Acknowledgement

I would like to express my deepest gratitude to my supervisor Professor JY Richard Liew for his high expectation, generous support, continuous guidance and encouragement during my PhD project. I would also like to express my special thanks to Dr Vu Khac Kien and Dr Krish Sivam for their very helpful mentorship and valuable discussions during this phase.

Sincere thanks go to Professor Koh Chan Ghee, Professor Somsak Swaddiwudhipong, and Dr Qian Xudong for their valuable judgements and comments on my research work.

I would like to appreciate the supports from my teammate Ms Ma Chenyin. I also give my thanks to Mr Ang Beng Oon, Mr Koh Yian Kheng, among other staffs from Structural Laboratory for their technical supports along the projects.

My gratitude also extends to my teammates from CORO team for sharing your various ideas and intense passions during the NAB competition. Special thanks are expressed to my mentor Joy Rouse in the XCC programme for your guidance on knowledge out of the box.

Special thanks and loves go to my dear family for your patience, sacrifices and unconditional loves throughout the years passed. Thank you my best friends for sharing your joys and passions during these years in NUS.

The research work reported in this thesis has been carried out at the Department of Civil and Environmental Engineering, National University of Singapore. Financial supports offered by National University of Singapore are greatly appreciated.

Table of Content

Summary

Efficient use of material can be achieved in metal structures when they are designed to act in tension rather than to resist actions that generate compression and bending in structural members. Thus, lightweight structures take benefits of membrane action. For instance, arch, vault, and dome are preliminary designs to resist compression; while pre-tensioned cable and membrane are normally adopted for structures to resist tension.

With the intention to combine advantages of efficient structural forms for both compression and tension, this thesis proposes and develops two novel lightweight tensile restrained structures: Tension Strip Structures (TSSs) and Deployable Cable Chain Structures (DCCSs). In TSSs, membranes are adopted to restrain curved member from lateral buckling. In DCCSs, cables are applied to stabilize single-layer grid shells consisting of hinged struts.

Morphology studies have been carried out to investigate various structural forms for TSSs. Different types of connections between fabric and strut are proposed and compared to each other in terms of strength and stiffness, ease of installation, as well as manufacture cost. Similarly, a series of structural forms of DCCSs in vault, dome, boom shapes are created for different applications. Transforming patterns are investigated for both vault-shaped and dome-shaped DCCSs. High deployment ratio (volume in deployed status divided by that in compact status) can be achieved in DCCSs due to their ability to transform in two directions compared with conventional deployable plate structures or foldable bar structures which can only transform in one direction. Geometric rules governing the deployability of the structures are discussed

and the locking mechanisms are explained. A new type of socket joint is proposed as a hub connecting struts and cables for deployable structures similar to DCCSs.

Structural behaviour of the proposed TSSs is investigated by advanced nonlinear structural analyses. A proposed corotational scheme provides an efficient methodology to perform geometrical nonlinear analysis of TSSs as planar curved beams with membrane restraints. Effects of design parameters such as length to depth ratio, cross section resistance of struts, elastic stiffness of restraints, number of struts, etc. on the stiffness and critical load of TSSs are investigated. Nonlinear inelastic analysis has been carried out for DCCSs to predict the load-displacement behaviour up to the maximum load. Comparison with other existing foldable shelters indicates that DCCSs have high structural efficiency in terms of strength to weight ratio. Dynamic effects of accidental removal of cable are investigated, which shows that the structure is sensitive to sudden loss of cable forces. However, the robustness of proposed structures against dynamic impact due to sudden damage of cables can be enhanced by providing safety ties at strategic locations.

Three full scale specimens for TSSs are manufactured and tested. Reduced scale prototypes for DCCSs are also fabricated. The practical issues related to fabrication of tensile restrained columns are discussed and recommendations for improvement are given. Test results such as maximum load, failure modes and load-displacement curves are obtained and compared with the numerical results so that the accuracy of the proposed analysis method can be verified for use in design.

List of Awards and Publications

Awards

2011 1st Prize of Novel Automobile Barrier Challenge, MHA&NUS, Singapore.

The best design proposal selected with the potential to arrest a vehicle with weight of 1800 kg travelling at 60 km/h within a stopping distance of 1 m is developed together with other CORO teammates.

2010 Hangai Prize, IASS 2010 at annual Symposium of International Association of Shell and Spatial Structures, Shanghai, China.

The criteria for the awards are innovation and scientific soundness of the presented technical paper.

2010 Extra Chapter Challenge (XCC) Awards, NUS, Singapore.

The applicants for this program are evaluated on the commercial feasibility of the discoveries and their passion for innovation and entrepreneurship.

2009 KKCNN Best Presenter Awards, Thailand.

Best presenter for the paper on deployable cable chain structures and deployable protective structures.

Publications

Journal Papers

2011 Y Li, KK Vu & JY Richard Liew. "Deployable Cable-Chain Structures: Morphology, Structural Response and Robustness Study", Journal of the International Association for Shell and Spatial Structures, v 52, n 168, p 83-96.

2010 Y Li, JY Richard Liew, KK Vu & A Krishnapillai. "Novel Hybrid Lightweight Tension Strip Structures", Journal of the International Association for Shell and Spatial Structures, v 51, n 166, p 263-270. (Hangai Prize)

Conference Papers

2012 CY Ma, Y Li, JY Richard Liew & KK Vu. "A Novel Deployable Vehicle Crash Barrier", in Proceedings of the 10thInternational Conference on Advances in Steel Concrete and Hybrid Structures, Singapore.

2010 Y Li, JY Richard Liew, KK Vu & A Krishnapillai. "Novel Hybrid Lightweight Tension Strip Structures", in Proceedings of the International Association for Shell and Spatial Structures (IASS) Symposium 2010, Shanghai, China.

2009 Y Li, JY Richard Liew & KK Vu. "Lightweight Tension Strip Structures", in Proceedings of the 6th International Conference on

Advances in Steel Structures 2009, Hong Kong, China.

2009 Y Li, CY Ma, JY Richard Liew & KK Vu. "Novel Deployable Protective Structures for Civil and Military Applications", in Proceedings of the 22nd KKCNN Symposium on Civil Engineering 2009, Chiang Mai, Thailand.

2008 Y Li, JY Richard Liew & KK Vu. "Deployable Cable Chain Structures: Concept Development", in Proceedings of the 21stKKCNN Symposium on Civil Engineering 2008, Singapore.

2007 KK Vu, JY Richard Liew, A Krishnapillai & Y Li. "Deployable Structure Systems: Meeting the Needs for Emergency and Safety", in Proceedings of the 5th International Conference on Advances in Steel Structures 2007, Singapore.

2007 KK Vu, JY Richard Liew & Y Li. "Deployable Boom Structures: Concept and Evaluation", in Proceedings of the 9th International Conference in Steel and Space Structures 2007, Yantai, China.

Public Seminars

2011 "Deployable Automobile Barrier" in Structural Steel Research Group (SSRG) 2011 Annual Seminar - Advances in Lightweight, Deployable and Steel Composite Structures, Department of Civil Engineering, National University of Singapore, Singapore.

2010 "Hybrid Lightweight Tension Strip Structures" in Hazard and Risk Mitigation Programme 2010 Annual Seminar - Advances in

Lightweight, Deployable and Steel Composite Structures, Department of Civil Engineering, National University of Singapore, Singapore.

2009 "Innovative Designs of Lightweight Structures" in Structural Steel Research Group (SSRG) 2009 Annual Seminar - Advances in Lightweight, Deployable and Steel Composite Structures, Department of Civil Engineering, National University of Singapore, Singapore.

2007 "Linkages Between Today and The Future of Deployable Booms" in Structural Steel Research Group (SSRG) 2009 Annual Seminar - Advances in Lightweight, Deployable and Steel Composite Structures, Department of Civil Engineering, National University of Singapore, Singapore.

Nomenclature

A	Cross sectional area
A_s	Cross sectional area of strut
B	B matrix
$C_{0,1,2,3,4}$	Constant coefficients
C_{pi}	Wind pressure coefficient
D	Diameter
$D_{\max}$	Maximum deflection of centre node in DCCS
D_r	Residual deflection
E	Young's modulus
E_m	Elastic modulus of the membrane
E_s	Elastic modulus of the strut
F	Force
F_c	Maximum tensile force of the critical cable
F_s	Maximum compressive force of the critical strut
H	Potential energy by external load
I	Moment of inertia
K	Tangent stiffness matrix
L	Length of the element, beam, or column
L_C	Length of the element at current configuration
L_O	Length of the element at initial configuration
M	Bending moment
M_{arch}	Bending moment in an arch
M_{beam}	Bending moment in a beam
M_c	End moment for a cantilever beam to rotate into a circle
$M_{i,j}$	Bending moment at end nodes i, j
N	Normal force in the analytical arch model
N_e	Axial force in the element
N_l	Axial strain due to end translation
N_n	Axial strain due to lateral deflection caused by end rotations

P	Applied force
P_{bk}	Buckling load
$P_{bk,norm}$	Normalized buckling load
P_y	Yield load
Q	Shear force in the analytical arch model
U	Strain energy
$V_{i,j}$	Shear force at end nodes i, j
$X_{i,j}^{C,O}$	Coordinates of nodes i, j in x direction at current, initial configurations
$Y_{i,j}^{C,O}$	Coordinates of nodes i, j in y direction at current, initial configurations
$\{F\}$	Internal force vector
$\{P\}$	Reference load vector
$\{R\}$	Unbalanced force vector

c_{kfs}	Coefficient of elastic of restraint for strut
c_{kfc}	Coefficient of elastic of restraint for column
d	Depth of TSS
f	Length to depth ratio
h	Distance of points on the arch to the column axial, or hog/sag of arch
i	Numbering parameter
j	Numbering parameter
k	Curvature
k_c	Axial compressive stiffness
k_f	Elastic stiffness of restraint
$k_{\lim}$	Elastic limit of axial compressive stiffness
k_{norm}	Normalized stiffness
k_{te}	Material tangent stiffness matrix
k_{tg}	Geometry tangent stiffness matrix
l_e	Length of the element
l_n	Length of the connection cable in DCCS
l_r	Length of the surrounding cable in DCCS
l_s	Length of the strut in DCCS
n	Number parameter

$n_{i,j}$	End conditions (hinge or rigid) at nodes i, j
n_p	Number of pyramids in DCCS
p	Global variations
p_a	Internal air pressure
p_l	Local variations
p_{lv}	Local virtual quantity of variations
p_v	Global virtual quantity of variations
q	Distributed load
q_i	Global internal force
q_{li}	Local internal force
$q_{x,y,z}$	External load in x, y, z directions
r	Radius of circular arch
r_x	Horizontal component of the reaction force
r_y	Vertical component of the reaction force
s	Span of the beam/arch/column
t	Membrane thickness
u	Nodal displacement component in x direction
u_l	Axial displacement
v	Nodal displacement component in y direction
w	Nodal displacement component in z direction
y	Radial deflection in analytical model
α	Included angle parameter
α_t	Coefficient of thermal expansion
β_c	Current angle of the element
β_0	Initial angle of the element
β_i	Current angle at the node i
β_j	Current angle at the node j
δ	Transverse deflection
ε	True strain
ε_{cr}	Critical strain
φ	Angle in the analytical arch model

γ	Included angle of half arch
λ	Load increment parameter
θ	Nodal rotation
θ_c	Included angle corresponding to a pyramid in DCCS
θ_i	Global nodal rotation at node *i*
θ_{il}	Local nodal rotation at node *i*
θ_j	Global nodal rotation at node *j*
θ_{jl}	Local nodal rotation at node *j*
σ	True stress
σ_{cr}	Critical stress
σ_y	Tensile yield stress
σ_u	Ultimate stress
Δz	Axial displacement
$\{\Delta U\}$	Displacement increment vector
CCS	Cable Chain Structure
CHS	Circular Hollow Section
DCCS	Deployable Cable Chain Structure
DL	Dead Load
DTSS	Deployable Tension-Strut Structure
FBS	Foldable Bar Structure
FPS	Foldable Plate Structure
HNL	Horizontal Notional Load
IL	Imposed Load
MBL	Minimum Breaking Load
RHS	Rectangular Hollow Section
RMSE	Root mean square deviation
TSS	Tension Strip Structure
WL	Wind Load

List of Figures

List of Tables

Chapter 1

Introduction

1.1 Overview

"Lightweight structures", as defined by Lightweight Structures Association of Australasia, is a generic term for a broad category of structures that optimize the load carrying capacity of the members involving a critical loading case, regardless of the type of the material employed. Based on this definition, typical lightweight structures include space frames, concrete shells, surface stressed structures, tensioned cables, and pneumatic structures as well as arched systems, braced vaults and domes, and deployable structures. Different types of lightweight structures have been developed for different requirements and loading cases. For example, due to their high mobility, deployable structures have high potential to be used for the temporary construction, military, and aerospace industries (Gantes, 2001).

Lightweight structures possess several advantages. First of all, they are regarded to be economical in terms of material usage because their self weight is typically a small portion of the applied load or generated. In addition, the aesthetic appearance and innovative character of lightweight structures are widely recognized. These advantages have led to continuous research and development in this field by both architects and engineers. Consequently, wide applications of lightweight structures

have been seen in architecture, engineering and building construction such as long span roofs for stadiums and/or exhibition structures, covered shopping malls, landmark structures, aerospace structures, as well as environmental protection canopies.

To achieve lightweight structures, two directions could be adopted: (1) developing new lightweight materials, and (2) utilizing optimally existing materials. With limited existing material available, many studies concentrate on optimization of structural forms to utilize existing materials (Bletzinger and Ramm, 2001). The procedure of optimization on forms and shapes of structures is to minimize the internal bending or the strain energy as most structures fail from bending. For this purpose, typical lightweight structures take advantage of membrane actions. For instance, tensile structural elements, pre-stressed cables and/or membrane, are widely used in lightweight structures while arches and/or domes are usually adopted in lightweight structures as compressive structural elements. Historically, both these two types of structural elements have played key roles in lightweight structures.

To efficiently resist compressive loadings using limited material such as stones and bricks, arches and domes were widely used as lightweight structural forms in ancient time. For example, a large number of arch masonry bridges were built in ancient China while many dome shaped churches were constructed in ancient Europe. Among them, some buildings are now still standing there after hundreds of years. A key feature of arch and dome is their ability to efficiently transfer external loads through, mainly, compressive forces to their supports. However, a severe disadvantage of these compression-based structures is buckling. For instance, the buckling phenomenon couples the load bearing capacity and the length of an arch together. This may make

the arch to fail before yielding limit especially when the arch is slender, thus leading to a waste of material.

Tensile structural elements such as cables and membrane have been adopted for tent structures since ancient times when nomadic tribes moved from place to place. Being lightweight and flexible, they are adaptable to the unsettled lifestyle of the nomadic tribes. Besides, tensile structural elements are structurally efficient as they are free from buckling. For example, the load bearing capacity of a cable is independent of its length and solely determined by the material properties and the cross section area.

However, where there is tension there is compression. For instance, tent structures need poles to resist compressive forces, and then buckling phenomenon must be considered. To overcome this problem, various hybrid lightweight structures have been developed since the last century with the intensive development of wrought iron and composite fabric. Hybrid lightweight structures, which do not solely rely on efficient compressive structural elements or tensile structural elements, often take advantages of both these elements. The philosophy of hybrid lightweight structures is to find the optimized interplay between tension and compression forces.

1.2 Objectives and scope

From the overall review presented in Section 1.1, although arches and membrane have been recognized as lightweight structural elements since ancient time, efforts to combine them together as a compressive column are still limited.

To fill the research gap, the objectives of this research are to propose novel lightweight structures utilizing curved struts and tensile membrane to resist

compressive load and to investigate their structural behaviours through analytical, numerical, and experimental works. The specific objectives are as follows:

1) Propose and develop lightweight Tension Strip Structures (TSSs) with high structural efficiency in terms of strength to weight ratio to resist compression load.

2) Develop nonlinear analytical models to predict the load-displacement behaviour and the loading capacity of TSSs.

3) Determine the optimum design parameters of TSS through a series of parametric studies.

4) Expand the concept of TSSs and generate other lightweight tensile restrained structures for larger span applications with the added function of deployability. They are termed as Deployable Cable Strut Structures (DCCSs).

5) Propose and evaluate suitable connection methods or joints, and investigate other design issues for applications of TSS and DCCS through numerical modelling, prototype building, and experimental testing.

The study addresses main parts of a technology development research, such as concept development, analytical modelling, numerical modelling, prototyping verification and experimental testing of TSS. Although flexural torsion buckling could occur for compression members made of open-profile sections, these studies are beyond the scope of this study as the TSS is made of tubular sections to resist axial loads. In addition, the structure is regarded as a planar arch with continuous elastic restraints offered by membrane in the proposed numerical model and thus torsional buckling and flexural torsional buckling are not considered.

1.3 Organization of thesis

This thesis consists of 7 chapters, as follows.

Following the present, introductory chapter, Chapter 2 reviews the relevant background to lightweight structural systems, relative deployment designs, and nonlinear analysis of curved beams with or without elastic restraints. Firstly, more attentions are paid on the applications of arches for lightweight structures. Secondly, surface tensile structures are discussed and summarized with regards to the structural function of those tensile elements. These two subjects provide the inspiration for the proposed tensile restrained structures in the subsequent chapters. The final section reviews the background behind the development of numerical analysis models for curved beams with or without elastic restraints. The qualities and limitations of these methods are illustrated and general trends for the methods are summarized.

Chapter 3 introduces and develops the concept of proposed lightweight tensile restrained structures including Tension Strip Structure (TSS) and Deployable Cable Chain Structure (DCCS). Different structural forms are investigated through morphology studies. The transforming patterns of DCCSs are investigated as well. Different joints like honey-comb socket joint are developed to facilitate rapid deployment and on-site assemblies. Various scaled prototypes are built to verify the proposed concepts and/or their deployment mechanisms.

Chapter 4 presents numerical methods for nonlinear analyses of both TSS and DCCS. The geometrically nonlinear analysis of planar arches with lateral elastic restraints is developed in a corotational scheme. This membrane locking free analysis scheme is proposed to simplify the formulation in conventional approaches taking into account

the effect of curvature on the geometrical stiffness while maintain the quality standard of accuracy. The accuracy and applicability of the presented method is validated by comparing the results of a series of numerical examples with those from literatures.

Chapter 5 presents numerical studies on the response of both TSSs under axial compression forces and DCCSs under design load considering lateral wind forces. For the analysis of TSSs, a combination of an analytical model, the proposed finite element model based on corotational concept, and a finite element model by ABAQUS is used to the predict the stiffness and critical load for different geometries. These models are validated against to each other and results verify that the proposed predictive method is reasonably accurate for design purposes. The parametric study of the proposed TSS is performed using the proposed method because of the simplicity compared with numerical modelling by ABAQUS. Critical parametric factors are estimated and optimum design parameters are deduced. Nonlinear inelastic analysis is performed on DCCS to study its load-displacement behaviour and its structural robustness against the sudden loss of cable.

Chapter 6 presents a series of experimental investigations on TSSs as well as their components such as struts, membrane, membrane seams, and the connection systems between struts and membrane. Three TSSs with different length to depth ratios are tested and their structural behaviours are compared. The experimental results are used to verify the proposed finite element models.

Chapter 7 provides conclusion remarks. Directions for further research are recommended.

Chapter 2

Literature Review

Three main topics relative to the content of following chapters in the thesis are reviewed in this chapter. Firstly details of designs and characteristics of lightweight structural systems including arches, tensile structures, and tensile restrained arches are presented. Subsequently deployable structures based on cable and strut systems and mechanical aspects of their designs are introduced. Lastly an overview of methods on arches with elastic restraints is given.

2.1 Lightweight structural systems

Typical lightweight structures take advantage of membrane actions for the purpose of minimizing internal bending or the strain energy. For instance, tensile structural elements, pre-stressed cables and/or membrane, are widely used in lightweight structures while arches and/or domes are usually adopted in lightweight structures as compressive structural elements. A vast number of lightweight structure concepts exist, whereof only a few that are closely related to the proposed structures in this thesis will be presented in this section.

2.1.1 Arches as lightweight structures

The section reviews developments of the arch as lightweight structure (in a relative sense) in history from the ancient time through to the current century.

It is hard to know the exact date that saw the initial invention of the arch as building forms, but certainly the history of human beings using arches exceeds 5000 years. A few initial applications of arches for underground structures such as drains were developed in the Ancient Near East, the Levant, and Mexico (Rasch, 1985). In Ancient Europe, dominant arch buildings, mostly in the application of bridges, constructed by the Etruscans and ancient Greeks were in the shape of corbel arch. Mycenaean Arkadiko bridge is herein taken as an example as shown in Figure 2.1. It was imaged by Heinrich (1979) that ancient builders are occasionally motivated to use the arch instead of corbelled lintel because of false construction experience.

Figure 2.1: Mycenaean Arkadiko bridge in Greece from about 1300 BC (Author: David Gavin; Source: http://www.mike-epidavros.com/ARCHAIA/web-content/peloponnes/source/lerna5.html).

Ancient Romans learned the arch from the ancient Greeks and Etruscans, refined it, and tapped in the first time the full potential for above ground buildings such as

bridges, aqueducts, triumphal arch, and gates. Further, vaulted and domed structures that are morphed from arches were used for roofing large halls, churches, and temples. Generally these arch buildings bear mainly the compression force and hence built by stone blocks or bricks that are jointed together with wet mixed mortar. The shapes of Roman arch buildings were usually in semicircular and hence with relatively high depth to span ratios, although some were in a curve less than a semicircle (O'Connor, 1993). The choice of semicircular shape inherently has an advantage of low thrust force at the foundation and hence lower requirement of foundation abutments. Roman engineers used concrete and coffer dams for the structure that was usually covered with bricks or ashlars outside. These construction techniques make some of the buildings survive in use to the present day, one of which is shown in Figure 2.2.

Figure 2.2: Pons Fabricius in Rome from 62 BC (Author: Matthias Kabel; Source: http://en.wikipedia.org/wiki/File:Pons_Fabricius.jpg).

After the falling of Roman Empire, no significant development of arch constructions could be recalled in Europe until the 12th century. In China, Zhaozhou Bridge built at Zhao Xian from 605 to 616 with massive limestone wedges reinforced with iron

showed new features not to be repeated in almost 1000 years. From Figure 2.3, it can be seen that the special combination of shallow segmental arch and open spandrels of the Zhaozhou Bridge distinguishes itself from Roman arches that usually adopted semicircular arches and filled spandrels. The open-spandrel design can not only reduce the total weight of the bridge by about 15.3% or approximately 700 tons but also allow water to pass through the spandrels during a flood.

Figure 2.3: Zhaozhou Bridge (Source: Shijiazhuang Government Official Website).

During the late medieval ages, Gothic pointed arches were employed to a large extent in the construction of the cathedrals and bridges. The horizontal thrust developed at the supports was reduced as a result. As shown in Figure 2.4, the Gothic arches are distinguished by their pointed apex, pushes the weight above to the side of the windows or doors and finally into flying buttresses and/or walls.

Particularly, the 14th century saw arch construction building renewed in new heights in Europe. Aesthetical requirement called for increasing spans for arch structures, which means narrower piers, thinner arch barrels and lower span-rise ratios. Span lengths of 40 m to 72 m were reached with different arch types such as semi-circular,

pointed and segmental arches (Troyano, 2003). The span-rise ratio reached as high as 5.3 to 6.4. However, arch structures collapsed mainly because of the high trust force at the abutments. The principle reason is that the horizontal thrust force at the abutments is proportional to the span and total load and inversely proportional to the rise of the arch.

Figure 2.4: Gothic arches featured in the Notre Dame in Paris (Author: Joseph Cesare; Source: Transferred from en.wikipedia).

Figure 2.5: The Iron Bridge from 1779 (Author: Roantrum; Source: http://en.wikipedia.org/wiki/File:Ironbridge_6.jpg).

In more modern times, new materials such as cast iron, steel, concrete made it possible to build even longer and more elegant arch buildings although masonry and brick arches continued to be built. The Iron Bridge as shown in Figure 2.5 was the first arch bridge built of cast iron in the world. The employment of new material significantly decreased both construction time and the weight for long-span arch bridges, which led to great economic benefits. Besides, the slender arch ribs stabilized by bracing struts and connectors brought the bridge elegant appearance. This further promoted cast iron as a constructional material and particularly the growth of other iron bridges.

Figure 2.6: A span of St. Louis Bridge from 1874 (Author: William Rosmus; Source: http://en.wikipedia.org/wiki/File:SaintLouisMetroLinkEadsBridge.jpg).

Steel was the first construction material that is almost equally good for both tension and compression. The introduction of steel as a construction material dramatically changed the landscape of the arch buildings. With the help of steel, arch buildings became more flexible than masonry arch buildings with major spans. The St. Louis Bridge, a massive arch, completed in 1874 is a good example. It consists of three

spans, the centre one being 158.5 m long, and the other two 153 m each. The piers upon which these spans rest were built of limestone carried down to bed rock. The steel members in this bridge are mainly in compression, which does not fully take the advantage of the potential of the material.

Figure 2.7: The Lupu Bridge from 2004 (Author: Jurgenlison; Source: http://en.wikipedia.org/wiki/File:Lupu_Bridge_Shanghai_at_World_Expo_2010_Seen_from_Pudong.jpg).

Together with the morphology evolution, development in steel wire technology makes longer span arch bridges practical. A through arch bridge, with different structural forms from previously mentioned, is a bridge in which an arch rises above the deck so it passes through the arch and steel wires/cables in tension suspend the deck from the arch. With this type of design, more major span arch bridges were built all over the world. One arguably the most famous of this type is the Sydney Harbour Bridge built in 1932. The arch has a span of 503 m and a rise of 134 m. Since then, construction of mega steel arches became popular. Other famous steel through arch bridge includes: Silver Jubilee Bridge with a span of 330 m, Bayonne Bridge with a span of 510.54 m, the Lupu Bridge with a span of 520 m, the Sixth Crossing Bridge, etc.

The reinforced concrete technique makes it possible to utilize the physical properties of both concrete and steel. This propelled both steel and concrete to being the most popular construction materials for arch buildings today. Reinforced concrete arch buildings such as bridges and dams bear some of their load by tension within the structure, which reduces the horizontal thrust against the abutments and allows their construction on weaker ground. To reduce the self-weight in reinforced concrete bridges, lightweight materials such as lightweight concrete or steel are employed for major span constructions. This type of design can be seen in both Stolmasundet Bridge in Norway and Second Shibanpo Bridge in China, both which are with a span of exceeds 300 m.

It is noteworthy that other constructions also adopt the form of arch such as concrete dams, arch steel buildings, arch stadium supports, etc. In arch dams, stability is obtained by a combination of arch and gravity action. And the safety of the arch dam also depends on the strength of the side wall abutment, which means the supporting rock should be carefully inspected.

Figure 2.8: Bird's eye view over Lake Hodges Dam (Author: Phil Konstantin; Source: http://en.wikipedia.org/wiki/File:LakeHodgesDamByPhil Konstantin.jpg).

There are two types of arch dams: single-arch dams and multiple-arch dams. In a single-arch dam, the normal hydrostatic pressure is resisted by the cantilever in vertical direction and the arch action in the horizontal direction. Two types of single-arch dams are in use, namely the constant-angle and the constant-radius dam. The constant-radius type employs the same face radius at all elevations of the dam, which means that as the channel grows narrower towards the bottom of the dam the central angle subtended by the face of the dam becomes smaller. Jones Falls Dam, in Canada, belongs to this category. In a constant-angle dam, this subtended angle is kept a constant and the variation in distance between the abutments at various levels is taken care of by varying the radii. Parker Dam is a constant-angle arch dam.

The multiple-arch dam consists of a series of single-arch dams with concrete buttresses as the supporting abutments, as for example the Daniel-Johnson Dam, the Lake Hodges Dam, Big Bear Valley Dam, etc. The multiple-arch dam does not require as many buttresses as the hollow gravity type, but requires good rock foundation because the buttress loads are heavy. Normally, the upstream faces of the arches and buttresses are inclined into the reservoir to take advantage of a vertical component of hydrostatic pressure enhancing the stability. Compared with concrete gravity dams, multiple-arch arch dams possess of high structural efficiency, some design could reduce concrete quantities by 80%.

Steel arch buildings are freestanding prefabricated metal structures made from connecting sheets of arched steel. They are easy to be constructed, able to be recycled, and also efficiency in the cost. Because the arch roof barely stands on straight walls and hence no strong horizontal thrust component can be resisted, deep arches are normally used in steel arch buildings. As the roof and walls are formed as one, no

columns and beams inside are required to support the roof. Low cost is another huge benefit of these modular steel arch buildings. However, there are also some disadvantages, such as fixed shape, limited light penetration among others.

To achieve larger and larger interior space in stadium, lightweight roofs become preferable options by the designers. In such case, the heavy inside supporters are ruled out as this will clearly increase the self-weight. A cross arch over the roof become a popular design in major stadiums. Examples include the Wembley Stadium Arch with a maximum height of 133 m, the Olympic Stadium Arch, and Durban Stadium with a maximum height of 220 m. In the two conservatories at marina bay in Singapore as shown in Figure 2.10, a series of arches are used to bear the loadings from entire elegant shell-like roofs. In addition, it is noteworthy that memorial gates and arches are a special category of constructions built with an intention of celebration and/or remembrance. The Arch de Triomphe in Paris and the Gateway Arch in St. Louis, Missouri are among the most famous monuments.

Figure 2.9: Steel arch building.

Figure 2.10: Conservatories at Marina Bay in Singapore.

In this section, the compression elements especially the arch are reviewed as the lightweight structures from a historic point of view. In the next section, tensile members are reviewed based on their functions as structural components.

2.1.2 Tensile structures

Different from the arch, compressive structures, tensile elements rely on prestress for stability and adequate stiffness and have negligible bending and shear stiffness, but effective resistance against tension force. Because the flexibility of the material used in the surface tensile structures, the structural form easily varies under different load conditions.

The usages of tension elements, such as membrane, cables, and so on, can be classified into three categories. In the first category, tension elements are used as main structural components in "tension-only" structures, i.e., cable nets or tension membrane structures. This category is termed as surface tensile structures. The shape

of a surface tensile structure should be carefully designed so that pre-tension can be introduced into every part of the structure and minimum surface can be achieved. Various form finding methods have been developed such as the soap experimental method (Drew, 1976) and numerical methods investigated by many researchers (Bletzinger and Ramm, 2001), which is not within the research scope of the current work.

The second usage of tension elements is found in "tension–compression" structures in which all elements are pin-jointed and no moment exists. Tensegrity (Calladine, 1978), cable strut structures (Wang, 1998), as well as pneumatic structures (Herzog, 1976) belong to this category. A "tension–compression" structure becomes stable only when pre-tension is introduced. In order to obtain a "tension–compression" structure which can be pre-tensioned, a form finding process is also necessary.

The third usage of tension elements can be found in tensile restrained structures, which is the focus of the current work. In a tensile restrained structure, tension elements are used to restrain a primary stable structure, which can be a column, a beam or even a single layer lattice shell. Structural properties, such as buckling load, stiffness, stabilization, etc., can be significantly improved through stiffening primary structures with tensile elements. Cable stayed columns (Chan *et al.*, 2002) or pre-tensioned bowstring structures (Liew and Li, 2006), Tensairity structures (Breuer and Luchsinger, 2010), cable-stiffened pneumatic structures (Yoo *et al.*, 2007), and tensile restrained arches (Burford and Smith, 1999) fall in this category.

2.1.2.1 Surface tensile structures

Two primary advantages of surface tensile structures are as follows. Firstly, they are lightweight as their loading resistance capacity is derived from their pre-stressed form

rather than the mass of the material used. Secondly, surface tensile structures' lightweight components are easy to transport and erect on site, hence they are cheap options for enclosing vast interior spaces.

Depending on the prestress manner, surface tensile structures can be generally derived into two categories, e.g. anticlastic surface structures/tensile membrane structures, and synclastic surface structures/pneumatic structures. Tensioning of membrane structures is realized by the edge loads and common examples include normally used tents in civil engineering and solar sails in aeronautical applications. Tensioning of pneumatic structures is realized by inside air pressure with examples such as inflatable beams, air-supported sports stadium, etc.

In anticlastic tensile structures, anticlastic surfaces or portions of them are as primary structures to carry loads. An anticlastic surface is of a double-curved surface, of which the two curvatures transverse to each other and the sum of all positive and all negative curvature is zero. Of these two curvatures, one normal section is concave and the other one is convex.

Anticlastic tensile structures include both flexible membranes and cable nets with double curvature forms/shapes. In the thesis, the term "membrane" represents both membrane and cable net surfaces. In anticlastic tensile structures, loads are distributed along the surface and the lines of the edge forming the shape of the membrane. Tensile stress is most prominent in tensioned membranes, while compression forces are distributed into the posts and/or anchors.

Without external loads, the form of anticlastic tensile structures depends on boundary conditions and constraints given the specific membrane property. The effective

form/shape should follow the minimal surface criteria. A minimal surface is a surface with a mean curvature of zero, which can be an anticlastic surface or a flat surface. Flat membranes are unstable structure in the normal direction, while anticlastic membranes can carry downward load by a concave curvature and upward load by a convex curvature. Boundaries in a flat surface will lead to flat and unstable surface, hence a minimum of four support points in different flat surfaces is required to make a tensile membrane structure.

Great varieties of elegant tensile membrane structural forms have been obtained by the designers through manipulating the basic elements inside that support or restrain the membrane. These elements include anchors, posts/masts, arches, trusses, rings, cables, etc. Although numerous different structural forms exist, there are only a few basic doubly curved forms. Among them, the saddle form and the cone form are the commonly used anticlastic tensile structural forms.

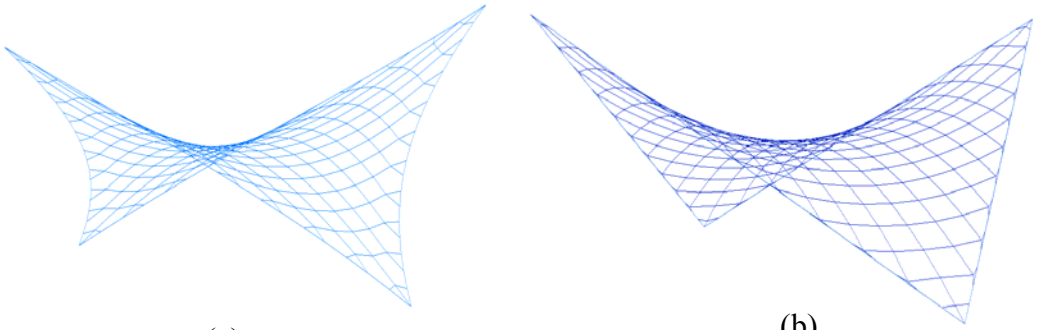

(a) (b)

Figure 2.11: Saddle forms with: (a) curved edges; (b) straight beams.

In the saddle, a membrane is stretched between supporting elements with elevation variations with either curved edges (restrained by cables) or straight edges (restrained by beams). Together with rigid grid or orthogonal grid at the centre, a basic module could be gained. In the saddle, a common variation is the arch/curved boundary supported tensile membrane structures as shown in Figure 2.11.

In the corn, the membrane is stretched between two vertically displaced concentric boundaries to shape a hyperboloid surface (Shaeffer, 1996). The changes in the configuration of the concentric boundaries lead to various membrane corns. The shape of these two boundaries could be drastically different although rings are commonly applied in practice.

2.1.2.2 Tension-compression structures

This category mainly includes the pneumatic structures, tensegrity, and cable strut structures.

Pneumatic structures are tension membrane structures in which the compression required to balance the membrane tension is provided by air pressure. In pneumatic structures, air acts as the compressive element (main contributor for the weight for most other structures) and hence they are probably the lightest structures and have the potential to cover largest span enclosures with a capacity for easy deployment and storage. Commonly used applications of this kind include the inflatable boat as well as life jackets. Besides, the most commonly used pneumatic structures are the tires for vehicles although they are not included in this review because they have to meet specific requirements and extensively studied.

Offering these benefits, pneumatic structures have wide applications in different fields such as: civil engineering, aeronautical and outer space exploration. In this section, pneumatic structures are divided into two subcategories to make the discussion simple: one is characterized by relatively large radii and a low inside pressure differential while the other possesses small radii and a high pressure differential. Some examples will be provided below and the emphasis will be given to the

applications in civil engineering.

For pneumatic structure with large radii, pressure difference between the interior and the exterior of the building is used to stabilize the membrane structures. They have been in use since the construction of a “Radome” by Walter Bird in the mid nineteen forties. Since then, this kind of elegant solution for easily erected and economical means of enclosing fairly long-span spaces had drawn considerable attention from architects and engineers. This technology was then expanded into some pneumatic sports stadium or pool roofs with semi-cylindrical shapes. All these buildings shared similar characters with the “Radome”. For instance, the height to the span ratio is fairly high and the inside air pressure must be maintained at a high level. The inward wind pressure on the steeply sloped walls of a high-profile (like Radome) air-supported structures must be resisted by the high-level inside air pressure.

A low-profile (low height to span ratio) air-supported design by David Geiger for the US Pavilion at Expo ’70 in Osaka (Japan) represents a true revolution (Huntington, 2004). The shortest span is about 13 times of the height of the roof. Roofs with such low slope are subject to upward “lift” forces only, and much of these wind pressure forces will be transferred to the anchors through the fabric. Hence, only low inside air pressure is required in such buildings while the cost is that high-tension stresses exist in the fabric membrane. Normally, this is overcome by using additional cables over the fabric to reinforce the membrane. In this way, the fabric is patterned to dimple upward between cables to yield small curvature radii and hence reduce the tension forces in the membrane.

Given promising development of new material such as polytetrafluoroethylene (PTFE) coated fibreglass fabrics, large span low-profile air-supported roofs were

further applied on stadiums, the silver dome of Pontiac in Michigan for example. However, the doubts about the air-supported roofs rose because numerous and sometimes costly full or partial deflations occurred due to combinations of severe storms together with either failure of the mechanical system.

Different from an air-supported structure discussed above, air-inflated structures are normally characterized by small radii and relatively high air pressure inside. Small space is enclosed to shape structural elements like beams, columns, arch frames, and walls. The load carrying capacity of such structures depends on the internal pressure level, the membrane material properties and the structural form of the element. Compared to air-supported structures, a constant air-supply would not be necessary in theory because air-inflated structures are self-contained and a completely airtight structure and a periodic replenishment of air are usually required (Veldman, 2005). Veldman (2005) developed a modified load deflection theory for straight inflated beams and investigated the influence of material and geometry on the load deflection behaviour. A series of inflated beams placed parallel to each other were also discussed in his work. Le van and Wielgosz (2007) derived a finite element for inflatable beams from the virtual work principle. Only straight air-inflated beams are included in their work. The bending response of inflatable, braided beams and arches was investigated numerically and experimentally by Brayley *et al*. (2012). Recently, Ritzel *et al*. (2009) conducted a program of numerical modelling and experiments on the blast, ballistic and earthquake response of the deployable shelter systems supported by air-inflatable beams showing improved ballistic protection and blast mitigation with a special tethering system and an external curtain wall.

Due to their lightweight, small packed volume and simple inflation, the use of

inflatable structure directly satisfies the needs of temporary structures including ease of deployment, simple erection, and minimal shipping volume and weight. However, pneumatic structures also have some disadvantages. For example, the stiffness of the whole structure is very sensitive to local penetration. In addition, it is found that most pneumatic structures have, more or less, suffered from asymmetric severe wind or snow load.

2.1.2.3 Tensile restrained structures

In a tensile restrained structure, tension elements are used to support a primary structure to improve the structural properties. Most popular structures from this category include (a) cable stiffened pneumatic structures, (b) cable stayed columns, (c) tensile restrained arches, and (d) Tensairity structures.

(a) Cable stiffened pneumatic structures

Inflatable structure with large radii and low profile suffer from large tension force in the membrane while inflatable structures with small radii normally suffer from distortion and collapse due to wrinkling. As discussed previously, using additional cables over the fabric to yield small curvature radii and hence reduce the tension forces in the membrane is a common practice to strengthen air-supported structures. For inflatable structures with small radii such as air beams and inflatable booms, cables or high strength strips are attached along the membrane to reduce the wrinkling region and delay the wrinkling occurrence. Yoo *et al*. (2007) stated that using shape memory alloy wires can remove the wrinkling region and hence improve the maximum load of the inflatable booms. Another way to enhance the pneumatic structures is to use external cables to support the inflatable arch/frames and improve the global response as given by Lukasiewicz and Warner (2010).

(b) Cable stayed columns

Cable stayed columns adopt cable stays and a crossarm system to stabilize a central slender column and to inhibit the primary buckling displacement. By such meanings, a lightweight structural solution can be achieved and the load bearing capacity of the column can be enhanced. The understanding of such structures has been continuously enriched by contributions from many aspects: the critical buckling load, the effect of imperfection, the ultimate axial strength, and the post buckling behaviour. Chu and Berge (1963), Smith *et al*. (1975), Hafez *et al*. (1979) among others investigated the critical buckling load. Wong and Temple (1982), Chan *et al*. (2002), and Saito and Wadee (2009b) evaluated the imperfection sensitivity. Temple *et al*. (1984), Smith (1985), Liew and Li (2006), and de Araujo *et al*. (2008) examined the cable stayed column ultimate axial strength. The buckling behaviour has been studied by Temple *et al*. (1984), Smith (1985), and Saito and Wadee (2009a).

(c) Tensile restrained arches

In a tensile restrained arch system, the bending in arch chord produced by the large differences between the thrust lines and the main geometry is to be significantly reduced by tensile restraining system (cables or membrane) bounded to the arch chord at the inward side. The system also effectively reduces the buckling length of the arch chord and hence an efficient lightweight structure solution can be achieved. Burford *et al*. (2009) presented the evolution of arches as lightweight structures in details from an historical point of view. Several principle types of cable restrained arch were derived in Burford *et al*. (2009) as follows.

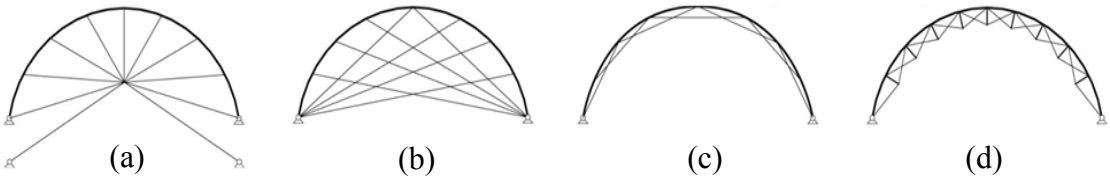

Figure 2.12: Types of tensile restrained arch from Burford *et al*. (2009): (a) hub type systems; (b) radial type systems; (c) chord type systems; (d) truss type systems.

In a hub type system, the restraining elements connect points on the arch chord to a fixed or free hub located at the centre. These systems are typically used in roof enclosures where arch is proposed on walls or columns and the internal volume enclosed by the arch is not functional. Figure 2.13 shows a general arrangement of arch and radial cables at Pargo Bugis Junction in Singapore.

Figure 2.13: Tensile restrained arch shape roof (Liew *et al.*, 2001).

In a radial type system, the restraining elements connect points on the arch chord to the arch support. These solutions are claimed to have higher levels of structural and material efficiency because the ties directly restrain the arch chord to a fixed support (Burford *et al.*, 2009).

In a chord type system, the restraining elements connect points on the arch chord to each other. This arrangement has larger clear heights compared to the former; hence this solution is preferable for shelters supported by arches. An example can be seen

from Lukasiewicz and Warner (2010).

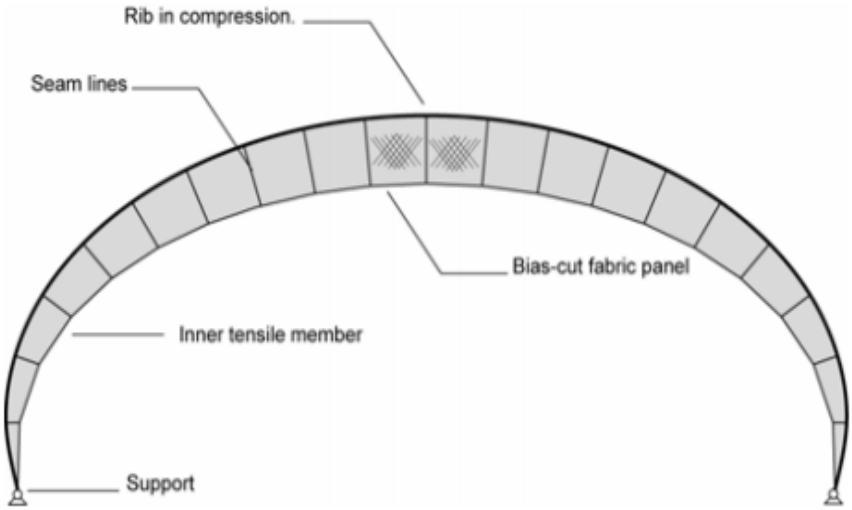

Figure 2.14: General arrangement of a web restrained arch (Burford and Gengnagel, 2004).

In a truss type system, the restraining elements closely follow the path of the arch chord providing improved ergonomics to that of radial and hub systems and better structure efficiency to that of chord systems. The restraining system has flexible locations such as inside, outside or both sides of the chord depending on the ergonomic and structural limit.

In some cases, these systems combine one or more of the above systems in a single structure and are normally used in situations where there are a number of dominant load cases.

The buckling behaviours of an arch stiffened by cables are investigated by Wu and Sasaki (2007) and the buckling load of the arch greatly increases after it is stiffened with a cost of slightly reduced stiffness.

Burford and Gengnagel (2004) proposed a novel restraining system including fabric

panel, rib, inner tensile member as shown in Figure 2.14. The structural response of this system was numerically investigated and some key design parameters such as connection of the inner tensile member, the orientation of the fabric panel, the size of the membrane panel are recommended by Alpermann and Gengnagel (2009). It was concluded that the deformation reduced by 45% compared to the one without restraining system.

(d) Tensairity structures

Tensairity is a recently proposed lightweight structural concept with the intention to gain mechanical advantages for low mass using inflated airbeams and attached stiffeners or cables. The key principle of this structure is to use low pressure air to stabilize compression elements against buckling and hence improve the load bearing capacity (Luchsinger *et al.*, 2004). A series of structural forms sharing this exact concept have been developed from Tensairity beams (Pedretti and Luscher, 2007) to Tensairity columns (Plagianakos *et al.*, 2009), from Tensairity kites (Breuer and Luchsinger, 2010) to Tensairity girders (Luchsinger *et al.*, 2011). Some realized applications of Tensairity include bridges, roof structures, wing structures, kites, etc.

A preliminary test carried out on both straight Tensairity beam and curved Tensairity beam by Breuer and Luchsinger (2010) shows that Tensairity beams have a clear increase with an increasing with air pressure inside and the stiffness and ultimate load of the Tensairity beam is much larger than air tubes with the same material and internal air pressure. They also claimed some potential applications of such structure, such as ultralight aircraft and hang-gliders. Unfortunately, only one specimen for each was tested in their work.

Load displacement response of Tensairity girder under a central load has been

investigated and the results indicated that the force has a linear relationship with applied load and displacement under bending load can be considerablely reduced when the chord is tightly connected with the fabric (Luchsinger and Crettol, 2006). The FE model developed can well predict the displacement versus load curve at the compression chord but the prediction at the tension chord is not as good. This suggests the difference between these two chords for Tensairity girders and the shear force may play important role in such structure.

A symmtric spindle-shaped Tensairity girder with a length of 8 m is tested under bending loads (Luchsinger *et al.*, 2011). A refined FE model was developed using ABAQUS to simulate the structural response carefully considering the contact between different components, the friction parameters, initial position of the cable, etc. Good correlation was found between the experimental and FE results. The experiments show better structural load carrying capacity compared to the cylindrical girder.

The spindle-shaped Tensairity columns are constituted by three curved columns or arches restrained by a spindle-shaped air hull at the centre. The curved columns are connected to the hull membrane by fabric pockets. Tensairity columns show the potential as poles in temporary structrues by comparing with similar curved truss-type structures (Plagianakos *et al.*, 2009). Tensairity columns have been further refined by applying fabric webs into the inflatable hull with the intention to improve the stability enhancement. The experimental and numerical investigations by (Wever *et al.*, 2010) on such structure show a considerable improvement of the structural behaviour interms of both stiffness and buckling load. However, significantly higher stiffness predicted by the FE model than the test results suggests ineffective connection

between fabric and struts. Besides, ignoring the fabric material nonlinearity and the fabrication imperfection leads to the overestimation on the structural capacity.

2.2 Deployment designs relative to lightweight/tensile restrained structures

Normally, the term deployable structure means the structure with the ability of transit from a compact state to one or more unfolded functional states (Hanaor and Levy, 2001). However, this term has not been well defined so far and contains quite many meanings behind it. For instance, deployable structures are sometimes known under other names like expandable, extendible, developable, retractable, transformable and foldable structures (Tibert, 2002).

It is hard to clearly state all deployable structures using only one criterion. Hence, in this thesis, deployable structures are to be classified based on deployment mechanisms and elements. Only those closely relative to the current work including deployable pantographic structures, deployable truss-assembly structures, and deployable tension strut structures will be reviewed in the following sub-sections. At the end, a survey on the deployment mechanisms is summarized to get the insight of these deployable structures.

2.2.1 Deployable pantographic structures

As predominant type of deployable structure for both outer space and terrestrial applications, pantographic structure refers to those systems relying on scissor-like kinematics. The use of scissor-like elements for deployable structures on an architectural scale traces back to works of several pioneers including Escrig (1996),

Krishnapillai (1988), You and Pellegrino (1996; 1997a), Ziegler (1997), and Gantes (2001), etc. In their work, three basic pantographic modules have been proposed: plane scissor module, radial scissor module, and scissor combination module.

Among these basic pantographic modules, the simplest one is 2D usage, the most common basic unit is plane scissor unit; space can be enclosed with three or more such units as show in Figure 2.15(a). The less common pantographic structures are composed of radial scissor unit developed by Skelton (1995), where pairs of scissors share one common pivot at the centre of the unit as shown in Figure 2.15(b). The most complicated unit is a 3D combination of scissor units such as the 'clicking unit' employed by Krishnapillai (1988), providing improved stiffness and a locking device as shown in Figure 2.16.

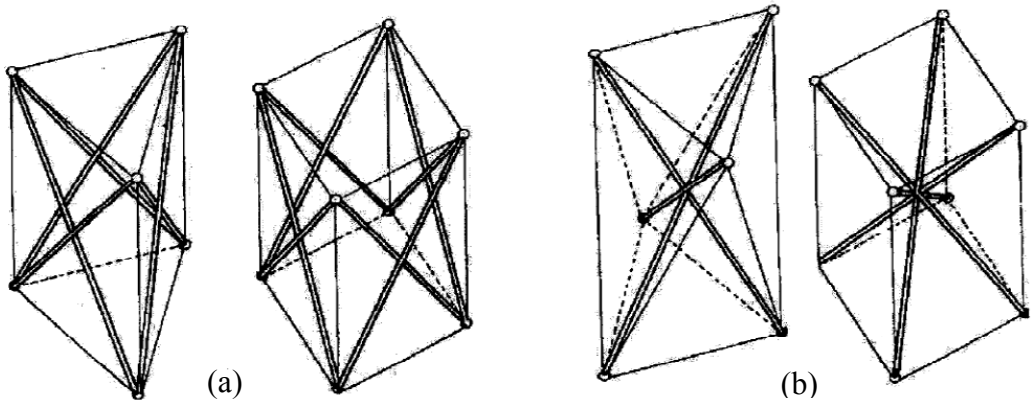

Figure 2.15: Basic pantographic units: (a) plane scissor unit; (b) radial scissor unit.

Different ways to assemble these basic modules shapes different structural forms. The simplest one is a 2D usage such as angulated scissors and retractable roofs proposed by You and Pellegrino (1997b). These structures attribute low stiffness due to the low structural depth and out plane braces; hence, they are just suitable for toys or exhibition. To eliminate this drawback, arch shaped or curved pantographic elements

have been engineered to form double layer grids or pantographic grids. In this kind of pantographic structures, “off-centred” scissors are used to achieve the curved shape. Another option is adopting tensile elements such as cables to stiffen the deployed pantographic structures (You and Pellegrino, 1996; 1997a).

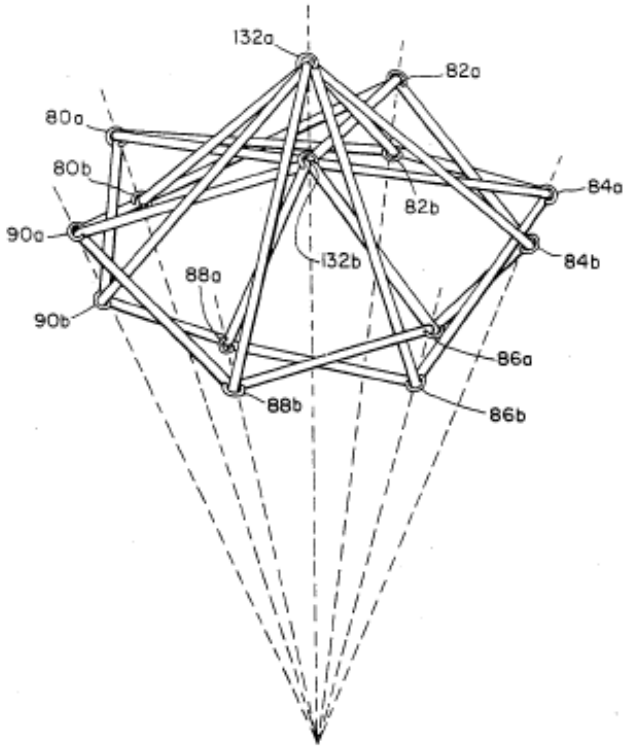

Figure 2.16: Deployable structures by Krishnapillai (1988).

Some more complex forms of scissor elements were used by Wei *et al*. (2006) to create new expandable structure for spatial objects as shown in Figure 2.17. The unit can be regarded as mechanism composed of two sets of scissors and some additional chords. According to Grubler-Kutzbach criterion, the freedom of the mechanism is one, which means the freedom of entire structure is determined by how many units are used in the system. Some examples of application are given and the volume ratio can be at least 2.83 if all of the links are thin enough. However, the structure given by the author is hard to control, and the stiffness is very low because they are not well braced.

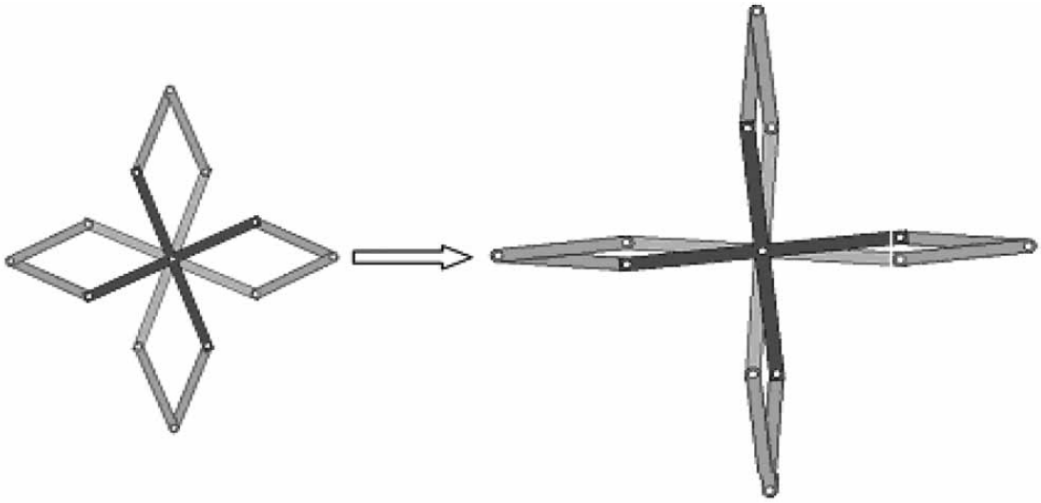

Figure 2.17: Complicated form of scissor like element by Wei *et al*. (2006).

In addition, to design practical structures any solution that would work in two dimensions can be projected vertically onto a 3-dimensional surface. However, the support conditions need to allow this motion as the perimeter of the structure varies during retraction. Kassabian *et al*. (1999) showed that it is possible to support the structure on a number of fixed points each corresponding to the centre of one of these circles if a rigid body rotation of the structure is allowed as demonstrated in Figure 2.18.

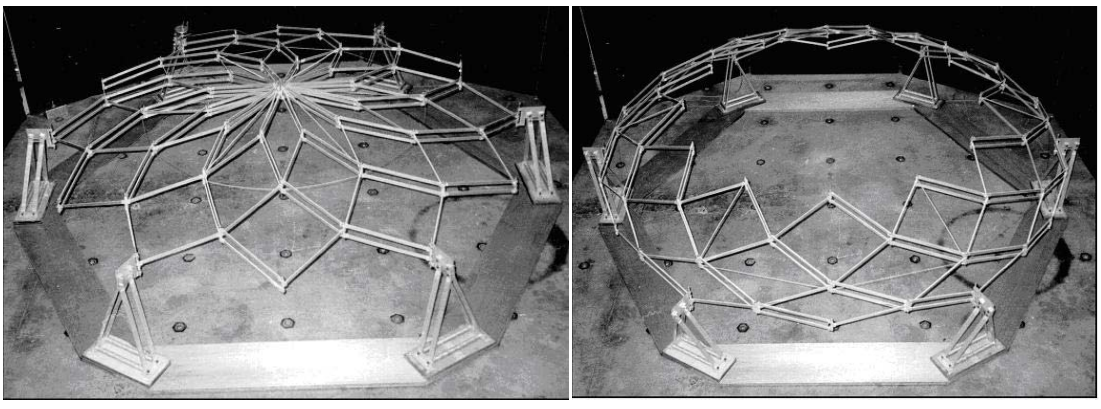

Figure 2.18: Deployable "spherical" structure by Kassabian *et al*. (1999).

In general, the pantograph in a plane on its own lacks structural depth and therefore

would have quite low structural efficiency. Beyond this, double-layer or curved pantograph structure eliminates this disadvantage and have wide applications. Normally, these structures have only one kinematic degree of freedom, which facilitate the deployment of the whole structure especially for outer space application where manual intervention is not available.

2.2.2 Deployable truss-assembly structures

Deployable truss-assembly structures or folding truss structures are systems made of pin connecting struts. The deployment of such structures depends on releasing the rotation of joints. Most such deployable structures have typically focused on the deployment of general truss-assembly designs rather than specific deployable structure designs. Most of these inventions address new approaches with the intention for outer space applications.

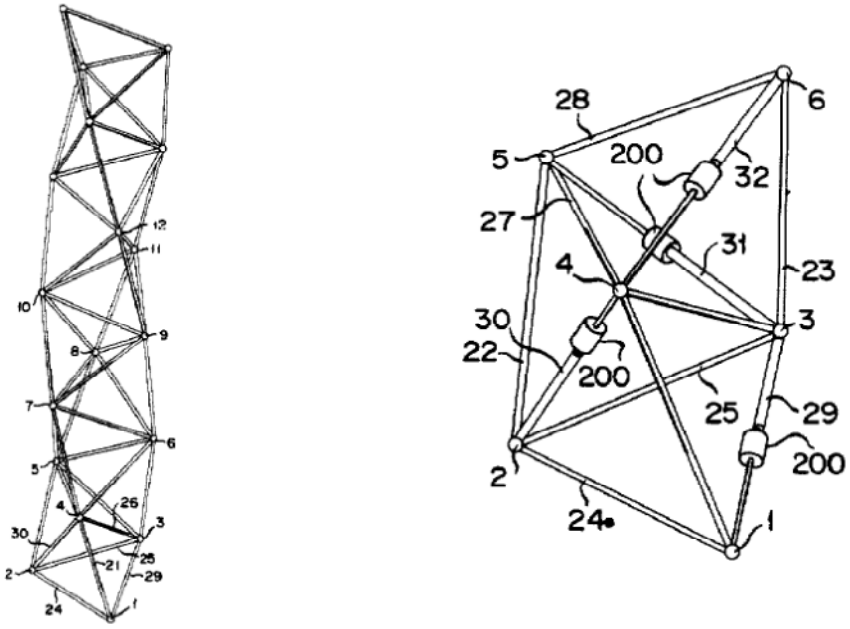

Figure 2.19: Deployable booms by Natori (1985).

For example, beams and triangular plates were used by Natori (1985) to form a

tetrahedral unit. These units composed of a linear truss to form a deployable boom as shown in Figure 2.19. The deployment mechanism of such structure is realized by flexible joint and some hinged struts. Special joint and hinge details and stowage/deployment kinematics are involved in his job.

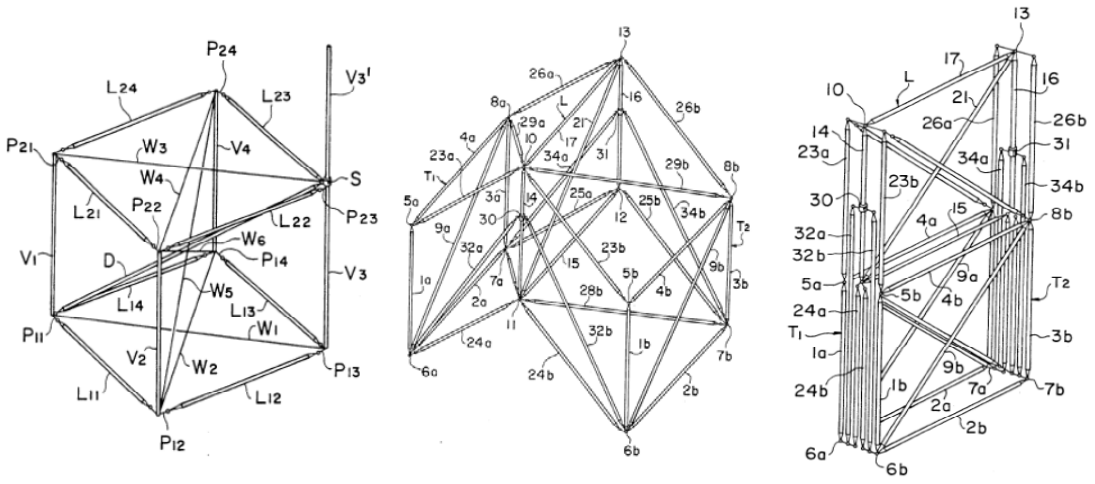

Figure 2.20: Deployable booms by Onoda (1991).

Onoda (1986; 1987a; 1987b; 1988; 1991) patented numerous and interesting collapsible or deployable square truss units using struts and special joints. The ties or joints can move along the vertical trusses as shown in Figure 2.20. Some applications suggested include box sections, curved frames for building, as well as solar reflectors or antennas. Besides, the structural and especially the joints' behaviour during deployment require detailed investigation.

Generally speaking, the deployable truss-assembly structures are flexible in both kinematics and shapes and therefore have various potential applications. The structure efficiency depends on specific cases and the reliability of those specially designed joints. Such complicated joints may require careful manipulation for pre-assembly, which limits their applications.

2.2.3 Deployable tension-strut structures

Deployable tension-strut structures include deployable cable-strut structures, deployable tensioned membrane strut structures, and deployable tensegrity. Although cable is most popular tension element in these systems, sometimes, fabric membrane is employed to brace struts as well. Hence tension-strut structure is more suitable description of these kinds of systems than deployable cable strut structures.

The principle has high potential due to the idea of improving the structural efficiency by separate tension and compression. Tensegrity structures are definitely under this principle because in purest form, it is not allowed that bars are connected to each other. Like deployable structure, the term tensegrity is not defined clearly either. But it is generally regarded that K. D. Snelson's X-Piece structure shown in Figure 2.21, constructed in 1948, represents the birth of the tensegrity structures. Gunnar Tiber developed tensegrity structures deployable for space usage through introducing bi-stable hinges into the struts (Tibert, 2002).

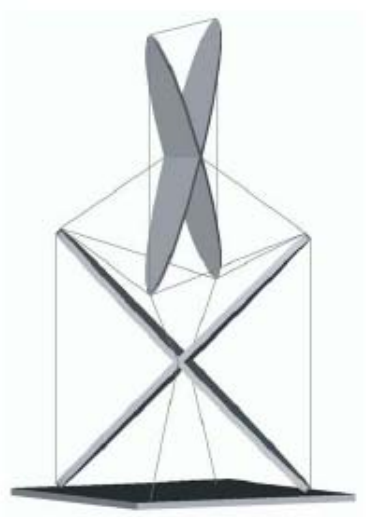

Figure 2.21: K. D. Snelson's X-Piece structure (Tibert, 2002).

Deployable Tension-Strut Structures (DTSS) are spatial structures developed by Vu *et*

al. (2006) on the base of cable strut structures proposed by Wang (2004) and Liew *et al*. (2003). The desire is combining the advantages of rapid deployment and structural efficiency of cable strut structures. According to the study of DTSS by Vu (2007), these systems have high potential in both outer space and terrestrial applications.

Structural efficiency of deployable tensegrity structures is relatively low because of improperly braced. However, the DTSS possess higher structural efficiency than conventional two layer grid structures.

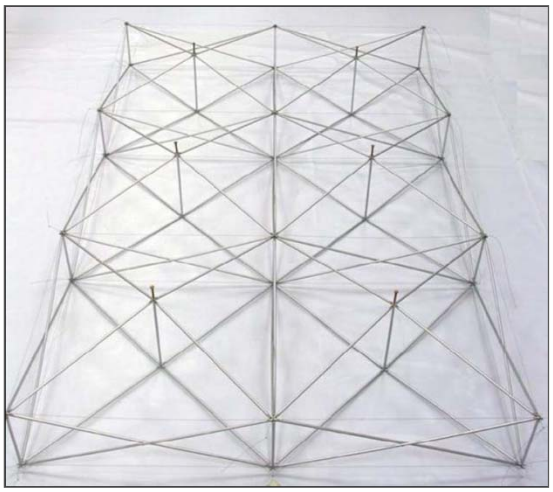

Figure 2.22: One DTSS proposed by Vu *et al*. (2006).

The concept of deployable strut-tensioned membrane is the outcome of the inspiration of combining a system of deployable strut skeleton with high strength membrane to span over large space in a short erection time (Liew and Tran, 2006). Two novel DSTMS were developed based on this concept: one is the Umbrella DSTMS and the other is Cone-shaped DSTMS.

Both of them are composed of short struts, cables and membrane. Struts are members bearing the compression and cables and membrane are tensioned components to achieve the self-stress equilibrium in the deployed configuration of DSTMS. At the

same time, members tensioned at the deployed configuration stabilize and provide restraint to the structural system for loading bearing purpose.

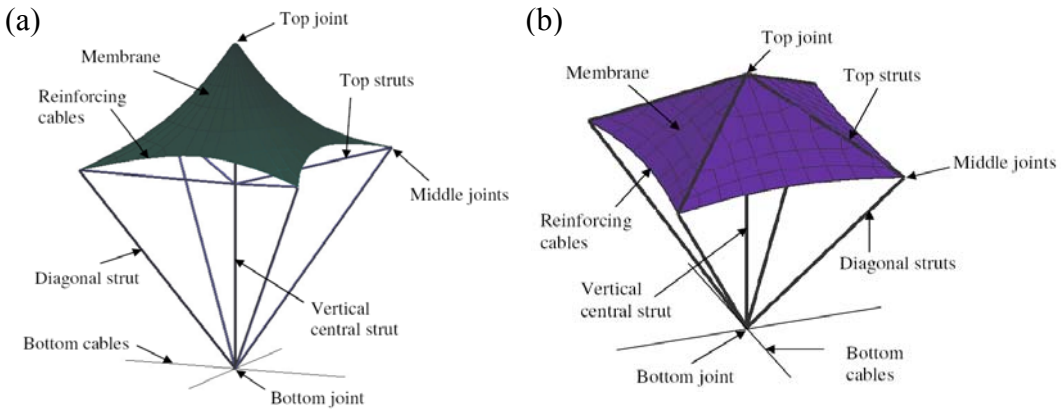

Figure 2.23: Deployable strut-tensioned membrane: (a) umbrella simplex; (b) cone-shaped simplex (Liew and Tran, 2006).

In deployable strut-tensioned membrane structures, the deployment is realized by sling the common joint of the top struts along the direction of the vertical central strut. The structural depth is controlled by the distance from the top struts to the bottom cables. The structure constituted by such simplexes needs fixed supports at the two ends to resist the outward load from the inside. Compared to other deployable tension strut structures, the covering membrane also contribute to the structural load bearing capacity as an integrated primary structural components for roof applications.

2.2.4 Deployment mechanism survey

Deployment movement can be investigated by studying basic structural modules and elements. These components of deployable structures include plates, bars, cables, joints, etc. Deployable structures can be unfolded or folded because they are mechanisms; otherwise they become rigid body only. There are two aspects that define the geometry of deployable structure: (a) the way individual elements are

arranged to form a basic module; (b) the way individual deployable modules are arranged to form a grid. Here, existing deployment methods relative to reviewed structures as above are presented and investigated at the level of forming a deployable module.

2.2.4.1 Pantograph

Pantograph, which sometimes is regarded as scissor-like elements, was first introduced in 1961 into civil engineering by Spanish architect, Emilio Perez Pinero. As shown in Figure 2.24, a pantograph is composed of two bars, each of which has three nodes, one at each end, connected to other members by hinges and one at an intermediate point, connect to the intermediate point of another member by a pivotal connection. The pivotal connection allows two bars to rotate freely about the axis perpendicular to the plane of the pantograph.

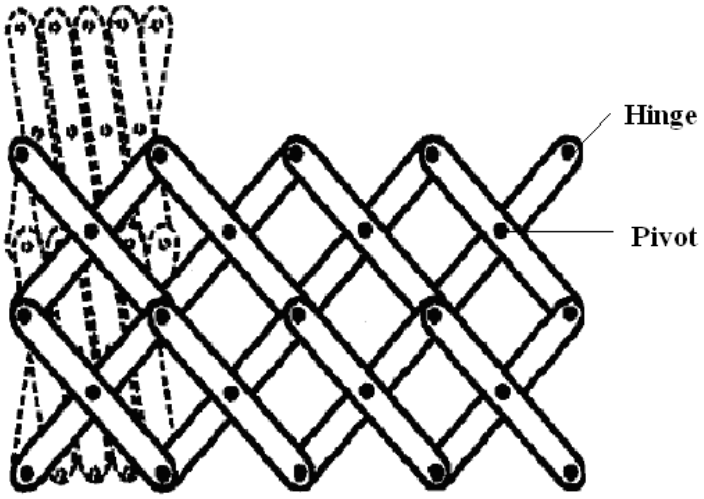

Figure 2.24: Basic pantograph elements (Hanaor and Levy, 2001).

The whole structure behaves as a mechanism because there is no stress during deployment process. The kinematic degrees of freedom of the mechanisms are removed by two types of releases at the ends of the rigid links- a hinge, releasing a

rotational degree of freedom and a pivot, releasing a translational one (Hanaor and Levy, 2001). Obviously, the pantograph system has only one degree of freedom. This system represents very good deployment control in the sense of that only one points needs to be controlled to determine the whole structure. The deployable tension strut structures (DTSS) studied by Vu *et al*. (2006) can be taken as an example to illustrate how to deploy structures using pantograph. When one module is deployed, the whole grid is unfolded to the final status because all of the scissors are connected to each other.

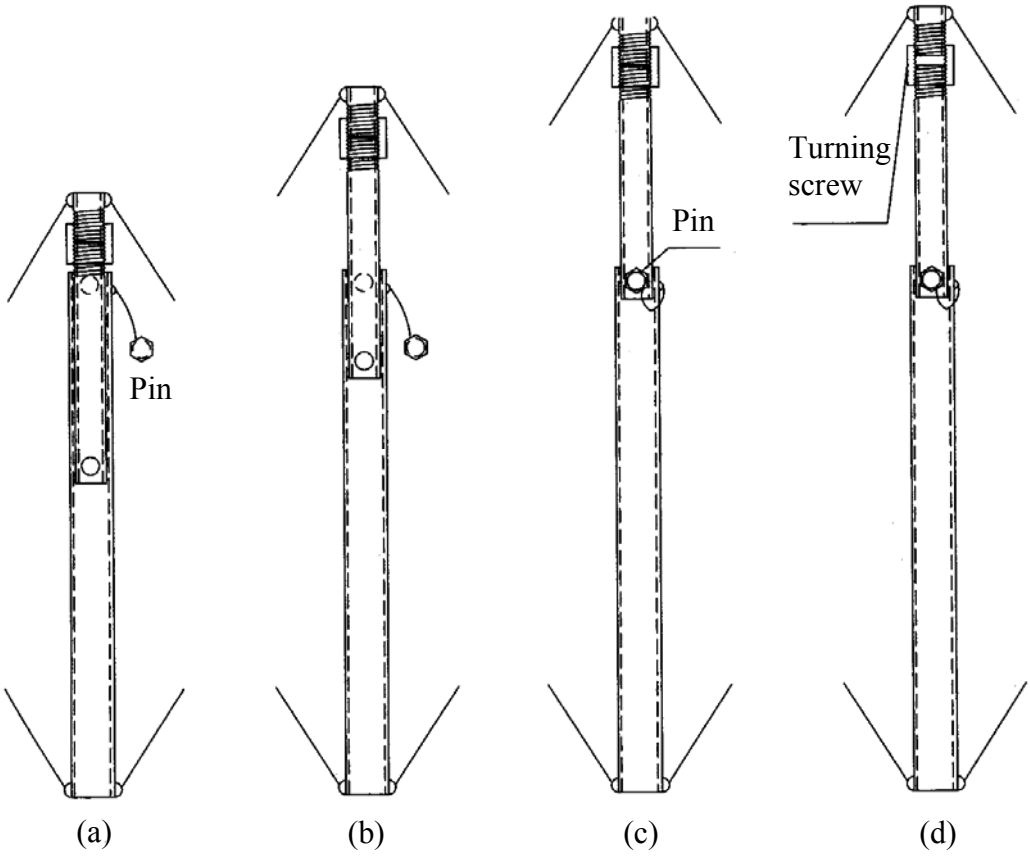

Figure 2.25: A telescopic strut locked by a pin: (a) stowed; (b) lifting; (c) locked; (d) fastened (Reproduced from (Wang, 2004)).

2.2.4.2 Telescopic struts

A telescopic strut can be lengthened or shortened manually or activated by fluid

pressure in the direction of the axis of strut. This method attempts to restrict axial translations of two struts in one direction and it is quite common in hydraulic jack, antenna of television, etc.

At stowed status, upper strut is inserted into the lower strut, which is longer than the former. Then the upper inner tube is lifted manually or other forces like liquid pressure to pre-determined position. After that pin is used to lock these two tube segments and screw is applied to fasten the whole structure as shown in (c) and (d). The umbrella simplex for deployable strut-tensioned membrane structures utilized this mechanism.

2.2.4.3 Energy-releasing devices

At folded status, the strain energy is stored in the members. When the energy is released, the structure can be deployed at the same time. Deployable truss-assembly structures may use this mechanism to unfold the structure for outer space applications where manpower control is not available. Herein, Folding Articulated Square Truss (FAST) developed by AEC-Able Engineering Company is taken as an example to illustrate this method.

The mast has revolute hinges along the vertical direction with axes parallel to the sides of the square bays and two pairs of diagonal bracing cables on each face of the bays (Miura and Tanizawa, 2000). Folded and transition parts and part of deployed mast are in the canister. For folded part, cables are slackened and the bow bends, where strain energy is stored inside. When it is deployed, bows become straight and strain of the cables increased gradually during this process. Hence, the strain energy stored in the bows facilitates the deployment and converted partly into the cables.

2.2.4.4 Tension element deployment

Tensioned members such as cables, rods, membranes, etc. can be released easily because of the material properties. In many cases, tension elements like cables are used to stabilize deployable structures by tension inside. When the cable is released, the structure can be changed into a mechanism and can be folded into compact configurations.

For this method, Wang (2004) summarized two ways: one is releasing individual cables and the other one is sliding cable. When a triangular Di-Pyramid is deployed by releasing cables, for instance, upper inclined cables are lengthened to allow the horizontal struts to rotate downwardly in the vertical plane. When upper inclined cables and bottom cables are continuous through the joints, sliding cable can be applied.

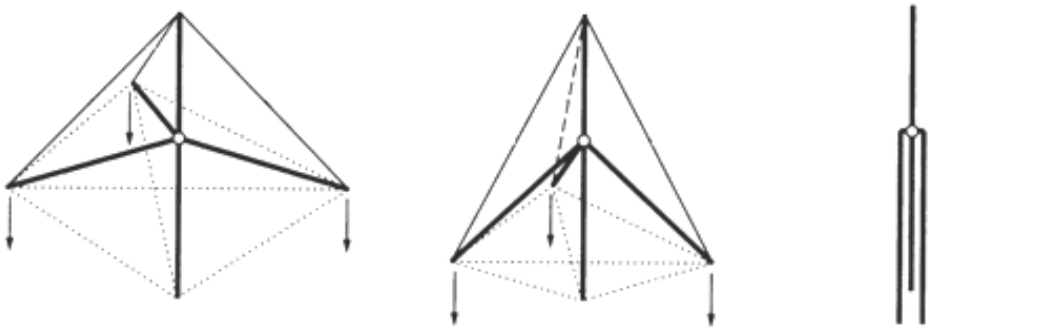

Figure 2.26: Folding a triangular Di-Pyramid by releasing cable method (Reproduced from (Wang, 2004)).

2.2.4.5 Hinge mechanism

Basically speaking, most deployable structures can be transformed (folded or unfolded) because they have more than one free degree of freedom. Most deployment

structures achieve these freedoms by combining several kinds of deployment method together. For example, when releasing cable method is discussed hinges releasing is not illustrated for the concentration of ideas. However, hinges releasing methods are the most popular among the deployable structures. Most deployable plate structures realize free rotation between two plates by introducing hinges. For example, deployable truss-assembly structures usually depend on the releasing the hinge mechanism at the joint or on a strut. Furthermore, deployable structures with movable struts always have hinges inside.

2.3 Nonlinear analysis of tensile restrained structures as curved beams with elastic restraints

2.3.1 Kinematic structural descriptions

An accurate and efficient nonlinear analysis has gained intense research interests for the past decades. Except for problems with simple geometries and load conditions, analytical or closed form solutions are usually not approachable. Notable contributions therefore have been made to develop finite element (FE) methods to address those problems among other methods such as boundary element and/or finite difference methods. Regarding the kinematic description in FE formulations with the ability to address large displacement problems, three main procedures are usually adopted including: (a) Total Lagrangian (TL) description, (b) Updated Lagrangian (UL) description, and (c) Corotational description.

In a TL description, the motions of the body are referred to the initial undeformed configuration. In an UL description, the motions of the body are referred to the most

recent known configuration or last configuration. Comparison of these two motion descriptions for the large displacement analysis of three-dimensional beams shows that the UL description is a computationally more efficient approach (Bathe and Bolourchi, 1979). Therefore UL description has been widely used for thin-walled structures under large displacement (Conci, 1992; Omidvar and Ghorbanpoor, 1996).

The corotational description is the most recent and the least utilized and developed among these kinematic description methods (Alsafadie *et al.*, 2011). In this description, a local co-ordinate system attached to each element translates and rotates with the element overall rigid body motion without deformation. Nodal variables are defined in the local co-ordinate system resulting in an element-independent formulation for local internal force vector as well the element tangent stiffness matrix. The geometric nonlinearity is considered during the transforming matrix from the local to the global co-ordinate system. In such a way, the rigid body motion is separated from the local strain producing deformation.

The term 'corotational' used to refer to the motion of the local system was introduced by Belytschko and Glaum (1979), followed by most researchers afterwards. However, the development of such concept can be traced to the early 1960s. Argyris (1964) introduced the similar concept termed as "natural approach" for calculation of the geometrical stiffness matrices of wings and flanges under membrane and bending stresses. Wempner (1969) applied this concept for analyzing the finite rotations of flexible shells. Argyris *et al*. (1979) summarized the initial advances of such concept and a series of applications. Oran (1973) and Oran and Kassimali (1976) recognized the importance of differentiating the local-global transformation matrix in obtaining a consistent tangent stiffness matrix and applied this method for frame structures under

static and dynamic load. Crisfield (1991) developed a corotational plane frame element including the additional axial strain caused by end rotations. However, numerical tests to validate the method were not reported therein.

Many existing high performance elements for geometrically linear problems can be implemented in the corotational approach to solve large displacement and rotation problems in recent works. Urthaler and Reddy (2005) implemented Euler-Bernoulli, Timoshenko, and simplified Reddy 2-dimensional elements into corotational beam approach. Felippa and Haugen (2005) developed a unified formulation of small strain corotational finite elements and summarized the benefit of such approach as well as the limitation. Chen *et al*. (2006) presented a consistent corotational total Lagrangian FE formulation for the geometric open cross section. Li (2007a; 2007b) proposed a beam element using vectorial rotational variables in both displacement field and mixed formulation using the Hellinger-Reissner functional and successful avoidance of shear locking. Alsafadie *et al*. (2010) proposed elasto-plastic local bema elements for the analysis of 3-dimensional thin-walled beams with generic open cross section with the capacity to capture both the Saint-Venant and warping torsional effects of open cross sections. Balling and Lyon (2011) extended the corotational element of Crisfield (1991) to include hinged and semi-rigid end conditions including plastic hinges.

2.3.2 Formulation of curved beam elements

Regarding the finite element formulation of a curved beam, those based on the curvilinear strain description for the static and dynamic analysis of curved structures are intensively developed (Friedman and Kosmatka, 1998; Prathap, 1985; Prathap and

Bhashyam, 1982; Wang and Chen, 2006). The initial modelling of curved structures by means of lower-order independent isoparametric beam formulations led to excessively stiff behaviour (shear locking) and these beam elements exhibited excessive bending stiffness (membrane locking) for modelling thin and deep arches.

Intensive studies have been conducted to overcome these shear and membrane locking phenomena. Among them, reduced integration methods, mixed and hybrid methods, and field-consistent redistribution approaches are the diffuse topics. The reduced integration methods removing the energy terms corresponding to the membrane energy were developed by Prathap and Bhashyan (1982) and Prathap (1985). However, arbitrarily chosen reduced integration may introduce zero energy modes, or violated the required membrane bending coupling (Stolarski and Belytschko, 1983). Prathap and Babu (1986) then developed a field-consistent redistribution method to overcome this drawback by predicting and removing the spurious constraint of the inconsistent strain field using a least-squares strain smoothing. Nevertheless, this method reduces the order of strain interpolation and suffers from lower convergence rate. In hybrid-mixed formulations, independent interpolation functions are used for different variables in different fields. It is possible to develop an effective element without the locking problems by carefully selecting appropriate parameters for assumed fields. Such approach has attracted many attentions from researchers such as Stolarski and Belytschko (1983), Saleeb and Chang (1987), Kim and Park (2006), among others.

The higher-order bending curvature components due to bending and the axial deformations of the bending deformation have been ignored in most conventional FE formulation of curved beam elements. Pi and Trahair (1998) developed a curved beam

element for nonlinear analysis of arches by considering the higher-order curvature components. Pi *et al*. (2007) extended the work of Pi and Trahair (1998) by including the material nonlinearity and elastic restraints. Both of these works are only for in-plane arches. A nonconventional structural approach was presented by Yau and Yang (2008) to simulate a plane curved beam with two straight-beam elements by utilizing the rigid body concept.

2.3.3 Analysis of curved beams with elastic restraints

Since the early works by Hetenyi (1946), who developed the differential equation approach, a number of studies on the analysis of beams resting on elastic foundation have been conducted. The static and dynamic behaviour of circular beams resting on the classical Winkler and Zimmerman hypotheses have been investigated in great depth by Volterra (1952; 1953). The vibration of elastic arches under static load has been studied by Wasserman (1977; 1978), and Plaut and Johnson (1981) with the consideration of the effects of different boundary conditions, initial thrusts, and elastic foundation. The stiffness matrix of a finite beam element on elastic foundation were derived including the shear and axial effects by Mourelatos and Parsons (1987). Different types of foundation such as Winkler foundation, Pasternak elastic foundation, Filonenko-Borodich foundation are discussed therein. The method is based on small displacement and small strain only. To model the practical problems such as multi-span bridges, horizontally curved beam element with elastic foundation has been studied by Dasgupta and Sengupta (1988) and Banan *et al*. (1989). A mixed finite element formulation for circular beams on the Winkler foundation has been developed by Akoz and Kadioglu (1996). More complex foundation such as uncertain

elastic foundation and unilateral contacts supported structural elements were studied by Chakraborty and Sarkar (2000) and Silveira *et al*. (Silveira *et al.*, 2008). In such situations, advanced nonlinear solution techniques are normally required, i.e. Ritz type approach adopted in the latter.

2.4 Summaries

As can be seen from the review of lightweight structures, arch has been tested by time to be an effective option for lightweight compressive elements. Tensile elements such as cables and membrane can be used not only as secondary structural elements but also the primary structural elements. With the fast development of materials for cables and membrane, the high potential of combining the advantages of these two types of structural components can be foreseen. Well designed arches restrained by tensile elements have shown good structural efficiency. However, most such structures are restricted in applications of roofs. Spindle-shaped Tensairity structures developed with different initials share the similar concept of tensile restrained arches have shown advantages as temporary of semi-permanent structures compared to truss structures with similar shapes. Nevertheless, the connections between the strut and the membrane hull are proven to be ineffective. It can be concluded that there are still rooms for innovations and improvements in this topic to fulfil the potential of tensile restrained arches.

Deployable structures can easily meet the requirement of temporary or mobile structures because of the inherent benefit such as the deployability, compact packaged volume, and easy storage and transportation. The reviewed existing deployable structures have shown such advantages. Expanding the concept of tensile restrained

arches for larger span applications and including added features of deployability is another task of this work.

Considering the structural analysis of arches resting on elastic foundation, there is still lack of a simple and straightforward approach for formulating curved beams on foundation models suitable for the tensile element used (membrane). This inspires the author to develop accurate and efficient numerical model for the structures presented in this work.

Chapter 3

Tensile Restrained Structures

3.1 Introduction

This chapter provides a detailed description of the concept development of two novel concepts on Tensile restrained structures, while the structural behaviour studies are to be presented in Chapters 5. In this current chapter, the background and motivation behind each structural concept are briefly discussed in the first place. In the second place, different structural forms sharing the same concept are illustrated along with some examples. These are followed by some discussions on other relative key issues like: connections, geometric relationship, and transforming patterns.

3.2 Tension Strip Structures – tensile restrained structures as compressive members

3.2.1 Concept proposal

This section presents the concept of a new structural form that utilizes tensile restrained structures as compressive members. This kind of structure is termed as Tension Strip Structures (TSSs).

For a slender column with boundary conditions shown in Figure 3.1, it buckles like a bow after a critical axial load as illustrated in the middle of this figure. Buckling is a sudden failure mode for a slender column subject to high compressive stress, where the applied compressive stress is much lower than the ultimate compressive stress of the material. This leads to a waste of material or lower structural efficiency. Lateral buckling restrained braces that are composed of struts and/or cables along the column are common solutions in practice. Another option is proposed herein, in which continuous tensile restrained braces are adopted.

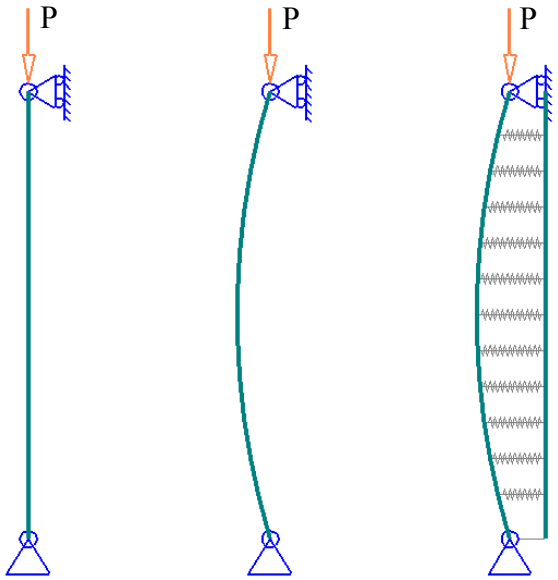

Figure 3.1: Buckled columns under compression.

The buckling resistance of the slender column is improved if “pull back” forces are provided by springs attached along the column as shown on the right side of Figure 3.1. If the whole scheme shown in Figure 3.1 is rotated by 90 degree in clockwise, this is similar the case where an arch bridge is loaded by massive self weight along its length. The bending moment inside the column struts can be regarded as minimum if the springs are continuous and the “pull back” forces are uniformly distributed along the curved strut. This phenomenon can be briefly explained by a simple example

given in next paragraphs.

A large number of arch stone bridges had been built in ancient China and many dome shaped churches had been built in ancient Europe because it has been well known that arches and domes are good at resisting compressive forces with limited materials since long time ago. The secret beneath is that both forms minimize the internal bending, which is critical to most structures. This could be illustrated as shown in Figure 3.2, where the arch is taken as an instance. For one beam with simply supported boundary conditions and under uniform load q, the bending moment at the middle section is:

$$M_{beam} = qs^2 / 8 \tag{3.1}$$

In the arch with the same span *s* as shown on the left, the bending moment at the middle section is reduced into:

$$M_{arch} = qs^2 / 8 - r_x h = 0 \tag{3.2}$$

One method to search for proper shapes of arches or domes is simulating hanging models. In funicular structures, e.g. cables or chains under the gravity loadings, no bending exists inside and thus the material could be optimally utilized. The optimal shape of arch under the same loading conditions could be obtained if the funicular is inversed.

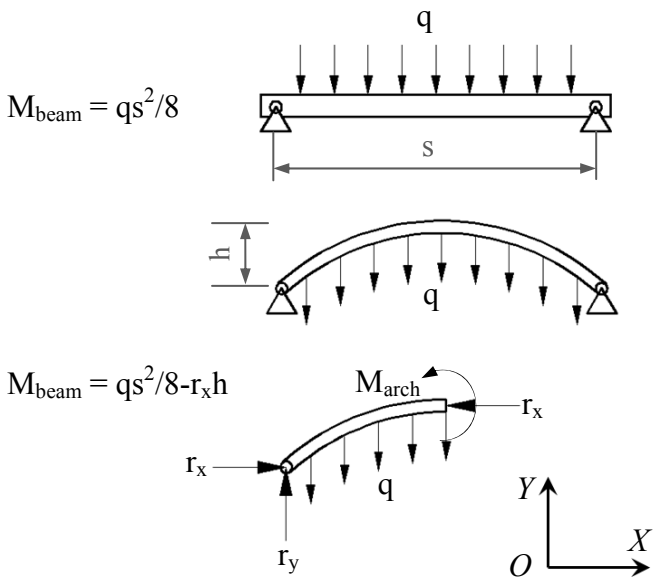

Figure 3.2: Funicular and arch models under uniform loadings.

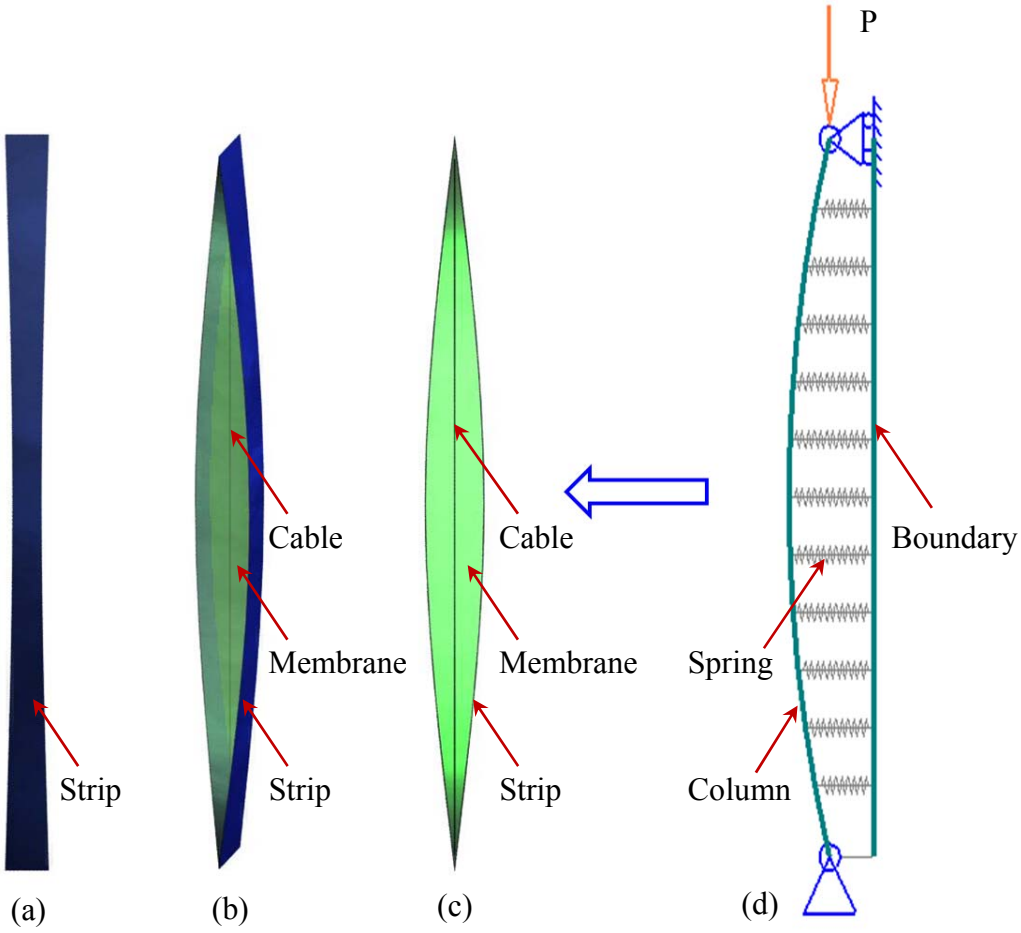

Figure 3.3: Tension Strip Structure: (a) left view; (b) trimetric view; (c) front view; derived from (d) a spring restrained pre-curved column model.

An explicit hybrid structure is proposed as shown in Figure 3.3, consisting of struts or strips as compressive members as well as membrane and cable as tensile members. This Tension Strip Structure (TSS) can be regarded as an assembly of two curved strut restrained by two pieces of membrane. The cable inside is adopted to resist tension forces. To make this structure self-standing, pretension in the membrane should be introduced into the membrane at the initial stage by prestressing the cable inside. It is explicit that the Tension Strip Structure is derived from the concept described previously of a pre-curved column restrained by springs along the height of the column as shown in Figure 3.3.

3.2.2 Morphology evolution

Some different forms with the same concept beneath could be derived from the basic Tension Strip Structure as shown in Figure 3.4(a). Wrinkles will be produced on the membrane when the structure is under axial load even though pre-tension is applied in the membrane in vertical direction. To handle this problem, design with discontinuous membrane as shown in Figure 3.4(b) could be adopted to reduce these wrinkles without affecting the structural load bearing capacity. As can be seen from Figure 3.4(c), tubes with relatively small section could be used instead of strips as compressive members, which provide more flexible forms, e.g. 4 tubes restrained by 4 pieces of membrane.

For each compressive element (tube in this case), the out of plane stability is enhanced by two adjacent membranes while for structures shown in Figure 3.4(a) and Figure 3.4(b), the lateral stability is provided by the width of the strip. Besides, Tension Strip Structures with different number of struts can be employed: e.g. 3

struts, 4 struts, 5 struts, etc. More complex joint designs are normally required for Tension Strip Structures with more struts.

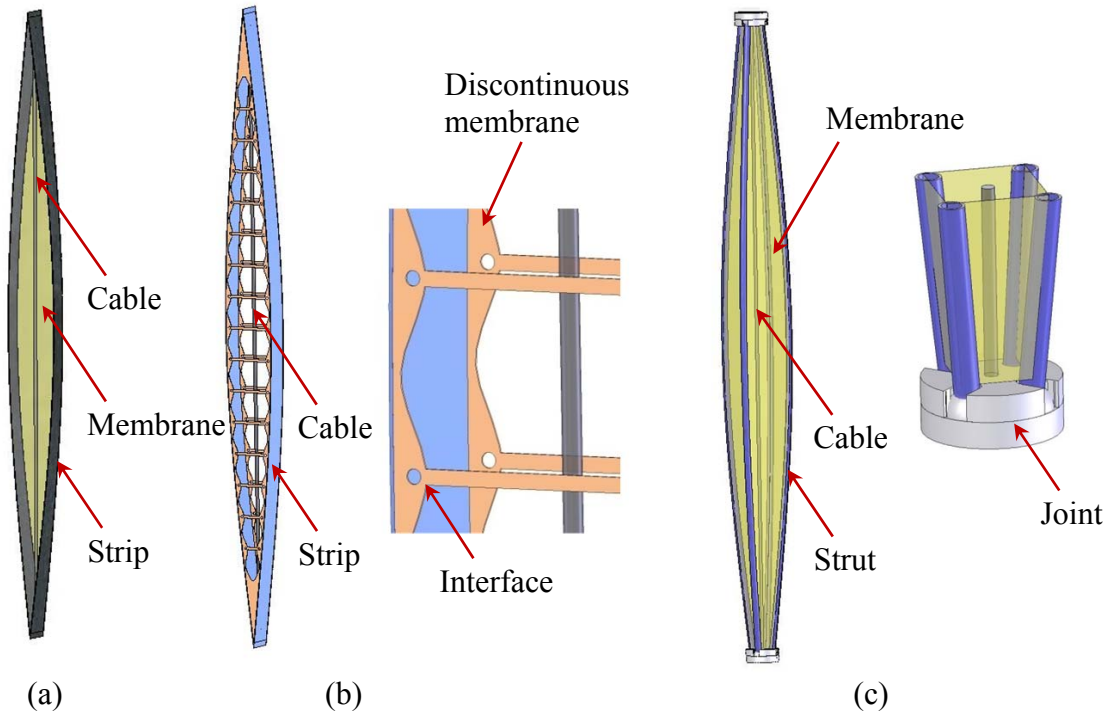

Figure 3.4: Structural forms of Tension Strip Structures with: (a) two strips; (b) two strips and discontinuous membrane; (c) four struts.

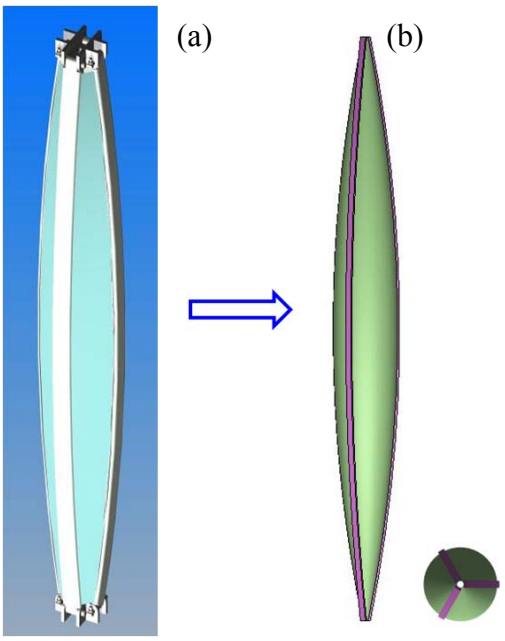

Figure 3.5: From (a) Tension Strip Structure to (b) air-supported Tension Strip Column.

Besides, another form combines the basic Tension Strip Structure with the air-beam concept: high pressure air is pumped into a membrane hull slotted inside the column as shown in Figure 3.5. Internal air with high pressure could be adopted to enhance the structure by preventing early local buckling of struts. The air-supported Tension Strip Structure has a circular shape cross section as can be seen in plan view. In this structure, the high pressure air inside rather than the membrane stabilizes the structure, which is different from previous Tension Strip Structures.

Internal cable is not required in air-supported Tension Strip Structure because the high pressure air inside and the membrane hull together can resist some level of tension forces on the tips. This idea is exactly the same with Tensairity columns (Plagianakos et al., 2009), although which is developed from a totally different derivation of concept termed as Tensairity beams (Luchsinger et al., 2004).

3.2.3 Connections between membrane and strut

For structures involving membrane, connections between key elements of such structures such as surface tensile structural elements and supporting elements are important issues. There are two practical ways in literatures to connect the strip or strut with the membrane for tensile structures (Burford and Smith, 1999; Wever *et al.*, 2010). In the first design, the strut is inserted into a pocket sewed on the membrane hull as shown in Figure 3.6. In this connection, arbitrary strut cross section shapes can be used and the connection design is simple. However, the connection between the pocket and the membrane is not strong enough due to the stress concentration effect at the sewed area between the pocket and the membrane hull especially when the system experiences high restraining forces. This drawback is indicated in the paper by Wever

et al. (2010), where the membrane web cannot be utilized due to the ineffective connection using the pockets.

In the second design as shown in Figure 3.7, struts with special profiles are used. Keders or cables wrapped in the membrane are embedded into two holes on the strut so that the membrane will be tightly connected to the strut. The membrane is independent for each section in this connection design, which makes the system more flexible and modularized. This design benefits from reliable connection between the membrane and the strut/strip using a Keder or a rope and reduced on-site erect and strike times. The main disadvantage of the connection is that the proprietary component is quite expensive especially for long struts.

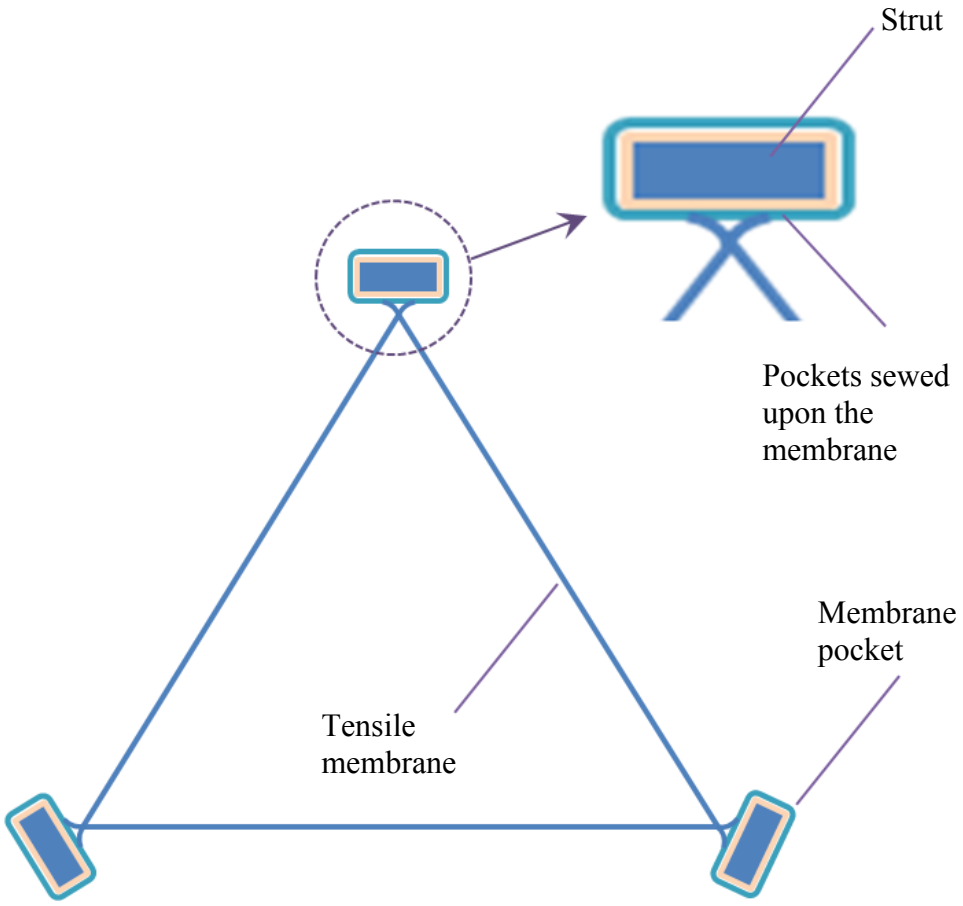

Figure 3.6: Connection with pockets.

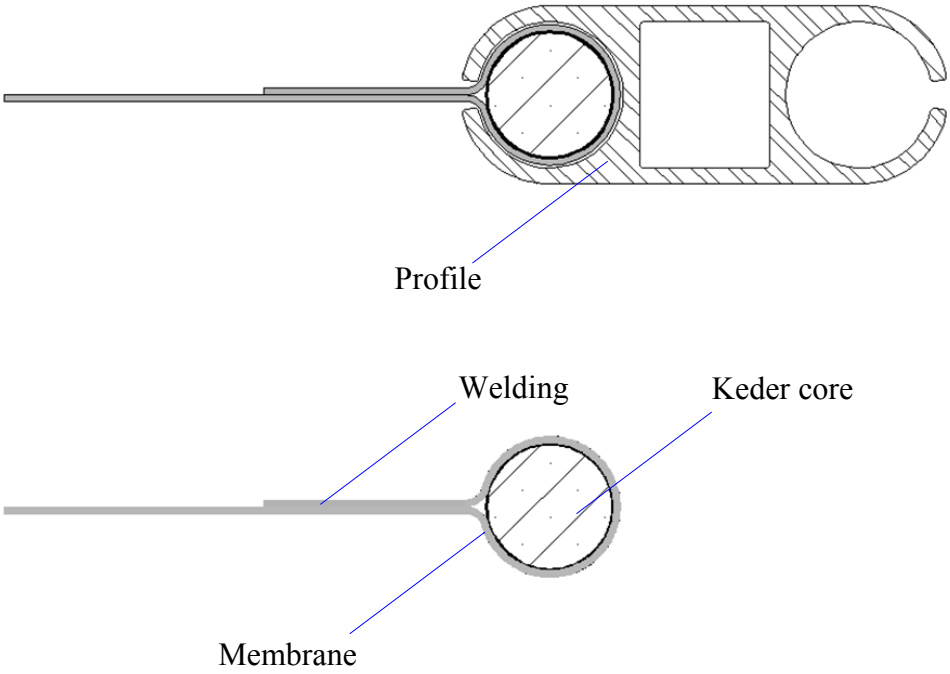

Figure 3.7: Connection with special cross section profile.

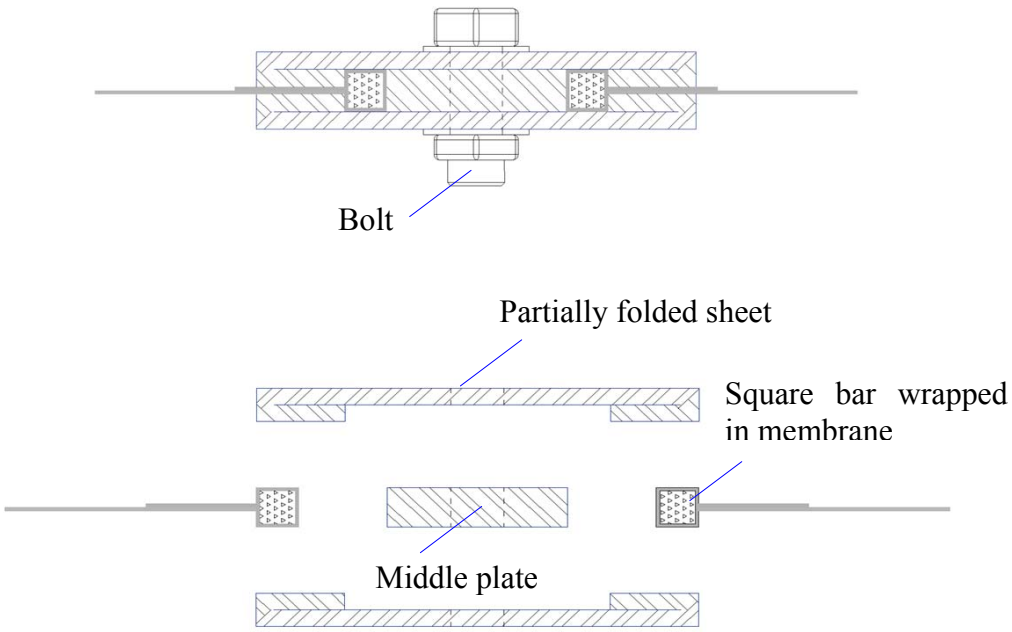

Figure 3.8: Connections using partially folded sheet.

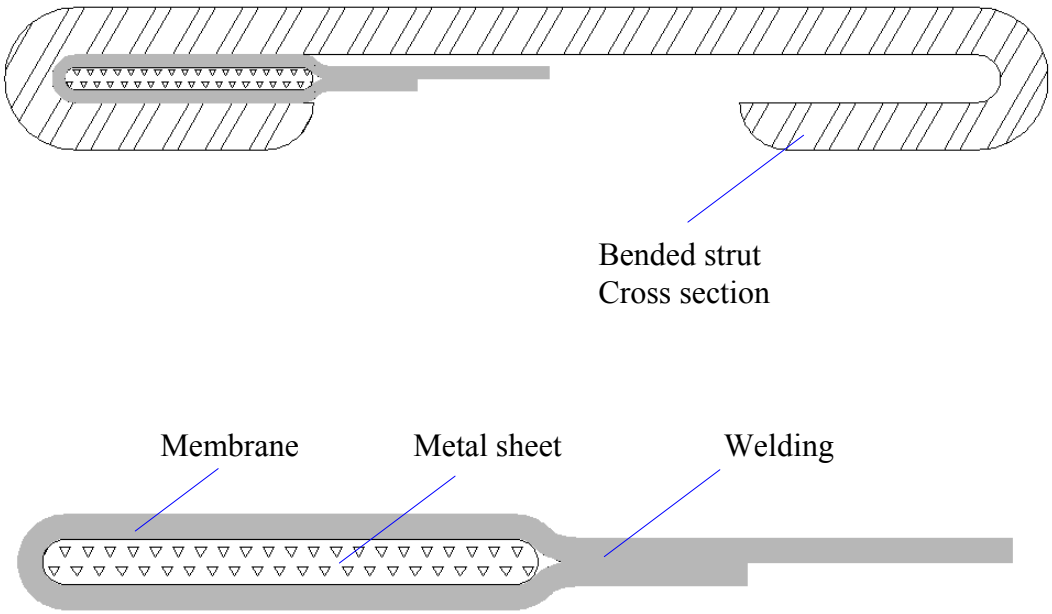

Figure 3.9: Connections using bended struts (not proportional).

This section presents two new systems with the intention to offer reliable connections between the strut and membrane. In the first proposed connection as shown in Figure 3.8, all components such as folded sheets, square section plates, square bars, bolts, etc. are available from market with relatively low cost. Different components are independent from each other, which makes the structure potentially modularized. With similar usage of cable/square bar wrapped in membrane, the connection of this design is as reliable as that of previous one.

In the second proposed connection as shown in Figure 3.9, metal sheets are utilized because of the low cost and easy fabrication. The slender flat sheet is bended at the two sides and a strut with a narrow "C" shaped cross section is formed. Small sized metal sheet wrapped in membrane as shown at the below part of Figure 3.9 is positioned between the two layers of the strut. These constitute an open connection between the membrane and the strut, in which only outward load can be applied to the membrane. The second connection is also a modularized design while maintains tight

bond between the strut and the membrane. Compared to the first proposed connection, the second one benefits from continuous integral strut where no bolt holes are used.

3.2.4 Fabrication issues

The fabrication of a structure requires a wide-ranging consideration of material, procedures and execution at both component and assembly levels. Tension Strip Structures involve membrane, struts, joints, and cables. The connections among these components need flexible designs to meet the requirements of easy assembly, dismantlement and the ability to be replaced after failure. The connection between struts and membrane has been discussed in Section 3.1.3 in details. For connection between joints and struts, pins are used. Clips are equipped for those pins to prevent possible slip. Cables including swaged sockets with threads are adopted to tighten the Tension Strip Column with nuts locating at the ends of the cable.

Struts initially in straight shape are bent by rolling machine to the desired arch geometry with certain curvature, which results in residual stress with the highest value in the outer most fibres of the section. It is essential minimize the stresses produced by the pre-bending in order to keep enough residual capacity in the member to resist the additional stresses from the applied load. It is practical that the residual stress caused by the pre-bending should not exceed 50% of the total yield stress of the material used. Regarding this, three parameters need consideration including the curvature of the desired geometry, the section depth, and the modulus of the material. With limited material available (aluminium, steel, composite, etc) and section depths, the minimum radius of the curvature can be obtained explicitly.

Commonly used structural tensile membrane includes three types: PVC coated, PTFE

coated and ETFE coated membrane. Polyester Reinforced PVC Architectural Membranes are the most cost effective and the most prevalent in Tensile Architecture. These fabrics, which are typically coated with PVDF lacquer on both surfaces to improve the life of the membrane and also provide for effective cleaning of both surfaces, have a lifespan exceeding 20 years. Woven fibreglass coated with polytetrafluoroethylene (PTFE) is the most durable Architectural Membrane available today. PTFE is essentially inert to environmental contaminants, ultra-violet light, has fire resistant properties and a proven lifespan exceeding 30 years. Ethylenetetrafluoroethylene (ETFE) is an extremely lightweight, transparent film with similar light transmission to glass while only 1% of the weight. ETFE has been used on many high profile sports centres and stadiums. ETFE has excellent weathering properties and a lifespan exceeding 20 years. For Tension Strip Structures, membrane shapes a double curvature configuration in the desired load-carrying status. To obtain this 3-D configuration from 2-D material, form-finding analysis and cutting pattern analysis should be performed. The membrane is cut into small pieces and attached together according to the analysis results. Laser cutting machine with high precision and suitable welding machine are used to fabricate the membrane component.

Once all components are fabricated, the Tension Strip Structure can be assembled together as follows. In the first step, the struts are connected to the membrane with the method discussed in Section 3.1.3. In this procedure, the membrane needs to be aligned to each other at both tips. It should be ensured that all membrane pieces should remain intact. In the second step, the struts are connected to the joints by pins that are well secured later by clips. In this step, the cable should be positioned in the hull enclosed by the membrane and strut pieces with a tip attached to a joint. In the third step, the Tension Strip Structure is compressed and the membrane is in

pretension to shape a desired configuration. The cable is fastened to another joint with a nut to stabilize the whole structure.

3.2.5 Potential applications

The proposed Tension Strip Structures are deemed as better options than existing slender hollow section tubes widely used now due to their potential benefits including lightweight, flexibility, rapid installation, etc. As shown in Figure 3.10, potential applications include poles in tents, members in various truss systems for both civil and aerospace industries.

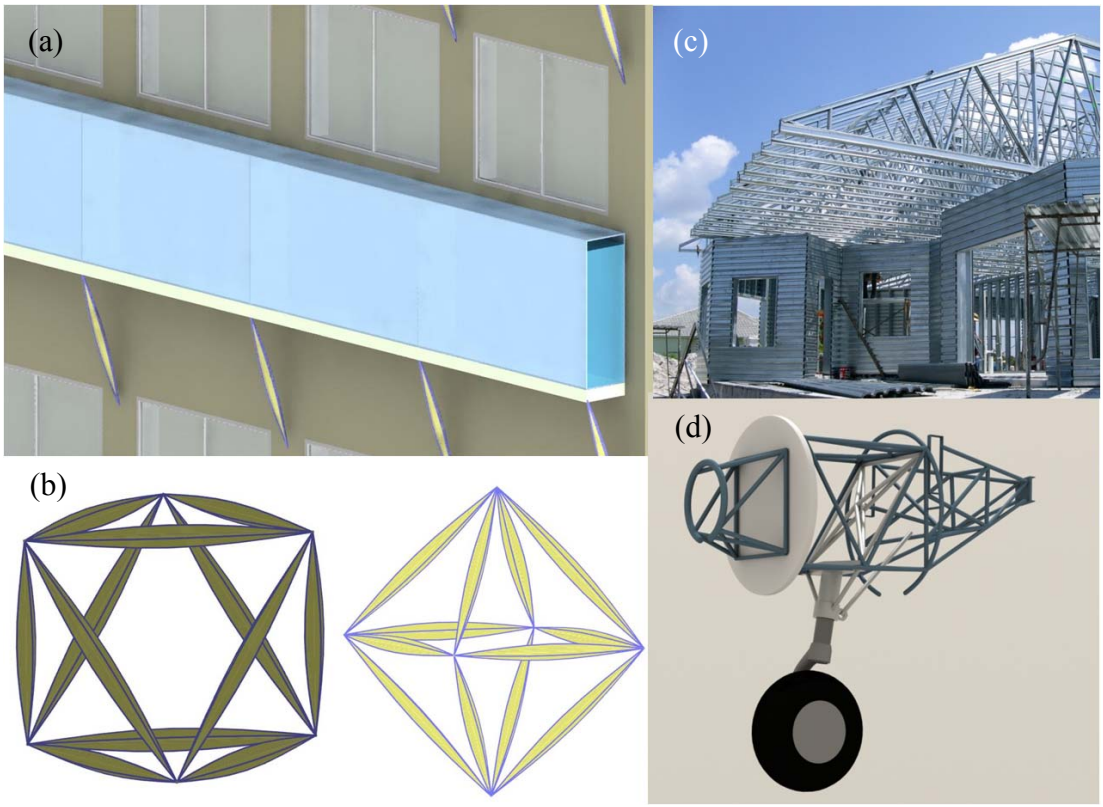

Figure 3.10: Potential applications of TSS: (a) a column supporting façade system; (b) truss systems; (c) truss in a building; (d) truss in a part of airplane.

Similarly to the cable stayed column, Tension Strip Structure tends to minimize the compression field and maximize the tension field for a compressive member,

potentially provide higher structural efficiency with the essentially minimum use of materials. In the concept level, Tension Strip Structure inherits higher structural efficiency compared to the conventional truss system because of a capacity to reduce the member weight with slender curved struts used. In cable stayed columns, the critical load is increased by reducing the effective length of the column and mitigating the global buckling. In Tension Strip Structure, the slender struts are well restrained along the whole length and hence minimizing the effective length. This shows that proposed Tension Strip Structure has a good chance to render a potentially more efficient compressive structure than truss systems and cable stayed columns.

3.3 Deployable Cable Chain Structures – tensile restrained structures with deployability

Cable strut structures proposed by Wang (1998) and Liew *et al.* (2003) have shown excellent structural efficiency in resisting gravity loads compared with the conventional space frame structures. Deployable structures have been continuously exploited and developed by researchers due to their ability to be folded for compact storage, easy transportation, rapid site-erection and dismantling (Gantes, 2001; Liew and Krishnapillai, 2009). Deployable Tension-strut Structures (DTSS) was first proposed by Vu *et al*. (2006) with the intention to combine the advantages of rapid deployment and high strength low weight characteristic of cable strut structures. However, these structures are formed by double layers of struts, which post some problems during the folding and opening procedure.

3.3.1 Concept proposal

While Tension Strip Structures can be regarded as assemblies of tensile restrained arches for compressive members, some vault shape shelters are composed by arch frames restrained by tensile membrane as shown in Figure 3.11. To make these kinds of shelters foldable in both longitudinal and transverse directions, the arch struts should be separated into several shorter straight struts connected end to end. The split arch struts as shown in Figure 3.12(b) are termed as the strut chain structure.

Figure 3.11: Shelter supported by tensile restrained arches (Courtesy of NK Burford, and C Gengnagel).

The strut chain structure is similar to scissor-like elements (SLE) as shown in Figure 3.12(a), which are the basic components of one kind of most popular deployable systems called pantographic structures. A common shortage of pantographic structures is that the axes of the struts that compose SLE connected by pivots are not lying in the same plane. This leads to secondary moment (or torsion) which needs to be considered in the design of the struts. The strut chain structures connected by hinge joints do not have this problem while they can still be foldable.

A module of SLE consists of two continuous struts (bars) and a pivot at the centre of

the strut; while a module of strut chain element consists of two struts connecting to each other by a hinge joint. In SLE, the two basic modules are connected together by two hinges, however, for strut chain structure, only a hinge is needed. This section proposes a novel Deployable Cable Chain Structure (DCCS) consisting of a single layer of cable strut system to achieve minimum weight and with sufficient strength and stiffness for small to medium span applications. The concept, geometric design, morphology study and deployment patterns of DCCS are discussed in following sections and their nonlinear load-displacement behaviour are investigated in other chapter.

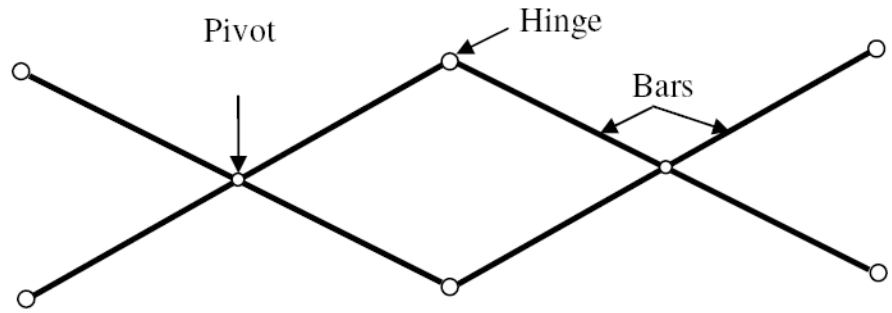

(a) Connection of SLE

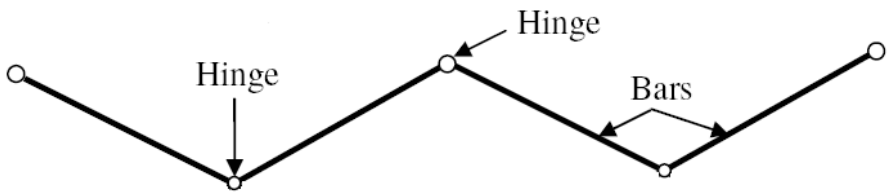

(b) Connection of Strut Chain

Figure 3.12: Connections in SLE and strut chain.

As mentioned above, strut chains could be applied as deployment mechanisms and in this proposed structure, cables rather than membranes are adopted to restrain the movement of struts and provide stability for the whole structure. Figure 3.13(a) shows a simply supported beam resisting an applied point load causing flexural bending in

the beam. If a strut chain is used to resist the same load, an additional bottom tension member is required to ensure equilibrium and stability as shown in Figure 3.13(b).

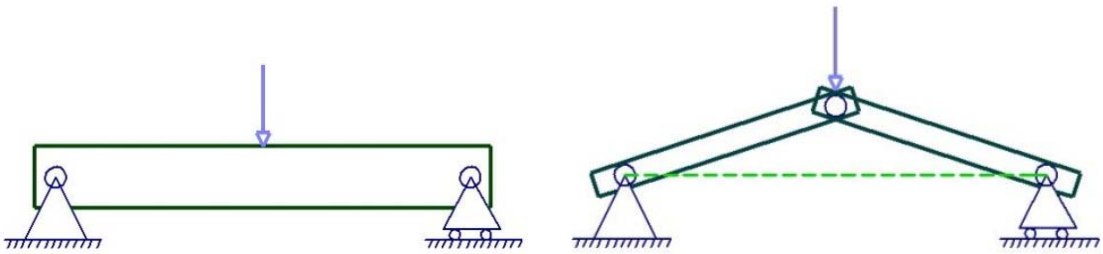

(a) Simply supported beam (b) Simplest cable chain

Figure 3.13: Beam and simplest cable chain under centre point load.

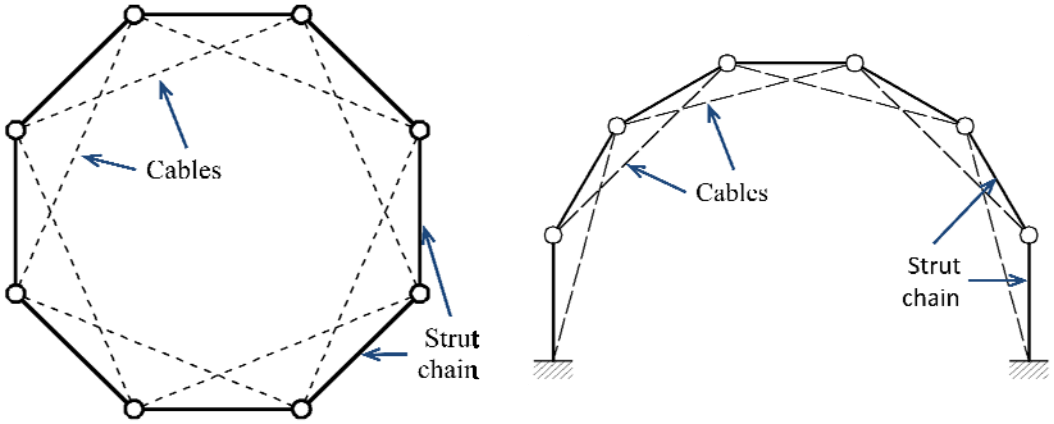

(a) Simple cable chain structure (b) Frame structure

Figure 3.14: Two-dimensional cable chain structures.

The simplest cable chain structure (CCS) as shown in Figure 3.13(b) consists of a strut chain element and a tensioned cable. The separation of tension and compression elements is similar to that of DTSS, which has been proven to have high structural efficiency (Vu *et al.*, 2006).

A two-dimensional cable chain structure may be formed as shown in Figure 3.14(a) with strut chains forming the outside ring that is stabilized by the cables inside. The adoption of strut chain facilitates deployment speed, while the cable helps to stabilize

the strut chains outside. The cable chain structure shown in Figure 3.13(b) is not stable because the cable will be slackened once a lifting force is applied at the centre node. Therefore an additional cable should be connected to the centre node to pull the centre node down to achieve overall stability. In the structure shown in Figure 3.14(a), every node maintains its equilibrium status due to adjoining four members: two cables and two struts. Part of CCS could be used to build the frame of a shelter in two-dimension as shown in the Figure 3.14(b).

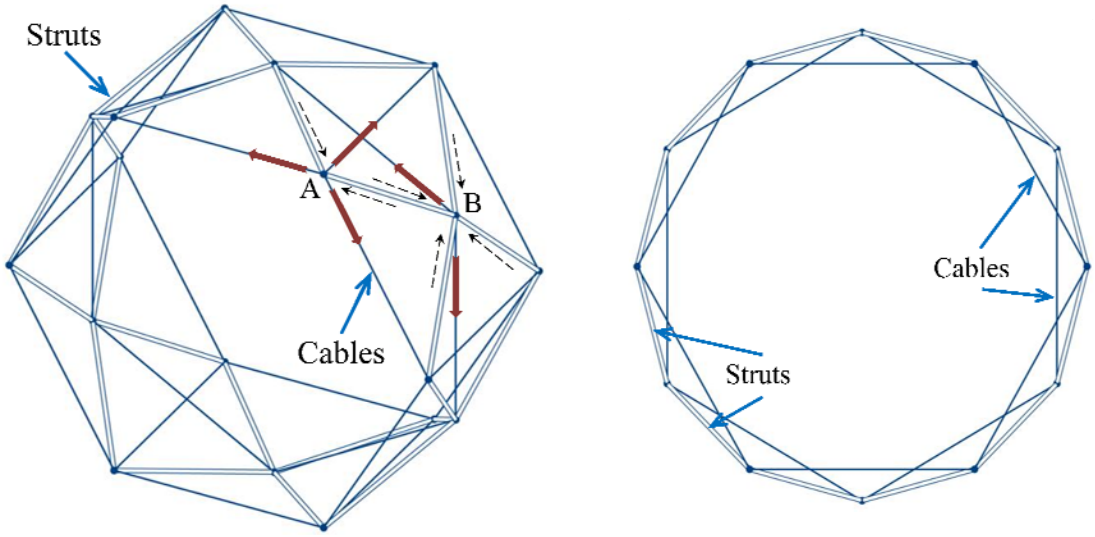

(a) Trimetric view and internal forces at joints A and B (b) Front view

Figure 3.15: Three-dimensional cable chain structures.

A three-dimensional cable chain structure could be obtained by substituting the outside hinged struts in Figure 3.14(a) into 4-strut grids as shown in Figure 3.15(a). Instead of a set of cables inside the two-dimensional cable chain structure, the three dimensional structure consists of two sets of cables: one set connecting the apex of pyramids shaped by the struts and the other set connecting the 4 separated nodes in the rectangular base. Front view of this structure shown in Figure 3.15(b) indicates that the same principle has been adopted for both two- and three-dimensional cable chain structures. Each node reaches the equilibrium status under the compression

forces of the struts and the tension forces of the cables, which are connected to a single node. Two typical nodes “A” and “B” are illustrated in Figure 3.15(a), where the thin and dash arrows along the strut mean the directions of compression forces and the thick and solid arrows along the cable indicate the directions of tension forces.

3.3.2 Morphology variation

Figure 3.16 illustrates a boom, a barrel vault and a dome composed of cable chain structures with/without the covering membranes. By connecting basic modules of cable chain structure end to end, a boom structure could be shaped as shown in Figure 3.16(a), which is the same as a deployable boom developed by Vu *et al*. (2007).

Further, a barrel vault and dome shaped shelter may be obtained by connecting half of the module of CCS as shown in Figure 3.16(b and c). However, it should be noted that ground anchors (dash lines in Figure 3.16(b)) are required at the two ends to increase the stiffness of the barrel vault in the longitudinal direction.

Various kinds of dome structure can be formed by using different basic modules. For instance, a dome composed of basic modules consisting of 3 struts and 3 cables may be shaped as shown in Figure 3.17. In addition, Figure 3.18 shows a dome structure consisting of 12 pyramids with 5 struts and 5 cables and Figure 3.19 illustrates a geodesic dome structure or Bucky ball consisting of 20 pyramids with 6 struts and 6 cables and 12 pyramids with 5 struts and 5 cables.

Further, a barrel vault and dome shaped shelter may be obtained by connecting half of the module of CCS as shown in Figure 3.16(b and c). However, it should be noted that ground anchors (dash lines in Figure 3.16(b)) are required at the two ends to

increase the stiffness of the barrel vault in the longitudinal direction.

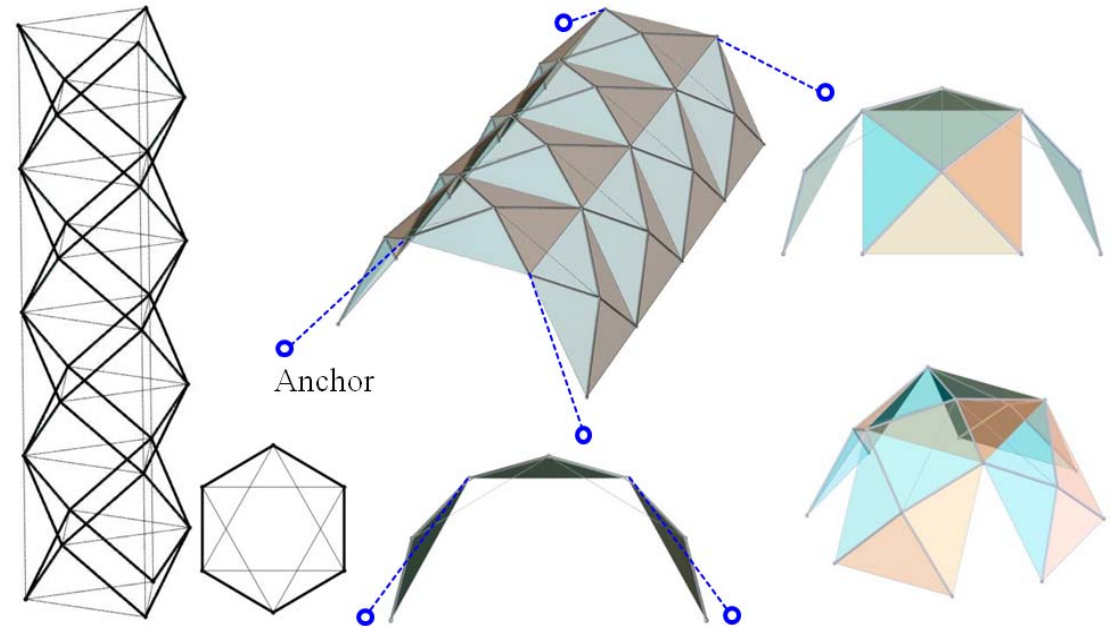

(a) Boom (b) Barrel vault with anchors (c) Dome

Figure 3.16: Boom, dome and barrel vault composed of CCSs.

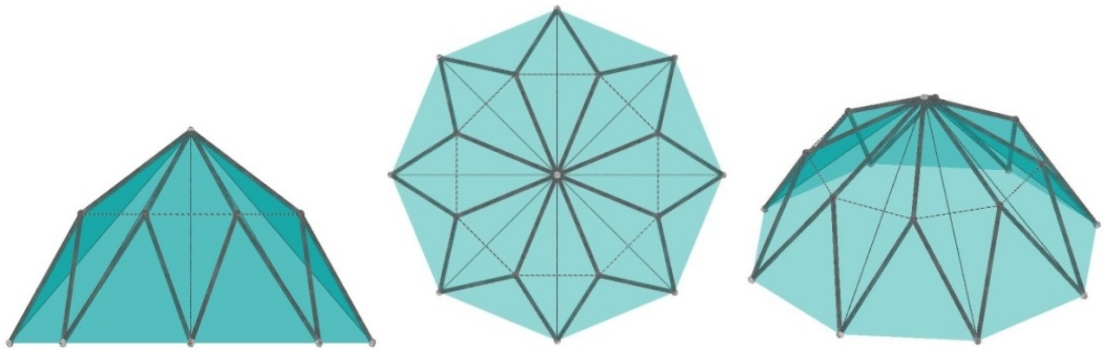

(a) Front view (b) Plan view (c) Isometric view

Figure 3.17: A dome composed of 3-strut CCSs.

Various kinds of dome structure can be formed by using different basic modules. For instance, a dome composed of basic modules consisting of 3 struts and 3 cables may be shaped as shown in Figure 3.17. In addition, Figure 3.18 shows a dome structure consisting of 12 pyramids with 5 struts and 5 cables and Figure 3.19 illustrates a geodesic dome structure or Bucky ball consisting of 20 pyramids with 6 struts and 6

cables and 12 pyramids with 5 struts and 5 cables.

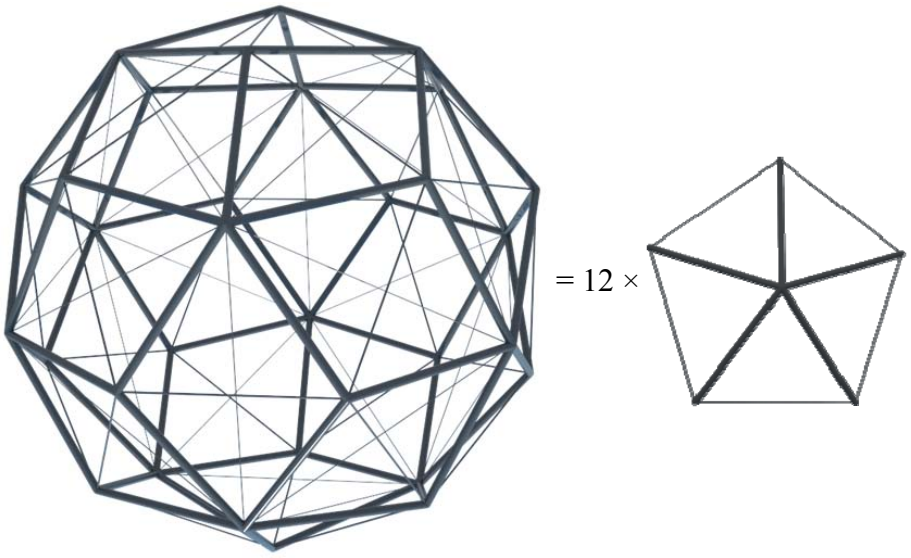

Figure 3.18: Geodesic dome composed of 5-strut CCSs.

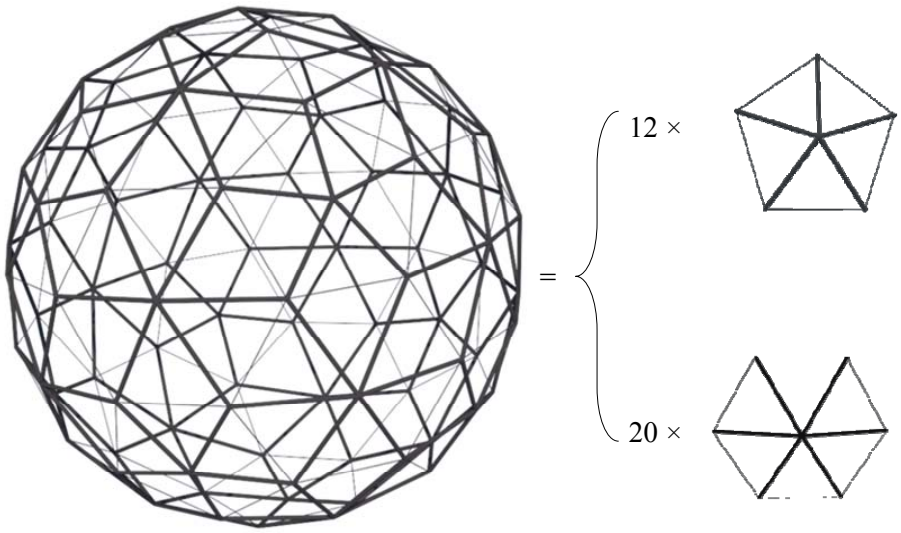

Figure 3.19: Geodesic dome composed of 5-strut CCS and 6-strut CCS modules.

Furthermore, new structural forms could be obtained by combining these different basic forms together. An example is shown in Figure 3.20, where a barrel vault consisting of 4-strut pyramid is connected to two halves of the dome structure shown in Figure 3.17. This new structure is in self-equilibrium in the longitude direction and does not require any anchor at the ends.

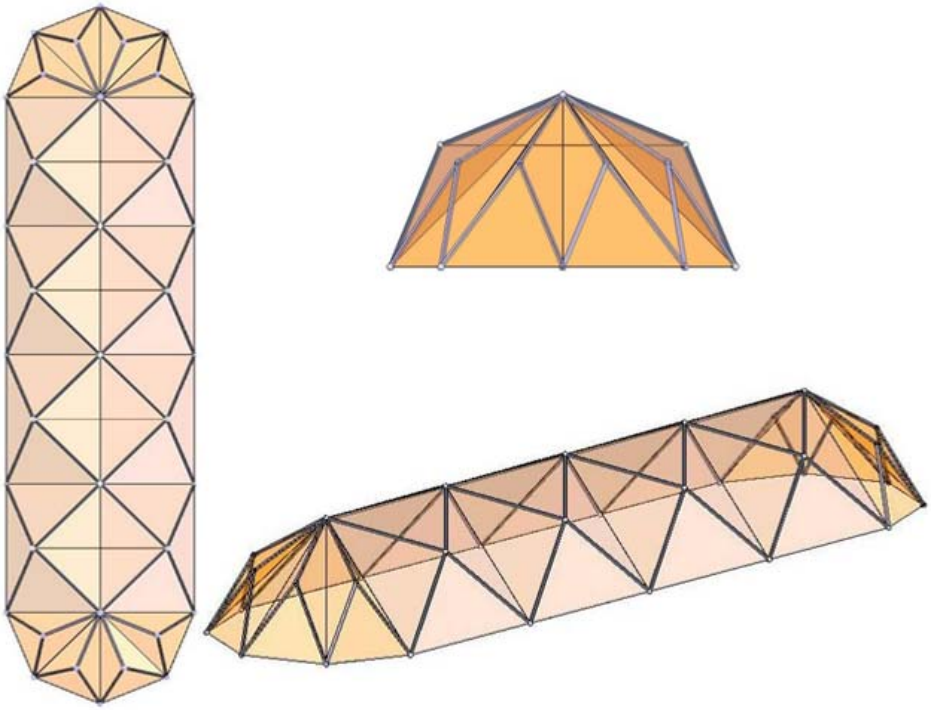

Figure 3.20: Combination of come and barrel vault.

To sum up, it has been shown from the previous discussion that different structural forms can be generated from the basic CCS modules by repetition.

3.3.3 Transforming patterns

For small and medium span applications, variety of mobile shelters has been proposed, like foldable panel structures (FPS) and foldable bar structures (FBS) (De Temmerman *et al.*, 2007; Trometer and Krupna, 2006). The transforming/deployment pattern of these shelters follows the same principle of Origami model or foldable tree leaves model (Guest and Pellegrino, 1994a; Guest and Pellegrino, 1994b; Guest and Pellegrino, 1996; Hachem *et al.*, 2005; Nojima, 2002). The basic module consists of several triangular plates connected to each other by hinges along their edges and could be folded into parallel plate series and/or unfolded into desired three-dimensional configuration with zigzag surfaces. The transforming/deployment pattern is very efficient and intuitionistic.

An illustration of the deployment of DCCS into a barrel vault is shown in Figure 3.21. Different from FPS or FBS, there are two transforming patterns: one is in longitudinal direction only and another one is in both longitudinal and transverse directions as shown in Figure 3.21, where membranes and cables are ignored for clarity.

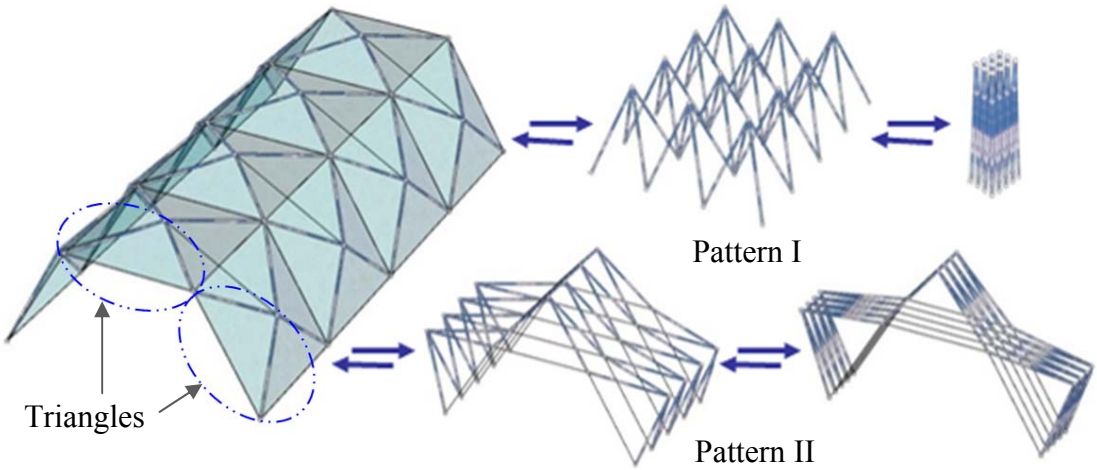

Figure 3.21: Two transforming patterns of DCCS.

The transforming pattern for 2-dimensional panel summarized by Gantes (2001) could also be adopted for presented DCCS barrel vault. The "Triangles" indicated in Figure 3.21 consisting of two struts, a cable in cross direction and the covering membrane act like the "triangular plate" mentioned in the last paragraph during the deployment or folding procedures. Other cables will be loosened as the structure is folded, which follows the same transforming pattern as FPS and FBS. On the other hand, the transforming Pattern II is based on pyramids shaped by four struts and four cables: the angles between the struts become smaller and smaller during the folding process. All cables will be loosened during the folding of the structure in this case.

Normally, the deployment ratio is defined as the specific value of the volume of deployed state divided by that of compact state of deployable structures. Obviously, the deployment ratio of Pattern II is 60, which is higher than that of Pattern I of 20.

The reason is that DCCS could be folded in two directions and the others can only be folded in longitudinal direction. However, from the prototype verification, it is noted that there is a "snap-through" phenomenon during the deployment, which means the deployment angle for some struts is larger than 180 degree. Thus the transforming is not as smooth and reliable when compared with FBS or FPS. In addition, it is worthy to note that the joint designs are different for these two patterns. Specific joints suitable for Pattern I could be found in the work by De Temmerman, *et al*. (2007), while a novel deployable joint for Pattern II will be presented in Section 3.3.5.

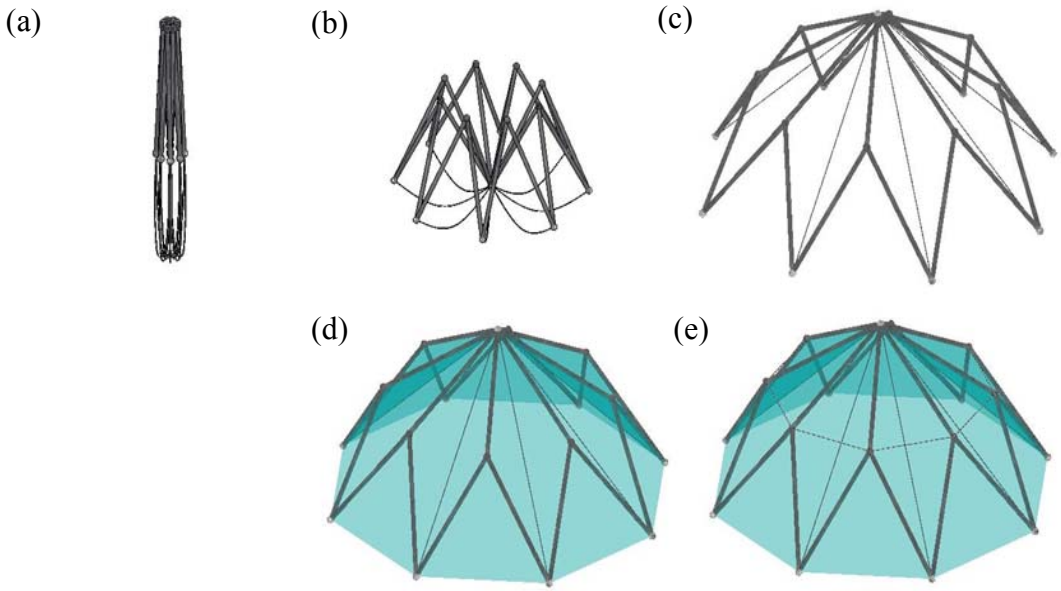

Figure 3.22: Deployment procedure of a dome-shaped DCCS in trimetric view: membrane is ignored in procedures (a), (b), &(c).

As shown in Figure 3.22, the deployment of DCCS shaping a dome can also follow those two patterns as given previously. Transforming Pattern II of such structure is based on pyramids including three struts and three cables. The angles between the struts become smaller and smaller during the folding process. All cables will be loosened during the folding of the structure in this case as can be seen from Figure 3.22(e) to (a). Figure 3.23 presents the plan view of different stages during the

deployment of DCCS shaping a dome.

In the transforming Pattern I of a dome-shaped DCCS, the structure transforms following the origami pattern in the toroidal direction.

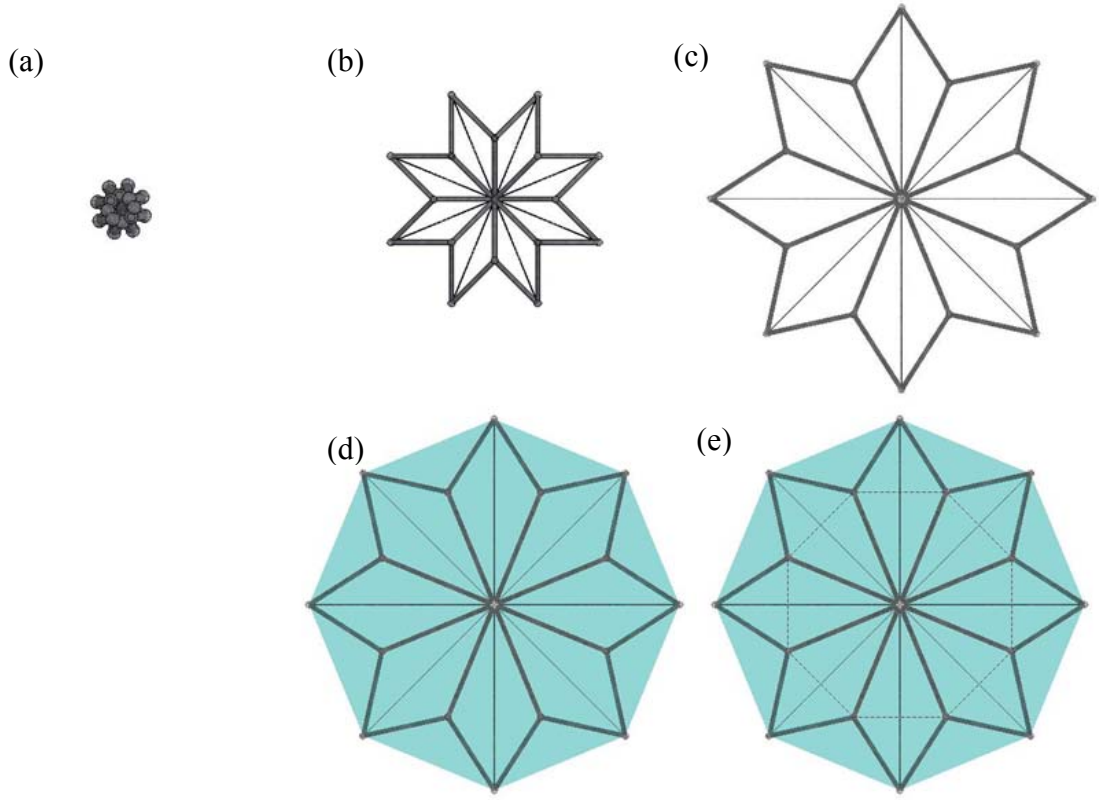

Figure 3.23: Deployment procedure of a dome-shaped DCCS in plan view: membrane is ignored in procedures (a), (b), &(c).

3.3.4 Geometric relationship

To understand the correlations of the parameters of cables and struts and their dependencies, geometric design for the proposed structure is developed. Some detailed researches on the parametric or geometrical design of *FPS* have been conducted by Guest and Pellegrino (1994a; 1994b; 1996) and De Temmerman, *et al.*(2007). The conclusions are also suitable for the proposed DCCSs if they follow the deployment Pattern I, which will not be repeated again herein.

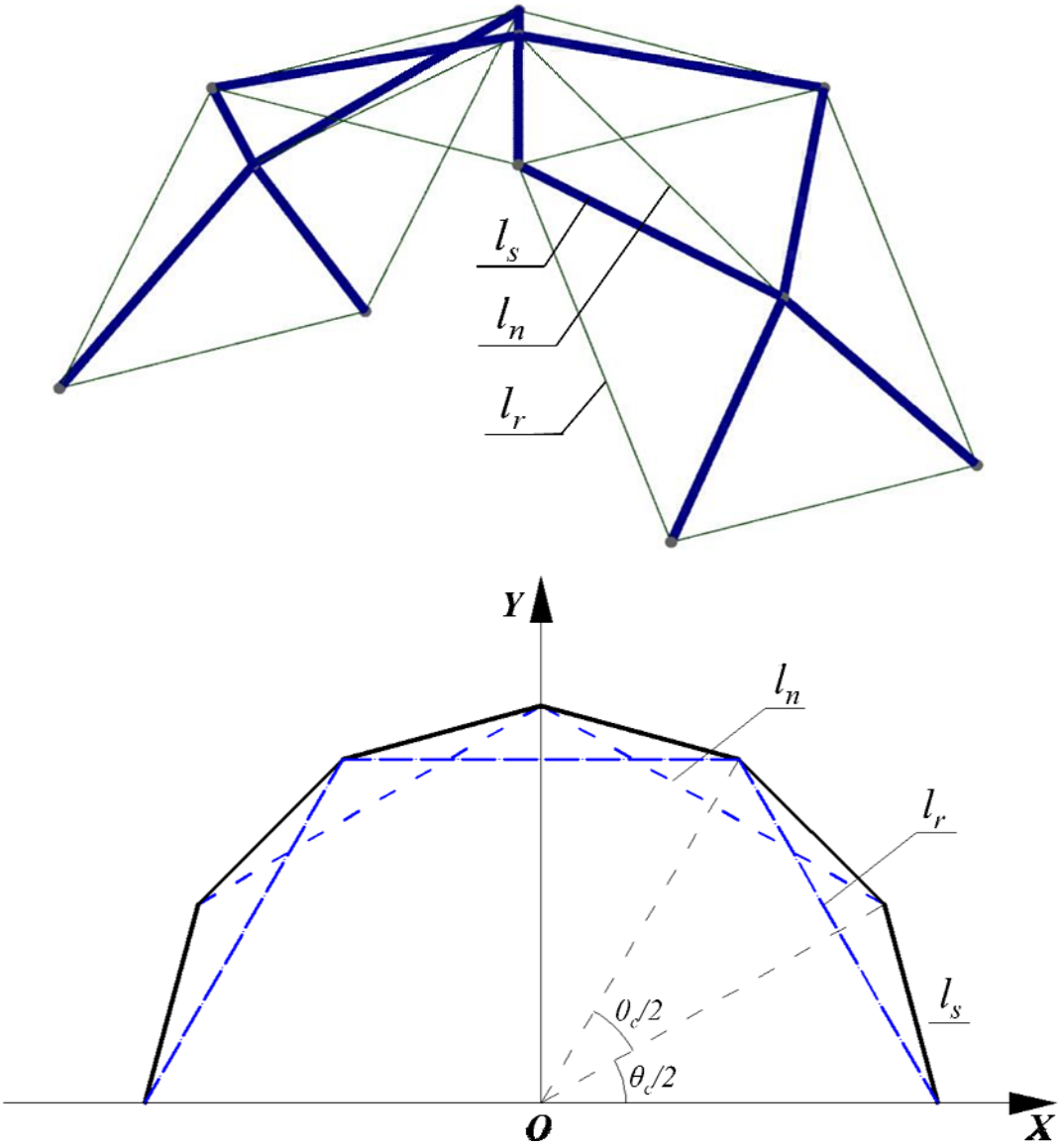

Figure 3.24: Parameters that define the configuration of DCCS.

For the deployment pattern II in Figure 3.21, the relevant parameters affecting the geometry of the structure include the number of modules in a frame, the length of strut in the basic pyramid, the length of surrounding cable in the basic pyramid and the length of connecting cable. In the present analysis, a basic pyramid module consists of 4 struts connected to each other at one common node and 4 surrounding cables connecting the other ends of the struts. All the struts have the identical length of s. The length of surrounding cable is r and that of connecting cables is n. In the case shown in Figure 3.24, 6 modules are connected to each other by 12 points and 6

connecting cables. The geometric relationship could be defined as follows:

$$l_n < \sqrt{2} l_s \tag{3.3}$$

$$\cos(\frac{\theta_c}{2}) l_r < l_n < \frac{1}{\cos(\frac{\theta_c}{2})} l_r \tag{3.4}$$

$$\frac{\sqrt{2}}{2} l_r < l_s < \frac{\sqrt{1+\cos^2(\frac{\theta_c}{2})}}{2\cos(\frac{\theta_c}{2})} l_r \tag{3.5}$$

where, $\theta_c =$ included angle corresponding to a pyramid in DCCS module,

$l_c =$ length of connecting cable,

$l_r =$ length of surrounding cable,

$l_s =$ length of the strut.

Equation (3.3) and the left term of Equation (3.5) ensure that the cable is not slackened or too long to provide stability to the whole structure, while Equation (3.4) and the right term of Equation (3.5) are derived from the requirement that the nodes (apexes) should be on the outside of the cable loops. The surrounding cables may be made the same length as the connecting cables. In such case, the following geometric relationship can be established:

$$l_s = \frac{\sqrt{1+\cos^2(\frac{\theta_c}{4})}}{2\cos(\frac{\theta_c}{4})} l_r \tag{3.6}$$

3.3.5 Bionic honeycomb joints

The design of joints for deployable structures are normally more complicated than that of conventional double layer space structures because the latter does not require the function of deployability. Liew *et al*. (2008), among others, have proposed several kinds of joints for deployable structures and prototypes have been made and tested. These joints consist of two critical parts: one is the pin and another one is the flange as shown in Figure 3.25(a).

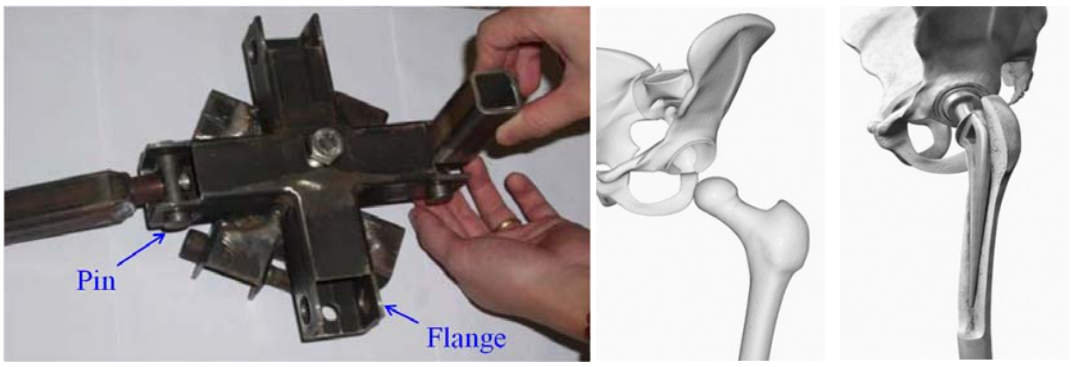

(a) Deployable joint (Liew *et al.*, 2008) (b) Hip Femur Joint (www.corbis.com)

Figure 3.25: Deployable joints.

Another type of joint is called “socket” inspired from hip femur joints, as shown in Figure 3.25(b). The natural design of human joints makes it possible for people to walk and even run smoothly. The observation of skeleton of human beings and the joints leads to the proposed honeycomb socket joint to be used in deployable structures. The unique feature of presented honeycomb socket joint is that it allows free rotation of the strut surrounding its own central axis, which leads to more flexible and safer connection avoiding secondary moment or torsion due to the joint eccentricity.

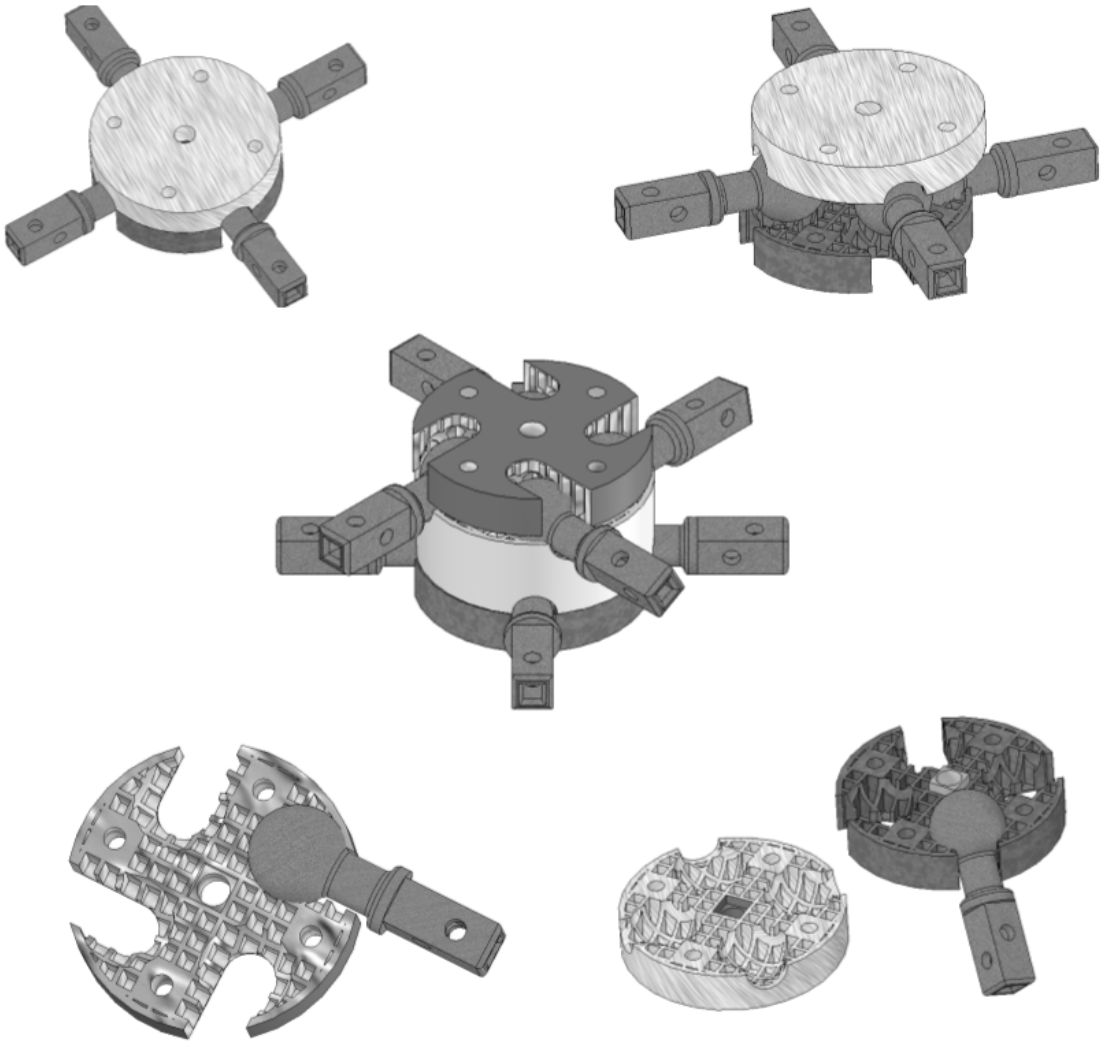

Figure 3.26: Details of honeycomb socket joint.

The proposed honeycomb socket joint is illustrated in Figure 3.26, which includes top cap, bottom cap, strut connectors and self-tightening screws. Screws are not shown in this figure for the purpose of clarity and can be assembled through the five holes penetrating the top and bottom caps. The ball-like connector and socket release the rotation around the axis of connected struts. In addition, four cuts at the bottom cap allow the four struts to rotate downward up to 90 degree in the downward direction (maximum 180 degree if cuts are also provided to the top cap) to facilitate large deployment of DCCS.

Honeycomb-like ribs are adopted inside instead of solid material to reduce weight while keeping the required strength and stiffness and to achieve easy manufacturing. As shown in Figure 3.26, male-female matching design in the centre of both caps is utilized to facilitate the installation on site. Furthermore, it should be noted that the socket is shaped like an olive rather than a spherical ball, which may prevent the ball joint from being blocked because of the lack of tolerance.

In addition, the design could be adjusted for different forms of the structure. For instance, 2-layer or 3-layer novel deployable joints could be designed for connecting 4 struts or 8 struts. Strut eccentricities in the sockets are unavoidable for application to the conventional deployable pantographic structures as shown in Figure 3.26.

3.3.6 Fabrication issues

To verify the proposed concept of DCCS and to check the feasibility of deployment and manufacturing, small scaled aluminium prototypes of the barrel vault and dome as shown in Figure 3.16 (a) and (b) are built. Figure 3.27 and Figure 3.28 show the deployment procedures of the barrel vault and dome prototypes. The typical joints shown in Figure 3.27 and Figure 3.28 are rather easy to manufacture.

However, the joints shown in Figure 3.27 and Figure 3.28 are not as robust as the proposed honey-comb socket joints and two of the plastic nodes shown in Figure 3.27 and Figure 3.28 were broken because of the high local stress during deployment. The deployment ratios of the prototyped barrel vault and dome are quite high (about 60) as shown in Figure 3.27 and Figure 3.28, where the covering surfaces are not included. It is worthwhile to note that all deployable joints for space structures should be used with caution as they are susceptible to joint instability, which may lead to structural

instability problems. Computation procedures to address these problems could be found in the works by Hanaor (1999) and Hanaor *et al*. (2000).

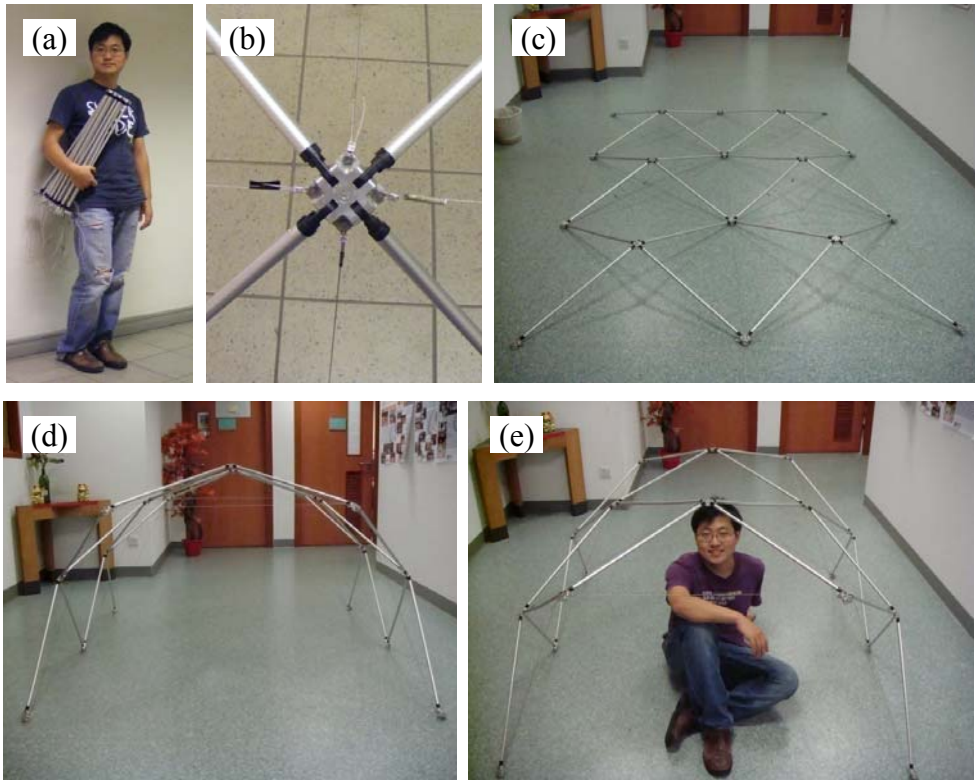

Figure 3.27: Prototype of a barrel vault-shaped DCCS: (a) compact state; (b) joint details; (c) during deployment; (d) deployed state; (e) accommodation demonstration.

In the prototype, only skeleton members (primary structural members) like struts and cables are fabricated and assembled, while the membrane/fabric for the cover is not included. Attentions should be paid on the connection of the membrane to joints and struts. For the connection of the membrane to the joints, a sphere cap as presented by Tran (2007) can be designed for membrane placed over on it. The connection between the membrane and the strut can be realized by a similar system as shown in Figure 3.6.

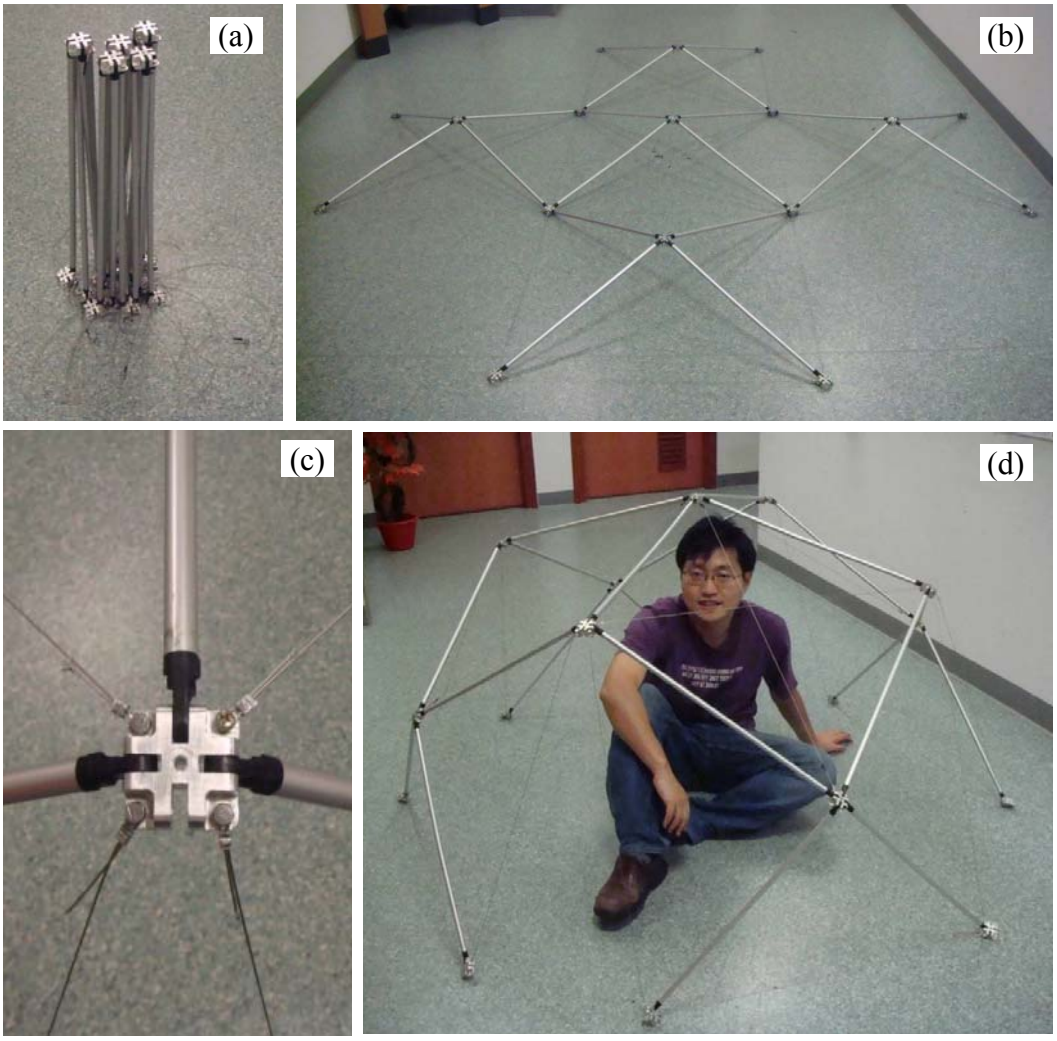

Figure 3.28: Prototype of a dome-shaped DCCS: (a) compact state; (b) during deployment; (c) joint details; (d) deployed state.

3.3.7 Potential application

Deployable Cable Chain Structures are aimed at space enclosures as shown in Figure 3.29. Since they are deployable for rapid on-site erection and foldable for easy relocation, they suit applications with the requirements of mobility and safety. For example, they could be used for exhibition enclosures, disaster relief shelters, and military deployable protective shelters. DCCS in a boom shape can serve as back bones for space exploitation structures.

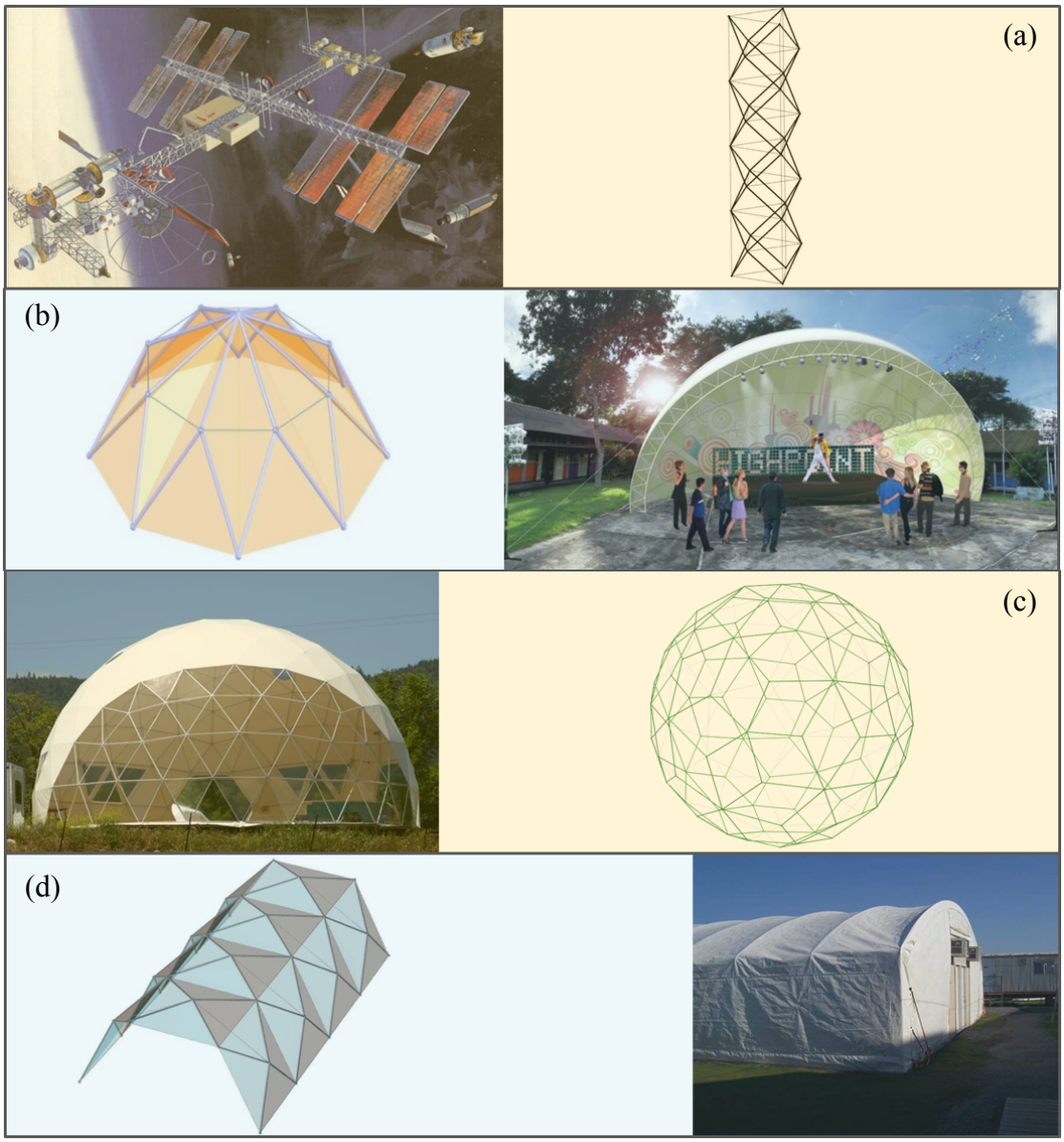

Figure 3.29: Potential applications of DCCSs: (a) outer space supporting systems; (b) exhibition enclosure; (c) geometric domes; (d) disaster or military shelters.

DCCS systems are expected to be lightweight because they inherent the high structural efficiency of cable-strut structures. Compared to conventional deployable structures using scissor-like-elements, complex joint designs are avoid. Compared to existing deployable shelters based on foldable bar or foldable plate structures, DCCSs possess high deployment ratio because they can be folded in two orthogonal directions.

3.4 Summaries

In this Chapter two new types of structures based on tensile restrained arch concepts have been proposed and developed: Tension Strip Structures as compressive structural members and Deployable Cable Chain Structures as shelters.

Tension Strip Structures have been presented to mitigate the buckling phenomenon of slender columns by combining arches restrained by membrane. Different structural forms with various purposes such as reducing wrinkles on membrane, and preventing early local buckling of struts have been proposed. Reliable and low-cost connection between membrane and struts/strips is designed to combine advantages of existing or similar connection methods in literature.

Deployable Cable Chain System has been presented based on the improvement and complementarities of scissor-like element structures and deployable tension-strut structures. Various structural forms such as barrel vaults, dome geodesic domes, boom structures and their combinations have been generated. Investigation on the deployment pattern shows that the pyramid module based pattern has higher deployment ratio than the origami-like deployment pattern. Based on the pyramid module, the geometry relationship among struts, surrounding cables and connecting cables is derived. Allowing free rotation of struts surrounding their own axes, novel deployable honeycomb socket joint adopting socket-connection concept for DCCS and other deployable structures has been proposed.

Chapter 4

Nonlinear Analysis Methods for Tensile Restrained Structures

4.1 Introduction

In Chapter 3, two tensile restrained structures, Tension Strip Structures (TSSs) and Deployable Cable Chain Structures (DCCSs), have been developed on the conceptual level. TSSs are proposed as a compressive member while DCCSs are proposed with the ability to be deployed. The analysis of these structures is not an easy task because of the tensile components involved as well as the possible large deformations experienced.

The first part of Chapter 4 aims to develop an efficient and accurate geometrically nonlinear analysis procedure to simulate TSSs, which can also serve as an optional tool for the planar frames w/o elastic foundation. In the analysis scheme, Tension Strip Structures is deemed as a curved beam (struts/strips) restrained by elastic foundation (membrane). The second part of Chapter 4 provides background information and discussions on a general FEM-package to be employed to evaluate the structural behaviour of DCCSs. Some key issues such as simulating pretension in cables and introducing geometrical imperfection in struts are discussed.

4.2 Nonlinear analysis corotational method for TSSs

To provide an efficient option for the nonlinear analysis of Tension Strip Structures, a method based on co-rotational concept is presented in this section. This method, however, may also apply to nonlinear analysis of general planer frames. In this method, struts of TSSs are treated as curved beams while membrane in between are deemed as elastic foundation. Because of the relatively flexible foundation and slender struts used, TSSs may experience large displacement but moderate strain. The geometrical nonlinearity needs to be taken into account. Considering these structural features, the corotational concept is adopted in this method.

Assumptions in this section are listed as below. Relationship between bending moment (M) and beam curvature (k) is expressed as $M = EI \cdot k$, in which EI is the bending stiffness. There is no large deformation and all strains of curved beams are limited to be moderate. Cross section of the planar curved beams is consistent along the length and the shape is doubly symmetric. Shear deformation is negligible and no torsion is considered.

4.2.1 Corotational concept and background

In the linear description of the motion of beams it is assumed that the displacements are very small and that the material is linearly elastic. In addition, the equilibrium equations are derived using the initial configuration of the body due to the fact that geometry does not change with the loading. However, in geometrically nonlinear analysis of structures, geometric changes are significant and the geometrical coordinates of the system must be updated during the deformation process. Consequently, it becomes necessary to distinguish between various measures of stress

and strain in the element level, and descriptions of motion in the global level.

In the local (element) level, most curved beam elements are developed based on the curvilinear strain description for the static and dynamic analysis of curved structures, such as Friedman and Kosmatka (1998), Wang and Chen (2006), among others. Classic modelling of curved structures by means of lower-order iso-parametric beam elements led to excessively stiff behaviour (shear locking) and some beam elements exhibited excessive bending stiffness (membrane locking) for modelling thin and deep arches. Extensive studies have been conducted to overcome these shear and membrane locking phenomena. Among them, reduced integration methods were developed by Prathap and Bhashyan (1982) and Prathap (1985). However, indiscriminate use of these methods may introduce zero energy modes.

In the global level, the development of accurate and efficient computational procedures to accommodate large rotation capability of beams and frame structures has become a subject attracting considerable interest among researchers. Conventional procedures can be grouped into two categories: the classical Lagrangian descriptions of motion, and corotational description of motion. In the Lagrangian description, the motion of the body is either referred to the initial undeformed configuration (total Lagrangian description) or to the latest known configuration (updated Lagrangian description). In a total Lagrangian description, it is imperative to build smooth interpolation curves which can closely express the curvature of the initial geometry. The arch geometry description is normally based on cubic Hermite or B-spline functions such as Dorfi and Busby (1994), Chakraborty and Majumdar (1997), among others.

As an unconventional approach, the rigid body rule is adopted to simplify geometric nonlinear analysis into the small-deformation linearized theory by Yang *et al*. (2007a). The rigid body concept for geometric nonlinear analysis has been applied to arches, 3D frames, plates and shells based on updated Lagrangian formulation in Yang et al. (2007b) as well as Yau and Yang (2008).

In the corotational description, the motion of the body is decomposed into rigid body motion and strain producing deformation. Figure 4.1 shows the initial and current configurations of a typical corotational beam element. Two types of coordinate systems are introduced in corotational description: the global coordinate system and the local coordinate system. To separate the rigid body motion from the general motion of the beam, a local coordinate system ($X_l O_l Y_l$) is attached to the beam element with the ability to continuously translate and rotate together with the beam element. The X_l direction is defined by two end nodes while Y_l axis has an orthotropic direction compared with the former. In this local coordinate system, the rigid body motion is successfully removed. In such a way, the corotational method provides a non-linear framework in which linear measures of stress and strain can be applied locally, thus simplifying the Lagrangian governing equations without significant loss in accuracy. For this reason, the corotational description is adopted in this work to simulate the nonlinear analysis of Tension Strip Structures.

4.2.2 Local element resistance vector

4.2.2.1 Axial force including end rotation effect

In Figure 4.1, the coordinates of the end nodes *i* and *j* in these two configurations are ($X_{i,j}^O, Y_{i,j}^O$) and ($X_{i,j}^C, Y_{i,j}^C$), respectively. The element length values thus in these two

configurations are

$$L_O = \sqrt{(X_j^O - X_i^O)^2 + (Y_j^O - Y_i^O)^2} \tag{4.1}$$

$$L_C = \sqrt{(X_j^C - X_i^C)^2 + (Y_j^C - Y_i^C)^2} \tag{4.2}$$

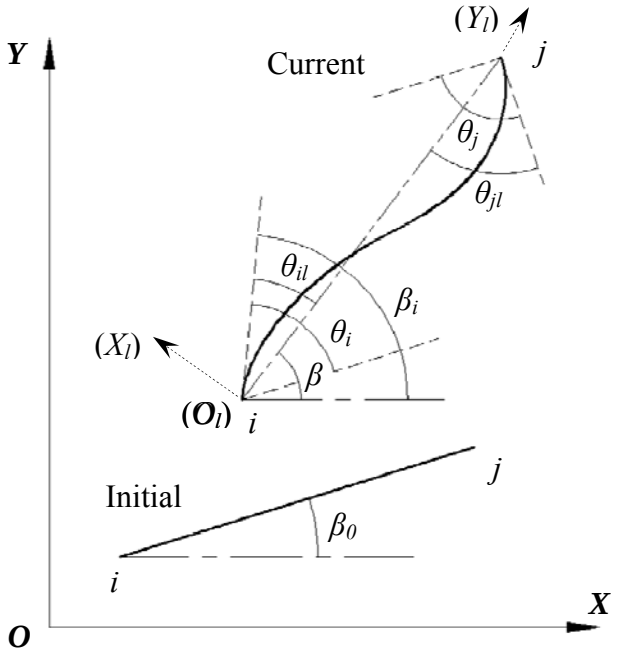

Figure 4.1: A beam element at different configurations.

The axial displacement of the beam element is

$$u_l = L_C - L_O = \sqrt{(X_j^C - X_i^C)^2 + (Y_j^C - Y_i^C)^2} - \sqrt{(X_j^O - X_i^O)^2 + (Y_j^O - Y_i^O)^2} \tag{4.3}$$

This is rewritten as suggested by Crisfield(1991) to avoid numerical problems as follows.

$$u_l = \frac{L_C{}^2 - L_O{}^2}{L_C + L_O} \tag{4.4}$$

The axial force due to the end translations is

$$N_l = \frac{EA}{L_O} u_l \tag{4.5}$$

Axial strain is also attributed to lateral deflection of beam caused by end rotations, which produce additional axial force as well. This so-called bow effect along the length of the beam can be written as

$$N_n(x) = \frac{EA}{L_O} \cdot \frac{1}{2} (\frac{dv}{dx})^2 \tag{4.6}$$

Assuming a constant axial force, the average value can be obtained by integration as follows.

$$N_n = \int_0^{L_0} \frac{EA}{L_O} \cdot \frac{1}{2} (\frac{dv}{dx})^2 dx \tag{4.7}$$

In the local coordinate system, the transverse deflection relates only to the end rotations. This can be approximated by a cubic polynomial as follows.

$$v = (\frac{\theta_{il} + \theta_{jl}}{L_O^2}) x^3 - (\frac{2\theta_{il} + \theta_{jl}}{L_O}) x^2 + \theta_{il} x \tag{4.8}$$

Thus the average axial force caused by end rotations can be written as

$$N_n = \frac{L_O}{15} (2\theta_{il}^2 - \theta_{il}\theta_{jl} + 2\theta_{jl}^2) \tag{4.9}$$

The total axial force is

$$N = \frac{EA}{L_O} u_l + \frac{L_O}{15} (2\theta_{il}^2 - \theta_{il}\theta_{jl} + 2\theta_{jl}^2) \tag{4.10}$$

4.2.2.2 Moment and rotation relation

The sine and cosine values of angles for the local coordinate system abscissa at the initial and current configurations are as follows.

$$\begin{cases} \sin\beta_O = \dfrac{Y_j^O - Y_i^O}{L_O}, \cos\beta_O = \dfrac{X_j^O - X_i^O}{L_O} \\ \sin\beta_C = \dfrac{Y_j^C - Y_i^C}{L_C}, \cos\beta_C = \dfrac{X_j^C - X_i^C}{L_C} \end{cases} \tag{4.11}$$

Given angles defined in Figure 4.1, the local nodal rotations (de Souza, 2000) are

$$\theta_{il} = \arctan\left(\frac{\cos\beta\sin\beta_i - \sin\beta\cos\beta_i}{\cos\beta\cos\beta_i + \sin\beta\sin\beta_i}\right) \tag{4.12}$$

$$\theta_{jl} = \arctan\left(\frac{\cos\beta\sin\beta_j - \sin\beta\cos\beta_j}{\cos\beta\cos\beta_j + \sin\beta\sin\beta_j}\right) \tag{4.13}$$

where, $\beta_i = \theta_i + \beta_0$ and $\beta_j = \theta_j + \beta_0$.

For a beam element under axial force N and end moments M, the governing differential equations for second-order beam theory are

$$\begin{cases} \dfrac{d^2M}{dx^2} + N\dfrac{d^2v}{dx^2} = 0 \\ M = EI\dfrac{d\theta}{dx} \\ \theta = \dfrac{dv}{dx} \end{cases} \tag{4.14}$$

The moment and rotation relation can be obtained by solving the governing differential equations as follows.

$$\begin{Bmatrix} M_i \\ M_j \end{Bmatrix} = \left(\frac{2EI}{L_O} \begin{bmatrix} 2 & 1 \\ 1 & 2 \end{bmatrix} + \frac{NL_O}{30} \begin{bmatrix} 4 & -1 \\ -1 & 4 \end{bmatrix} \right) \begin{Bmatrix} \theta_{il} \\ \theta_{jl} \end{Bmatrix} \tag{4.15}$$

Assuming only nodal load applied, the shear force at the end nodes are

$$\begin{cases} V_i = \dfrac{M_i + M_j}{L^C} \\ V_j = -\dfrac{M_i + M_j}{L^C} \end{cases} \tag{4.16}$$

The expressions of variables (end moments, shear forces, axial forces) in the local member resistance vector have been obtained hereto.

4.2.2.3 Relation between local and global variables

The relationship between local and global nodal displacements can be obtained by geometric approach. The current configuration is assumed to experience a small variation δd_{ij} as shown in Figure 4.2. The corresponding local deformation in the axial direction (e_1) and small rigid rotation (in e_2 direction) from the current configuration are two components of the small variation. The dot products of the direction vector and the virtual global variation δd_{ij} yield the relation between local variation and global variations as follows.

$$\delta p_l = B \delta p \tag{4.17}$$

The B matrix reads

$$B = \begin{bmatrix} -c & -s & 0 & c & s & 0 \\ -s/L & c/L & 1 & s/L & -c/L & 0 \\ -s/L & c/L & 0 & s/L & -c/L & 1 \end{bmatrix} \tag{4.18}$$

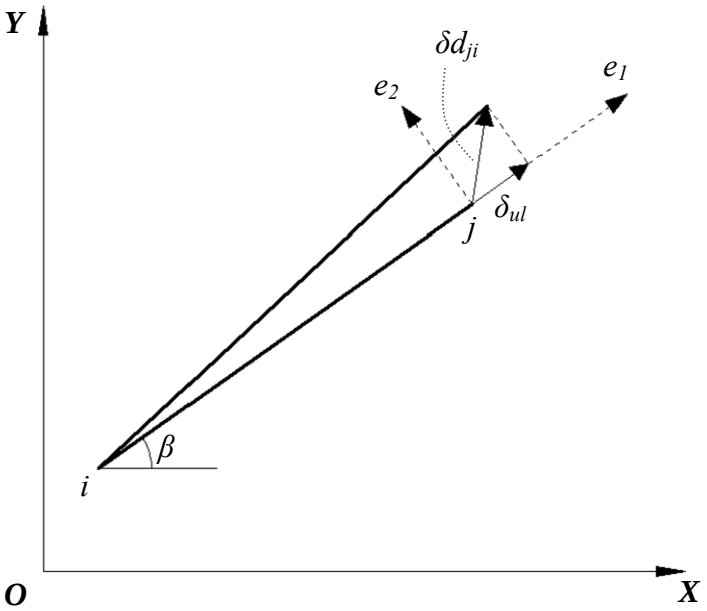

Figure 4.2: A small displacement from the current configuration.

4.2.3 The virtual work

The equivalent internal virtual work in local and global systems gives

$$\delta p_v^T q_i = \delta p_{lv}^T q_{li} = \delta p_v^T B^T q_{li} \tag{4.19}$$

where q_i is the global internal force vector for element i and a subscript v implies a virtual quantity. Because the virtual displacements are arbitrary, the global internal force vector can be calculated from the known local internal force vector as follows.

$$q_i = B^T q_{li} \tag{4.20}$$

4.2.4 Tangent stiffness matrices

Differentiation of the previous equation gives the tangent stiffness matrix as follows.

$$\delta q_i = B^T \delta q_{li} + \delta B^T q_{li} + N\delta B_1 + M_i \delta B_2 + M_j \delta B_3 = (k_{te} + k_{tg})\delta p \tag{4.21}$$

where B_1, B_2, and B_3 is the first, second and third column in the matrix B^T, k_{te} and k_{tg} are the material stiffness and geometrical stiffness matrices at the global level, respectively. Substitute the axial force and end moment equations in terms of local nodal displacements into the variations in the middle part of the previous equation gives the tangent stiffness matrices as follows.

$$k_{te} = \frac{EA}{L_O}\begin{bmatrix} 1 & 0 & 0 & -1 & 0 & 0 \\ 0 & 0 & 0 & 0 & 0 & 0 \\ 0 & 0 & 0 & 0 & 0 & 0 \\ -1 & 0 & 0 & 1 & 0 & 0 \\ 0 & 0 & 0 & 0 & 0 & 0 \\ 0 & 0 & 0 & 0 & 0 & 0 \end{bmatrix} + \frac{EI}{L_O}\begin{bmatrix} 0 & 0 & 0 & 0 & 0 & 0 \\ 0 & \frac{12}{L^2} & \frac{6}{L} & 0 & -\frac{12}{L^2} & \frac{6}{L} \\ 0 & \frac{6}{L} & 4 & 0 & -\frac{6}{L} & 2 \\ 0 & 0 & 0 & 0 & 0 & 0 \\ 0 & -\frac{12}{L^2} & -\frac{6}{L} & 0 & \frac{12}{L^2} & -\frac{6}{L} \\ 0 & \frac{6}{L} & 2 & 0 & -\frac{6}{L} & 4 \end{bmatrix} \tag{4.22}$$

$$k_{tg} = \frac{F}{L}\begin{bmatrix} 0 & 0 & 0 & 0 & 0 & 0 \\ 0 & 1 & 0 & 0 & -1 & 0 \\ 0 & 0 & 0 & 0 & 0 & 0 \\ 0 & 0 & 0 & 0 & 0 & 0 \\ 0 & -1 & 0 & 0 & 1 & 0 \\ 0 & 0 & 0 & 0 & 0 & 0 \end{bmatrix} + FL_O \begin{bmatrix} 0 & 0 & 0 & 0 & 0 & 0 \\ 0 & \frac{1}{5L^2} & \frac{1}{10L} & 0 & -\frac{1}{5L^2} & \frac{1}{10L} \\ 0 & \frac{1}{10L} & \frac{2}{15} & 0 & -\frac{1}{10L} & -\frac{1}{30} \\ 0 & 0 & 0 & 0 & 0 & 0 \\ 0 & -\frac{1}{5L^2} & -\frac{1}{10L} & 0 & \frac{1}{5L^2} & -\frac{1}{10L} \\ 0 & \frac{1}{10L} & -\frac{1}{30} & 0 & -\frac{1}{10L} & \frac{2}{15} \end{bmatrix} + \frac{M_1 + M_2}{L^2}\begin{bmatrix} 0 & 1 & 0 & 0 & -1 & 0 \\ 1 & 0 & 0 & -1 & 0 & 0 \\ 0 & 0 & 0 & 0 & 0 & 0 \\ 0 & -1 & 0 & 0 & 1 & 0 \\ -1 & 0 & 0 & 1 & 0 & 0 \\ 0 & 0 & 0 & 0 & 0 & 0 \end{bmatrix}$$

$$+EA\begin{bmatrix} 0 & -\frac{\theta_1+\theta_2}{10L} & \frac{\theta_2-4\theta_1}{30} & 0 & \frac{\theta_1+\theta_2}{10L} & \frac{\theta_1-4\theta_2}{30} \\ -\frac{\theta_1+\theta_2}{10L} & L_O(\frac{\theta_1+\theta_2}{10L})^2 & \frac{L_O(4\theta_1-\theta_2)(\theta_1+\theta_2)}{300L} & \frac{\theta_1+\theta_2}{10L} & -L_O(\frac{\theta_1+\theta_2}{10L})^2 & \frac{L_O(4\theta_2-\theta_1)(\theta_1+\theta_2)}{300L} \\ \frac{\theta_2-4\theta_1}{30} & \frac{L_O(4\theta_1-\theta_2)(\theta_1+\theta_2)}{300L} & L_O(\frac{4\theta_1-\theta_2}{30})^2 & \frac{4\theta_1-\theta_2}{30} & -\frac{L_O(4\theta_1-\theta_2)(\theta_1+\theta_2)}{300L} & \frac{L_O(4\theta_1-\theta_2)(4\theta_2-\theta_1)}{300L} \\ 0 & \frac{\theta_1+\theta_2}{10L} & \frac{4\theta_1-\theta_2}{30} & 0 & -\frac{\theta_1+\theta_2}{10L} & \frac{4\theta_2-\theta_1}{30} \\ \frac{\theta_1+\theta_2}{10L} & -L_O(\frac{\theta_1+\theta_2}{10L})^2 & -\frac{L_O(4\theta_1-\theta_2)(\theta_1+\theta_2)}{300L} & -\frac{\theta_1+\theta_2}{10L} & L_O(\frac{\theta_1+\theta_2}{10L})^2 & -\frac{L_O(4\theta_2-\theta_1)(\theta_1+\theta_2)}{300L} \\ \frac{4\theta_2-\theta_1}{30} & \frac{L_O(4\theta_2-\theta_1)(\theta_1+\theta_2)}{300L} & \frac{L_O(4\theta_1-\theta_2)(4\theta_2-\theta_1)}{300L} & \frac{4\theta_2-\theta_1}{30} & -\frac{L_O(4\theta_2-\theta_1)(\theta_1+\theta_2)}{300L} & L_O(\frac{4\theta_2-\theta_1}{30})^2 \end{bmatrix} \tag{4.23}$$

Both material and geometry tangent stiffness matrices are in symmetric forms. The geometry stiffness considers the effects of end rotations on the axial strain.

4.2.5 Issues in implementation of corotational method for TSSs

4.2.5.1 Hinged end conditions

Different from common problems, the foundation (membrane) is located between beams (struts) in Tension Strip Structures as shown in Figure 3.3. In the corotational models, the beam elements should form a loop to simulate the real TSS structure and the tips should be modelled as hinges to allow free rotations. At these nodes, the end moments are released and the displacements are not consistent. The model with hinged end conditions as introduced by Balling and Lyon (2011) is adopted herein.

Two variables, n_i and n_j, are used to imply the end conditions at nodes i and j in the beam element in Figure 4.1, respectively. The end condition is hinged if the variable equal to 0; the end condition is rigid if the variable is equal to 1.

In such conditions, the solution to the differential equation discussed in Section 4.2.2.2 should be changed as follows.

$$\begin{Bmatrix} M_i \\ M_j \end{Bmatrix} = \left(\frac{EI}{L_O} \begin{bmatrix} n_i(3+n_j) & 2n_in_j \\ 2n_in_j & n_j(3+n_i) \end{bmatrix} + NL_O \begin{bmatrix} C_1 & C_2 \\ C_2 & C_3 \end{bmatrix} \right) \begin{Bmatrix} \theta_{il} \\ \theta_{jl} \end{Bmatrix} \tag{4.24}$$

If the axial load in an incremental step is limited to be small compared with EI, the coefficients in the second term of the right side of the equation above read

$$C_1 = \frac{n_i(3-n_j)}{15} \quad C_2 = -\frac{n_in_j}{30} \quad C_3 = \frac{n_j(3-n_i)}{15} \tag{4.25}$$

Due to these changes, the material tangent stiffness matrix and geometry tangent stiffness matrix should be

$$k_{te}=\frac{EA}{L_O}\begin{bmatrix}1&0&0&-1&0&0\\0&0&0&0&0&0\\0&0&0&0&0&0\\-1&0&0&1&0&0\\0&0&0&0&0&0\\0&0&0&0&0&0\end{bmatrix}+\frac{EI}{L_O}\begin{bmatrix}0&0&0&0&0&0\\0&\frac{3(n_i+2n_in_j+n_j)}{L^2}&\frac{3n_i(1+n_j)}{L}&0&-\frac{3(n_i+2n_in_j+n_j)}{L^2}&\frac{3n_j(1+n_i)}{L}\\0&\frac{3n_i(1+n_j)}{L}&n_i(3+n_j)&0&\frac{3n_i(1+n_j)}{L}&2n_in_j\\0&0&0&0&0&0\\0&-\frac{3(n_i+2n_in_j+n_j)}{L^2}&-\frac{3n_i(1+n_j)}{L}&0&\frac{3(n_i+2n_in_j+n_j)}{L^2}&-\frac{3n_j(1+n_i)}{L}\\0&\frac{3n_j(1+n_i)}{L}&2n_in_j&0&\frac{3n_j(1+n_i)}{L}&n_j(3+n_i)\end{bmatrix} \quad (4.26)$$

and

$$k_{tg}=\frac{F}{L}\begin{bmatrix}0&0&0&0&0&0\\0&1&0&0&-1&0\\0&0&0&0&0&0\\0&0&0&0&0&0\\0&-1&0&0&1&0\\0&0&0&0&0&0\end{bmatrix}+FL_O\begin{bmatrix}0&0&0&0&0&0\\0&\frac{n_i-n_in_j+n_j}{5L^2}&\frac{n_i(2-n_j)}{10L}&0&-\frac{n_i-n_in_j+n_j}{5L^2}&\frac{n_j(2-n_i)}{10L}\\0&\frac{n_i(2-n_j)}{10L}&\frac{n_i(3-n_j)}{15}&0&-\frac{n_1(2-n_j)}{10L}&-\frac{n_in_j}{30}\\0&0&0&0&0&0\\0&-\frac{n_i-n_in_j+n_j}{5L^2}&-\frac{n_i(2-n_j)}{10L}&0&\frac{n_i-n_in_j+n_j}{5L^2}&-\frac{n_j(2-n_i)}{10L}\\0&\frac{n_j(2-n_i)}{10L}&-\frac{n_in_j}{30}&0&-\frac{n_j(2-n_i)}{10L}&\frac{n_j(3-n_i)}{15}\end{bmatrix} \quad (4.27)$$

$$+\frac{M_1+M_2}{L^2}\begin{bmatrix}0&1&0&0&-1&0\\1&0&0&-1&0&0\\0&0&0&0&0&0\\0&-1&0&0&1&0\\-1&0&0&1&0&0\\0&0&0&0&0&0\end{bmatrix}+EA\begin{bmatrix}0&-D_3&-D_1&0&D_3&-D_2\\-D_3&L_O(D_3)^2&L_OD_1D_3&D_3&-L_O(D_3)^2&L_OD_2D_3\\-D_1&L_OD_1D_3&L_O(D_1)^2&D_1&-L_OD_1D_3&L_OD_1D_2\\0&D_3&D_1&0&-D_3&D_2\\D_3&-L_O(D_3)^2&-L_OD_1D_3&-D_3&L_O(D_3)^2&-L_OD_2D_3\\-D_2&L_OD_2D_3&L_OD_1D_2&D_2&-L_OD_2D_3&L_O(D_2)^2\end{bmatrix}$$

where $D_1=\frac{n_i(3-n_j)}{15}\theta_{il}-\frac{n_in_j}{30}\theta_{jl}$, $D_2=\frac{n_j(3-n_i)}{15}\theta_{jl}-\frac{n_in_j}{30}\theta_{il}$, $D_3=\frac{D_1+D_2}{L}$.

4.2.5.2 Membrane restraint matrix

The membrane restraint effects are redeemed as special foundation that can only provide restraint on the beam in a tensile manner rather than compressive manner. However, the foundation matrices are derived in a general sense with the intention to include general problems. Two types of considerations on foundation are described in this section. In the first type, the foundation is considered in the global level. The foundation force applied to the primary structure is related directly to the displacement of the two end nodes for the spring-like foundation element. In the

second type, the foundation is considered in the local level. The foundation force is related to the strain of the foundation element. In both cases, the foundation matrix needs to be conducted and coupled with the tangent stiffness matrices.

A Winkler elastic foundation is assumed to provide spring-like downward proportional vertical reaction $k_f \cdot v$, at any point, where k_f is the elastic stiffness of the restraint, and v is the vertical displacement at that point. And the twist of the beam is independent to the foundation. Hence, the foundation spring matrix relating reactions and displacement of the curved beam is

$$\{r\} = \begin{bmatrix} 0 & 0 & 0 \\ 0 & k_f & 0 \\ 0 & 0 & 0 \end{bmatrix} \begin{Bmatrix} u \\ v \\ \theta \end{Bmatrix} \tag{4.28}$$

where, the left side is the reaction vector and the vector on the right shows the displacements and rotation variations. For Tension Strip Columns, the value of k_f is treated as 0 if the current length of the two connected nodes is not larger than the initial value.

4.2.6 Nonlinear solution algorithm

4.2.6.1 Equilibrium path searching methods

Nonlinear solution techniques have gained extensive interests from engineering and research community together with finite element method to solve nonlinear problems in terms of geometry and material. Load controlled Newton-Raphson method was the first method of this kind with the capability to search the equilibrium path. However, this method is not able to find the path after critical load. Displacement controlled

Newton-Raphson method can overcome this point but cannot tackle snap-through or snap-back behaviour. Advanced incremental iterative procedures such as arc-length control, work control, generalized displacement control, and orthogonal residual are proposed for those complex nonlinear problems.

In this work, a numerical solution algorithm adopting the generalized displacement control (GDC) method proposed by Yang and Shieh (1990) is used. The GDC method is discussed in the first place, followed by the detailed nonlinear solution steps presented for solving the nonlinear corotational equations.

The GDC method has features as follows: (a) robustness in changing the load direction at the limit points; (b) numerical stability at critical points; (c) proper adjustment technique for changing the step size (Yang *et al.*, 2007b). To illustrate how GDC method works, the incremental form of an equilibrium equation is given for the *j*th iteration of the *i*th incremental step as follows.

$$[K_{j-1}^{i}]\{\Delta U_{j}^{i}\} = \{P_{j}^{i}\} - \{F_{j-1}^{i}\} \tag{4.29}$$

In Equation (4.29), $[K_{j-1}^{i}]$ is the tangent stiffness matrix from the previous iteration of the *i*th incremental step, $\{F_{j-1}^{i}\}$ is the internal resistant force of the structure, and $\{\Delta U_{j}^{i}\}$ denotes the displacement increments generated at the *j*th iteration. The initial conditions of Equation (4.29) come from the last iterative step of the (*i*-1)th incremental step.

The iterations may be performed with variable applied load steps to avoid numerical instabilities, i.e.,

$$\left\{P_j^i\right\} = \left\{P_{j-1}^i\right\} + \left\{\Delta P_j^i\right\} = \left\{P_{j-1}^i\right\} + \lambda_j^i \left\{\hat{P}\right\} \tag{4.30}$$

where λ_j^i is the load increment parameter for the *j*th iteration of the *i*th incremental step, and the $\{\hat{P}\}$ is the reference load vector. The unbalanced forces from the difference between the applied loads $\{P_{j-1}^i\}$ and internal forces $\{F_{j-1}^i\}$ in the previous step are given by

$$\{R_{j-1}^i\} = \{P_{j-1}^i\} - \{F_{j-1}^i\} \tag{4.31}$$

Substituting Equation (4.30) and Equation (4.31) into Equation (4.29) leads to

$$[K_{j-1}^i]\left\{\Delta U_j^i\right\} = \lambda_j^i \left\{P_j^i\right\} + \left\{R_{j-1}^i\right\} \tag{4.32}$$

which can be decomposed into two parts as

$$[K_{j-1}^i]\left\{\Delta \hat{U}_j^i\right\} = \left\{\hat{P}\right\} \tag{4.33}$$

$$[K_{j-1}^i]\left\{\Delta \bar{U}_j^i\right\} = \left\{R_{j-1}^i\right\} \tag{4.34}$$

The displacement increment vector hence can be calculated by

$$\left\{\Delta U_j^i\right\} = \lambda_j^i \left\{\Delta \hat{U}_j^i\right\} + \left\{\Delta \bar{U}_j^i\right\} \tag{4.35}$$

and the total displacements of the structure at the end of *j*th iteration can be accumulated by

$$\left\{U_j^i\right\} = \left\{U_{j-1}^i\right\} + \left\{\Delta U_j^i\right\} \tag{4.36}$$

In the GDC method, a load increment parameter λ_j^i is determined from a constraint condition. The load increment parameter at j = 1, which means the beginning of the ith incremental step, is given by

$$\lambda_1^i = \lambda_1^1 \left| GSP \right|^{0.5} \tag{4.37}$$

where λ_1^1 denotes the preset load increment parameter for the 1st incremental step. The GSP is defined as

$$GSP = \frac{\left\{\Delta \hat{U}_1^1\right\}^T \left\{\Delta \hat{U}_1^1\right\}}{\left\{\Delta \hat{U}_1^{i-1}\right\}^T \left\{\Delta \hat{U}_1^i\right\}} \tag{4.38}$$

The load increment factor λ_j^i for $j \geq 2$ is

$$\lambda_j^i = \frac{\left\{\Delta \hat{U}_j^{i-1}\right\}^T \left\{\Delta \bar{U}_j^i\right\}}{\left\{\Delta \hat{U}_j^{i-1}\right\}^T \left\{\Delta \hat{U}_j^i\right\}} \tag{4.39}$$

where $\{\Delta \hat{U}_j^{i-1}\}$ denotes the displacement increments generated by the reference load $\{\hat{P}\}$ at the first iteration of the previous incremental step, and $\{\Delta \hat{U}_j^i\}$ and $\{\Delta \bar{U}_j^i\}$ denote the displacement increments generated by the reference loads and unbalanced forces, respectively, at the jth iteration of the ith incremental step.

4.2.6.2 Incremental iterative nonlinear analysis algorithm

The detailed procedures of incremental iterative nonlinear analysis coupled with GDC method are as follows.

Step 1. Select a reference load vector $\{\hat{P}\}$, the initial load increment λ_1^1, the allowed

total number of incremental steps, and the tolerance for the unbalanced load. Set the initial conditions: $\{P_0^1\} = \{0\}$, $\{U_0^1\} = \{0\}$, and the residual $\{R_0^1\} = \{0\}$, etc.

Step 2. For i = 1, set GSP = 1.

Step 3. For the first iteration (j = 1) at each incremental step i:

(a) Form the global stiffness matrix $[K_0^i]$;

(b) Solve for $\{\Delta\hat{U}_j^i\}$;

(c) Calculate the load increment parameter λ_1^i: Set $\lambda_1^i = \lambda_1^1$ for i = 1; for i > 1, obtain the GDC using Equation (4.40) and calculate λ_1^i using Equation (4.41). The sign of λ_1^i remain the same with λ_1^{i-1} unless GSP is negative in which case the direction of loading should be reversed through multiplying λ_1^i by -1.

Step 4. For the remaining iterations, i.e. $j \geq 2$:

(a) Update the tangent stiffness matrix $[K_{j-1}^i]$;

(b) Solve for $\left\{\Delta\hat{U}_j^i\right\}$ and $\left\{\Delta\bar{U}_j^i\right\}$, respectively, using Equation (4.42) and Equation (4.43).

(c) Determine λ_j^i using Equation (4.44).

Step 5. Compute the total external loads $\{P_j^i\}$ and structural nodal displacements $\{U_j^i\}$ by Equation (4.45) and Equation (4.46).

Step 6. Update the all structural nodal displacements.

Step 7. Loop over each node and calculate the internal forces $[F_j^i]$ using equations in Section 4.2.2.

Step 8. Loop over each node and calculate the unbalanced forces $\{R_j^i\}$ remaining at the end of each iterative step.

Step 9. Check if the ratio of the norm of the unbalanced forces to the norm of the applied load is smaller than preset tolerance given in Step 1. If the criteria is not satisfied, let $j = j+1$ and go back to Step 4. Otherwise, go to Step 10.

Step 10. If the total number of steps is smaller than the preset number in Step 1, let $i = i+1$ and go to Step 3 for next incremental load step. Otherwise, stop the procedure.

4.2.7 Numerical verifications

In this section, the formulation and procedure presented in previous sections are applied and computer programs are developed to solve a series of planar beam problems with and/or without elastic foundations, for which the exact or approximate solutions are available in literature for comparison. The curved beam element developed is degenerated into straight beams where applicable.

4.2.7.1 Cantilever beam with end moment

In the first numerical example, the response of a cantilever beam as shown in Figure 4.3, subjected to a concentrated clockwise moment at the free end, is analyzed using the presented method. This numerical example is studied to show the efficiency and large rotation capability of the presented formulation and iterative scheme in this

work.

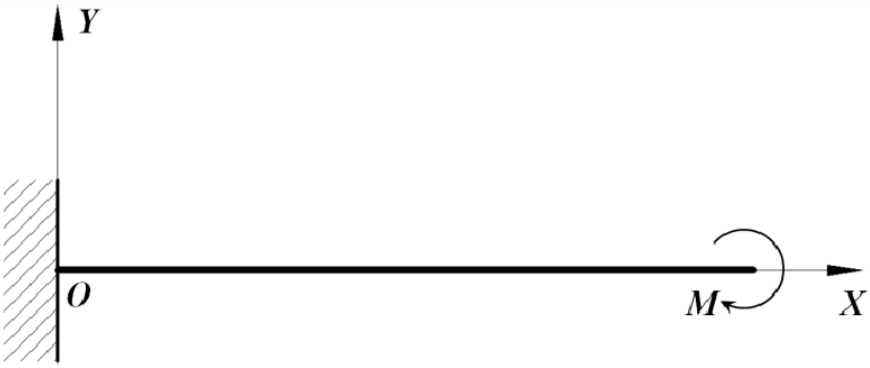

Figure 4.3: Cantilever beam under moment force at the tip.

The dimensionless end moment parameter required for the cantilever beam to curl into an exact complete circle is

$$M_c = 2\pi(EI / L) \tag{4.47}$$

For this example, all beam elements share the same cross section area ($A = 4$), second area moment of inertia ($I = 1.3333$), as well as modulus of elasticity ($E = 100$). The length of the beam is 10 inches and discretized into 16 elements and 17 nodes. The tolerance used for equilibrium iterations is 1.0e-4. The deformed configurations of the cantilever beam subjected to end moments (until M_c) are obtained in 20 load increments as shown in Figure 4.4.

To illustrate the robustness of the presented formulation and iterate procedure and the ability to handle arbitrarily large rotations, Figure 4.5 shows the deflected configurations of the cantilever beam with end moments ranging from M_c to $3M_c$. Accordingly, the cantilever beam curls itself 1, 2, and 3 times.

The dimensionless displacements in two directions versus dimensionless end moments curves are obtained in 20 load increments as shown in Figure 4.6. The comparison of results before end moment reaches M_c with those given by Urthaler and Reddy (2005) shows a good agreement.

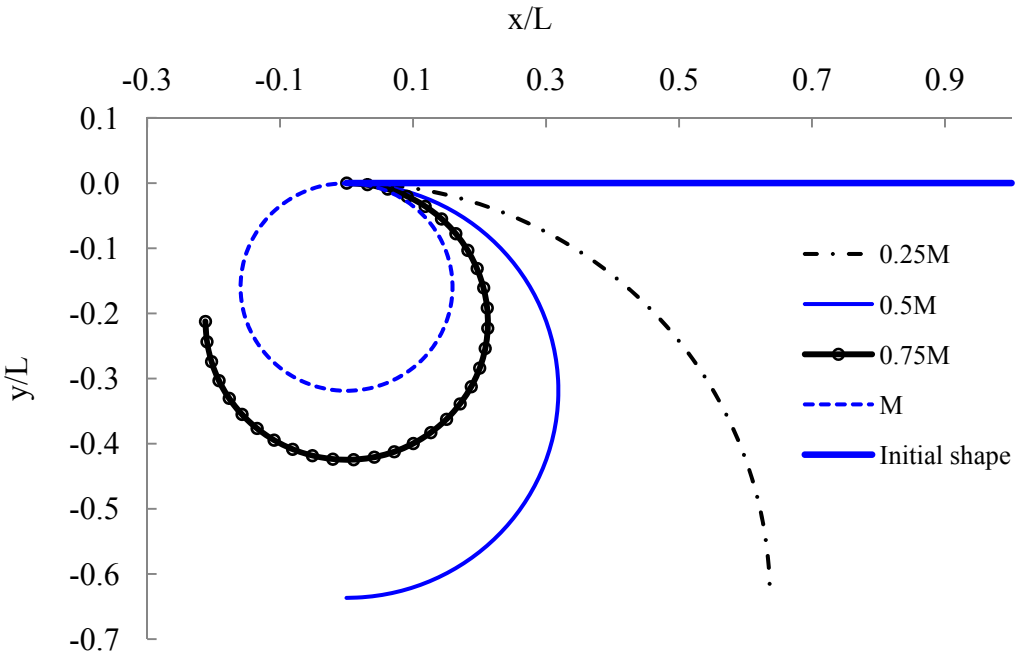

Figure 4.4: Deflected configurations subjected to end moment until Mc.

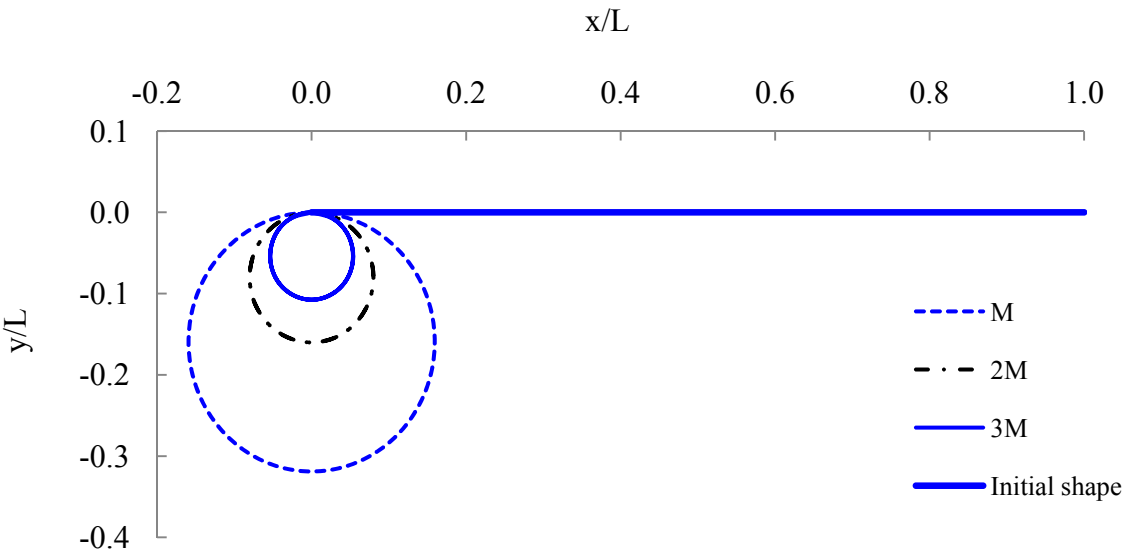

Figure 4.5: Deflected configuration subjected to end moment until 3Mc.

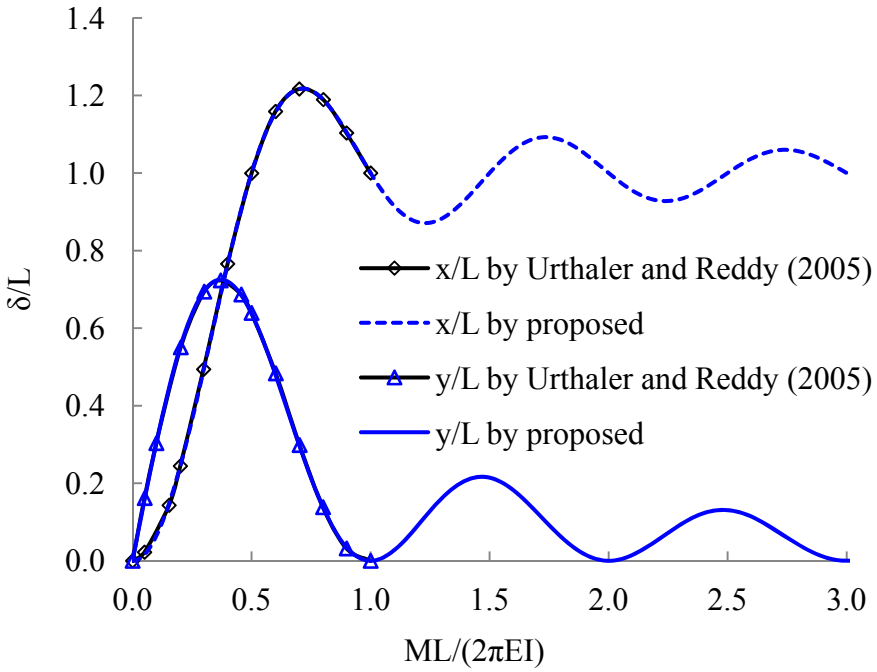

Figure 4.6: Free end dimensionless displacement subjected to end moment.

Table 4.1 contains the root mean square deviation/error (RMSE) values in terms of nodal displacements for this example. The convergence of the solution with mesh refinement is apparent from the results. The convergence studies with the similar approach are performed for all following examples, which are not presented in the text for concision purpose.

Table 4.1: Root mean square deviation (RMSE) values of the relative errors in the nodal deflections of a cantilever beam subjected to an end moment.

No. of elements	4	8	16	32
RMSE (%)	0.0688	0.0346	0.0176	0.0090

4.2.7.2 Cantilever beam subjected to end shear load

A cantilever beam as shown in Figure 4.7 subjected to a downward concentrated load at the free end is analyzed in this example. The length of the beam is 10 inches and discretized with 10 elements and 11 nodes. The tolerance used for equilibrium

iterations is 1.0e-4.

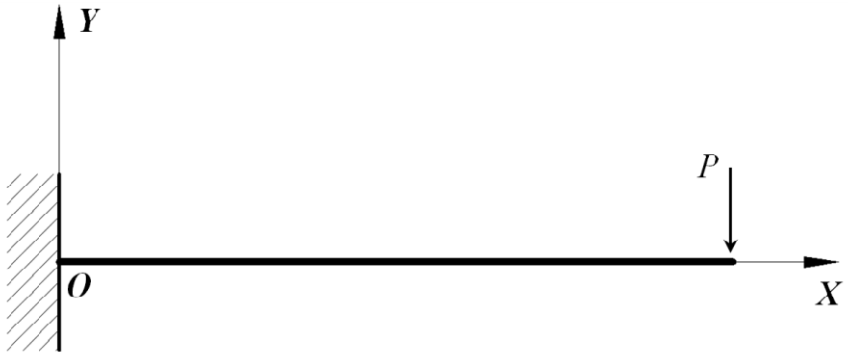

Figure 4.7: Cantilever beam subjected to end shear force.

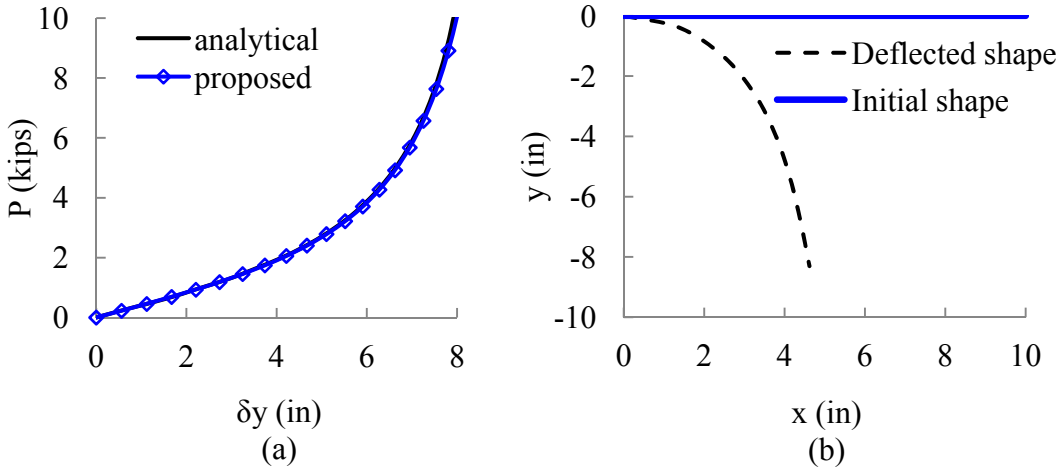

Figure 4.8: Cantilever beam subjected to end shear load: (a) P-δ curve; (b) Deflected configurations.

For this example, all beam elements share the same cross section area ($A = 4\,\text{in}^2$), second area moment of inertia ($I = 1.3333\,\text{in}^4$), and modulus of elasticity ($E = 100$ ksi). The load displacement curves are compared to the analytical solution given in Khosravi et al. (2007) as shown in Figure 4.8(a), while the deformed configurations are presented in Figure 4.8(b). The load and deflection at the tip have a linear relationship with small loads applied, but as the load increases the curve is apparently nonlinear due to the membrane hardening effect.

4.2.7.3 Lee's frame

Lee's frame subjected to a vertical concentrated load, located on the beam with a distance from the intersection point of 24 cm as shown in Figure 4.9, is analyzed in this example. Pin boundary conditions are applied at the supported tips. Both beam and column have a unified length of 120 cm and cross section area of 96 cm^2, moment of inertia of 2 cm^4 and linear elastic modulus of 7060.8 kN/cm^2.

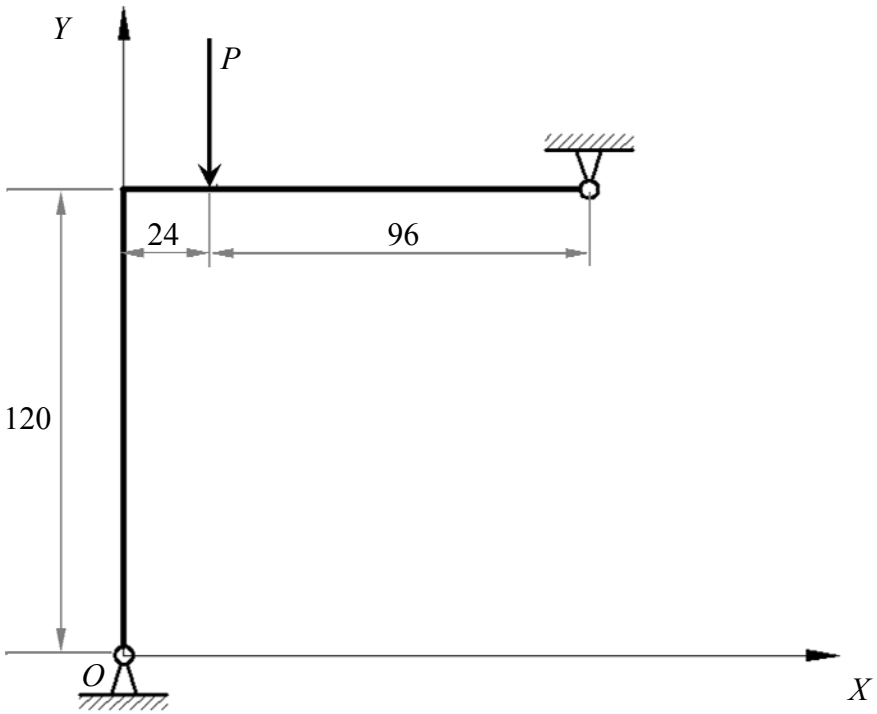

Figure 4.9: A Lee's frame (unit: cm)

Both beam and column are discretized with 10 equal length elements, which are sufficient to capture results approaching to that obtained by de Souza (2000) as shown in Figure 4.10, where the vertical applied load is plotted against the vertical displacement of the loaded point. This example also shows that generalized displacement control scheme applied can cope with tracing complicated equilibrium

pat including both snap back and snap through problems.

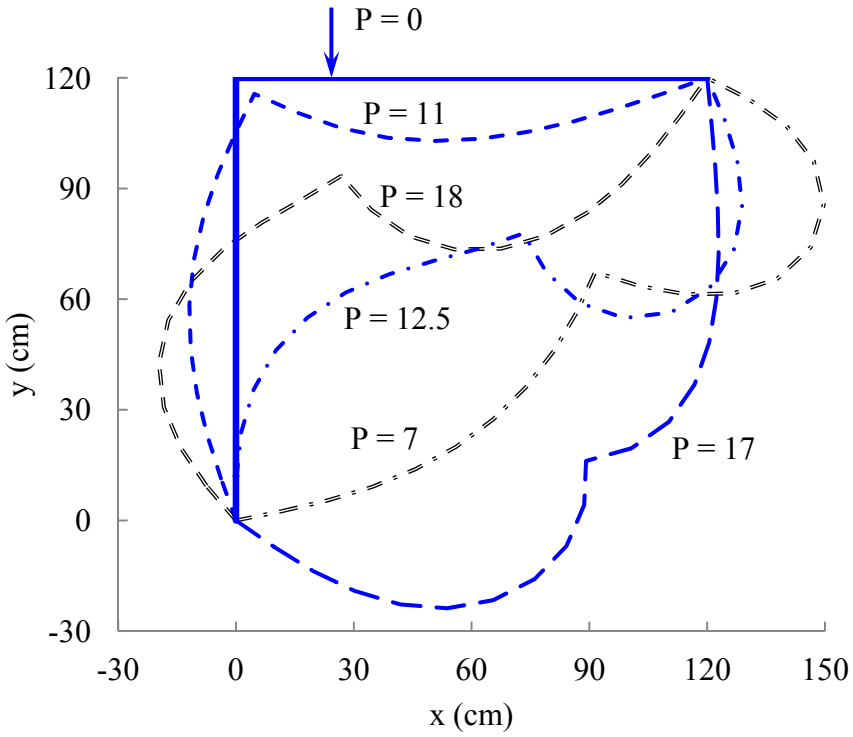

Figure 4.10: Deformed configurations of Lee's frame at various loads (unit: kN).

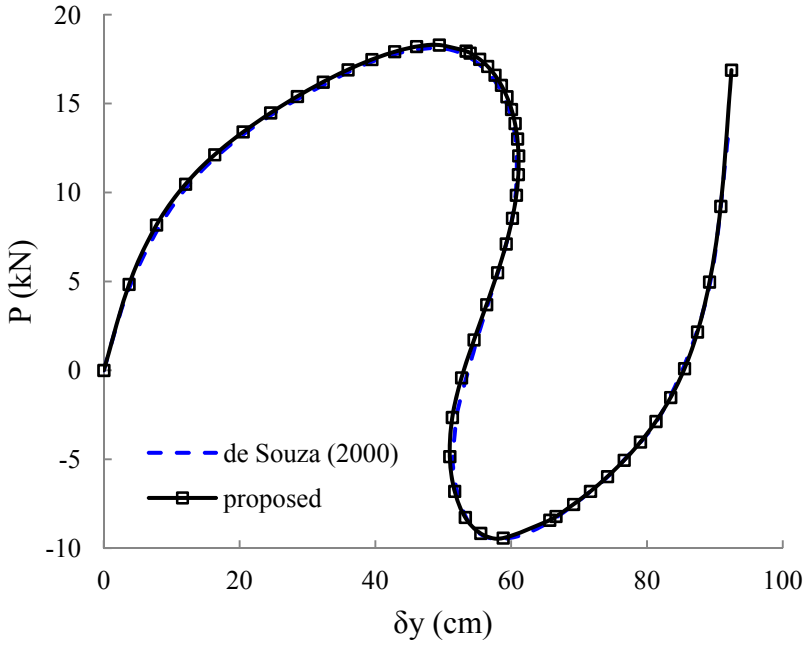

Figure 4.11: Load versus vertical displacement of Lee's frame.

4.2.7.4 Toggle frame

The toggle frame is loaded by a concentrated load at the point of intersection as shown in Figure 4.12. The two sided tips of the beams with a distance of 65.715 cm are clamped. The intersection point has a height of 0.98 cm. Both beams have unified cross section area of 0.408282 cm^2, moment of inertia of 0.0132651 cm^4, and linear elastic modulus of 19971.4 kN/cm^2.

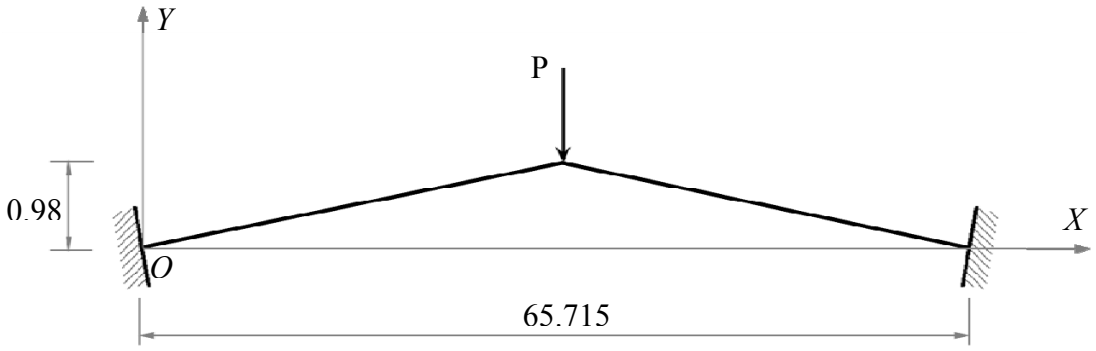

Figure 4.12: The dimension of a toggle frame (unit: cm)

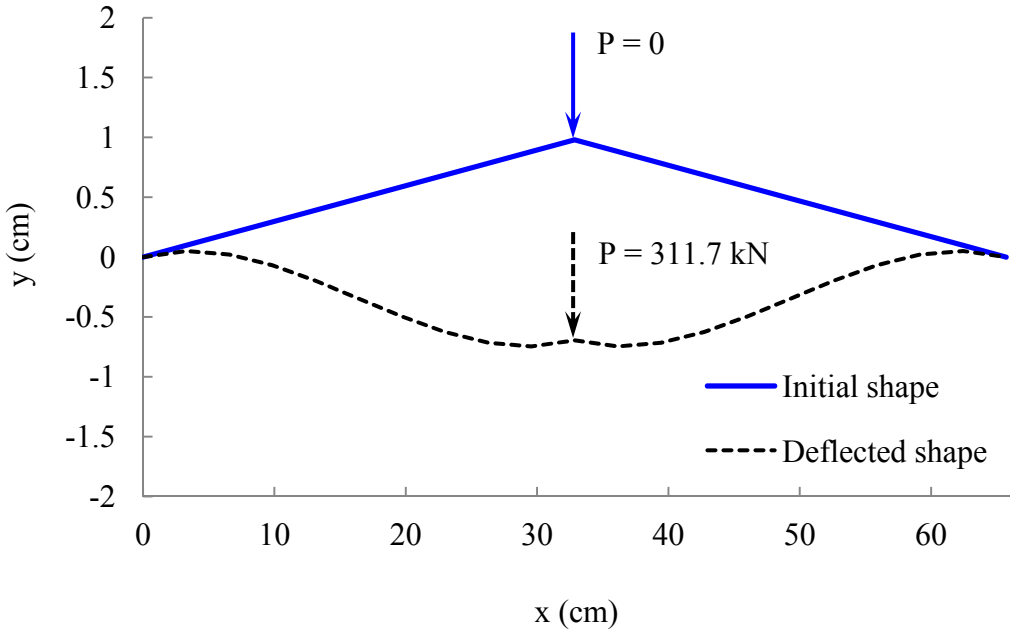

Figure 4.13: Initial and deflected configurations of toggle frame.

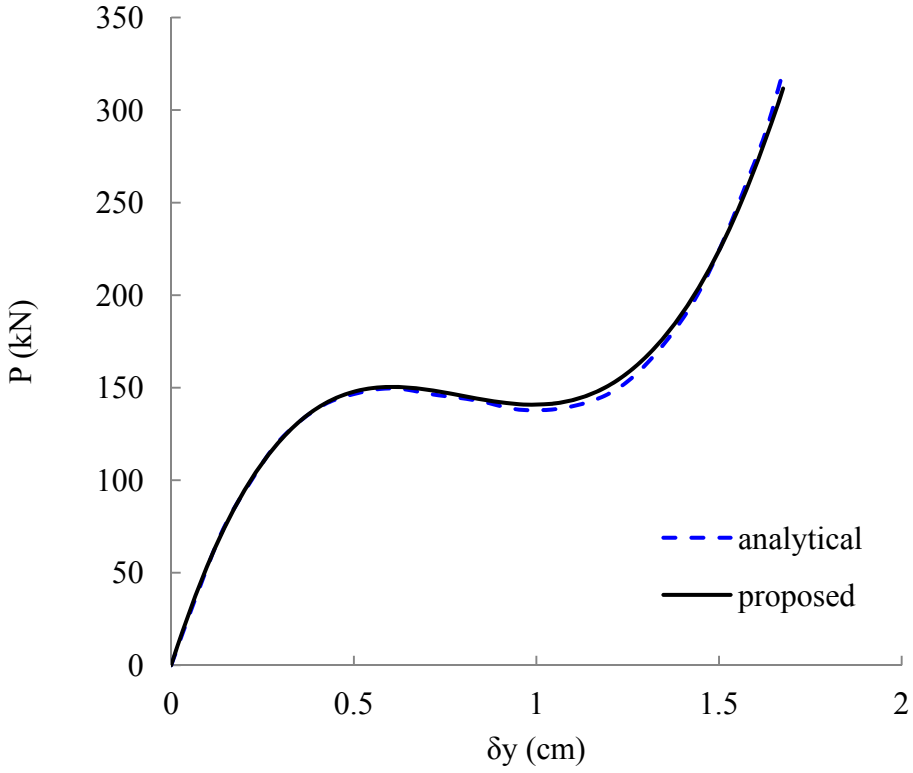

Figure 4.14: Load versus vertical displacement of toggle frame.

The two beams are both discretized with 10 equal length beam elements and 8 nodes, which is sufficiently fine to approach the analytical results obtained by Williams (1964). Figure 4.13 depicts the initial and deflected shapes of the toggle frame. Figure 4.14 depicts the applied load against the vertical displacement of the intersection point.

4.2.7.5 Pin-supported shallow arch at both ends

Figure 4.15 shows a shallow arch supported by two pins at ends subjected to a concentrated vertical load. The span of the arch is 100 in and the hog height is 5 in. The arch has unified cross section area of 1 in^2, moment of inertia of 1 in^4, and linear elastic modulus of 2000 psi.

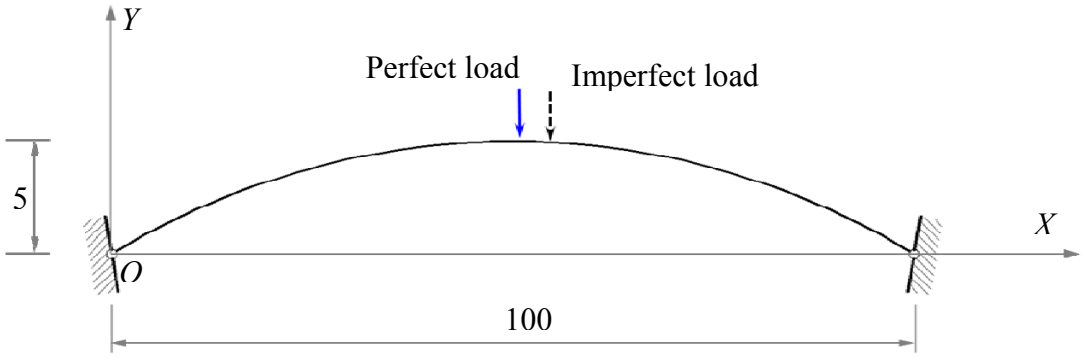

Figure 4.15: Dimensions of a shallow arch (unit: in).

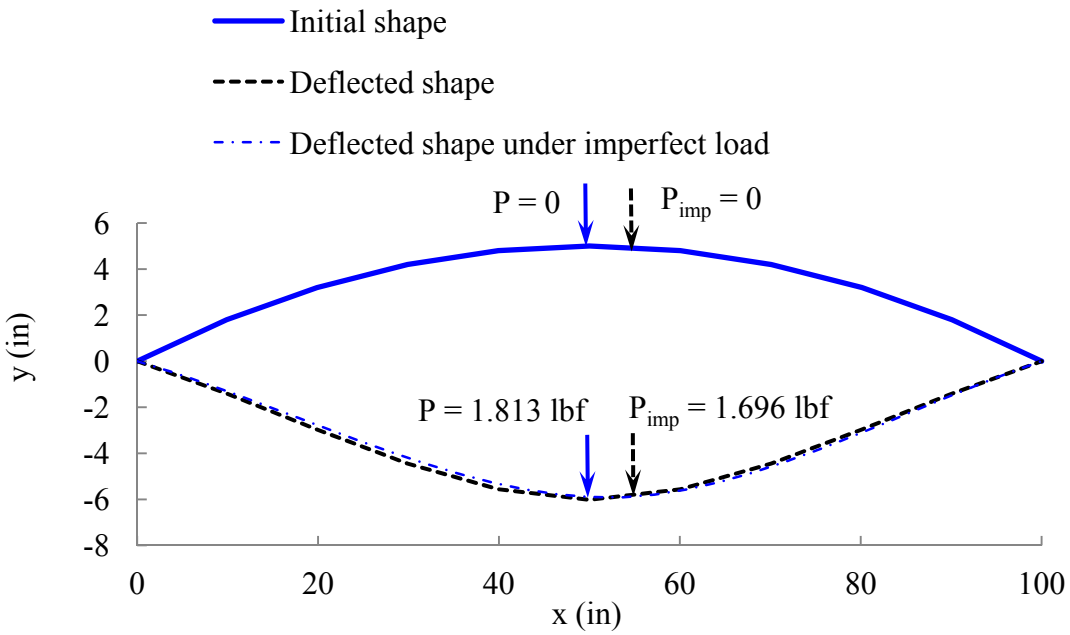

Figure 4.16: Initial and deflected configurations of a shallow arch.

In this example, the arch is discretized with 28 equal length beam elements and 29 nodes. Same with Yau and Yang (2008), two load conditions are analyzed. For the perfect loading case, the vertical load is applied at the apex of the shallow arch; while for the imperfect loading case, the concentrated load is applied on the nearest node next to the apex, with an offset of 3.571 in. It is apparent from Figure 4.17 that the results obtained by the proposed approach agree well with those by Yau and Yang (2008). This example confirms the validation and accuracy of the developed

procedure and scheme for curved shaped planer beams with large deflection problems and high numerical robustness for tracing equilibrium path for problems evolving both snap back and snap through.

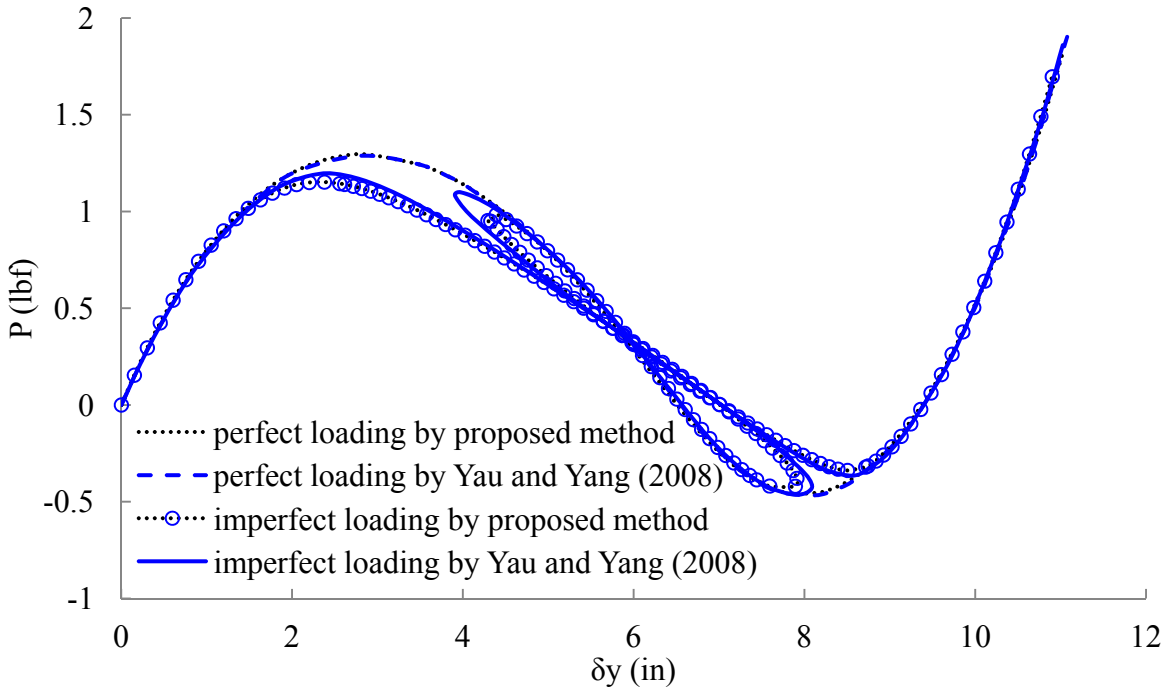

Figure 4.17: Load versus vertical displacement of a shallow arch.

4.2.7.6 Pin supported semicircular arch at both ends

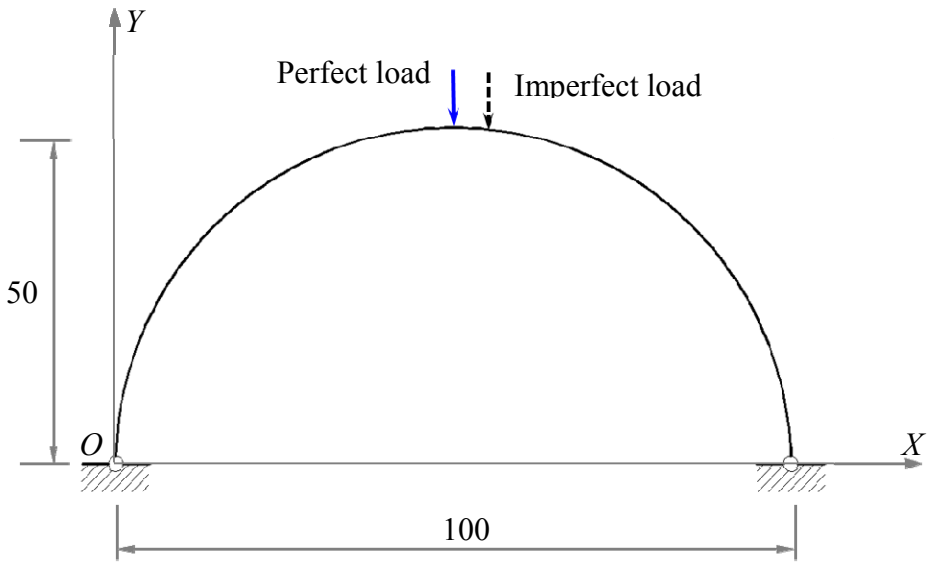

Figure 4.18: Initial and deflected configurations of a deep arch (unit: in).

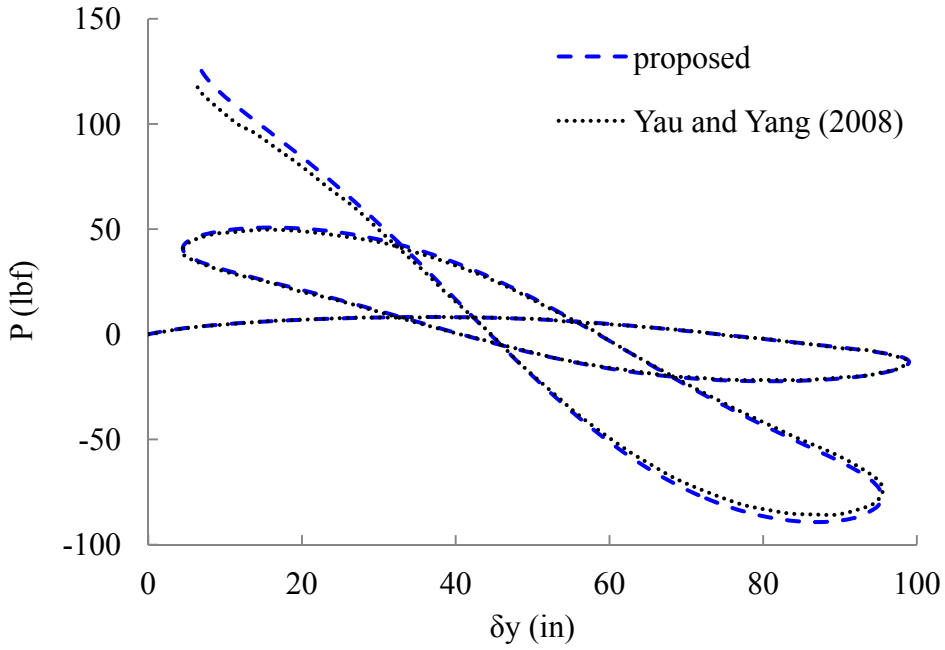

(a)

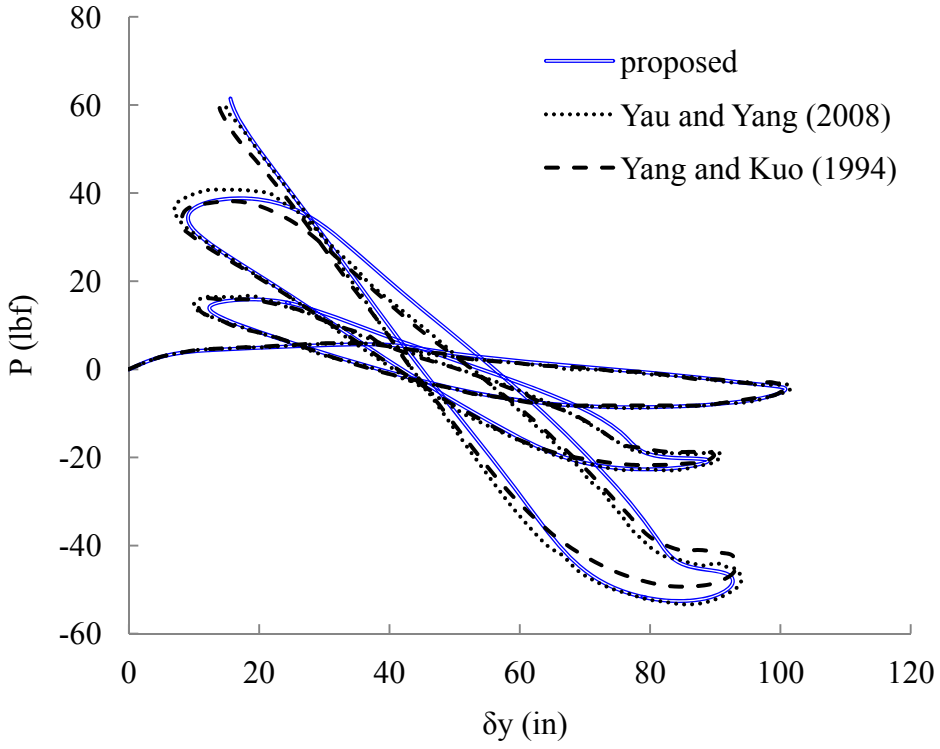

(b)

Figure 4.19: Load versus vertical displacement of a deep arch under: (a) perfect load; (b) imperfect load.

Figure 4.18 shows a hinged semicircular arch subjected to a concentrated vertical load. The arch with a radius of 50 in has a unified cross section area of 1 in^2, moment of inertia of 1 in^4, and linear elastic modulus of 2000 psi. Two loading cases are considered as well: one is the perfect/symmetrical loading in which case the load is applied on the apex while the second case is the imperfect/asymmetrical loading in which case the load is applied on the nearest node next to the apex with an offset of 6.283 in as indicated in Figure 4.18.

In this example, the arch is discretized with 50 equal length beam elements and 51 nodes. The analysis finishes in 800 incremental load steps. Figure 4.19(a) shows that the results obtained by the presented approach have a good match with those by Yau and Yang (2008). Figure 4.19(b) shows that the load versus apex displacement curve converge and match closely those given by Yau and Yang (2008) as well as Yang and Kuo (1994). During the analysis, the displacement of apex node almost reaches the span of the semicircular arch indicating the arch has experienced a very large deflection.

4.2.7.7 Straight beam on elastic foundation

A simply supported (pin-roller supports) beam resting on an elastic foundation is subjected to uniformly distributed load as shown in Figure 4.20. The span of the beam is 240 in and the magnitude of the uniform load is 43.4 lb/in. The beam has unified cross section area of 7.11 in^2, moment of inertia of 30 in^4, and linear elastic modulus of 3e7 lb/in^2. The Winkler-type foundation modulus is 26.041667 lb/in^2.

In this example, the beam is discretized with 20 equal length beam elements and 21 nodes. Results of both displacements and moment distribution along the beam are obtained using the presented method, which are very close compared to analytical

results obtained by Timoshenko and Woinowsky-Krieger (1959) as shown in Figure 4.21 and Figure 4.22. Only first half of the moment results are shown in Figure 4.22 due to symmetry.

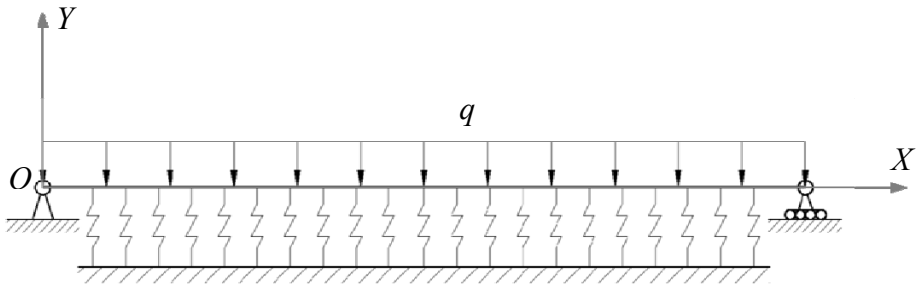

Figure 4.20: A straight beam on elastic foundation under uniformly distributed load.

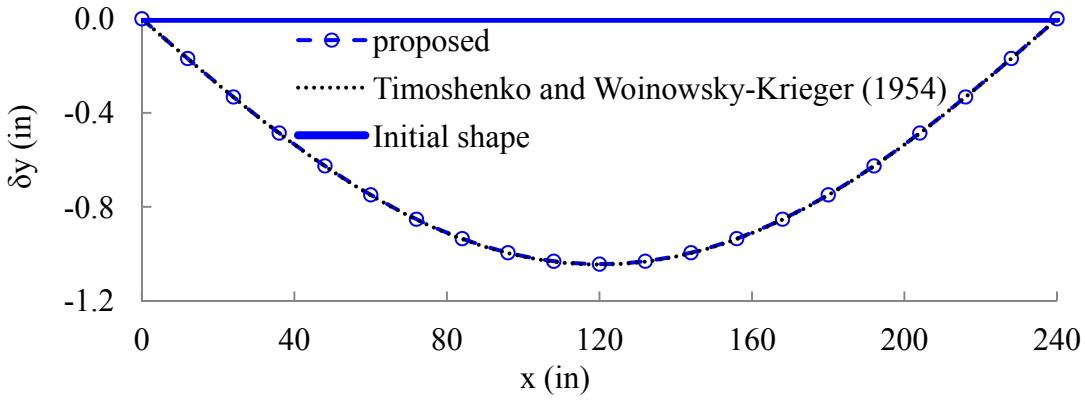

Figure 4.21: Initial and deflected configurations of a straight beam on elastic foundation.

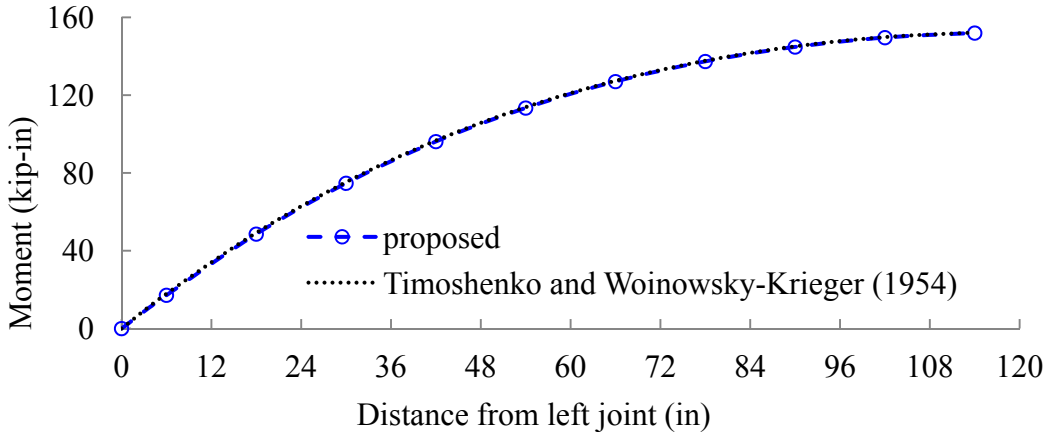

Figure 4.22: Moment distribution along first half length of the beam on an elastic foundation.

4.2.7.8 Arch restrained by membrane

In this section, an arch restrained by elastic-foundation-like membrane is analyzed using the presented method to illustrate the capacity to simulate curved beam with relatively soft foundations where large deformation may be evolved. Tensarity columns as shown in Figure 4.23 proposed by Plagianakos *et al*. (2009) are taken as an example. The column has a span of 5 m and a maximum diameter of 0.545 m. It consisted of an inflated membrane hull and three circularly curved struts placed at respective angles 120 along the section. The strut has unified cross section area of 30x10 mm^2 and linear elastic modulus of 68 GPa. According to Plagianakos *et al*. (2009), the modulus of the elastic foundation is a function of the inside air pressure (p_a) and independent of the hull properties, as follows

$$k_f = 1.69\pi p_a \tag{4.48}$$

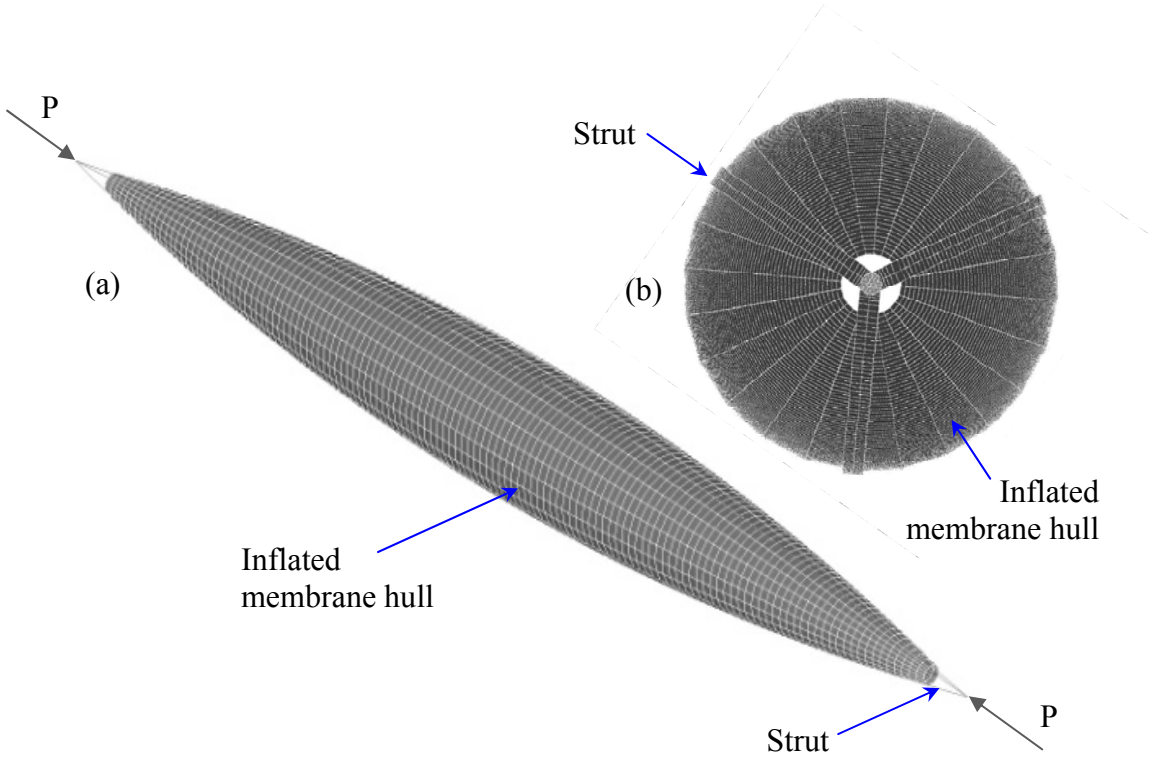

Figure 4.23: Tensairity column finite element model reproduced from Plagianakos *et al*. (2009): (a) isometric view; (b) plan view (not proportional).

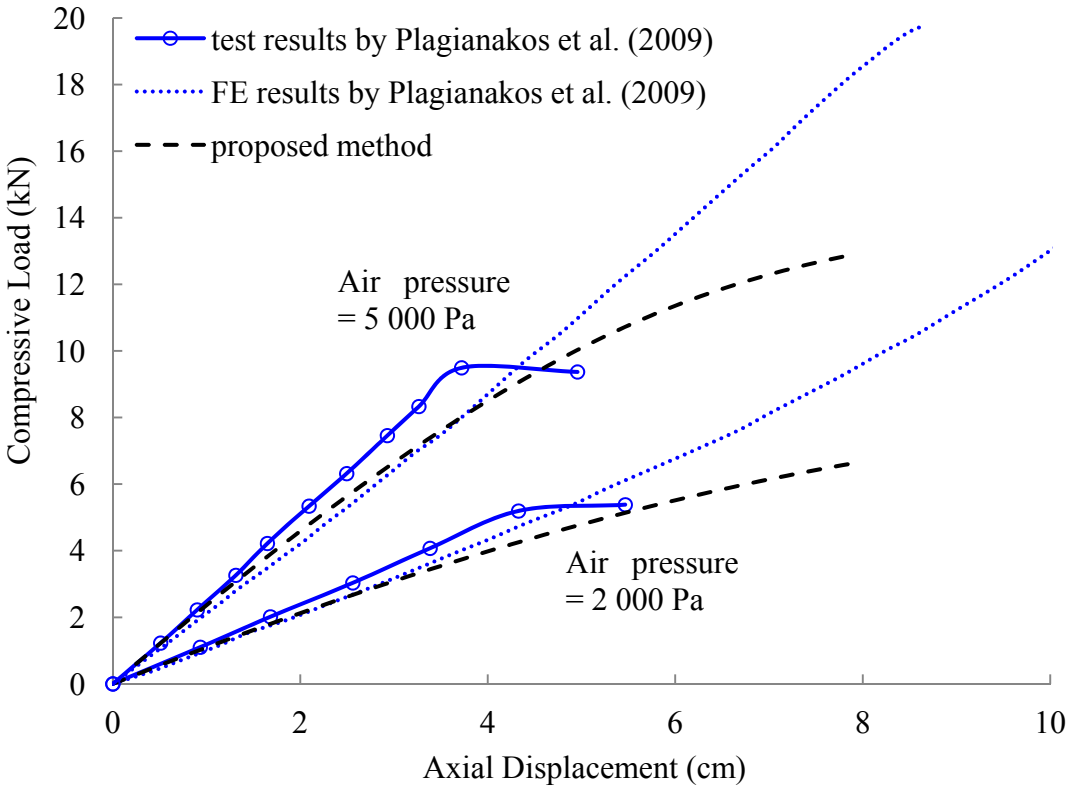

Figure 4.24: Load-displacement curves for different air pressures.

Two levels of air pressures (2 000 Pa and 5 000 Pa) are considered in this example. In the simulation using the proposed method, the arch strut is deemed as supported by pin-roller boundary conditions. The beam is discretized with 20 elements and 21 nodes. Results of axial load versus tip displacement are compared to test and finite element results given by Plagianakos et al. (2009). As can be seen from Figure 4.24, the developed method can predict the initial stiffness well. The predicted stiffness increases with an increase in the internal air pressure. In the test, the column buckled because of asymmetric radial displacements occurring near the end, which is due to local imperfections caused by local fibre misalignment. This effect is not considered in the proposed method because detailed information of such local imperfection is not available. This leads to deviation between the predicted buckling load and the measured value in the test. However, the difference between results obtained from the

proposed method and linear finite element model by Plagianakos et al. (2009) demonstrates that the geometrical nonlinearity should be considered for such problems.

4.3 Nonlinear analysis method for Cable Chain Structures

In Deployable Cable Chain Structures, struts and cables are the primary structural components while the effects of joints among these primary components are not considered herein. The struts are deemed as beam-column elements, and cables are tension elements with no compression or bending stiffness. In many cases, both of these elements are slender requiring a nonlinear analysis to consider the tensile stiffening effect of cables and the P-δ/P-Δ effect of struts. The strain in DCCSs is expected to be small under design load for safety. Hence, a nonlinear analysis programme with the capability to simulate large displacements and small strain problems is appropriate for DCCSs. In this study, the structural responses of DCCSs in the deployed status are predicted using a robust nonlinear numerical tool, USFOS (2012), with a verified capacity to yield the accurate column and beam-column behaviour for space frames.

The basic formulations behind USFOS and some key issues during the simulation of DCCSs during the load bearing period after deployment are discussed in this section.

4.3.1 Basic formulations

The 4^{th} order differential equation for a beam under end forces is

$$\frac{d^4w}{dx^4} + \frac{P}{EI}\frac{d^2w}{dx^2} = 0 \tag{4.49}$$

Exact displacement shape functions satisfying the governing differential equation above are employed in USFOS. All integration in the element stiffness expression can be carried out analytically, and the element stiffness matrices are presented as closed-form expressions. Course mesh, e.g. one element per physical member in a structure, is sufficient to capture the global nonlinear effects.

Nonlinear strain relationships (Green strain) are used to account for the effects of large displacements and the coupling effects between axial strains and lateral deflections. The coupling effect of the axial force on the bending stiffness of the element is considered by the nonlinear terms in the Green strain formulation. This enables accurate prediction of the flexural buckling load of columns with different boundary conditions with a limitation of moderate strains.

The continuum formation based on Green strains for a 3-dimensional beam element under is

$$\varepsilon_x = \mu_{,x} + \frac{u_{,x}^2}{2} + \frac{v_{,x}^2}{2} + \frac{w_{,x}^2}{2} \tag{4.50}$$

For moderate element deflection where the von Karman approximation applies, this can be simplified as

$$\varepsilon_x = \mu_{,x} + \frac{v_{,x}^2}{2} + \frac{w_{,x}^2}{2} \tag{4.51}$$

The virtual displacement principle is applied to derive the stiffness formulation. The total potential for an elastic element is

$$\Pi = U + H \tag{4.52}$$

The internal strain energy of a beam is

$$U = \frac{1}{2}\int_0^l [EA(u_{,x} + \frac{v_{,x}^2}{2} + \frac{w_{,x}^2}{2})^2 + EI_z v_{,xx}^2 + EI_y w_{,xx}^2]dx \tag{4.53}$$

The potential of external load is

$$H = -(F_i u_i + \int_0^l q_x u dx + \int_0^l q_y v dx + \int_0^l q_z w dx) \tag{4.54}$$

In the USFOS code, material nonlinearity is modelled by incorporating plastic hinges possibly at the ends and midpoint of the element. In the latter case, the original element is subdivided into two sub elements. The plastification of the element is assessed by comparing stress resultants against the total plastic capacity of the cross section. The behaviour of the hinges is controlled by plastic flow theory with two basic assumptions as: (a) Initial yielding conditions exists, which can be represented by an initial yield surface that is assumed to be a scaled down version of the bounding surfacing indicating the full plastification of the cross section, and (b) Both surfaces can translate without rotation in the stress resultant space controlled by a flow rule, relating plastic strain increments to stress increments.

4.3.2 Modelling pretension in cable elements

The method of using temperature changes in cable elements to produce a particular level of cable pretension is adopted in the nonlinear analysis of Deployable Cable Chain Structures. This concept is common practice for simulating structures involving cable elements. However, the choice of the magnitudes of the temperature is influenced by the deformation of other connected structural components due to the

introduced pretension in cable elements. This effect is significant for DCCSs because the connected parts (strut chains) can only gain proper stiffness with the help of cable elements in pretension.

The temperature decrease (ΔT) in the cable element needed to yield the desired pretension (P_c) is

$$\Delta T = \frac{P_c}{\alpha_t l_e}\left(\frac{1}{EA} + \frac{1}{k_r}\right) \tag{4.55}$$

where α_t is the coefficient of thermal expansion for the cable, l_e is the original length of the cable, EA is the axial tensile resistance of the cable, and k_r is the stiffness of the rest structural components subjected to internal load of the cable. Neglecting the $1/k_r$ term leads to inaccurate results especially for relatively flexible structures. For simple connection geometries with only one cable, it is easy to calculate k_r. However, this is not readily determined for complex geometries with a number of cables such as DCCSs. Preliminary analysis incorporating with the trial and error or iterative method is required for a proper pretension analysis.

4.3.3 Geometrical imperfection for struts

Structural members in practice have initial imperfection due to geometrical imperfection, residual stress, and workmanship. The analysis of buckling of structural members needs lateral displacement at the member mid-section in the form of initial imperfections or imposed by frame deformations in pre-buckled stage in order to provoke the buckling. Otherwise, the analysis tends to overestimate the compression resistance of the member as well as the whole structure.

Equivalent initial imperfection is usually used to model geometrical and material imperfections. Conservative choices on the magnitude and the direction of these equivalent imperfections should be adopted. Hellan *et al.* (1995) investigated the influence of initial imperfections in different directions and concluded that applying the imperfections in the same plane of applied member load or global base shear leads to smallest mean values and small standard deviation in terms of the first member failure strength and system collapse strength.

In the analysis of DCCSs, imperfections are applied in direction of global base shear and a magnitude of the imperfection is taken as 1/500 of the strut length. Interaction between local buckling and column buckling can be included with the dent formulation activated. This is not necessary for cases where the D/t ratio of the cross section is smaller than 35.

4.4 Summaries

This chapter presents numerical analysis methods for the proposed tensile restrained structures including both Tension Strip Structures (TSSs) and Deployable Cable Chain Structures (DCCSs).

Efficient and accurate beam finite element matrices based on large displacements and small to medium strain corotational formulations are developed. The element matrices are further expanded to include the membrane restraint effect on compression members. The attributes or advantages of this proposed method are summarized as follows:

— Capable of analysing rigid and hinge end members.

— Axial strain caused by both end translations and end rotations is considered in the calculation of internal force steps.

— The proposed element is implemented in a generalized displacement control method with a capability to trace load-displacement path involving both snap through and snap back problems.

The applicability and accuracy of the developed method have been verified by comparing the results with a series of classical problems from literature including straight cantilever beams, planar frames, shallow/deep arches, as well as straight/curved beam with elastic restraints.

Nonlinear finite element analysis method using Green strain as the strain measure is adopted for DCCSs. Exact displacement shape functions satisfying the governing differential equation above are employed. One element per physical member in a structure is sufficient to capture the global nonlinear effects. The presented method can model pre-tensioned cable and is capable of capturing the buckling behaviour of struts with initial imperfections.

Chapter 5

Numerical Investigation of Structural Behaviour

5.1 Introduction

The main objective of the study in Chapter 5 is to investigate the static structural behaviour of Tension Strip Structures (TSSs) with different geometrical and material parameters and the structural response of Deployable Cable Chain Structures (DCCSs) subjected to both applied static load and sudden loss of cable force.

Section 5.2 presents the development of analytical and numerical finite element models, results of parametric studies, as well as case studies to qualify the potential application of presented TSSs. Section 5.3 discusses the load-displacement behaviour for DCCSs, structural efficiency comparison to other similar shelter systems in literatures, and the robustness against sudden damage of cable.

5.2 Tension Strip Structures

5.2.1 Development of analysis models

5.2.1.1 Analytical model

To develop a simplified analytical model for the Tension Strip Columns, the restraint effect of the internal membrane is considered as an elastic foundation for curved struts under compression. Such a model has been presented by Plagianakos *et al*. (2009) based on a flat circular arch approximation and a parabola beam approximation by Wever *et al*. (2010) resting on elastic foundation. The latter approximation allows for simpler analytical expressions. In both models, all compression elements of the column are assumed to resist equal load, which is an identical behaviour. Therefore, only one compression element needs to be considered in both models.

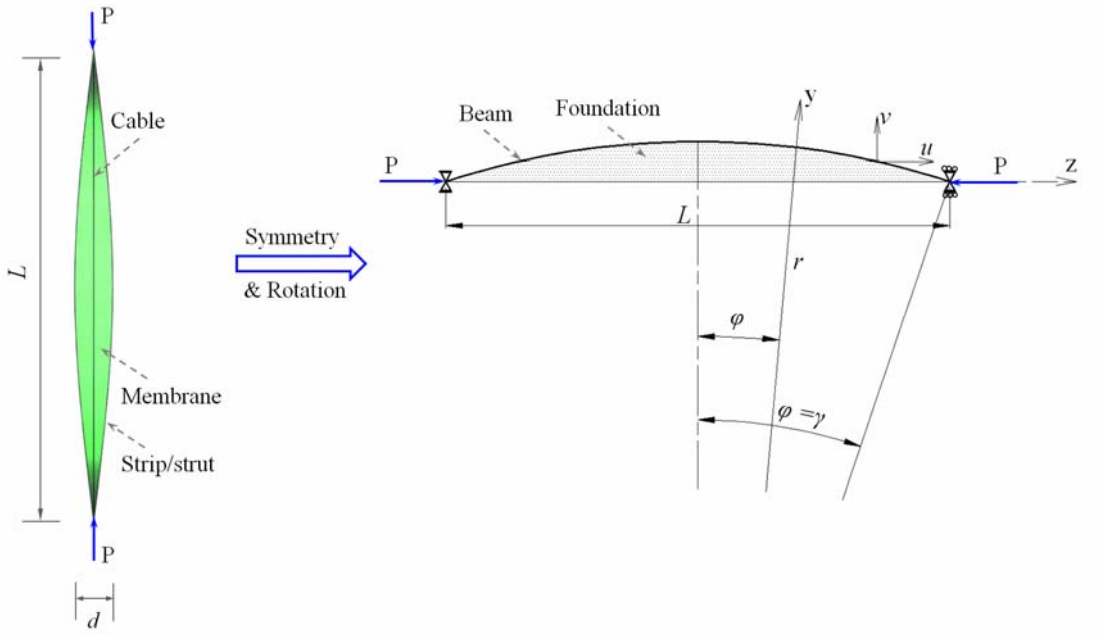

Figure 5.1: Analytical model of TSS as a curved beam resting on elastic foundation.

Tension Strip Structure can also be modelled as a curved beam restrained by elastic foundation formed by membrane with elastic stiffness of k_f as shown in Figure 5.1. The TSS given in Figure 3.3 is taken as an example for easy explanation. Owing to the symmetric geometry and the loading condition for this structure, a half model can be used to simulate the Tension Strip Structure. The membrane restraint effect on the

strip/strut is modelled by elastic foundation formed by a series of springs. A beam resting on elastic foundation model can be obtained for the exactly same structure by rotating the half model in clockwise by 90 degrees as shown in Figure 5.1. The beam is subjected to compressive concentrated axial load applied at the tips.

As derived by Hetenyi (1946), circular arches on elastic foundation are described by

$$\frac{d^5 y}{d\varphi^5} + 2\frac{d^3 y}{d\varphi^3} + \eta^2 \cdot \frac{dy}{d\varphi} = 0 \tag{5.1}$$

with

$$\eta = \sqrt{\frac{r^4 k_f}{EI} + 1} \tag{5.2}$$

In the Equation (5.1), y is the radial deflection, φis the angle, r is the radius of the circular arch, k_f is the elastic stiffness of restraints and EI is the bending stiffness of the arch as shown in Figure 5.1. The general solution of Equation (5.1) is

$$y = C_0 + \left(C_1 \cosh(\chi\varphi) + C_2 \sinh(\chi\varphi)\right)\cos(k\varphi) + \left(C_3 \cosh(\chi\varphi) + C_4 \sinh(\chi\varphi)\right)\sin(k\varphi) \tag{5.3}$$

where $\chi = \sqrt{\frac{\eta - 1}{2}}$ and $k = \sqrt{\frac{\eta + 1}{2}}$.

For the case of Tension Strip Structure (TSS), only symmetric solutions need to be tackled and thus $C_2 = C_3 = 0$. The following relation applies for most TSSs studied

$$\frac{r^4 k}{EI} \gg 1 \tag{5.4}$$

and one can yield

$$\chi = k = \sqrt[4]{\frac{r^4 k}{4EI}} = \lambda r = \rho \tag{5.5}$$

Then, Equation (5.3) can be written as

$$y = C_0 + C_1 \cosh(\rho\varphi)\cos(\rho\varphi) + C_4 \sinh(\rho\varphi)\sin(\rho\varphi) \tag{5.6}$$

For shallow arches (the angle of opening $2\gamma < 60^\circ$), the bending moment M, the shear force Q and the normal force N in the arch are given by Hetenyi (1946) as follows

$$M = -\frac{EI}{r^2}\frac{d^2 y}{d\varphi^2} \tag{5.7}$$

$$Q = -\frac{EI}{r^3}\frac{d^3 y}{d\varphi^3} \tag{5.8}$$

$$N = kry + \frac{EI}{r^3}\frac{d^4 y}{d\varphi^4} \tag{5.9}$$

The angular deflection θ, the horizontal displacement u and the vertical displacement v are defined by

$$\theta = -\frac{r}{EI}\int_0^{\varphi} M d\varphi' \tag{5.10}$$

$$u = u_0 - \int_0^{\varphi} \theta r \sin\varphi' d\varphi' \tag{5.11}$$

$$v = v_0 - \int_0^{\varphi} \theta r \cos\varphi' d\varphi' \tag{5.12}$$

where φ' is an integration variable. Explicit expressions for these quantities are given as below:

$$M = 2\lambda^2 EI(C_1 \sinh(\rho\varphi)\sin(\rho\varphi) - C_4 \cosh(\rho\varphi)\cos(\rho\varphi)) \tag{5.13}$$

$$\begin{aligned} Q = 2\lambda^3 EI\Big(&C_1\big(\cosh(\rho\varphi)\sin(\rho\varphi)+\sinh(\rho\varphi)\cos(\rho\varphi)\big)\\ &-C_4\big(\sinh(\rho\varphi)\cos(\rho\varphi)-\cosh(\rho\varphi)\sin(\rho\varphi)\big)\Big)\end{aligned} \tag{5.14}$$

$$N = rkC_0 \tag{5.15}$$

$$\begin{aligned}\theta = \lambda C_1\big(\cosh(\rho\varphi)\sin(\rho\varphi)-\sinh(\rho\varphi)\cos(\rho\varphi)\big)\\ -\lambda C_4\big(\cosh(\rho\varphi)\sin(\rho\varphi)+\sinh(\rho\varphi)\cos(\rho\varphi)\big)\end{aligned} \tag{5.16}$$

$$u = -\rho\big((C_1 - C_4)I_{u1} - (C_1+C_4)I_{u2}\big) \tag{5.17}$$

$$v = C_0 + C_1 - r\big((C_1 - C_4)I_{v1} - (C_1 + C_4)I_{v2}\big) \tag{5.18}$$

where

$$\begin{aligned} I_{u1}(\varphi) = &\frac{1}{4\rho}\sinh(\rho\varphi)\times\left(\frac{\rho}{\rho-1}\cos\big((\rho-1)\varphi\big)-\frac{\rho}{\rho+1}\cos\big((\rho+1)\varphi\big)\right)\\ &+\frac{1}{4\rho}\cosh(\rho\varphi)\times\big(\sin\big((\rho-1)\varphi\big)-\sin\big((\rho+1)\varphi\big)\big)\end{aligned} \tag{5.19}$$

$$\begin{aligned} I_{u2}(\varphi) = &\frac{1}{4\rho}\cosh(\rho\varphi)\times\left(\frac{\rho}{\rho+1}\sin\big((\rho+1)\varphi\big)-\frac{\rho}{\rho-1}\sin\big((\rho-1)\varphi\big)\right)\\ &-\frac{1}{4\rho}\sinh(\rho\varphi)\times\big(\cos\big((\rho+1)\varphi\big)-\cos\big((\rho-1)\varphi\big)\big)\end{aligned} \tag{5.20}$$

$$\begin{aligned} I_{v1}(\varphi) = &\frac{1}{4\rho}\sinh(\rho\varphi)\times\left(\frac{\rho}{\rho+1}\sin\big((\rho+1)\varphi\big)+\frac{\rho}{\rho-1}\sin\big((\rho-1)\varphi\big)\right)\\ &-\frac{1}{4\rho}\cosh(\rho\varphi)\times\big(\cos\big((\rho+1)\varphi\big)+\cos\big((\rho-1)\varphi\big)\big)+\frac{1}{2\rho}\end{aligned} \tag{5.21}$$

$$\begin{aligned} I_{v2}(\varphi) = &\frac{1}{4\rho}\sinh(\rho\varphi)\times\left(\frac{\rho}{\rho-1}\cos\big((\rho-1)\varphi\big)+\frac{\rho}{\rho+1}\cos\big((\rho+1)\varphi\big)\right)\\ &+\frac{1}{4\rho}\cosh(\rho\varphi)\times\big(\sin\big((\rho-1)\varphi\big)+\sin\big((\rho+1)\varphi\big)\big)\end{aligned} \tag{5.22}$$

The elastic stiffness of restraints (k_f) is directly related to the elastic properties of the membrane, which can resist outward lateral tensioning forces. With prestressing in the membrane, inward compressive forces up to the prestressing value can also be resisted. For a Tension Strip Column with n struts (evenly distributed in a circular pattern around the centre axis of the column), the elastic stiffness of restraints used for this analytical model is

$$k_f = 2\cos\left(\frac{(n-2)\pi}{2n}\right)\frac{E_m t}{h} \quad for\ n = 2,3,4,... \tag{5.23}$$

with E_m the elastic modulus of the membrane, t the membrane thickness, and h the distance from strut to the axis of the column. As h is not constant along the length of the column, the elastic stiffness of restraints studied is a function of the position along the column. The lowest value of k_f can be obtained at the centre position because h is largest at that point. Analytical solution given by Equation (5.4) is no longer valid and numerical solution is required. Nevertheless, a constant value of h is assumed to yield a conservative axial stiffness for benchmarking purpose.

The following three boundary conditions apply for the TSSs

$$v\big|_{\varphi=\gamma} = 0 \tag{5.24}$$

$$M\big|_{\varphi=\gamma} = 0 \tag{5.25}$$

$$N\cos(\varphi) - Q\sin(\varphi)\big|_{\varphi=\gamma} = P \tag{5.26}$$

The first boundary condition shows that there is no vertical displacement at the end of TSS because of the symmetrical behaviour of the compressive struts regarding the

axis of the TSS. The second condition implies that the struts are connected at the end with pins, which means there is no moment. The last conditions come from the force equilibrium at the connection end.

With these boundary conditions, the constant coefficients C_0 , C_1 and C_4 can be determined analytically. Accordingly, the general solution of the governing equation could be well quantified.

$$C_0 = (\frac{AD}{C} - B)C_4 \tag{5.27}$$

$$C_1 = -\frac{D}{C}C_4 \tag{5.28}$$

$$C_4 = \frac{P}{rk} / \left(\frac{\sin(\gamma)}{2\rho}(C + \frac{D^2}{C}) + \cos(\gamma)(\frac{AD}{C} - B) \right) \tag{5.29}$$

with the abbreviations

$$\begin{aligned} A &= 1 - \rho I_{v1}(\gamma) + \rho I_{v2}(\gamma) \\ B &= \rho I_{v1}(\gamma) + \rho I_{v2}(\gamma) \\ C &= \sinh(\rho\gamma)\cos(\rho\gamma) - \cosh(\rho\gamma)\sin(\rho\gamma) \\ D &= \cosh(\rho\gamma)\sin(\rho\gamma) + \sinh(\rho\gamma)\cos(\rho\gamma) \end{aligned} \tag{5.30}$$

The axial displacement of the column is defined as

$$\Delta z = 2\,u\big|_{\varphi=\gamma} - \frac{NL}{E_s A_s} \tag{5.31}$$

with E_s the elastic modulus of the strut and A_s the cross sectional area of the strut.

The axial compressive stiffness of the TSS is accordingly

$$k_c = \frac{P}{\Delta z} \tag{5.32}$$

With no detailed discussion considered necessary, a simple analytical expression for the axial stiffness of the TSS can be written as below given by Wever *et al*. (2010), following the similar procedure but using parabolic arch approximation

$$k_c = \frac{n}{8} k_f \frac{L}{2} (\frac{L}{d})^2 / \left(1 + \frac{k_f (\frac{L}{2})^2 (\frac{L}{d})^2}{4 E_s A_s} \right) \tag{5.33}$$

From Equations (5.31) and (5.32), the axial stiffness depends on the length to depth ratio L/d, the span L, the elastic stiffness of restraints k_f, as well as on the elastic modulus E_s and cross sectional area A_s of the strut.

5.2.1.2 Corotational model

An efficient and accurate locking-free beam finite element for the analysis of beams with small strains and large displacements are presented in Chapter 4. The general applicability and accuracy of the method and proposed procedure have been verified by a series of numerical examples. This corotational method is applied to the Tension Strip Columns with necessary adoptions as discussed in this section.

FE model with only one curved beam resting on elastic foundation cannot include the interaction effect between two struts connected by membrane, which is common for Tension Strip Columns with two or four struts. A spindle shape column with two arches connected at the tips as shown in Figure 5.2 is used instead of the model of only one arch as discussed in Chapter 4 with the attention to capture more accurate failure modes. In the model as shown in Figure 5.2, each strut is discretized with 16

elements and 17 nodes.

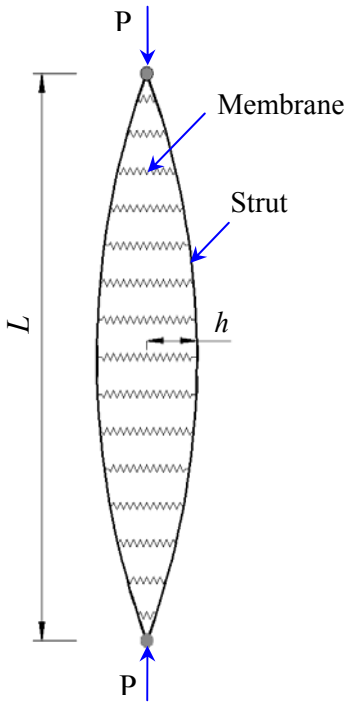

Figure 5.2: Corotational model for TSS with the whole loop with two struts.

Since the membrane can resist only tension force, it is necessary to model the behaviour of the cables with no compression resistance in order to capture the overall behaviour of Tension Strip Structures. In the present work, membrane is simulated using a series of axial spring elements with a force-extension relationship as shown in Figure 5.3. The axial spring element has negligible compressive stiffness; it is effective only when it is subjected to tension force.

Besides, both hinged and rigid joints at the tips can be modelled using the corotational method. In the former case, the internal moment at the tip is set to be 0 and the rotation at the boundaries is regarded as free. In the second case, the rotation at the boundaries is constrained.

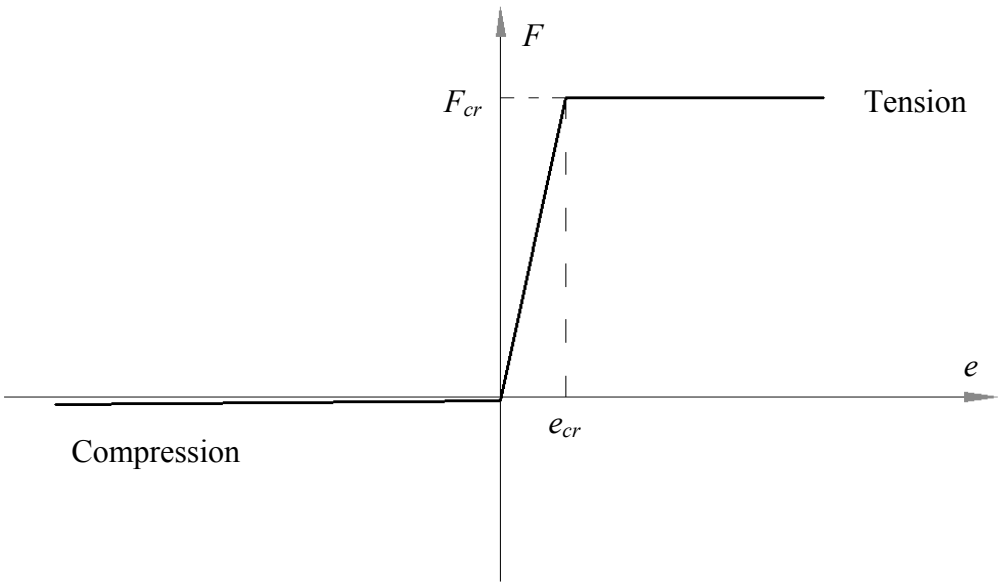

Figure 5.3: Force-extension relationship of membrane strip.

5.2.1.3 ABAQUS model

This numerical model is developed using the general purpose finite element (FE) software ABAQUS (2010). Figure 5.4 shows a typical finite element model for tension strip structures with more than two struts, while Figure 5.5 shows a finite element model for those with only two struts/strips.

All membrane and strips in Figure 5.5 are modelled by shell elements, while struts in Figure 5.4 are modelled by beam elements. ABAQUS offers several thin shell elements such as 3-node triangular and 4-node quadrilateral general purpose elements with full integration (S3, S4) and six degrees of freedom at each node as well as 4-node and 9-node reduced integration, thin-shell elements (S4R5, S9R5), with five degrees of freedom per node.

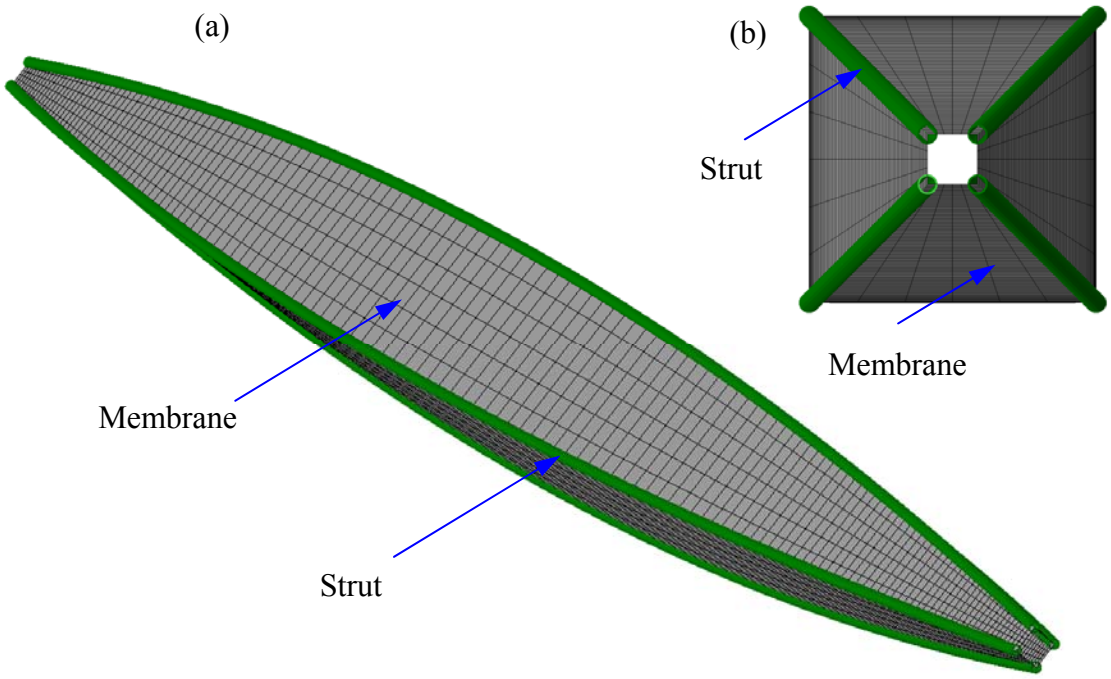

Figure 5.4: ABAQUS model of TSS with 4 struts: (a) isometric view; (b) plane view.

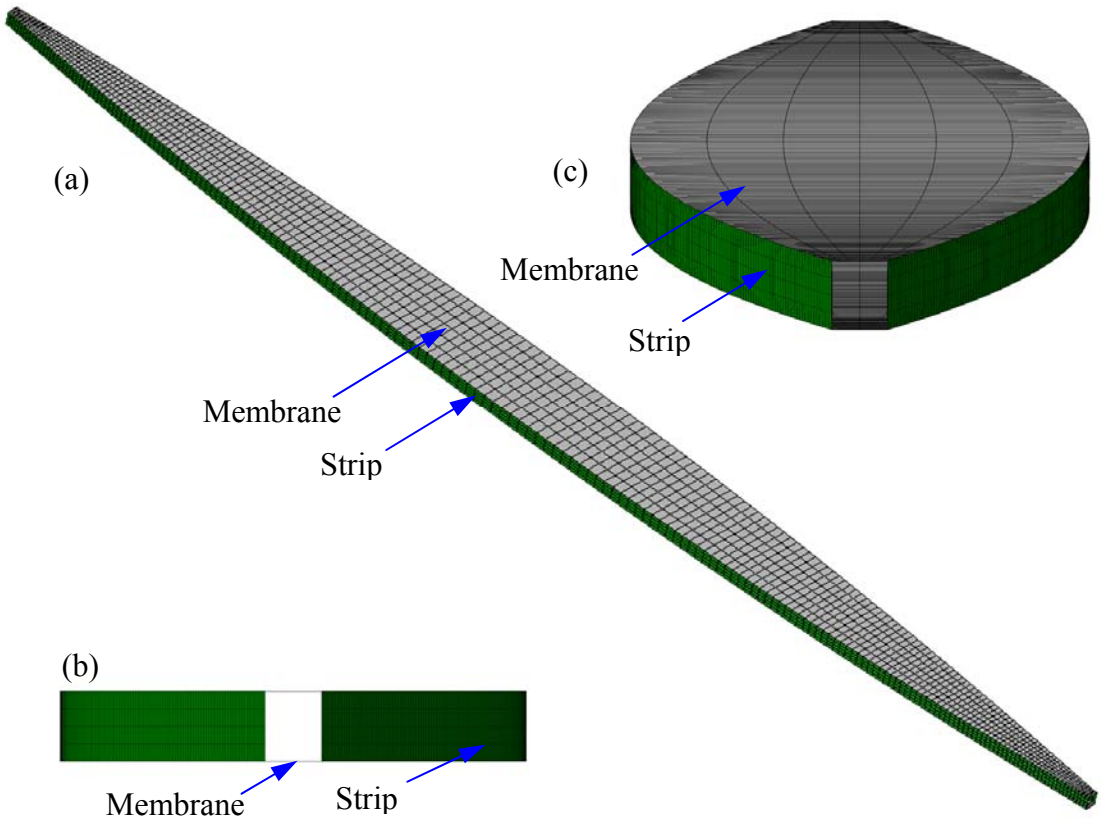

Figure 5.5: ABAQUS model of TSS with 2 struts: (a) isometric view; (b) plane view; (c) top back view.

The S3 element uses constant bending curvature and membrane strain approximations; therefore a very fine mesh is required to capture the bending deformation due to wrinkling. The formulation of element S4 is similar to S3 for bending, but the in-plane strain field has been enhanced to eliminate shear locking effects. Both S4R5 and S9R5 are thin shell elements with three in-plane translations and two in-plane rotation components. They use reduced integration with hourglass control to avoid shear locking. These elements are preliminary investigated by Wong and Pellegrino (2006), and both elements S4R5 and S9R5 are found to be fairly accurate and computationally more economical. In this work, all strips and membrane are modelled by 8-node quadratic shell element also with reduced integration. This element can provides for arbitrarily large rotation but small strains and the change in thickness with deformation is ignored in these elements. 3-node beam elements (B32) are used to model the struts, which also have quadratic geometric order.

Biased mesh is applied for both membrane and struts, being finer at the tips of the column and relatively coarse at the centre part. To avoid unstable solution and underestimation of the buckling load, coincident nodes rather than tie contact are modelled between strips/struts and membrane and are coupled in all nodal degrees of freedom except axial displacement in the element local coordinate system as suggested by Plagianakos *et al*. (2009).

The materials are taken to be linearly elastic-perfectly plastic with the Young's modulus, Poisson's ratio and yield stress being defined.

5.2.1.4 Model validation

The proposed corotational model has been verified against recently generated experimental results (Plagianakos *et al.*, 2009) in Chapter 4. In this section, the

analytical model, corotational model, and ABAQUS model as described previously are validated against each other by analyzing the same case.

Table 5.1: Material properties.

Material	Aluminium	Membrane (isotropic)
Elastic modulus (GPa)	68.80	3.46
Yield strength (MPa)	280	195
Poisson's ratio	0.3	0.4

In this case, a membrane strip column (referring to Figure 5.2 and Figure 5.5) with height (or span) of 6 m, width of 0.6 m, depth of 6 cm, strip thickness of 4 mm, and membrane thinness of 0.3 mm is analyzed. The column is constrained by a pin-roller boundary condition and subjected to axial compression load. The material properties for both membrane and strips are listed in Table 5.1. Overall, results for both stiffness and buckling load from all models agree well with each other except that the analytical model can only predict the stiffness.

It can be seen that the ABAQUS model predicts slightly higher stiffness than the other two models. This is due to two reasons: (a) membrane foundation in ABAQUS model is continuous along the struts, and (b) the shell element can still resist some compression forces even though the capacity is negligible for most cases. Although the analytical model is expected to predict lower stiffness because lowest modulus of elastic foundation is used along the column as discussed in Section 5.2.1, the result by this model is very close to that given by ABAQUS and almost same with that yielded by the proposed corotational method.

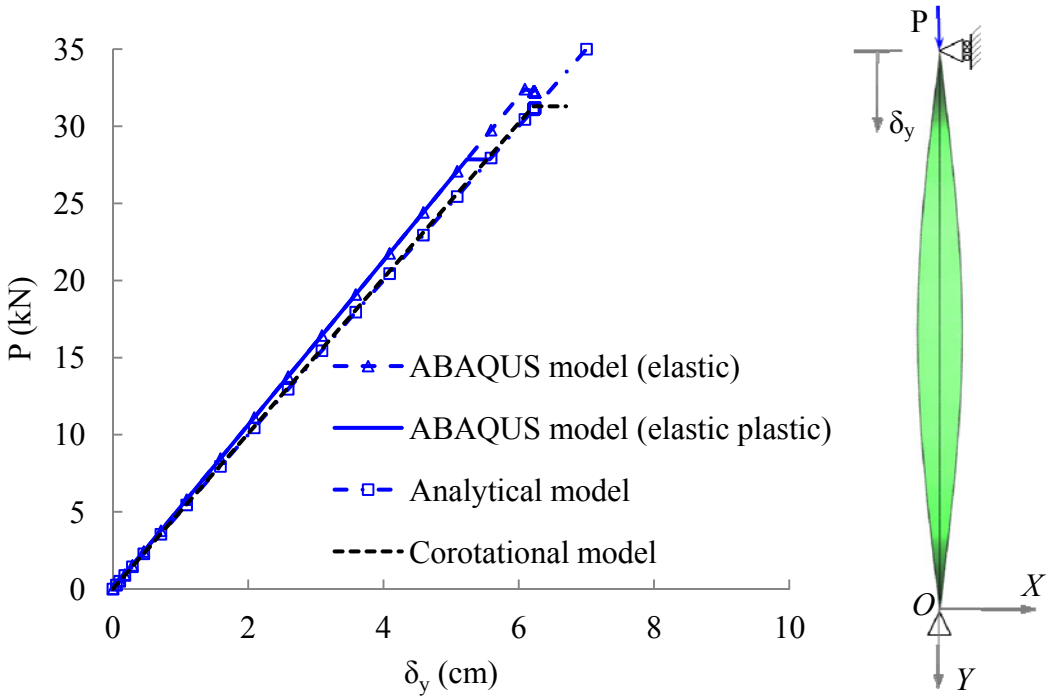

Figure 5.6: Load displacement curves of a TSS using different models.

The proposed corotational model can predict the buckling load well as compared to the results from ABAQUS model. The elastic plastic ABAQUS model yields slightly lower buckling load than the elastic ABAQUS model and the proposed corotational model because material nonlinearity is not considered in the last two models. It also shows that the effect of material nonlinearity is not significant because the strain in slender struts is small for TSSs.

It should be noted that mesh refinement convergence test is a precondition for analyzing any example in this work no matter which finite element model is utilized. With no detailed discussion considered necessary herein, an example for the proposed method can be found in Chapter 4, while the procedure to study the effect of mesh refinement in the ABAQUS model is the same with those given by (Plagianakos *et al.*, 2009).

In Section 5.2.1, three models for Tension Strip Structures are developed either

analytically or numerically, which are to be utilized in the next sections. The proposed corotational model is used to capture the buckling load for 2D problems, while the ABAQUS model is used to predict the buckling load when necessary. The analytical model based on the beam on elastic foundation theory given by Hetenyi (1946) is to be used to predict the stiffness of TSSs because of its simplicity and efficiency (a spreadsheet is enough) without significant accuracy lost.

5.2.2 Structural behaviour under axial compression

With these validated numerical models, a series of parametric studies is conducted. The aim is to investigate the influence of varying key parameters on the static system behaviour: the length to depth ratio L/d, the length of the columns, the elastic stiffness of restraints (k_f), and the cross sectional resistance of the struts, etc.

5.2.2.1 Stiffness

The work by Wever *et al*. (2010) reveals that the axial stiffness of the Tensairity column does not depend on the bending stiffness of the compression element, but strongly depends on the length to depth ratio of the column as given in Equation 5.34. Similarly, the length to depth ratio also plays an important role on the stiffness of Tension Strip Columns. Besides, other parameters such as height, the elastic stiffness of restraints as well as cross sectional resistance of the struts also influence the stiffness of the column. All these parameters are routed out into several groups and the effect of them are investigated as follows.

The combination effect of length to depth ratio and the elastic stiffness of restraints is investigated first. The height of the column is 6 m and the thickness of the membrane

is 3 mm. Three types of Tension Strip Columns are investigated: the column with 2 struts, the column with 3 struts, and the column with 4 struts. The total cross sectional area of struts for all columns remains same, i.e. 60 mm x 4 mm, 40 mm x 4 mm, 30 mm x 4 mm, respectively for each strut in these columns.

The length to depth ratio ranges from 2 to 40 for this study. For cases where length to depth ratio is higher than 20 the stiffness refers to the initial loading stage when no significant shape change happens due to any premature buckling, i.e. the deflected struts remain an arch shape.

Lower length to depth ratio leads to large difference in the elastic stiffness of restraints (k_f) along the length of the column, which leads to potential larger deviation. The simplified analytical model is validated herein against the proposed method to evaluate the deviation caused. A 2-strut column is considered with the same material and geometrical properties given in the previous paragraph and the elastic modulus of membrane is 0.353 GPa.

Figure 5.7 shows the curves of normalized stiffness against length to depth ratio obtained by the analytical model and by the proposed corotational model, respectively. The normalized axial stiffness (k_{norm}) is defined as

$$k_{norm} = \frac{k_c}{k_{lim}} \tag{5.34}$$

where k_{lim} is the elastic limit as given below.

$$k_{lim} = \frac{nE_s A_s}{L} \tag{5.35}$$

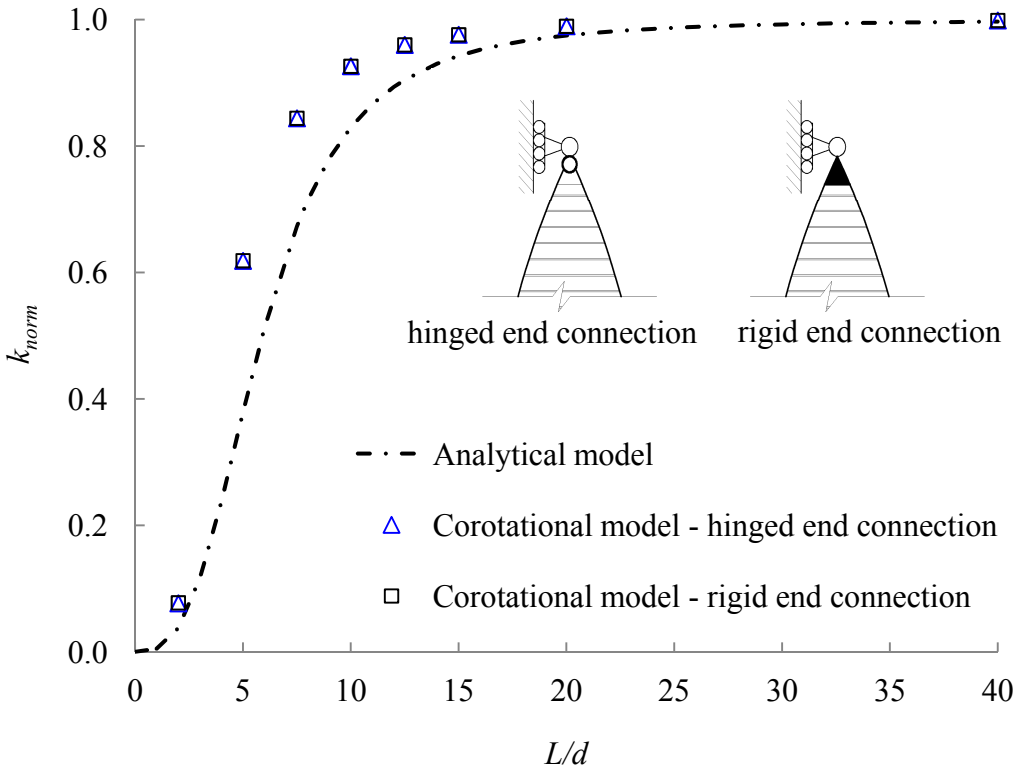

Figure 5.7: Normalized stiffness versus length to depth ratio by the analytical model showing comparisons against the proposed corotational model.

The proposed method can predict the normalized stiffness for two types of TSSs: one with hinged end connections and the other with rigid end connection. The analytical model, however, predicts only the type with hinged end connections.

The normalized stiffness for TSSs with hinged end connections is discussed first. The stiffness prediction of such structures by the simplified analytical model experiences large deviation compared with that obtained from proposed numerical model when the length to depth ratio is low. As can be seen from Figure 5.7, the normalized stiffness value predicted by the simplified analytical model is 50% of that predicted by the proposed method when length to depth ratio is 2.0. Nevertheless, the difference between the predictions by these two models dramatically decreases as the length to depth ratio gets higher. The deviation is within 20% when the length to depth ratio

reaches 7.5 and the trend continues. As the length to depth ratio reaches 20, no obvious difference can be observed. Besides, the curve of normalized stiffness to L/d obtained from the analytical model share the same pattern with those from the proposed method. Thus, the analytical model can be used to predict the stiffness for parametric studies.

Figure 5.7 also shows results predicted by proposed method for the case where rigid end connections are adopted at the tip of the TSSs. No clear difference is observed between these two cases especially for slender columns because of the effect of membrane restraints. Therefore, only hinged end conditions are studied in the further analyses.

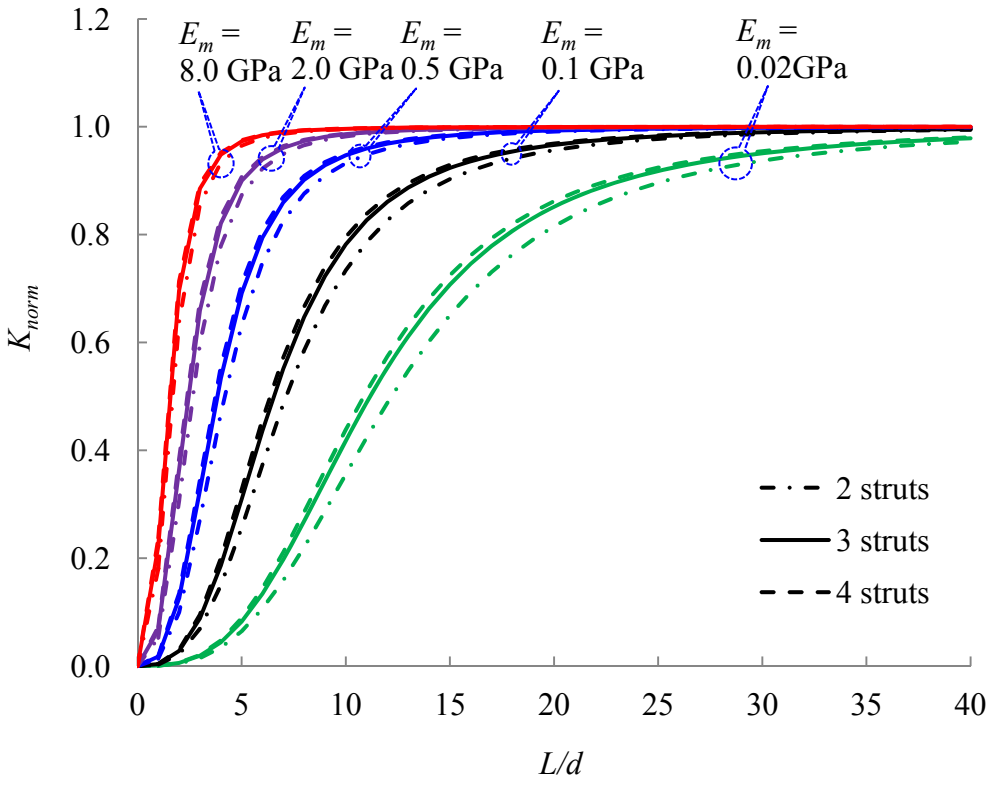

Figure 5.8: Normalized stiffness versus length to depth ratio for varying foundation modulus.

Figure 5.8 shows the normalized stiffness versus length to depth ratio for 3 types of

Tension Strip Columns with varying elastic modulus of membrane (k_f) from 0.02, 0.1, 0.5, 2, to 8 GPa with the intention to cover the commonly used architectural membrane. As can be seen, the stiffness increases as the length to depth ratio increases. The stiffness also gets higher when the elastic stiffness of restraints gets higher. The stiffness can reach 80% of the elastic limit at a L/*d* ratio not lower than 10 when the elastic modulus of membrane is higher than 0.1 GPa for the given columns. For higher length to depth ratio of the given column with a higher elastic stiffness of restraints, the axial stiffness eventually reaches the limit of the material elasticity. For the cases with an elastic modulus of membrane higher than 2 GPa, this limit is almost reached even with a length to depth ratio as low as 5.

For all cases, a 4-strut column has the highest stiffness, while a 2-strut column has the lowest stiffness. Equation (23) relates the elastic stiffness of restraints for TSS to the number of the strut with the assumption that all struts in the column share the same axial load distribution.

Equation (5.23) gives the elastic stiffness of restraints by membrane. The coefficient of elastic stiffness of restraints for each strut and the column can be written as Equation 5.36 and Equation 5.37, respectively.

$$\text{For struts, } c_{kfs} = 2\cos\left(\frac{(n-2)\pi}{2n}\right) \quad for\ n = 2,3,4,... \tag{5.36}$$

$$\text{For column, } c_{kfc} = 2n\cos\left(\frac{(n-2)\pi}{2n}\right) \quad for\ n = 2,3,4,... \tag{5.37}$$

Figure 5.9 shows that the coefficient of Equation (5.23) for a column with more struts is higher although the coefficient is lower for each strut when the number of struts

increases. This indicates the stiffness is higher for columns with more struts than those with fewer struts. In Figure 5.9, the number of struts ranges from 2 to 6. However, too many struts in TSSs make the joint very complex, which limits the application of Tension Strip Structures with more than 4 struts for civil engineering. Therefore, only TSSs with 2, 3, and 4 struts are investigated in this work.

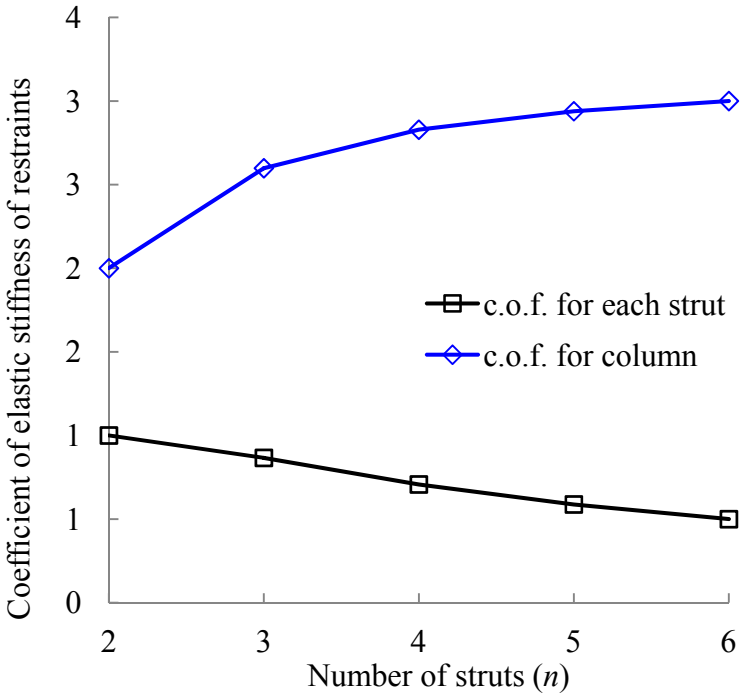

Figure 5.9: Coefficient of membrane foundation versus the number of struts.

Secondly, the effect of cross sectional resistance of the struts on the axial stiffness of the structure is studied. The length to depth ratio is fixed as 15, while other geometrical or dimensional parameters remain same as the previous case. A series of membrane with elastic modulus ranging from 0.02, 0.1, 0.5, 2, to 8 GPa is also included in this case. The variation of the cross sectional resistance of the struts is controlled by changing the elastic modulus. Constant cross sectional geometries are chosen to be compact and therefore no local buckling is considered necessary.

Figure 5.10 depicts the normalized stiffness against different elastic modulus of the

struts varying from 10 GPa to 1000 GPa with the intension to cover not only commonly used materials in civil engineering, i.e. aluminium alloy, steel, etc. but also materials used in military and aerospace industries. It shows the normalized stiffness decreases when the elastic modulus of struts increases for given elastic stiffness of restraints. It should be noted that the absolute value of the stiffness is getting larger and larger as the stiffness of struts increases. The normalized stiffness decreases due to the elastic limit of the stiffness for the column increases, indicating the efficiency of the material use can get lower even if stronger struts are used for given elastic stiffness of restraints.

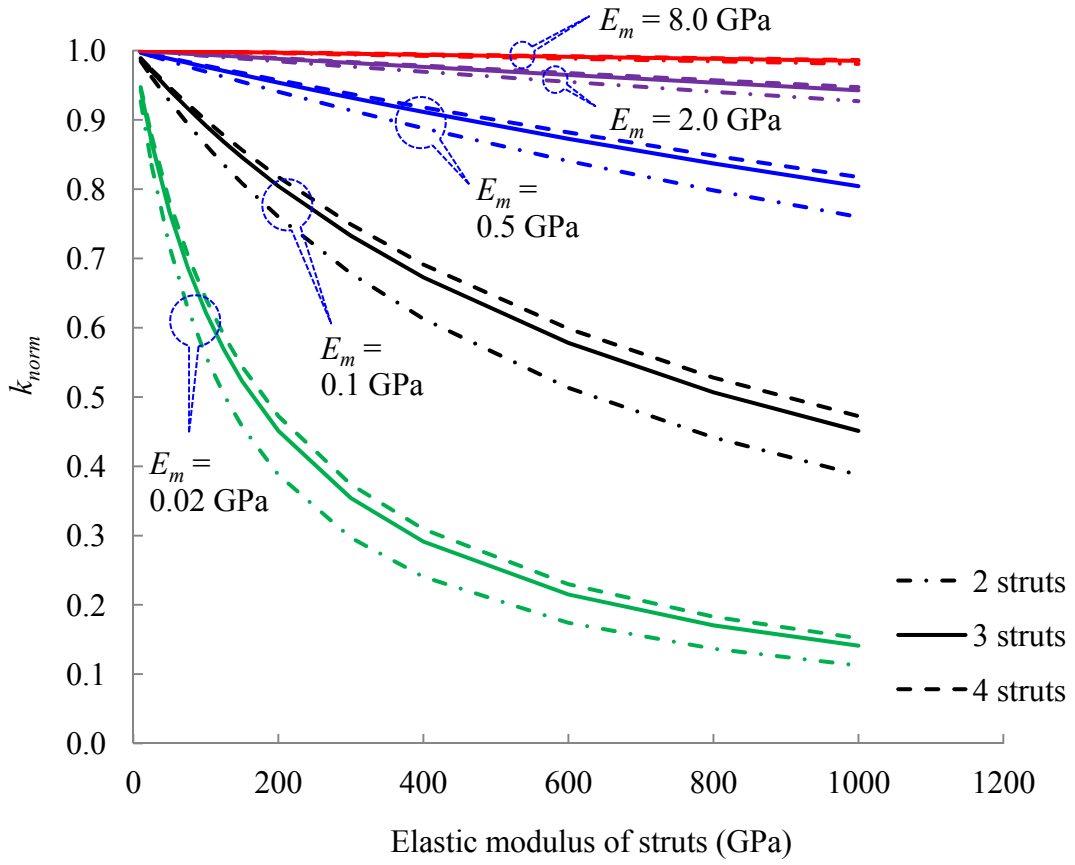

Figure 5.10: Normalized stiffness versus cross sectional stiffness.

As can be seen from Figure 5.10, increasing the elastic stiffness of restraints can improve the material use efficiency for the struts in terms of the stiffness for Tension Strip Columns under axial load. All columns investigated with E_m higher than 0.5 GPa possess high normalized stiffness (0.8 at least).

Thirdly, Figure 5.11 depicts the normalized stiffness of the Tension Strip Column against the length. In this case, the length to depth ratio keeps as 15 as well. The normalized stiffness increases as the length increases as shown in the figure, although it is known that the absolute stiffness decreases. However, the stiffness almost reaches the limit of the material elasticity for a small height of 0.5 m when the elastic modulus of membrane reaches 0.5 GPa.

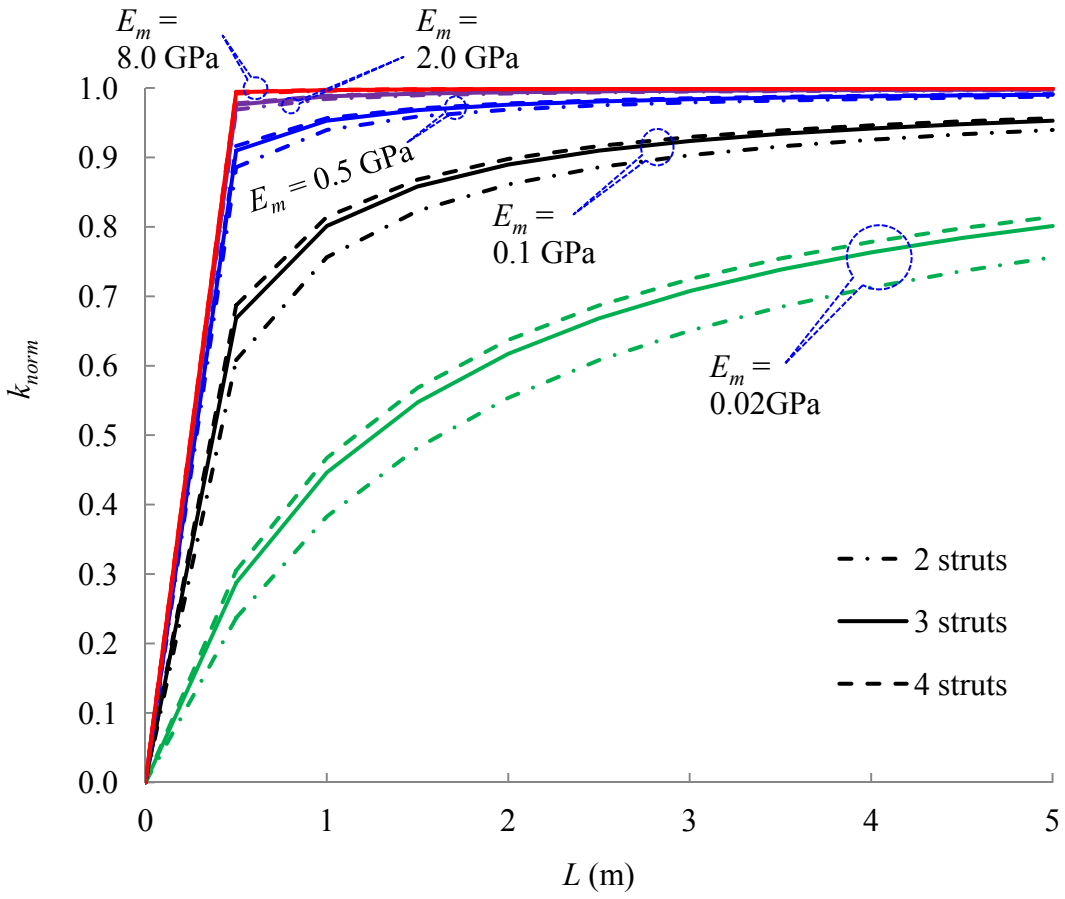

Figure 5.11: Normalized stiffness versus length.

In summary, the normalized stiffness of Tension Strip Structures increases with an increase of length to depth ratio, cross sectional resistance of struts, elastic stiffness of the restraints, and length with the condition that other parameters remain the same. However, these conclusions are based on the assumption that the struts in TSS keep the similar form to the initial status. The struts in the TSS are prone to experience first mode buckling in the reverse direction (i.e., the strut moves inward) when the length to depth ratio is higher than 20. In such cases, the stiffness during the whole compressive phase may be lower even though the stiffness at the very beginning is still high.

5.2.2.2 Critical load

Failure modes regarding Tension Strip Columns are discussed as follows. The discussion focuses on the failure or instability of main structural components such as struts and membrane. Other failure modes relating to the connection between the struts and membrane or the joints, however, are not included. Three types of failure modes are summarized as follows.

Under the stresses induced by axial compressive forces the membrane may fail by direct tensile failure. The peak tensile stress and the likely site for this failure mode to initiate are at the centre of the membrane. This failure mode (failure mode I) normally results in deteriorated tearing failure of the membrane and the consequential buckling failure of the struts in the first buckling mode. In failure mode I as shown in Figure 5.12(b), the membrane fails to provide sufficient restraints to the struts.

In failure mode II as shown in Figure 5.12(c) and failure mode III as shown in Figure 5.12(d), the struts together with the membrane experience a global buckling as a

whole. Failure mode II refers to TSSs with pin-roller boundary conditions and Failure mode III refers to TSSs with fixed boundary conditions. The curved struts are over-restrained in these failure modes. These are similar to the failure modes of conventional straight columns except that the first buckling mode of conventional straight column does not happen herein because of the initial spindle geometry of TSS. Figure 5.12 shows only the failure modes of Tension Strip Structures with 2 struts. Those with more struts have the similar failure modes to these structures.

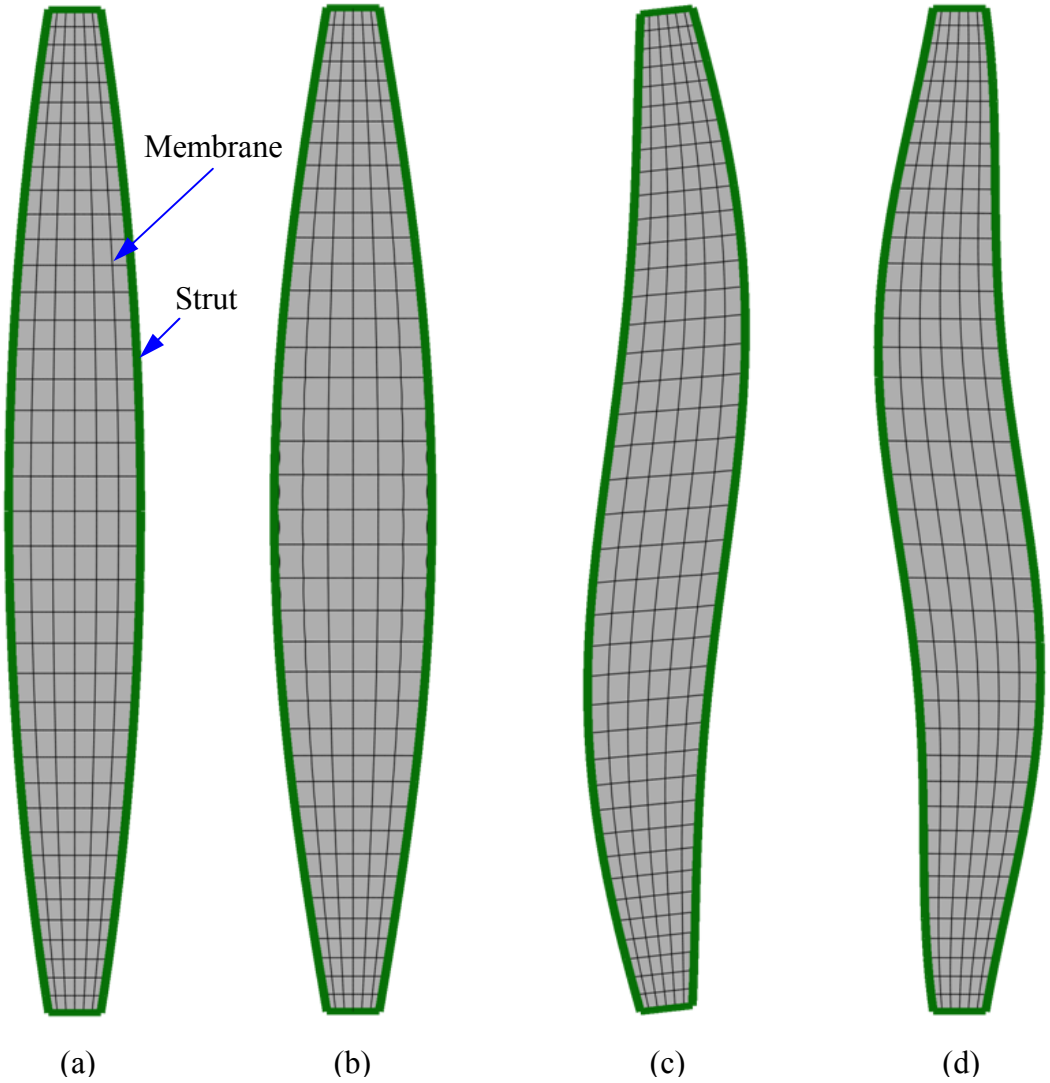

Figure 5.12: Failure modes of TSSs: (a) initial shape; (b) Failure mode I; (c) Failure mode II(pin-pin); (d) Failure mode III(fixed-fixed).

As far as the buckling of Tension Strip Structures is concerned, the effects of elastic stiffness of restraints, cross sectional resistance of struts, and length to depth ratio should be taken into account. Only global buckling modes are considered in this work, with the cross sectional properties of the struts chosen such that elastic local buckling, which is beyond the research scope of the present study, does not occur. Geometrically nonlinear analyses are conducted with the numerical method presented in Chapter 4 to obtain the ultimate load-carrying capacity and the corresponding buckling modes accordingly, for 2-dimensional problems.

In the first case, the effects of both length to depth ratio (L/d) and the elastic stiffness of restraints (k_f) on the buckling load are investigated. Same configurations and material properties in the first case of last section are used for the current study except that the elastic modulus of membrane varies from 0.02, 0.05, 0.1, 0.2, to 0.5 GPa. A normalized buckling load ($P_{bk,norm}$) is defined as the ratio of the buckling load (P_{bk}) divided by the cross section resistance (P_y) driven by the yield strength of the strut as given in Equation 5.38. In this case, the strut with a yielding strength of 270 MPa is taken as an example, which is a representative value for commonly used aluminium alloys.

$$P_{bk,norm} = \frac{P_{bk}}{P_y} \tag{5.38}$$

Figure 5.13 depicts curves of normalized buckling load versus length to depth ratio with different elastic modulus of membrane. Figure 5.13 shows that increasing the length to depth ratio increases the buckling load and increasing elastic modulus of membrane increases the buckling load as well. The normalized stiffness versus length

to depth ratio curves show higher slopes as the elastic of membrane increases. For instance, the buckling load of a column increases by 0.066 when the length to depth ratio increases from 5 to 20 for the case where the elastic modulus of membrane is 0.02 GPa. This value is 0.355 when the elastic modulus of membrane is 0.5 GPa.

The buckling response of a Tension Strip Column subjected to axial compression force is governed by first mode when the elastic stiffness of restraints is low. In Figure 5.13, the solid triangular markers locating at the left bottom corner suggest the column experience first mode buckling. When the elastic stiffness of restraints increases higher buckling mode begins to govern the load bearing capacity of the column.

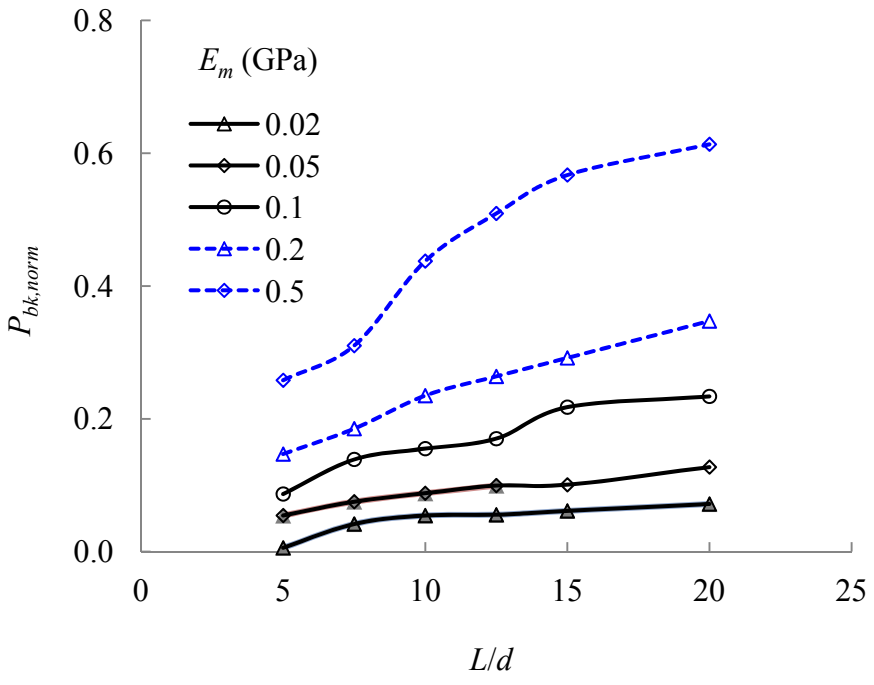

Figure 5.13: Normalized buckling load versus length to depth ratio.

The effect of the cross sectional resistance of struts on the critical load of Tension Strip Column is investigated using the same configuration except that the length to depth ratio remains 10 for all columns. The elastic modulus of membrane is varied as

0.05, 0.1, 0.2, 0.5, 1, to 2 GPa in this case. The cross sectional areas of the struts vary as 10x6, 20x6, 30x8, 45x8, 60x8, 90x8, 120x10, and 120x16 mm^2. The elastic modulus of the strut remains the same at 68 GPa.

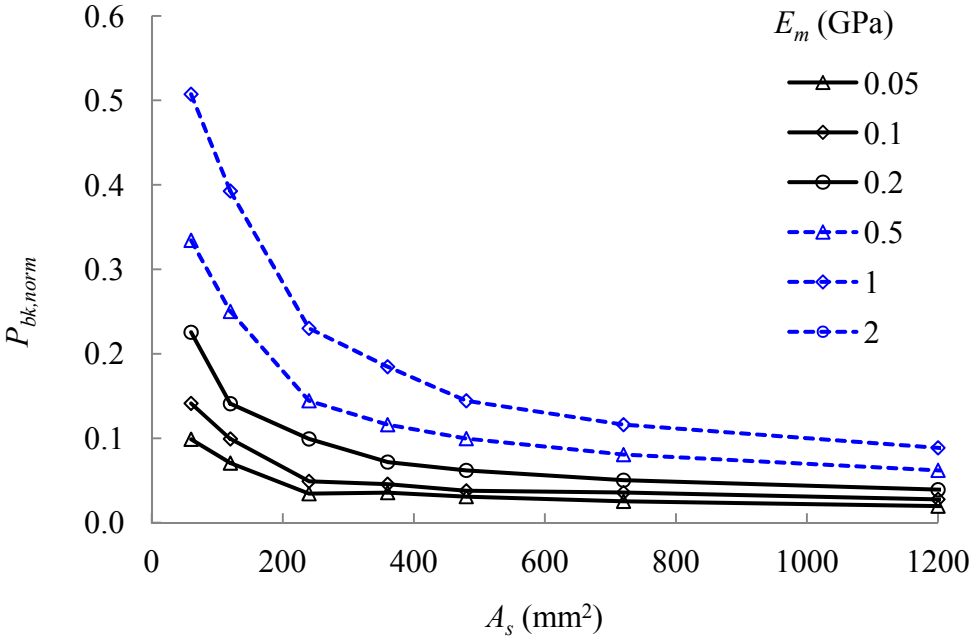

Figure 5.14: Normalized buckling load versus cross sectional resistance of struts.

The results shown in Figure 5.14 verify that the normalized buckling load increases as the elastic stiffness of restraints increases. For a given elastic modulus of membrane, the normalized buckling load decreases while the elastic modulus of the struts increases. The columns located at the left top corner have the relatively high normalized buckling load. The columns with stiffer struts (i.e. larger cross sectional areas) possess low normalized buckling load. For instance, if the area of the strut is higher than 200 mm^2 the normalized buckling load of all TSS columns analyzed is lower than 0.3. Higher elastic stiffness of restraints with lower cross sectional area is preferable for TSS columns in terms of normalized buckling loads. The tension strip columns with high elastic modulus of the strut and low elastic stiffness of restraints experience first mode buckling, which is same with what is discussed in previous

paragraphs in this section. The columns with relatively low elastic modulus of the strut and high elastic stiffness of restraints are limited by the high order buckling mode.

5.2.3 Structural efficiency

The study of structural efficiency in terms of strength to weight ratio is carried out by two case studies. In the first case study, the axial load capacity of a tension strip column is compared with a CHS tube (D = 80 mm and t = 2 mm) subject to a compressive axial load as shown in Figure 5.16.

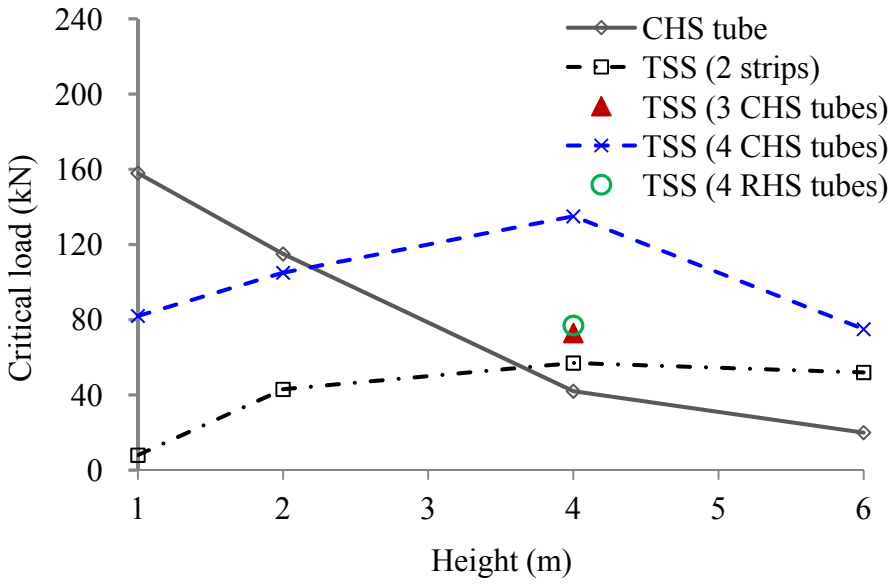

Figure 5.15: Ultimate load comparisons.

With the same depth of the middle section, different models in Figure 5.16 with various lengths ranging from 1 m to 6 m are analyzed and compared for Tension Strip Structures with different struts as shown in Figure 5.15. Moreover, in order to evaluate the effect of number and section shape of the tubes, two other Tension Strip Structures sharing the same height of 4 m but with different cross sections: 3 CHS tubes and 4 RHS tubes are also studied.

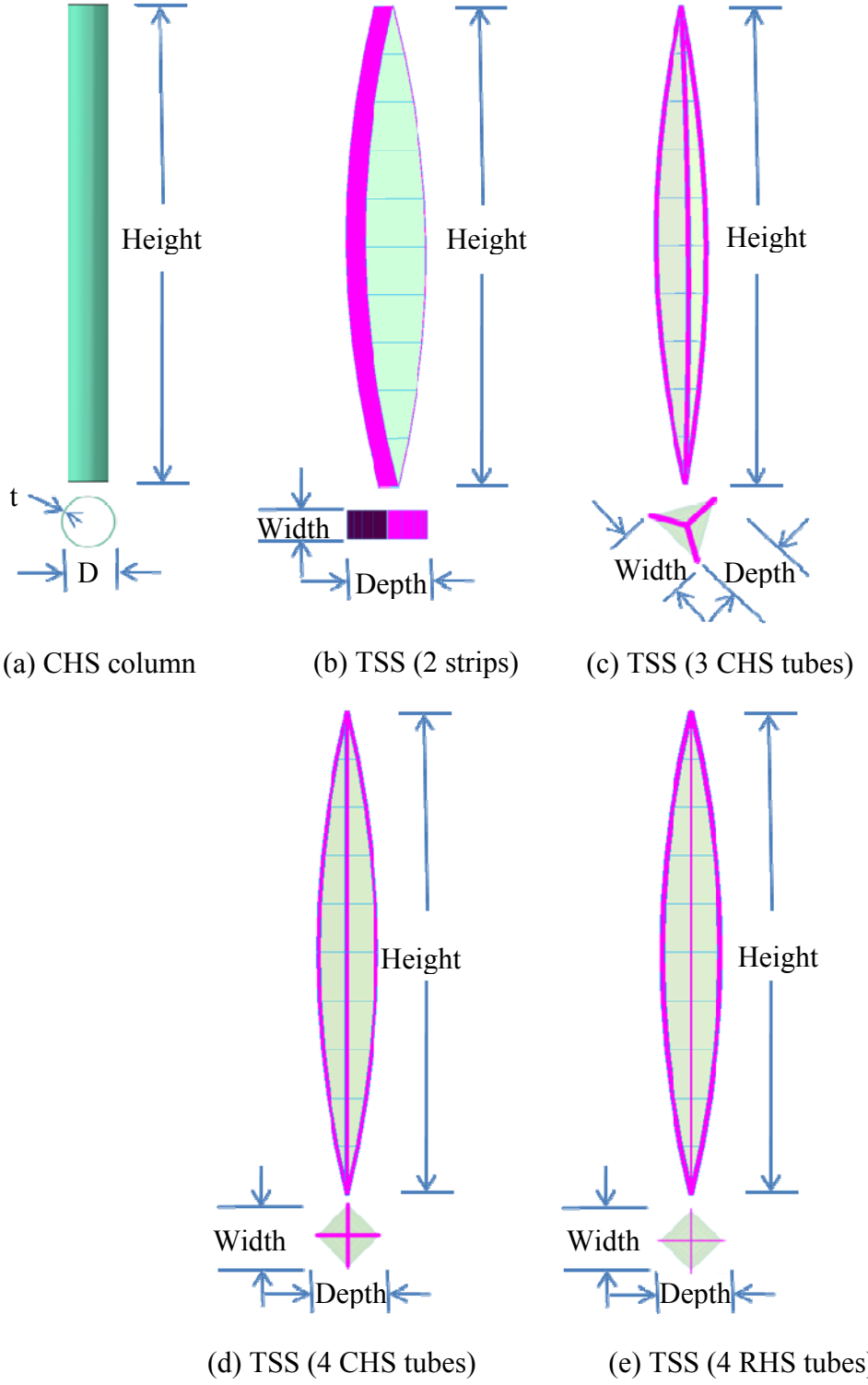

(a) CHS column (b) TSS (2 strips) (c) TSS (3 CHS tubes)

(d) TSS (4 CHS tubes) (e) TSS (4 RHS tubes)

Figure 5.16: Configuration definitions of Different TSSs and a tube.

The structural weight of all membrane restrained systems shown in Figure 5.16 remains the same as the single CHS member (with outer diameter of 80 mm and thickness of 2 mm). For simplicity, the weight of the membrane and cable is ignored

due to their negligible weight. Detailed parameters of these models used herein are listed in Figure 5.17.

Models	Name	Forms	Geometry Description
1	TSS (2 strips)	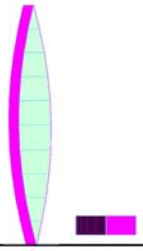	Thickness of Membrane 0.5 mm Thickness of Strips 4.0 mm Depth 60 mm Width 400 mm Heights 1, 2, 4 & 6m
2	TSS (3 CHS tubes)	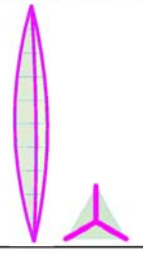	Thickness of Membrane 0.5 mm Outer Diameter of Tubes 25 mm Thickness of Tubes 2.1 mm Depth 346 mm Width 400 mm Heights 4m
3	TSS (4 CHS tubes)	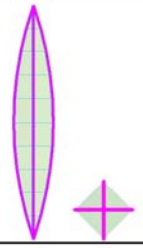	Thickness of Membrane 0.5 mm Outer Diameter of Tubes 20 mm Thickness of Tubes 2.0 mm Depth 400 mm Width 400 mm Heights 1, 2, 4 & 6m
4	TSS (4 RHS tubes)	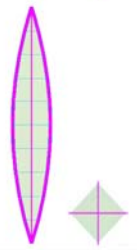	Thickness of Membrane 0.5 mm Height of Box 26 mm Width of Box 6 mm Thickness of Box 2 mm Depth 400 mm Width 400 mm Heights 4m

Figure 5.17: Details of different TSSs.

As shown in Figure 5.15, for shorter columns of length 2 m and 1 m, there is no advantage for membrane strips or membrane tubes in terms of compression resistance. However, the axial resistance of both membrane strips and membrane tubes is much higher than that of a single tube when the length is taken 4 m and 6m. The length to depth ratio for the ordinary tube of 6 m is higher than 150. This quantifies the potential of Tension Strip Structures for being used as compressive members instead

in cases when high length to depth ratio (>100) of CHS tubes is required.

In the second case study, the structural efficiency of TSS in terms of the strength to weight ratio has also been compared to other two column systems available in the literature (Plagianakos *et al.*, 2009). As shown in Figure 5.18, all of these three column systems to be compared are in a spindle shape: (a) Tension Strip Structure; (b) Tensairity column; and (c) truss column. Three struts with the same cross section: 30 mm x 10 mm are used in both TSS column and Tensairity column. In the Tensairity column, a membrane hull with an internal air pressure of 250 mbar is connected to three struts.

In the truss column, diaphragms are equally located along the length to transfer axial forces and bending moments. The elements in the truss have the equal inertia moment (case 1) or an equal area (case 2) to the rectangular struts. Figure 5.19 compares the load-axial displacement curve of a truss with four or five diaphragms for both cases to the Tensairity column and the TSS column. The displacement values for TSS column and truss columns are shifted to the main compressive region of the Tensairity column for explicit comparison. The total weights for both TSS column and Tensairity column are 16.2 kg, where 12.8 kg are the three struts plus end joints and 3.4 kg the hull plus the connection. The total weights of the truss columns with 4 and 5 diaphragms are 16.5 kg and 17.2 kg, respectively.

Figure 5.19 shows TSS column has the similar stiffness to the truss columns with 5 diaphragms, which is higher than the Tensairity column and the truss columns with 4 diaphragms. TSS column shows significant improvement on the buckling load compared with the other column systems. In addition, the TSS column, similar to

Tensairity column, has a compact transportation or storage volume with a rapid deployment on site. This is another advantage over the conventional truss column systems.

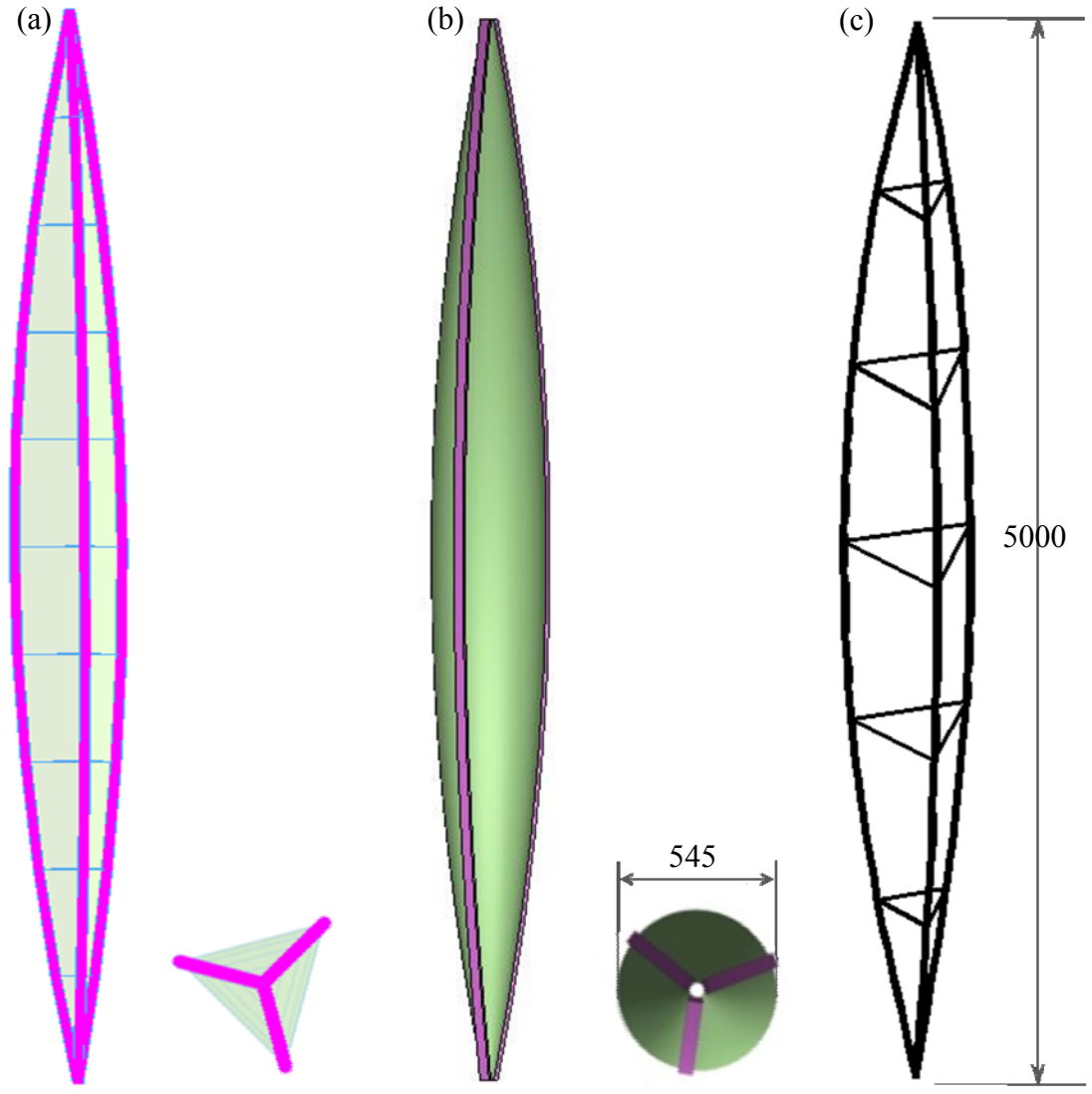

Figure 5.18: Main dimensions of three column systems to be compared: (a) TSS column; (b) Tensairity column; and (c) truss column (unit: mm).

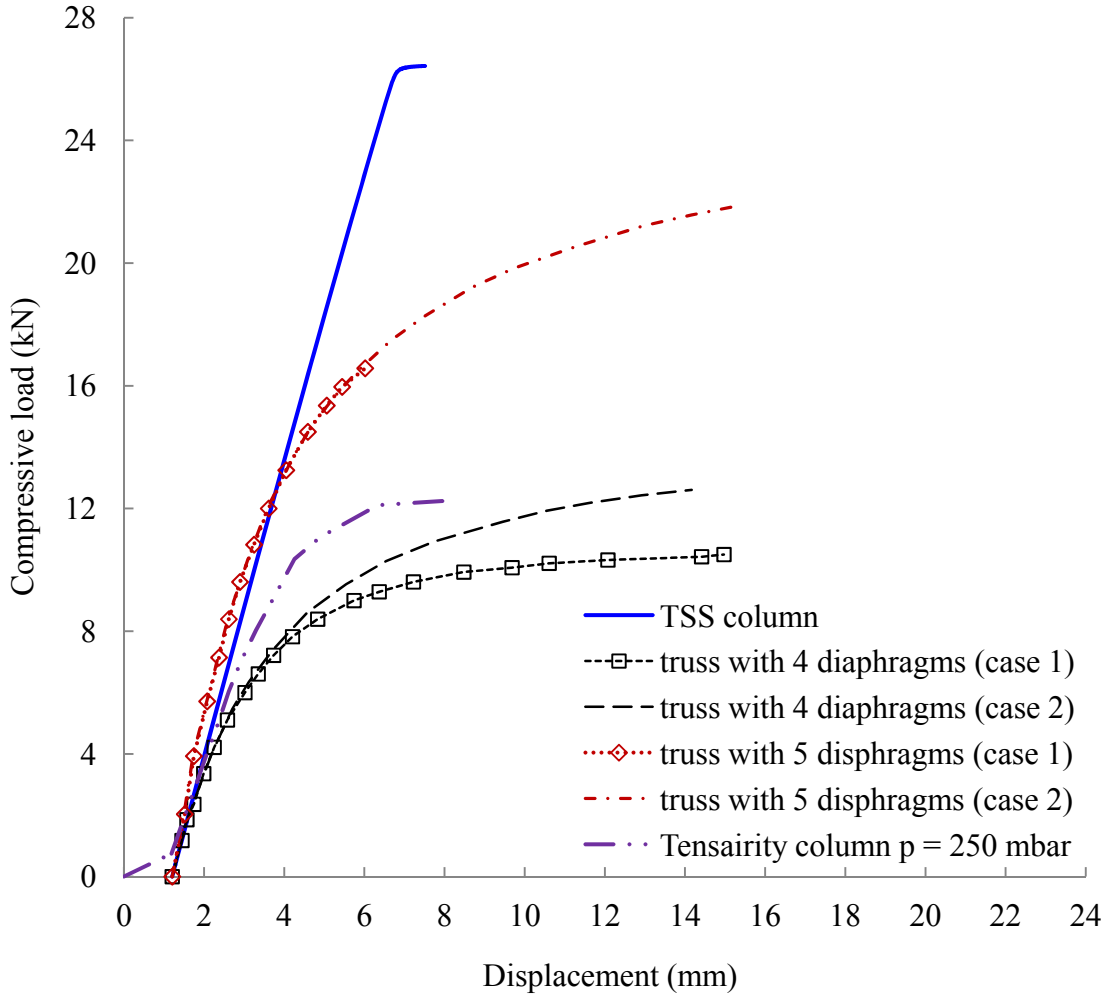

Figure 5.19: Load-displacement curves of TSS column, Tensairity column, and a series of truss columns.

5.3 Deployable Cable Chain Structures

5.3.1 Load-displacement behaviour

Advanced analysis for the design of steel frames has been under intense development during the last two decades, by Chan and Zhou (1995), Kim and Chen (1996), and (Chan and Gu, 2000), among others. Liew and his colleagues (2001; 2000) developed an advanced inelastic analysis for the design of three-dimensional cable strut and space frame structures. The main feature of the advanced analysis program is to use

one element per member to model each structural component and to obtain a realistic representation of member load-displacement behaviour at the pre- and post-buckling regions.

The analysis operates on element stress resultants, i.e., forces, bi-moments and torsion. The beam–column is subject to end forces acting on three transitional and three rotational degrees of freedom at each end node. The effects of large displacements and coupling between lateral deflection and axial strain are included by using nonlinear strain relations. The elastic tangent stiffness matrices are calculated from closed form expressions, with no numerical integration over the element cross section or over the element length. They contain the influence of axial force acting on lateral deformations of the member ($P-\delta$ effect). The detailed formulation of the three-dimensional inelastic beam–column is reported in the study by Liew and Tang (2000) and will not be repeated herein.

For tension members, the axial load–elongation relationship is obtained based on the bilinear elastic–plastic stress–strain curve of the material. The axial load–deformation relationships obtained for the strut and tie elements model the large displacement inelastic behaviour of an axially loaded member. By selecting an appropriate member initial out-of-straightness magnitude, the ultimate strength of an axially loaded member calculated from the advanced analysis matches the Eurocode 3 column strength, and hence no separate check is required for member stability and strength. A detailed description of the strut and tension element models for advanced inelastic analysis of space frame structures can be found in Liew et al. (2001).

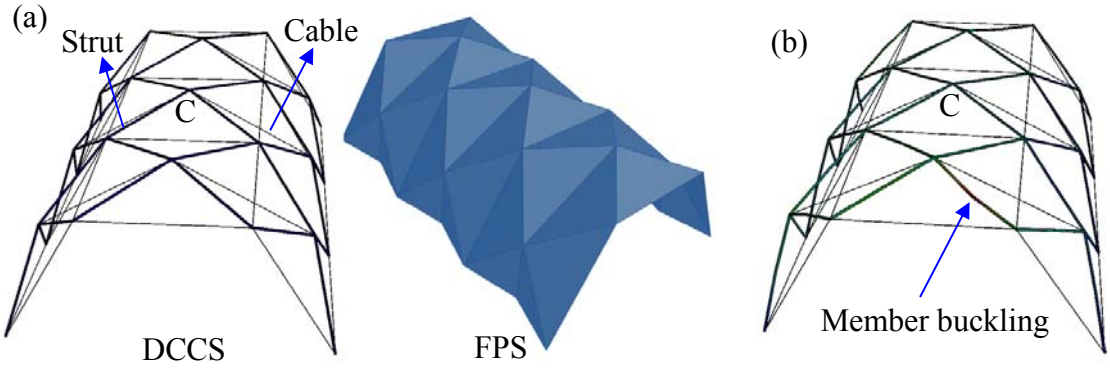

(a) Initial shapes of DCCS and FPS (b) Deformed shape of DCCS at ultimate load

Figure 5.20: Analysis model of a barrel vault.

Figure 5.20(a) shows the basic model, in which the thick lines indicate struts and thin lines represent the cables. The cables are modelled as tension elements while the struts are models as beam elements. The base supports are assumed to be pinned to the ground. Struts are made of circular tubes of diameter 50 mm and thickness 2 mm with design strength 275 N/mm^2 and modulus of elasticity 205000 N/mm^2. Cables are high strength strands of diameter 9 mm with breaking stress 1950 N/mm^2 and modulus of elasticity 195000 N/mm^2.

The structure is subject to a uniformly distributed dead load (*DL*), contributed by self-weights of structural elements: struts, cables, and covering surface (0.2 kg/m^2). Imposed load (*IL*) of 0.75 kN/m^2 is assumed in the preliminary design. Pretension force of about 30% of minimum breaking load (*MBL*) of the cable is introduced to the cables to increase the initial stiffness of the entire structure. Wind load (*WL*) computed using EN 1991-1-4 (2005) with basic wind velocity of 20 m/s as suggested in Singapore National Annex(2009). The wind load direction and net pressure on outside surface of the barrel vault is shown in Figure 5.21. In this stage it is not possible to estimate the permeability and openings in the shelter. So internal wind

pressure coefficient, Cpi , should be taken as the more onerous of -0.3 and +0.2. A horizontal notional load (HNL) of 0.5% of the factored reaction at the base is applied on the top nodes. Non-uniform imposed loading case is also investigated. In this study, it is assumed that only the right side of the barrel vault is subject to imposed load of 0.75 kN/m^2. All loads are applied as nodal loads.

The following six factored load combinations suggested by Eurocode (2002) are considered in the nonlinear analysis:

$$\begin{aligned}
&1.\ 1.35DL + 1.5IL + HNL \\
&2.\ 1.35DL + 1.5IL + 0.6 \times 1.5WL(Cpi = -0.3) \\
&3.\ 1.35DL + 1.5IL + 0.6 \times 1.5WL(Cpi = +0.2) \\
&4.\ 1.35DL + 0.7 \times 1.5IL + 1.5WL(Cpi = -0.3) \\
&5.\ 1.35DL + 0.7 \times 1.5IL + 1.5WL(Cpi = +0.2) \\
&6.\ 1.35DL + 1.5IL(nonuniform) + HNL
\end{aligned} \tag{5.39}$$

The most critical load combination is load case 2, in which the top struts at the ends are the most critical members that govern the failure of the system.

The curve shown in Figure 5.22 represents the relation between the deflection of the top centre node “C” after pre-stress phase and the load level which is defined as

$$Load\ Level = \frac{Applied\ Load}{Factored\ Load} \tag{5.40}$$

This curve is separated by the point ③ into loading and unloading phases. In the first phase, the top centre node “C” firstly moves downward linearly under the applied load until the load level reaches 1.0. Several cables then slacken, and the overall stiffness of the structure reduces gradually until the load level reaches 1.4. The structure reaches its maximum load resistance when a strut buckling occurs. The maximum load obtained from the analysis is about 1.65 times of the factored load.

The deformed shape of the structure is shown in Figure 5.20(b), which indicates that the top struts at the end of the vault have buckled. Generally, the curve in the loading phase suggests the proposed structure behaves in a linear manner even when some cables slacken. The gradually reduced slopes indicate that the status of the cable is important to the stiffness of the whole structure and has direct effect on the performance of the presented structure. Besides, it is worthwhile to note that the end struts are the most critical. The reason is that only two struts are connected to the end nodes compared with the internal nodes where four struts are connected.

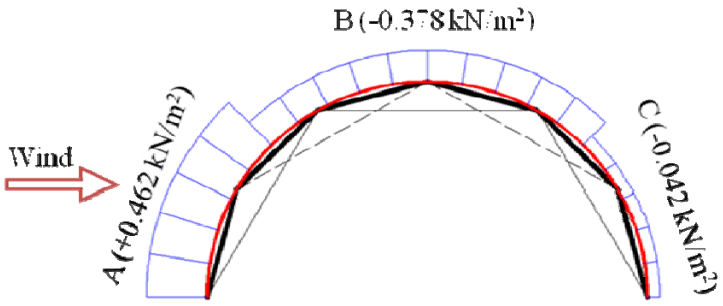

Figure 5.21: Wind load on barrel vaulted roof (Load case 2).

After the buckling of an end strut, as shown in Figure 5.22, the structure enters the unloading phase. The equilibrium of the system cannot be maintained and the external load has to be reduced to obtain a new equilibrium configuration. At this stage, a displacement control technique is used in the analysis model. During this phase as shown in Figure 5.22, there are two almost straight lines with different slopes: one is from point ③ to point ④ and another one is from point ④ to point ⑤. Both of these two lines are almost parallel to the relative curves in the loading phase. The system regains some strength when the load level drops to 0.7 and the structure continues to deform until point ⑥. Figure 5.23 shows the deformed shapes at some critical points denoted in Fig. 19. It may be argued that the structural behaviour during the unloading

phase may be quite different in practice and the load displacement curve may directly drop to point ⑥ from point ②. This needs to be verified by experiments in the future work.

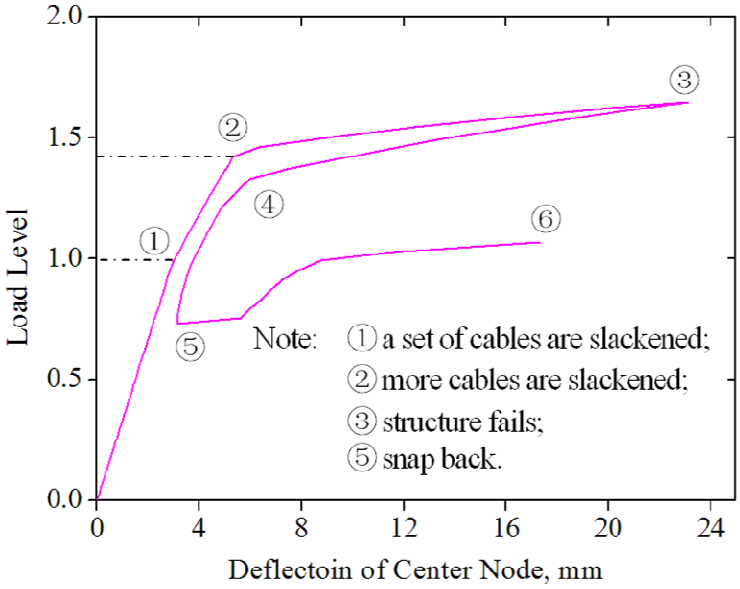

Figure 5.22: Load deflection curve of the barrel vault with cable prestress of 30% MBL.

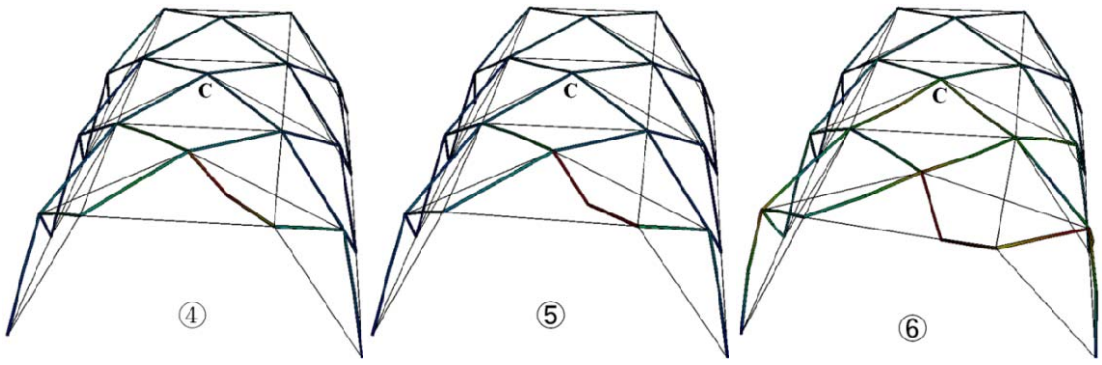

Figure 5.23: Deformed Shapes at Points ④, ⑤, and ⑥ (see Figure 5.22).

5.3.2 Dynamic response due to sudden loss of cable

Internal cables are susceptible to damage due to accidents or vandalism. Dynamic effect due to sudden release of energy can be significant as the failure is rupture in nature while cable is in tension. In this section, a nonlinear dynamic analysis is

performed to assess the robustness of the proposed structures in an accidental scenario where an internal cable is suddenly removed or cable end joint is failed in very short time. All structural element sizes, boundary conditions and cable pre-stress force remain the same as in section 5. Loading is taken in accordance with EN 1990 (European Committee for Standardization, 2002) and EN 1991 Part 1-7 (European Committee for Standardization, 2006) applied for accidental limit state.

The accidental load combination is

$$\begin{aligned} Accidental\ Load &= 1.0 \times Dead\ Load\ (DL) \\ &+0.5 \times Imposed\ Load\ (IL) + Sudden\ Loss\ of\ a\ Cable \end{aligned} \tag{5.41}$$

The damping ratio is assumed to be ranged from 0.01 to 0.02. Pre-stress and vertical load of 1.0DL+0.5IL is gradually applied to the structural at first. After that, an internal cable is suddenly removed and the axial force is assumed to be lost in 0.02 second.

Due to the geometric and loading symmetry, only eight cable removal scenarios need to be investigated. In each scenario (from case 1 to case 8), a cable (from cable 1 to cable 8 as shown in Figure 5.24) is removed one at a time. For example, in case 7, the time history of the vertical deflection at control point “C” due to the removal of cable 7 is shown in Figure 5.25. The deflection of the centre node is about 1.4 mm before the removal of the cable and after that the structure responses in a dynamic manner. The residual deflection is about 2.2 mm while the maximum value is 3.3 mm (50% higher).

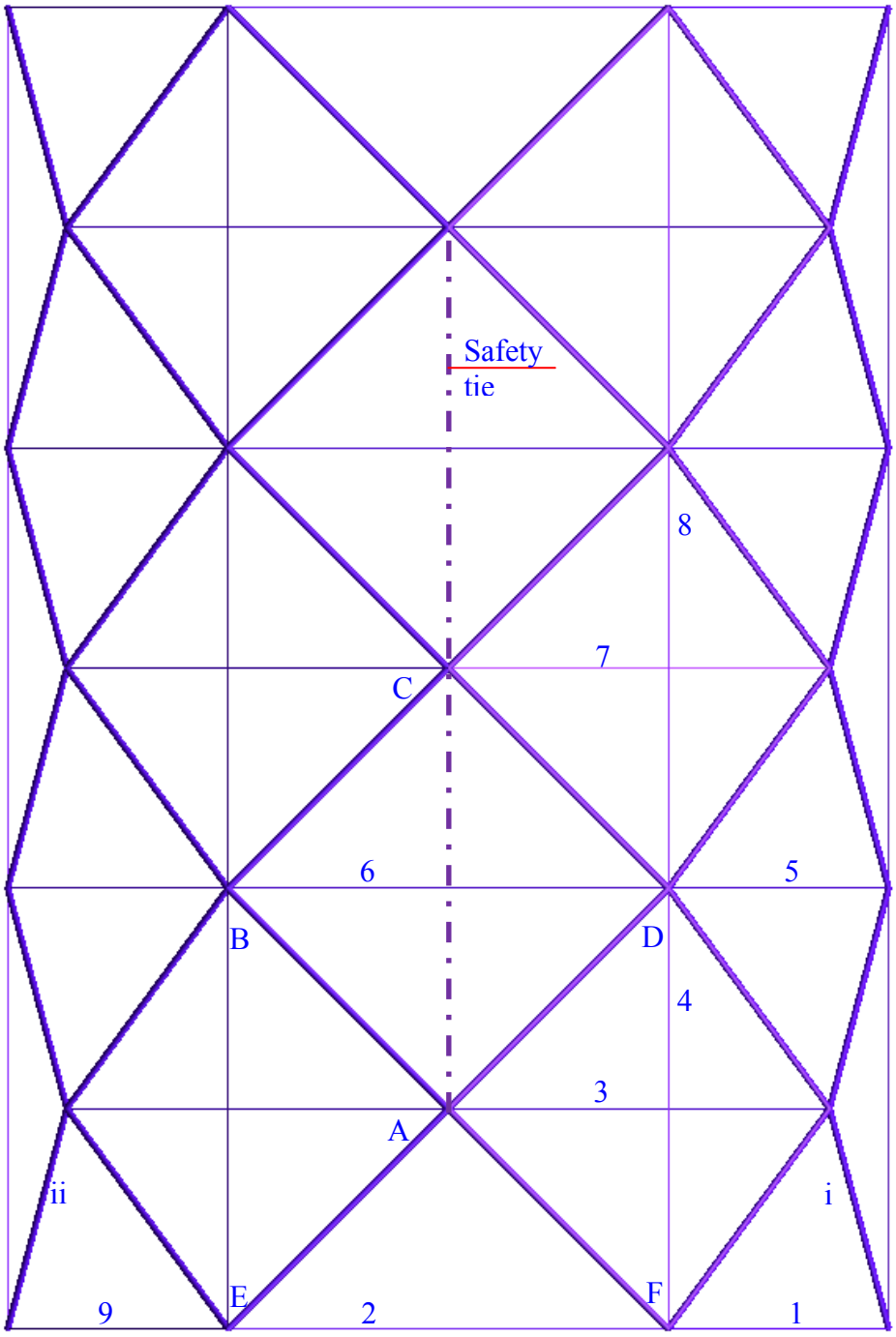

Figure 5.24: Numbering of cables and joints in plan view.

The vibration of the structure induces dynamic forces in the members. The maximum force of the critical cable, F_c, is 33 kN in tension, while the maximum compressive force of the critical strut, F_s, is 36 kN. The residual deflections, D_r, the maximum deflections of centre node "C", $D_{\max}$, maximum tensile forces in cables and maximum compressive forces in struts of other 4 cases are all listed in Table 5.2,

where downward is defined as a positive direction and tension force is in positive value. The maximum compressive and tensile forces are lower than buckling or breaking forces of the strut and cable, respectively. The structure does not fail for load cases 1, 3, 5, 7 and 8.

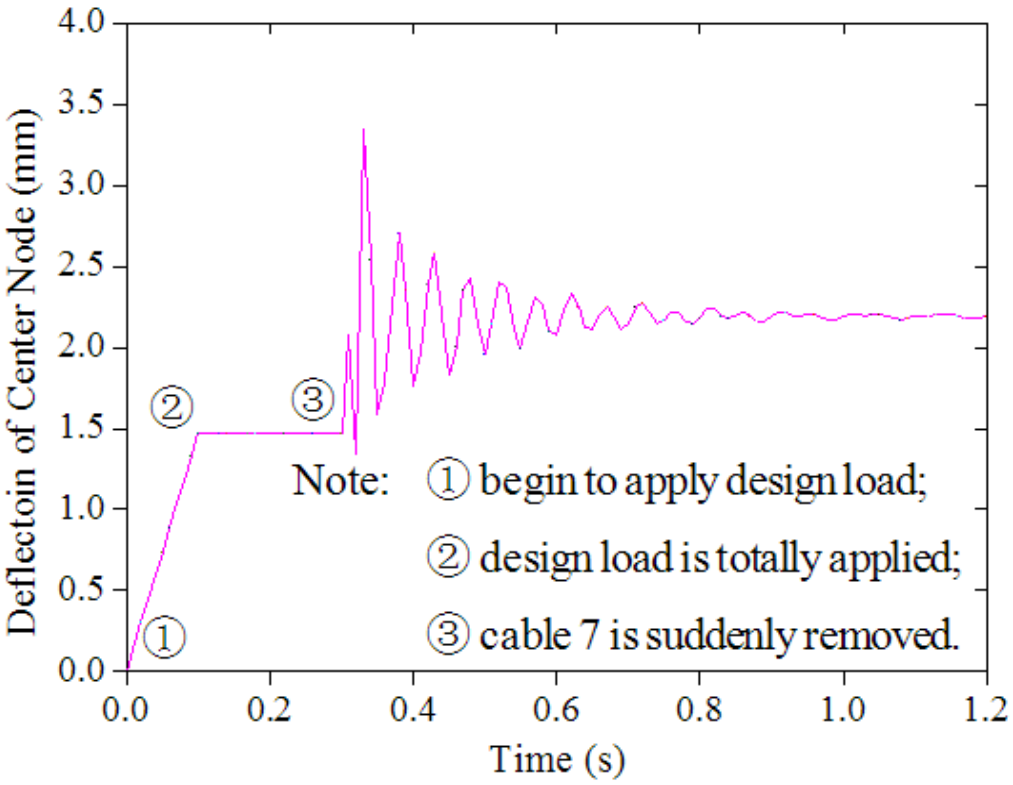

Figure 5.25: Deflection of Centre Node "C" due to the Sudden Removal of Cable 7.

Table 5.2: Representative deflections and element forces for different cases.

Case	No. of Removed Cable	D_r (mm)	D_{max} (mm)	F_c (kN)	F_s (kN)
1	1	1.03	1.48	33	-31
3	3	6.79	13.0	55	-35
5	5	-0.64	1.48	37	-31
7	7	2.20	3.30	33	-36
8	8	-7.13	2.27	44	-35

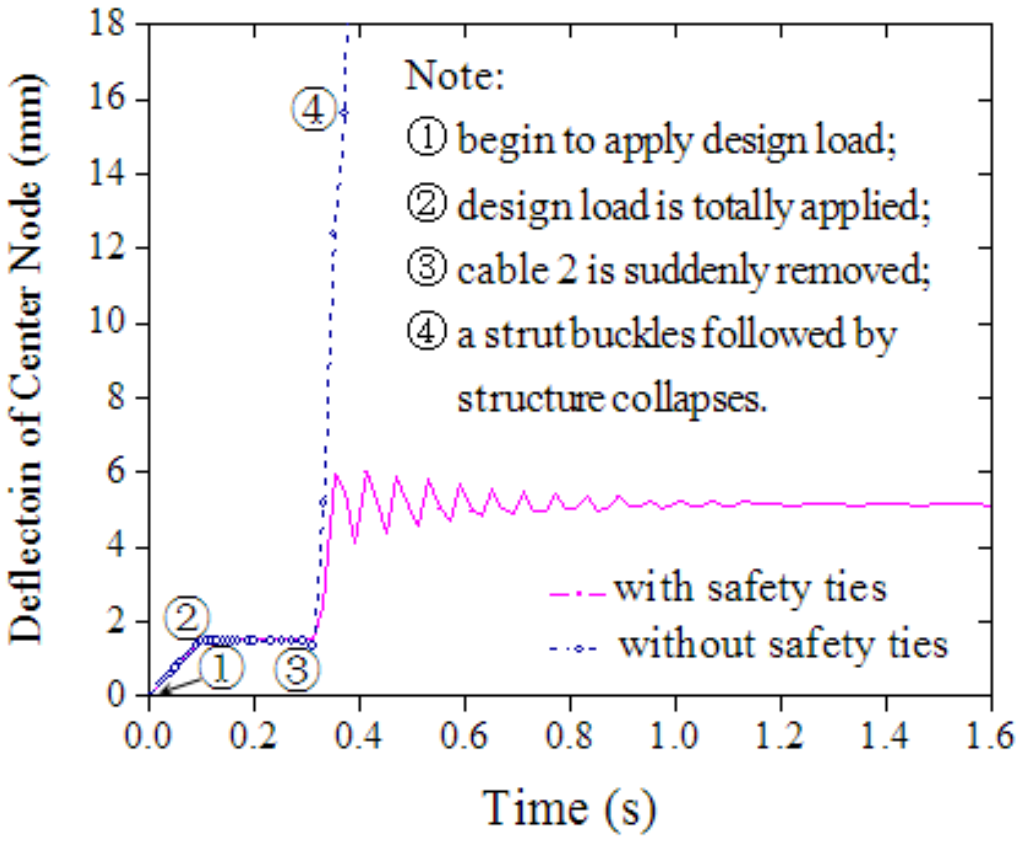

Figure 5.26: Deflection of Centre Node "C" due to the Removal of Cable 2.

The structure fails in a progressive manner in other cases where cable 2, 4 or 6 is suddenly removed. For instance, joints E and F will move apart when cable 2 is suddenly removed and cables 1 and 9 are slackened. After that, struts *i* and *ii* buckle and point "A" quickly moves downward, followed by the collapse of the whole structure.

To provide the structure with an acceptable level of robustness to sustain localized failure without disproportionate collapse, 2 horizontal safety ties are added shown as dashed lines in Figure 5.24. In this way, joints "A" and "C" are effectively connected and the safety tie tends to pull joint "A" back in cases 2, 4 and 6. Figure 5.26 shows the deflection curves in time domain for the case where cable 2 is suddenly removed. As can be seen from this figure, the maximum defection at the centre node is about 6 mm with the help of the additional safety ties.

5.3.3 Comparison of structural efficiency with other structural forms

To evaluate the structural efficiency, the proposed structure is compared with two existing structures: Foldable Bar Structure (FBS) and Foldable Plate Structure (FPS), the deployment pattern of which has been given in Section 3. FPS normally consists of hinged triangular plates, which can be folded or deployed according to an Origami-like pattern, as shown in Figure 5.20(a). FBS utilizes bars (struts) and specially designed joints, which can be regarded as a transition from FPS because of the same deployment pattern (De Temmerman et al., 2007).

Table 5.3: Comparison of DCCS, FPS and FBS.

Structural System	Span	Covered Area	Strut Diameter (Thickness) or	Cable Diameter	Weight /area
	(m)	(m^2)	(mm)	(mm)	(kg/m^2)
DCCS	6.67	67	50(2)	9	3.75
FPS	6.67	67	1	NA	12
FBS	7.05	55	50(2.5)	NA	5

A FPS model is built using the same span, width and load combination as proposed structure as shown in Figure 5.20(a). The analysis results show that the FPS shelter with plate thickness of 2 mm can only resist about 1.2 times the factored load. However, the deflection is much smaller and the stiffness is higher than that of DCCS. The preliminary structural analysis result of FBS sharing the similar parameters is obtained from De Temmerman et al. (2007). The detailed information of the models and results are summarized in Table 5.3. Under the similar span and covered area, the

weight of proposed structure (DCSS) is about 3.75 kg/m2, which is 25% lighter than FBS with self weight of 5 kg/m2. On the other hand, the weight of FPS is relatively high due to the thickness of the steel plates.

5.4 Summaries

Structural responses of both Tension Strip Columns and Deployable Cable Chain Structures are investigated in this chapter.

An analytical model based on beam on elastic foundation theory and two numerical models based on the finite element method for Tension Strip Columns have been constructed and validated against each other. It has been demonstrated that the stiffness of such structures rise with an increase of the length to depth ratio. Length to depth ratios ranging from 8 to 20 are recommended for Tension Strip Columns. Practical length to depth ratio, however, is also subjective to practical limitations such as the maximum depth, the connection keder size, etc. The structural efficiency in terms of stiffness increases with an increase in the elastic stiffness of restraints for given struts. It is also found that the stiffness of the column with more struts is higher than those with fewer struts while the total cross sectional area remains same. However, four struts are recommended because too many struts in a column require more complicated joint design and potentially less efficiency.

A clear trend is seen where higher elastic stiffness of restraints leads to higher normalized buckling load. The normalized buckling load increases when the length to depth ratio increases. However, TSS with a length to depth ratio higher than 20 is prone to experience a first mode buckling toward the axis. It is observed that low normalized buckling load is relative closely to the first mode buckling, which should

be avoided during the design. A careful tuning of the combination of length to depth ratio, the cross sectional resistance of the strut and the elastic stiffness of restraints would result in the most efficient design. The structural efficiency of TSSs has been demonstrated by two case studies in which TSS columns are compared with conventional CHS tube columns, Tensairity columns, and truss columns.

Nonlinear inelastic analysis on Deployable Cable Chain Structures has been carried out and comparison with other existing foldable shelters indicates that the proposed structure offers excellent structural efficiency in term of strength to weight ratio. In the robustness analysis, dynamic effects of accidental removal of cables are investigated, which shows the structure is sensitive to sudden loss of cable forces. However, the robustness of proposed structures against dynamic impact due to sudden damage of cables can be enhanced by providing safety ties at strategic locations.

Chapter 6

Experimental Investigation of Tension Strip Structures

6.1 Introduction

In this chapter, a series of full scale experiments on Tension Strip Structures as well as various component tests carried out are reported. The Tension Strip Structures constitute of aluminium alloy struts, PVC coated membrane, and joints made of constructional steels. The experiment aims to examine the structural behaviour of the proposed structure subjected to axial compressive load.

Three specimens with a uniform total height of 2120 mm have been manufactured and assembled. Figure 6.1 illustrates one of these manufactured Tension Strip Structures, in which the main components are indicated. Issues encountered during the fabrication are discussed first. Setups for both full scale structure experiments and component tests are introduced in the next section. Results of these tests are presented and discussed, which are followed by some conclusions.

6.2 Full scale fabrication challenges

Full scale prototypes of proposed Tension Strip Structures are manufactured to

integrate the tensile membrane, tensile cable, slender struts to form a system to resist compression force as shown in Figure 6.1. The membrane components, which are different from conventional structural materials such as steel and concrete, need careful processing to meet the stringent requirements so that they can achieve the desired form.

Figure 6.1: Manufactured Tension Strip Structure.

The connectors and joints are designed to allow rapid onsite erection and easy dismount for economic transportation and storage. Reliable connections between the membrane and struts are vital to achieve effective lateral restraints for the curved struts under compression. The following subsections explain the different aspects of the fabrication of Tension Strip Columns.

6.2.1 Fabrication of coated membrane

In order to effectively transfer load, the flat roll membrane should be divided into strips, cut and welded together according to the proper patterning according to geometrical and structural designs. This is the main procedure of the fabrication of coated membrane. In this project, a commercial PVC coated membrane material termed as Precontraint 502 S2 Translucent is used. The technical specification provided by the vendor is summarised in Table 6.1.

The precondition of these fabrication procedures is the determination of desired 3-dimensional shape of the membrane. As discussed in Chapter 2, the membrane relies on the geometry with double-curvatures to bearing load. The situation is slightly different in Tension Strip Columns, where lateral restraints to the struts are mainly provided by the yarns of the membrane in transverse direction. The curvature of the membrane in vertical planes depends on the geometrical form of the struts, which are slightly bent in all fabricated structures. This means the curvature of the membrane in vertical planes is also insignificant. The curvature in horizontal planes is associated with the boundaries. High boundary constrains apply to the membrane in the horizontal (transverse) direction; while low boundary constrains apply in the proposed structure. The curvature of the membrane in the horizontal planes is thus relatively

small when the column is under compressive load. Even in such cases, the equilibrium shape of the membrane is still in 3-dimensional, which should be divided into flat (2-dimesional) strips. The 3-dimensional geometry of the membrane is determined from a form-finding procedure by a general commercial program ForTen 3000 (D'Anza, 2008). The form-finding depends only on the boundary conditions, rather than material properties. The form-finding procedure however is not within the scope of this study. The following paragraphs therefore focus only on the procedures of the fabrication of membrane.

Table 6.1: Technical specification of membrane material used.

PRECONTRAINT 502 S2 TRANSLUCENT

Yarn	1100 dtex PES HT
Weight	590 g/m^2
Width	250/267 cm
Thickness	0.5 mm
Tensile Strength	
Warp	2800 N/5 cm
Weft	2800 N/5 cm
Tear Strength	
Warp	280 N
Weft	280 N
Adhesion	
Warp	100 N/5 cm
Weft	100 N/5 cm
Light transmission	19%
Handling temperature range	-30 ~ 70 ^{o}C

In the first procedure, the cutting patterns of the 3-dimensional membrane are established for individual membrane strips. In this stage the compensation value has to be anticipated, which is normally obtained from stress-strain curve yielded by biaxial tests under long-term loading of the actual stretch in the designated tensioned state. The compensation values are used to provide desired pre-stress in order to

correct the effect of the deformation or resulting strain of membrane under loading and temperature. A compensation value of 0.3% is used for both warp and weft directions as suggested by the membrane supplier. This procedure is also accomplished by ForTen 3000 (D'Anza, 2008). The arrangement of the strips in the height of the column direction is parallel. Pattern drawings indicating the detailed dimensions of the membrane and the welding edge are the outcome of this procedure.

For the current case, the width of the whole piece of membrane is from 72 mm to 182 mm and the length of the whole piece of membrane is about 1900 mm. It can be cut as one flat piece. Hence, no seam inside the membrane is required. However, seams are required as larger pieces of membrane are used in large scale columns. Therefore, the cutting and welding procedures are briefly discussed.

In the second procedure, 2-dimensional membrane strips are cut out from pattern drawings obtained from previous procedure. This procedure needs to reproduce the calculated patterning as precisely as possible. The cutting pattern drawings include the specification of the material, the edges and cutting shape of the strips. Seams widths and allowable are given also if necessary to enable proper joints between different strips. The cutting out of coated membrane is done with hand tools or preferable a cutting machine. This is limited, however, to cutting capacity, edge geometry, and layer thickness. The finished strips should be check against the patterning drawings in any case.

In the third procedure, strips are joined together with joints. Most joints between membrane strips fall into two categories: permanent surface joints and temporary or reusable joints. Permanent joints include welded seams, combination seams, sewn

seams and glued seams; temporary or reusable joints include clamping plates and keder rail joints, looped and laced joints as described by Seidel (2009). Welded seams are suggested to be used for Tension Strip Columns. The strength of welded seams depends on welding process and processing temperature, which should achieve 80% of the membrane strength at least for the current design. Two common processes for welding membrane strips together are high frequency welding and hot element welding. The former process is preferable because a largely homogeneous joint where the entire coating thickness of the two material sides to be joined are integrated.

6.2.2 Cold-form shaping of curved aluminium struts

The fabrication of current Tension Strip Columns adopts special aluminium profile for the struts as shown in Figure 6.2. The aluminium strut is bent with rolling machine to a desired arch shape with small curvatures. In such a way, a consistent curvature along the whole length of the strut can be achieved. Besides, a steel cable with a diameter of 18 mm is located into the hole of the struts during the procedure to prevent possible large deformation of the C channel under the compression of rolling machine.

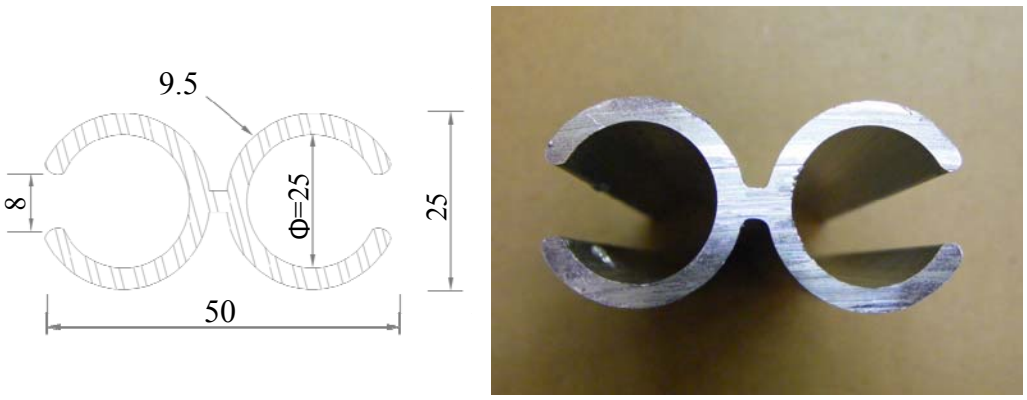

Figure 6.2: Cross section specifications of aluminium strut.

6.2.3 Connection between membrane and struts

In Chapter 3, several connections are discussed for Tension Strip Structures regarding the designs, advantages, and shortages. The connection using special cross section profiles and keders is adopted for the current fabrication as shown in Figure 6.3. Keder is made of a tube core with woven polyester single side PVC coated.

This connection ensures the reliable load transferring from the membrane to the struts. Under the axial compression struts in Tension Strip Columns tends to deflect outward, which results in a stretching in the membrane through the keder. In other words, the force in the membrane is transferred into the pressure between the keder core and the inside surface of the C channel of the struts at the contact area. This forms an effective force transferring mechanism.

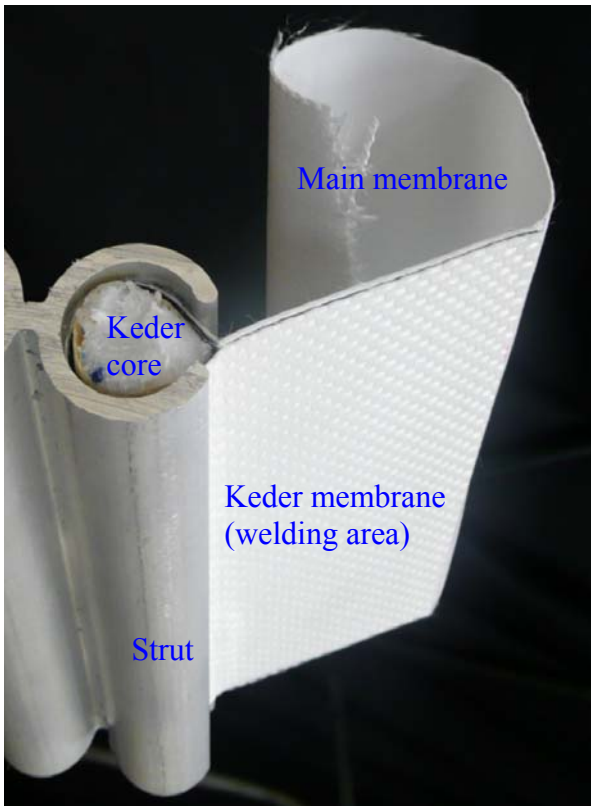

Figure 6.3: Connection between strut and membrane.

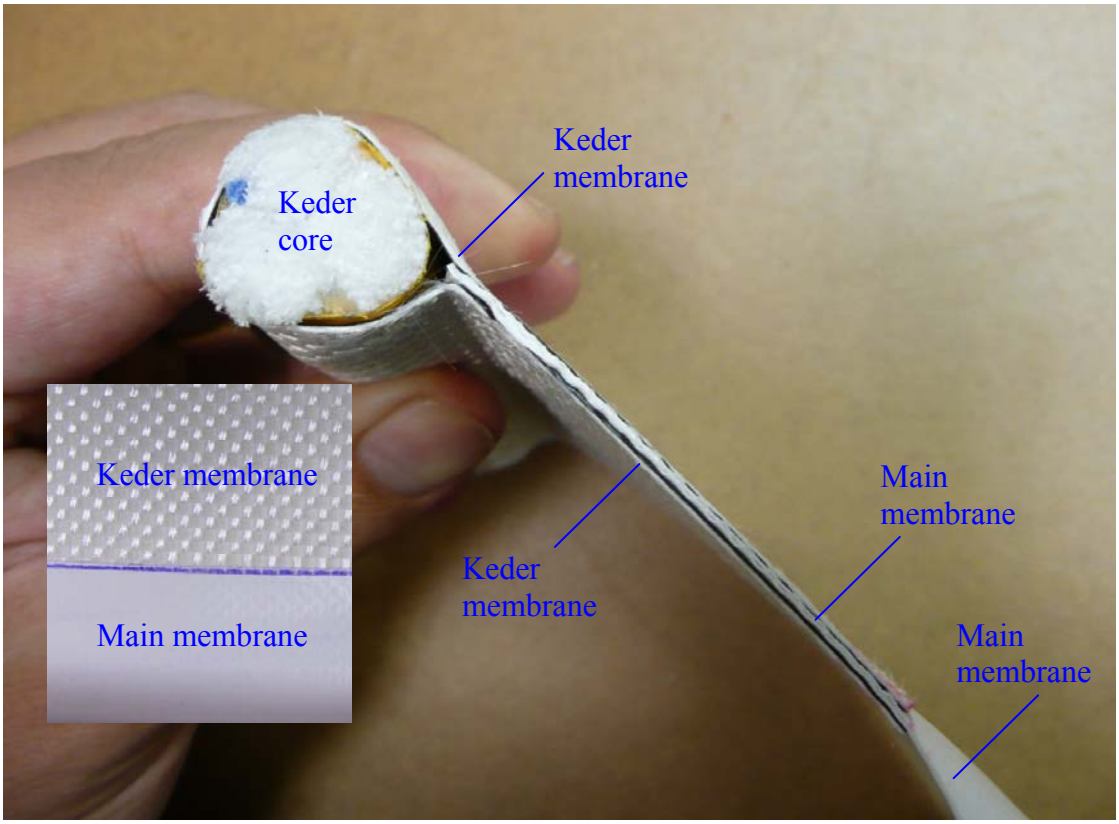

Figure 6.4: Keder welded with main membrane.

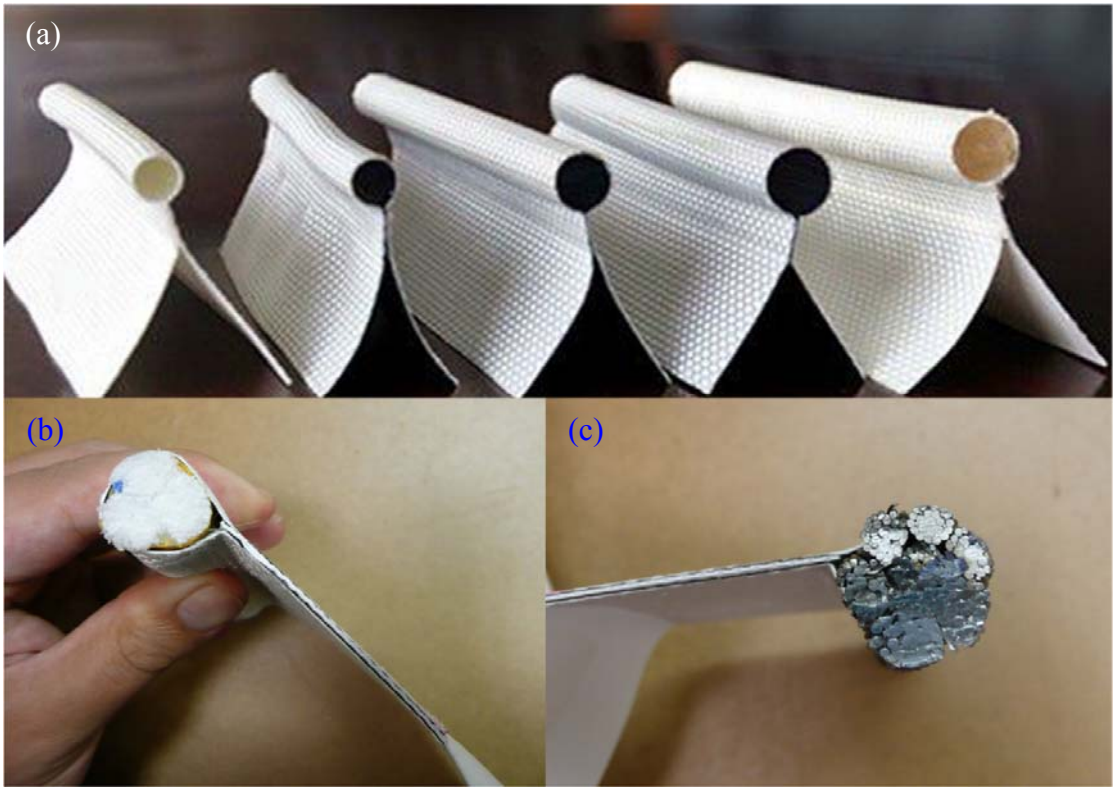

Figure 6.5: 3 types of keders: (a) PVC tube; (b) nylon rope; (c) steel cable.

A pocket is designed to connect the membrane with the keder as shown in Figure 6.4. In this connection, the rope keder is wrapped by a keder membrane that is welded to the membrane on both sides by high frequency machine. Keder membrane is different from main membrane in two aspects: (a) keder membrane is stronger in terms of mechanical properties to ensure a reliable connection, and (b) the weaver pattern in keder membrane is specially designed to be easy to slider into a keder hole (C channel in this case). The left bottom corner of Figure 6.4 shows the different appearance between keder membrane and main membrane. The keder membrane is weaved in a way that the friction between the membrane and contacted surface (inner surface of the C channel in the current project) is smaller because of reduced contact area.

Figure 6.5 shows three options available for the keder: (a) PVC tube, (b) nylon rope, and (c) steel cable. Steel cable typed keder offers highest restraints to the membrane pocket against deformation under stretching load in membrane, however limited to considerable weight. Nylon rope typed keder provides lightweight, however limited to slightly softer restraints. PVC tube typed keder combines the advantages of previous two types. However, the out diameter of PVC tube is smaller than what is required herein. Nylon rope and steel cable typed keders are the preliminary choices for the project. The final decision is due to the mechanical behaviours of these two types that are investigated by experiments as given in Section 6.4.

6.2.4 Dismountable joints

One of the potential applications of Tension Strip Columns is for temporary or semi-permanent buildings. It is vital to meet the general functional requirement for easy erection and dismount onsite as well as economic transportation and storage. Thus,

dismountable joints are a must for Tension Strip Columns.

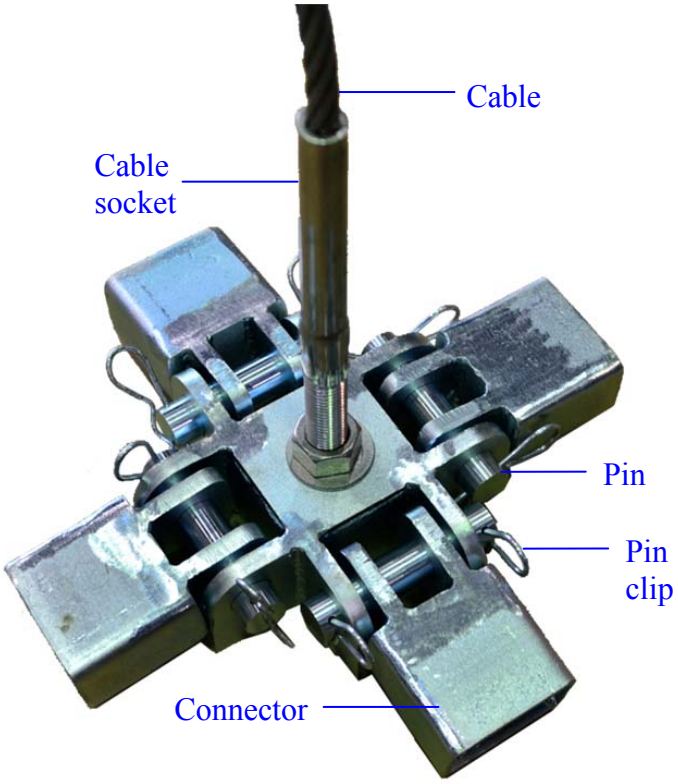

Figure 6.6: A joint fabricated for Tension Strip Columns.

Figure 6.6 shows a joint fabricated. The joint connects with aluminium struts via connectors. Struts along with the connectors are free to rotate along the axes of pins. Four pin connections are designed to accommodate four connecters. High strength steel S690 is used for all pins and flanges on the connectors and joint to ensure the ultimate load of the column is controlled by the membrane-strut system and not by joints. Pin clips are used to restrain the possible slip of pins. A hole is located at the centre of the joint to allow the internal cable to go through.

6.2.5 Installation and tensioning

The section presents the procedure as shown in Figure 6.7 to assemble a Tension Strip Column with all the components ready.

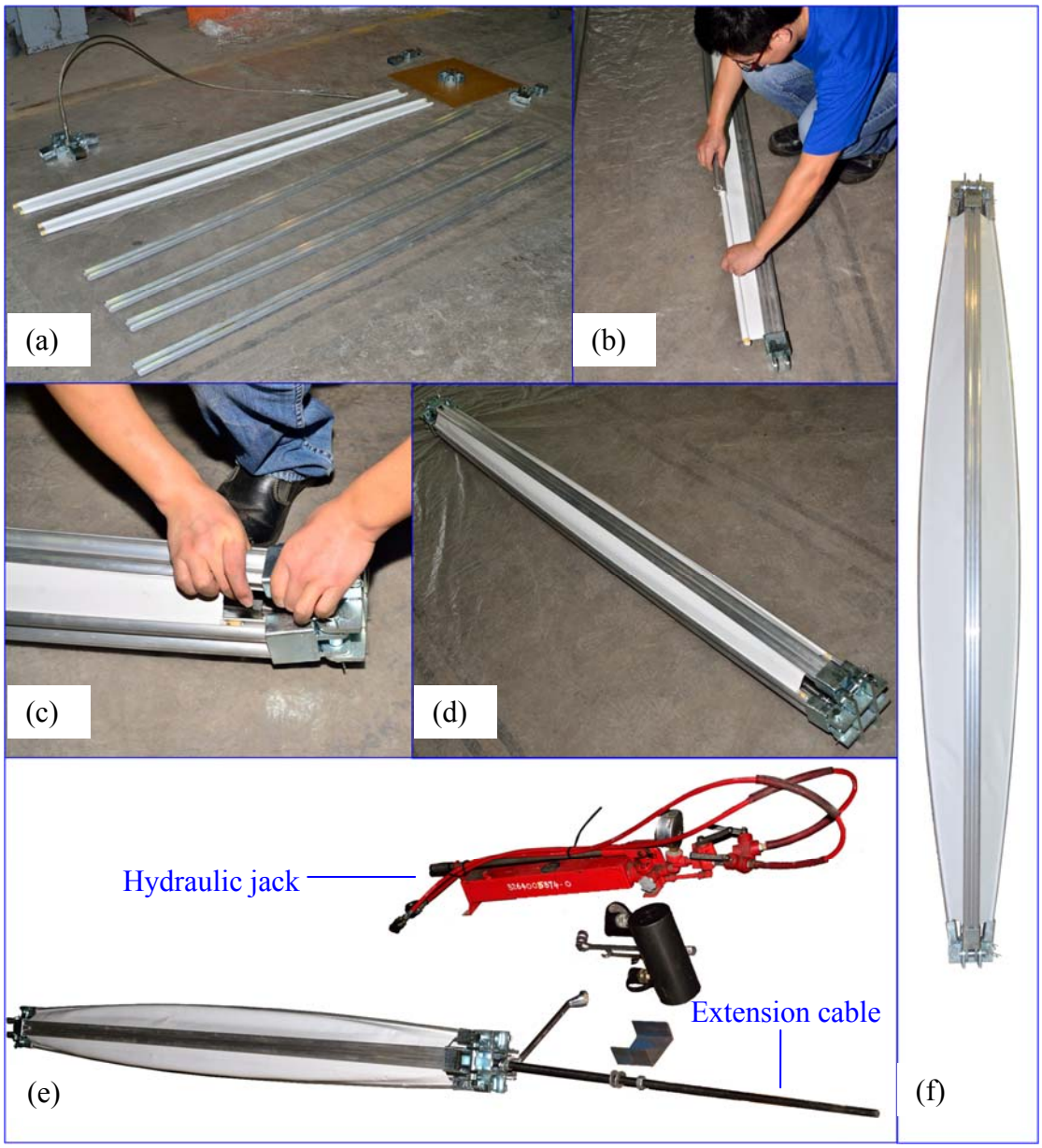

Figure 6.7: Assembly procedures of TSS: (a) main components; (b) slotting membrane into aluminium profile; (c) connecting joints; (d) TSS before pretension; (e) pretension with hydraulic jack; (f) tensioned TSS.

In the first step, the struts are connected to the membrane. Each piece of membrane is allocated properly by inserting the keders on the two sides of the membrane into the aluminium holes. No stretch can be left on the keder membrane pieces. Lubricating oil is recommended to apply on the contact area between the keder membrane and the inside surface of aluminium struts with the intention to reduce the friction. In the

second step, a joint is connected to one end of the four struts. The cable with thread terminals is fixed to this joint by nuts and washers at an end. In the third step, another joint is connected to the struts as well as the cable. Up to this step, all components are connected. However, the column is not stable because the membrane is still slackened. In the last step, the column is compressed with a hydraulic jack in the axial direction and the cable is fixed at the end. All membrane pieces should be pre-tensioned and the column is stabilized. The desired status can be obtained by monitoring the total height of the column or the width of the column during the tensioning procedure.

6.3 Test methodologies and setups

The whole test includes two categories: a series of component tests followed by a full scale monotonic load test. The objective of the component test is to obtain thorough understanding of the mechanical properties of the components used such as aluminium struts, membrane, jointed membrane, connection between the membrane and struts. In the full scale monotonic load test, the structural behaviour of Tension Strip Column under axial compressive load is investigated in terms of the ultimate strength, load-displacement diagram, stress distribution, etc.

In this section, the test methodologies and setups for all component tests and full scale column tests are discussed.

6.3.1 Coupon test on aluminium struts

Tensile plate coupon tests on four pieces of aluminium specimens with the same thickness (3 mm) with the C channel in aluminium struts are carried out following the

procedure recommended in the ASTM E 8/E 8M-08 (2008). The tests are performed on the MTS 250 kN test rig. The tensile aluminium coupons are cut off from the same batch of material for the struts.

Figure 6.8 shows the setup of the aluminium coupon test. An extensometer gauge is installed, while two post yield strain gauges are installed on both sides in between the extensometer legs. The data recorded by stain gauges and extensometer gauge found a basis to calculate engineering stress strain curve. This should be converted to true stress stain curve.

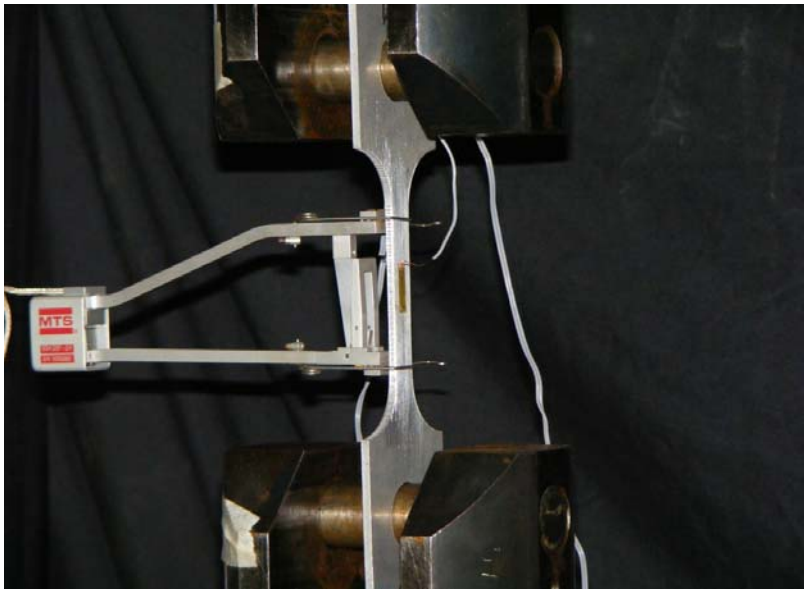

Figure 6.8: Aluminium coupon under test.

6.3.2 Uniaxial strength test on membrane

To obtain the uniaxial strip strength loaded parallel with the yarn direction, 50 mm wide samples of membrane cut parallel to the warp and weft directions are tested. 5 test pieces for the weft direction and 10 test pieces for the warp direction cut off from the same batch of the main membrane are prepared to obtain the average uniaxial

strength according to Eurocode.

All specimens are 50 mm in width, 300 mm in length, and 0.5 mm in thickness. To prevent premature damage around the griping area, two flat steel plates are used to clamp the membrane tips with a clamping area of 50 mm x 50 mm. Hence, the length in between the clamping plates is 200 mm. The applied load and the displacement of the stroke are recorded during the test. The slip of the membrane at the clamped tip is also recorded to calculate the true elongation. The uniaxial strip tests are carried out at a temperature of 26±1°C. An assumed reduction factor is introduced because the strength under a biaxial load that is difficult to measure is lower than that under a uniaxial load.

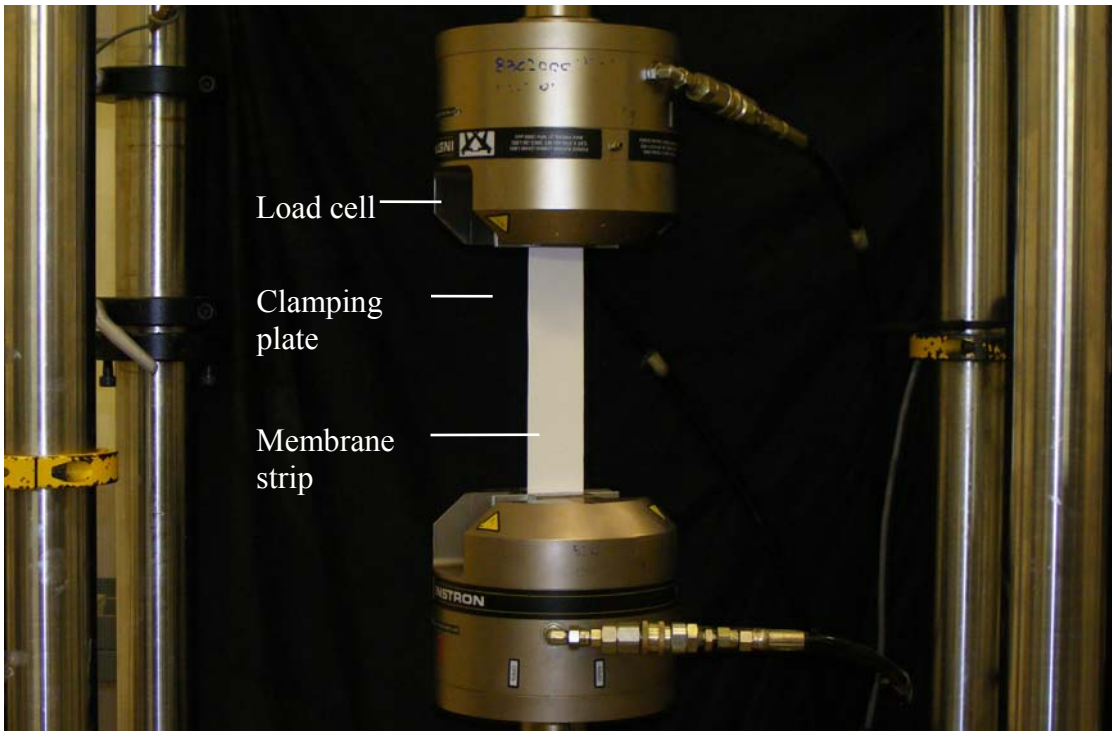

Figure 6.9: Uniaxial membrane strip strength test setup.

6.3.3 Uniaxial tear strength test on membrane

The tear strength test is carried out based on trapezoidal tear method suggested by

ASTM D5587-08 (2008). This test aims to measure the tear propagation resistance of a membrane with small tear initiated before testing. The result obtained is not directly related to the force required to start a tear.

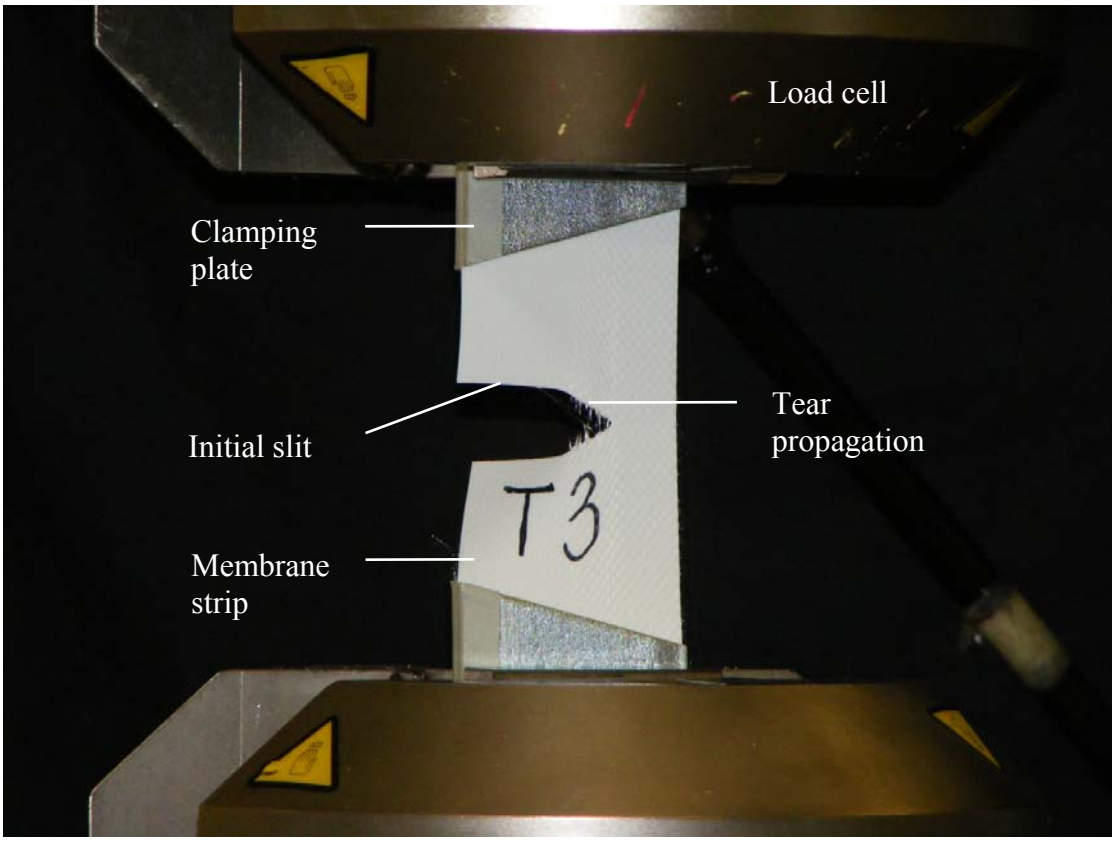

Figure 6.10: Trapezoidal tearing test setup.

The test is carried out on the INSTRON 500 kN test rig as shown in Figure 6.10. In this test, an outline of a trapezoid is marked on a rectangular specimen. The specimen is slit at the centre of the smallest base of the trapezoid to start the tear. The nonparallel sides of the marked trapezoid are clamped in parallel jaws of a tensile testing machine. The separation of the jaws is increased continuously at the rate of 20 mm/min to apply a tensile force to propagate the tear across the specimen. Force in the time domain is recorded and maximum forces are measured.

6.3.4 Uniaxial strength test on welded seams

Welded seams are necessary for wide-area membrane surfaces. Forces are transferred by the adhesive strength at the welding area, which is critical to the strength of the whole membrane surface. In this test, the seam strength is determined by a uniaxial tensile test similar to the one described in Section 6.3.2 except that a seam located at the centre of the membrane strip as shown in Figure 6.11. 6 test pieces for the weft direction and 9 test pieces for the warp direction cut off from the same batch of the main membrane are prepared to obtain the average uniaxial seam strength based on Eurocode.

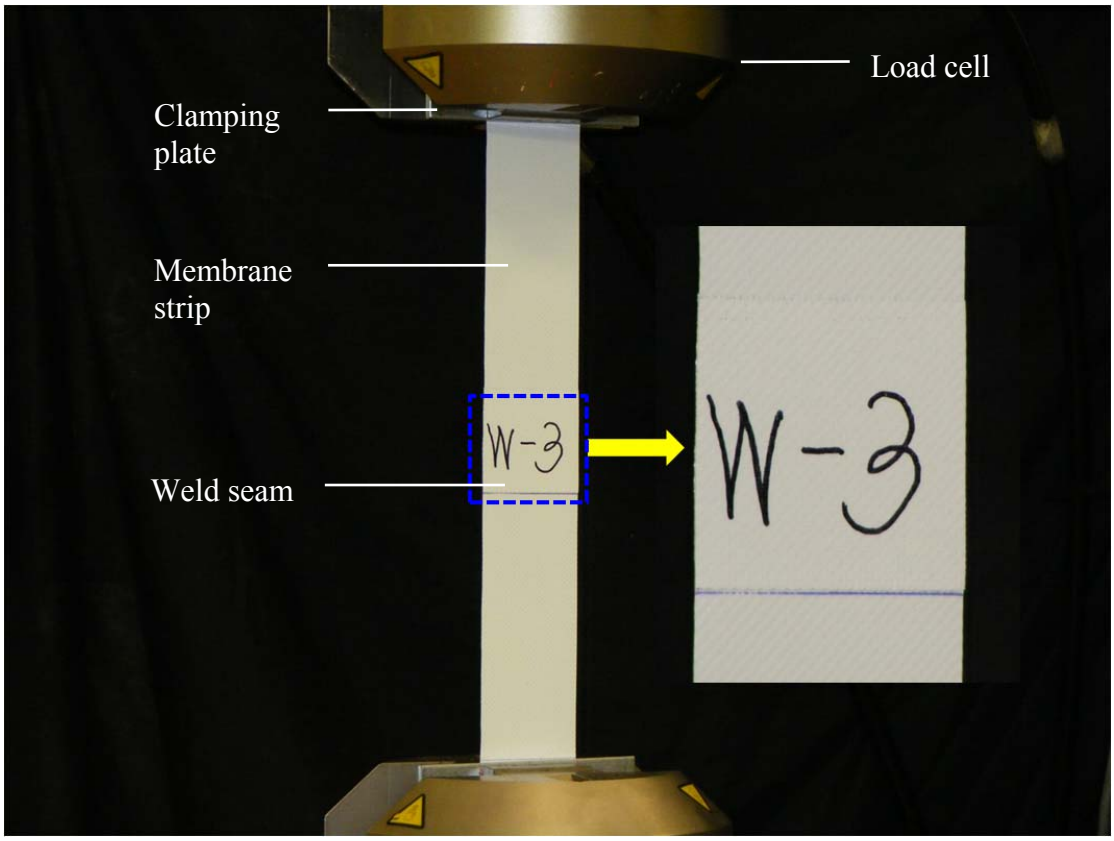

Figure 6.11: Uniaxial weld seam strength test setup.

All specimens are 50 mm in width, 300 mm in length, and 0.5 mm in thickness. In practice, the seams have an average width of 40 – 50 mm. The width of the seam is 50

mm for all specimens in both warp and weft directions. To prevent premature damage around the griping area, two flat steel plates are used to clamp the membrane tips with a clamping area of 50 mm x 50 mm. The length in between the clamping plates is 200 mm. The applied load and the displacement of the stroke are recorded during the test. The slip of the membrane at the clamped tip is also recorded to calculate the true elongation. The uniaxial strip tests are carried out at a temperature of 26±1°C.

6.3.5 Tensile strength tests on strut to membrane connection

The tensile strength of connection systems discussed in Section 6.2.3 is investigated by tensile strength tests. The tests are performed on the INSTRON 500 kN test rig as shown in Figure 6.12.

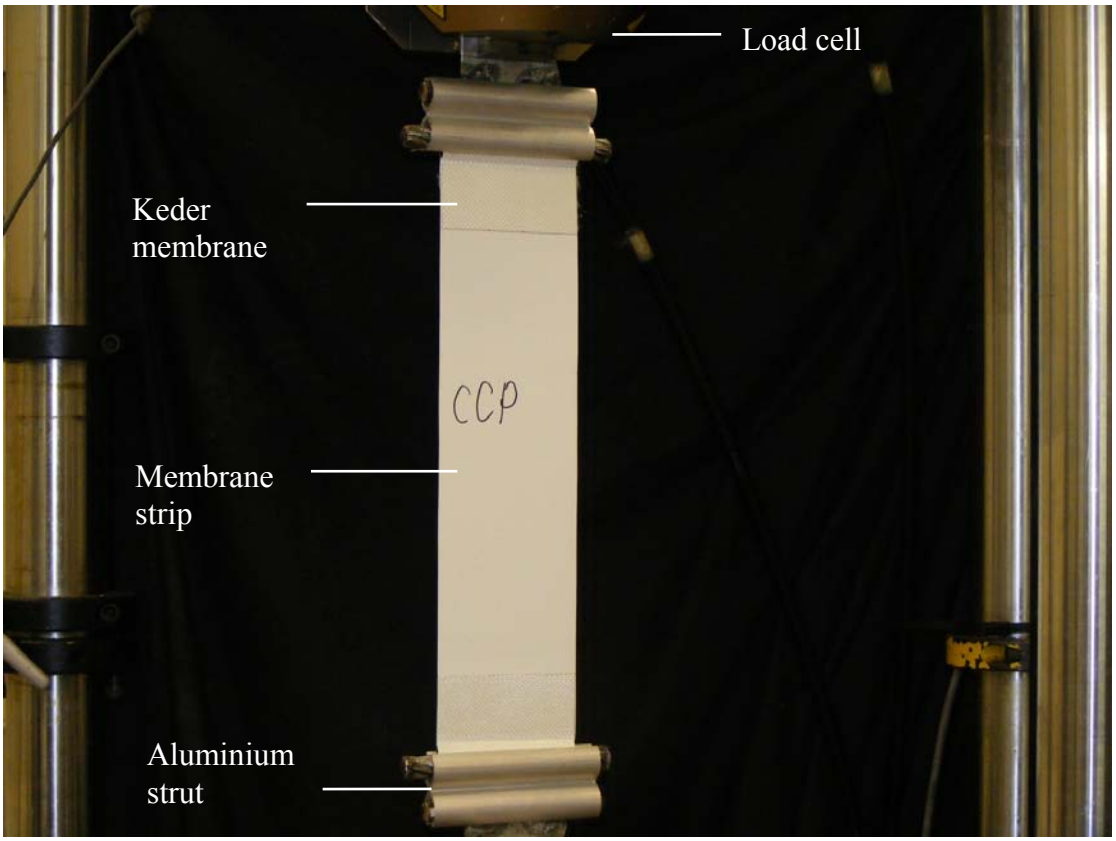

Figure 6.12: Tensile test setup on strut to membrane connection.

The membrane strip is connected to aluminium struts via keders, while the aluminium struts are connected to the griping jaws through a device as can be seen from the right top corner of Figure 6.12. The device constitutes a steel round rod and steel plate. These two parts are welded together. The tensile force is applied by the separation of the griping jaws. The cell load and stroke are recorded during the test procedure.

The main membrane specimens are cut off from the same batch of the material used for the column fabrication in both warp and weft directions. The main membrane specimens have a length of 450 mm, a width of 100 mm, and a thickness of 0.5 mm. The welding area between keder membrane and main membrane has a height of 50 mm and a width of 100 mm. The strut in the test is cut off from the same batch of the material used for columns with a length of 12 mm and the same cross section with those discussed in Section 6.2.2. Both steel cable typed keder and nylon rope typed keder are tested. The diameter of keder cores in both types is 17.6 mm. In both direction, 5 specimens with nylon rope typed keders and 1 specimen with steel cable typed keders are tested at a room temperature of 26±1°C.

6.3.6 Monotonic load test on Tension Strip Columns

The setup of the monotonic load test on the Tension Strip Columns is shown in Figure 6.13. The column is mounted on the 250 kN actuator rig in the structural engineering laboratory in the National University of Singapore. Two rollers allowing free in-plane rotations are attached to ends of the column to simulate a pin-pin boundary condition.

Twelve linear strain gauges are installed at the centre and quarter positions on the left side of all four struts. Besides, transducers are used to measure the axial load-shortening at the tip as well as the lateral deflection at the centre and quarter points.

The detailed locations of the transducers and strain gauges are illustrated in Figure 6.13.

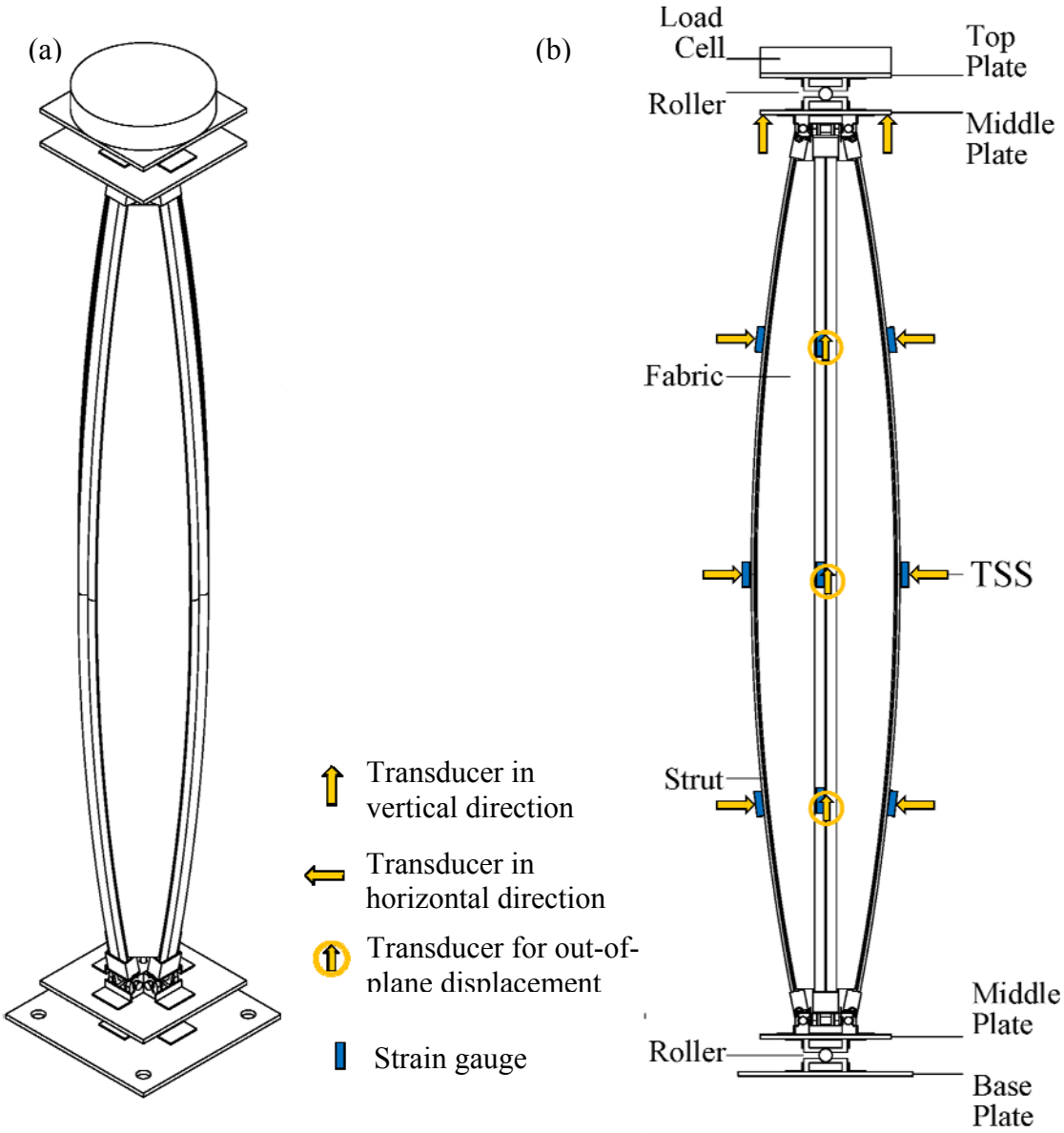

Figure 6.13: Setup of monotonic load test on a Tension Strip Column: (a) trimetric view; (b) front view.

The monotonic load test is displacement-controlled. The prescribed displacement increment is in the range of 0.2-0.4 mm/min: loading rate is 0.2 mm/min and unloading rate is 0.4 mm/min. In the preloading phase, the column is loaded to 10 kN for twice to verify the readings of all transducers and strain gauges. After that, the

specimen is loaded until the column fails.

6.4 Test results and discussions

Test results are presented and discussed in this section for monotonic load tests on Tension Strip Columns and all component tests. The component tests include coupon tests for aluminium struts, uniaxial strength and uniaxial tear strength tests for membrane, uniaxial strength tests for membrane seams, as well as tensile strength tests of the connection systems between membrane and aluminium struts.

6.4.1 Coupon test on aluminium struts

The mechanical properties of aluminium material used for the struts in Tension Strip Columns are measured in this test. Figure 6.14 shows the engineering stress-strain curves measured from coupon tests as well as the representative true stress-strain curve for finite element models.

Table 6.2: Coupon test results of aluminium struts.

Specimen	E (GPa)	σ_y (MPa)	σ_u (MPa)	Elongation
alum1	68.3	269	296	12.0%
alum2	72.2	276	303	11.7%
alum3	68.6	264	290	10.9%
alum4	71.6	270	296	12.3%
Average	70.2	269.8	296.3	11.7%

The test results are summarized in Table 6.2. As can be seen from the table, mechanical properties for different specimens from the aluminium material used are consistent and average values are used.

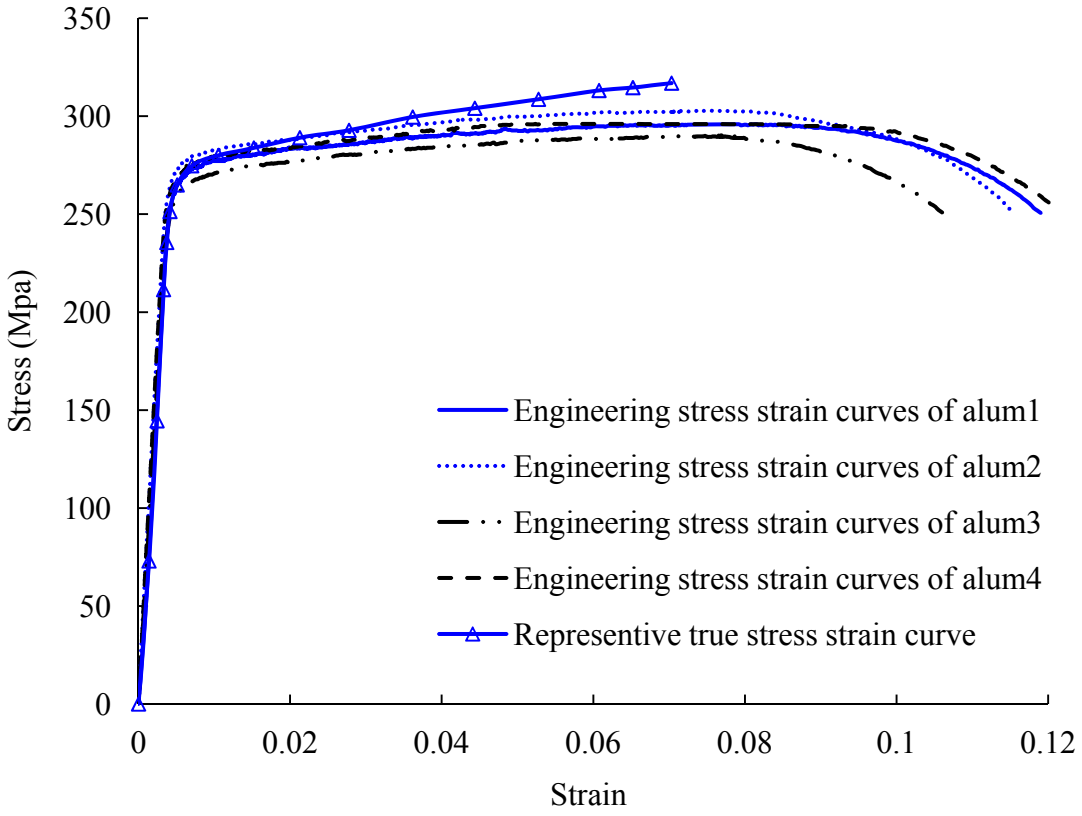

Figure 6.14: Stress strain curves measured from aluminium coupon tests.

6.4.2 Uniaxial strength test on membrane

Figure 6.15 shows the force-extension diagram for membrane in both warp and weft directions measured from uniaxial strength test. The results are consistent in both directions. Tensile strength and stiffness in warp direction are noticeably higher than those in weft direction. The different weaving and coating of the yarns in these two directions contribute to these differences.

The force-extension diagram for tensioned membrane strips in both warp and weft directions exhibits 3 regions, which correspond to the zigzag structure of the polymer chain in the micro-level. In region I, the angle of the zigzag chain is initially widened with restraints by the surrounding coating material. In region II, zigzag chains start to extract themselves from amorphous area, showing more ductile behaviours. In region

III, the behaviour becomes stiffer because of jamming of the drawn-out chains and growth of crystalline areas.

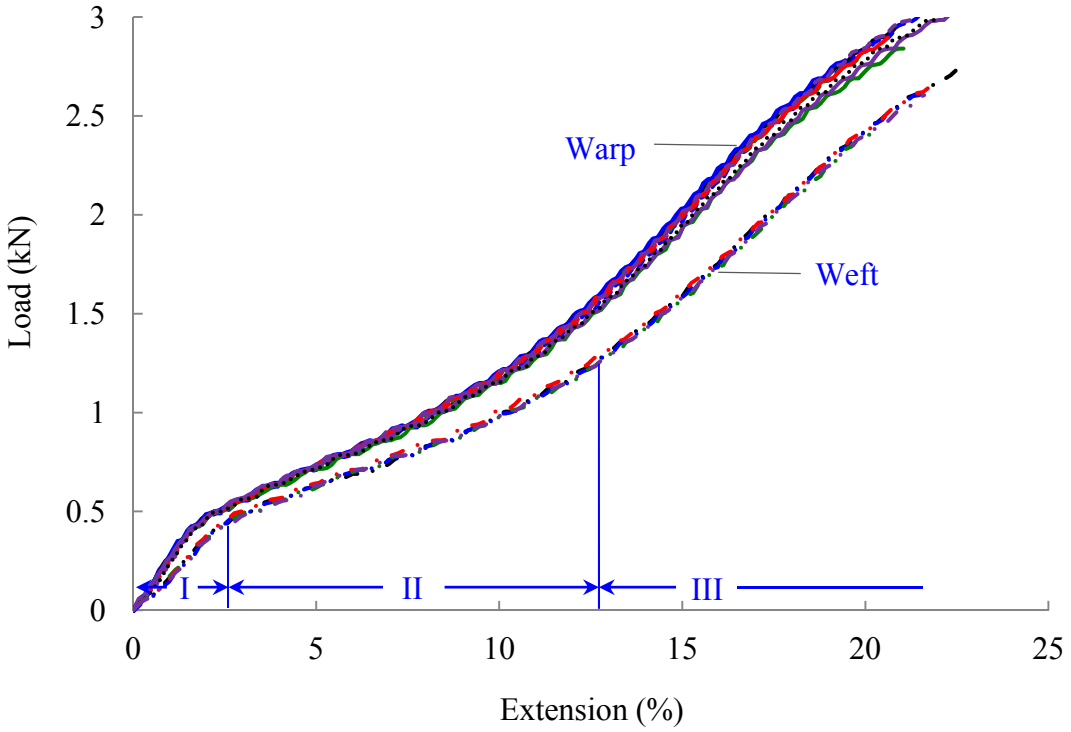

Figure 6.15: Force-extension diagram for membrane in both warp and weft directions.

Table 6.3: Uniaxial strength of membrane strip.

Warp direction		Weft direction	
Specimen No.	Uniaxial strength (kN/5 cm)	Specimen No.	Uniaxial strength (kN/5 cm)
1	2.965	1	2.735
2	2.820	2	2.620
3	2.780	3	2.405
4	3.040	4	2.645
5	2.840	5	2.605
6	2.785	-	-
7	2.895	-	-
8	3.010	-	-
9	3.050	-	-
10	2.985	-	-
Mean value	2.917	Mean value	2.602
Standard deviation	0.100	Standard deviation	0.122

Table 6.3 summarizes the ultimate strength for membrane strips tested in both warp and weft directions. The standard deviations of both cases are lower than 5% of the average values. The membrane strips fail in a rupture manner at the ultimate strength. All specimens listed in Table 6.3 break at the centre area in between the two clamping areas at tips.

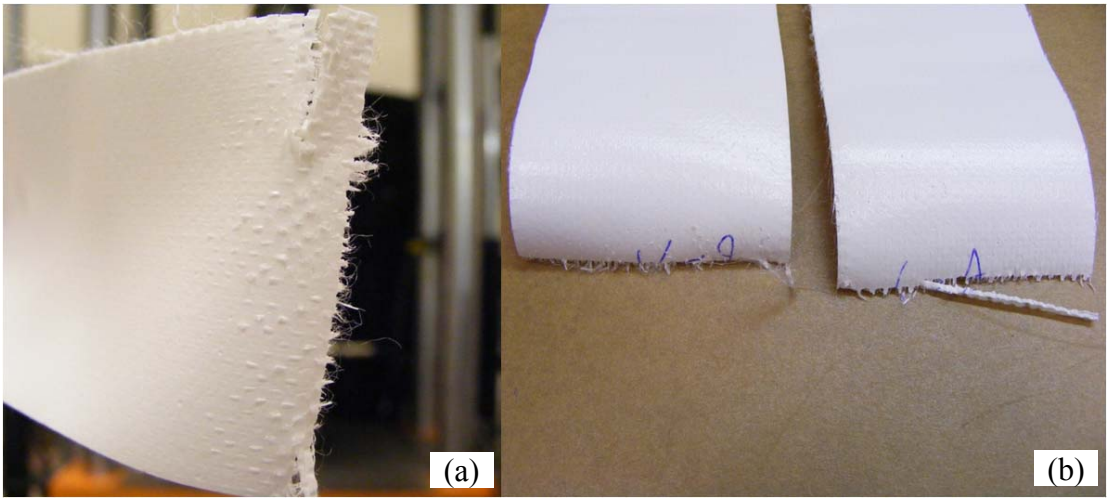

Figure 6.16: Breaking pattern of membrane strips in uniaxial tensile tests.

Figure 6.16 shows the typical breaking type of membrane strips under uniaxial tensile load in both warp and weft directions. The failure mode is a dynamic brittle rupture in the width direction. Figure 6.16(a) shows the salient coating around the failure area due to the dynamic failure of the yarns inside.

6.4.3 Uniaxial tear strength test on membrane

The uniaxial tear strength of membrane strips serves as a check method for acceptance of the material. Figure 6.17 and Figure 6.18 display tensile force versus displacement curves of test specimens in warp and weft directions, respectively. The curves in both directions share a similar pattern. In the initial region (displacement

ranges from 0 to 9), the applied force increases until the crack propagation threshold force. In the remaining region, the crack propagates rapidly and the applied force forms a plateau followed by a dramatic drop to zero.

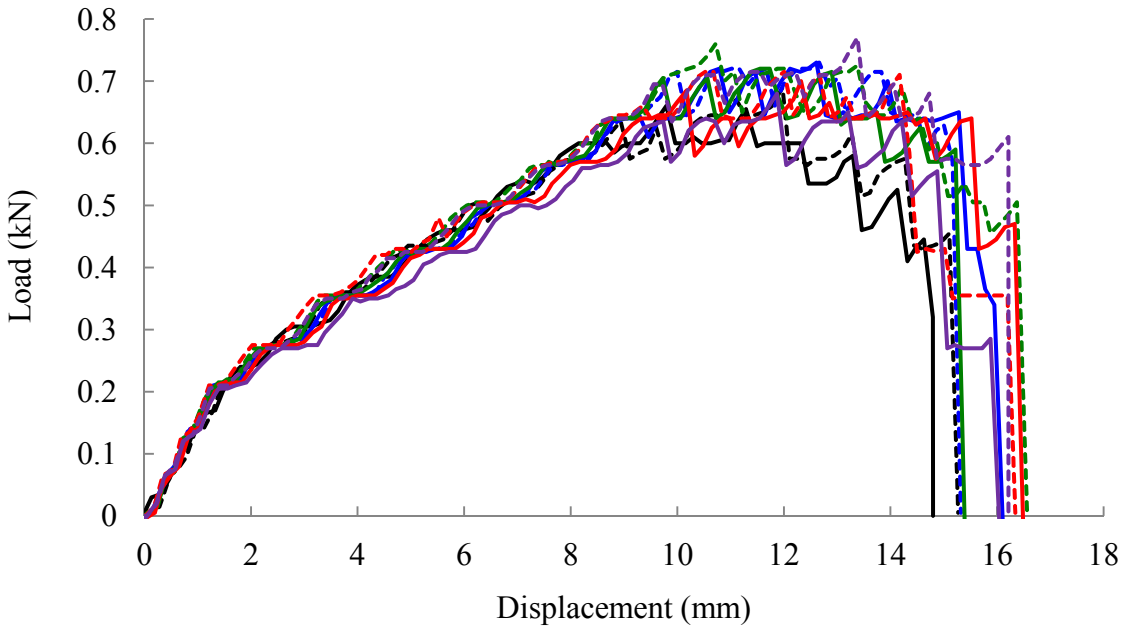

Figure 6.17: Uniaxial tearing load-displacement diagrams of 10 membrane strip specimens in warp direction.

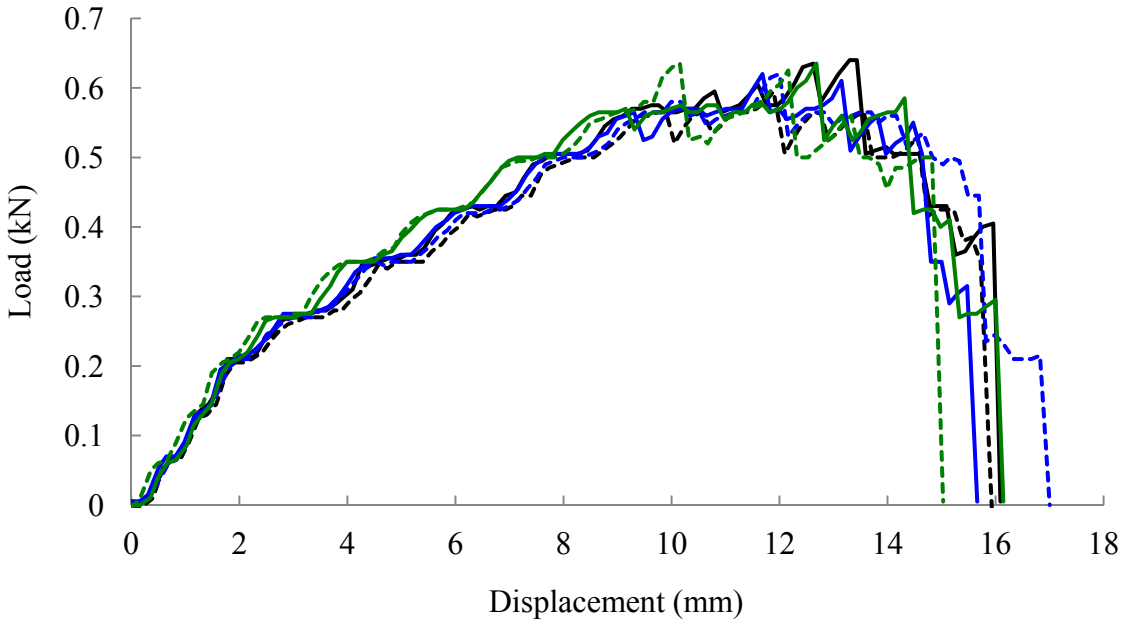

Figure 6.18: Uniaxial tearing load-displacement diagrams of 6 membrane strip specimens in weft direction.

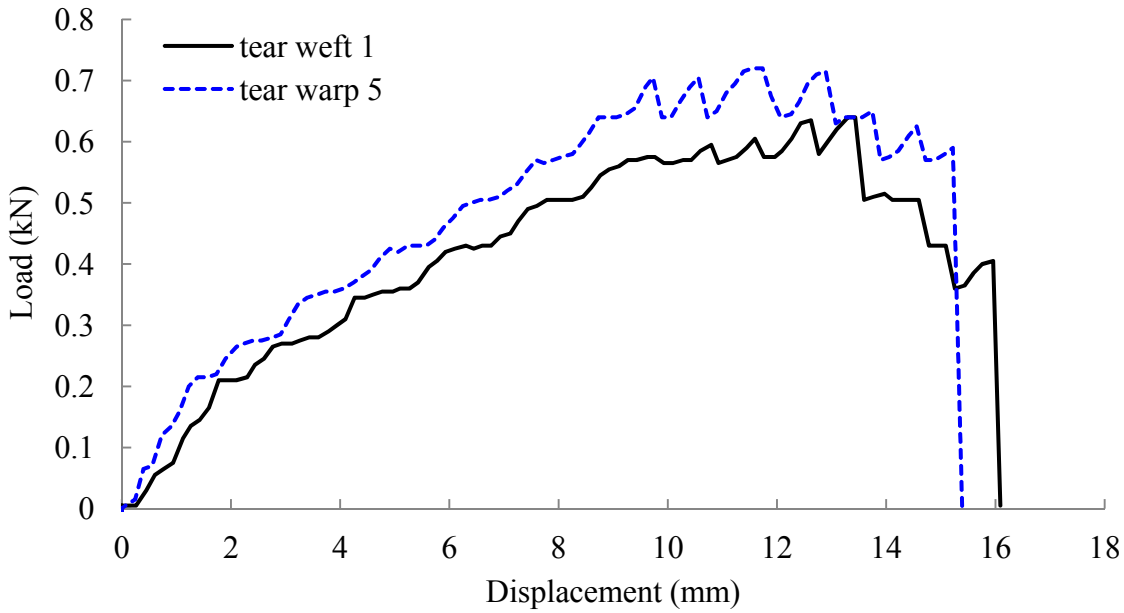

Figure 6.19: Preliminary comparison between typical uniaxial tearing load-displacement curves of membrane strip in warp and weft direction.

Table 6.4: Tear strength of membrane strip.

Warp direction		Weft direction	
Specimen No.	Tear strength (kN)	Specimen No.	Tear strength (kN)
1	0.66	1	0.64
2	0.69	2	0.60
3	0.73	3	0.62
4	0.73	4	0.62
5	0.72	5	0.64
6	0.76	6	0.63
7	0.70	-	-
8	0.72	-	-
9	0.65	-	-
10	0.77	-	-
Mean value	0.713	Mean value	0.622
Standard deviation	0.037	Standard deviation	0.015

Figure 6.19 compares the force to displacement response of membrane strip in warp direction to that in weft direction by using two typical curves extracted from Figure 6.17 and Figure 6.18. It shows that the tear strength of membrane strip in warp

direction is higher than that in weft direction. Besides, the membrane strip in warp direction also presents higher stiffness than that in weft direction.

Table 6.4 summarizes the tear strength for membrane strips tested in warp and weft directions, respectively. The standard deviations of both cases are lower than 6% of the average values. The average tear strength values in both directions fall in the normal range of PVC coated membrane and are close to the values given in the technical properties provided by the vendor.

6.4.4 Uniaxial strength test on welded seams

The uniaxial strength tests are used to evaluate the coating adhesive strength of the membrane as well as the welding quality of the workshop. 9 specimens in warp direction and 6 specimens in weft direction are tested. Figure 6.20 shows that membrane strips with welded seams have the similar pattern of load-extension diagrams with those without welded seams. Membrane strips in warp direction with welded seams also show higher uniaxial tensile strength than those in weft directions. The former also has higher stiffness than the latter.

Table 6.5 summarises the ultimate strength of welded membrane strips in warp and weft directions, respectively. The standard deviations of both cases are lower than 5% of the average values. The average values of the tested ultimate strength for welded membrane strip specimens in warp and weft directions are 2.838 and 2.561 kN/5 cm respectively, which achieves 97% and 98% of those for intact specimens in warp and weft directions. This shows a satisfactory welding quality and sufficient adhesive strength of the coating for the material.

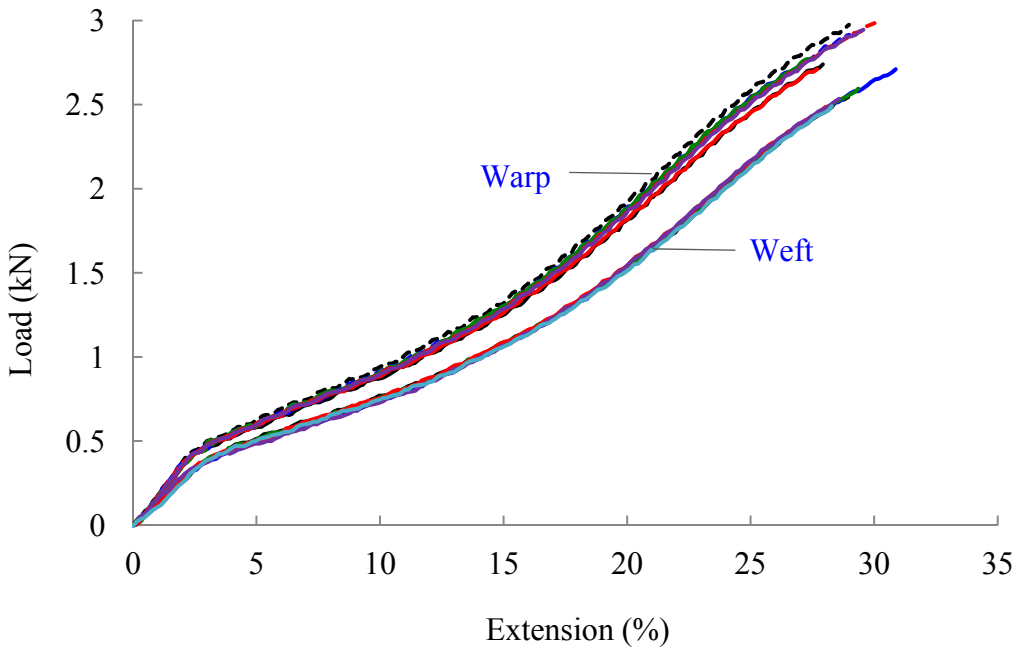

Figure 6.20: Force-extension diagram for membrane strips with welded seam in both warp and weft directions.

Table 6.5: Ultimate strength of membrane strip in warp direction with welded seam.

Warp direction		Weft direction	
Specimen No.	Weld strength (kN/5 cm)	Specimen No.	Weld strength (kN/5 cm)
1	2.74	1	2.55
2	2.98	2	2.71
3	2.69	3	2.60
4	2.92	4	2.49
5	2.78	5	2.54
6	2.72	6	2.49
7	2.74	-	-
8	3.02	-	-
9	2.98	-	-
Mean value	2.838	Mean value	2.561
Standard deviation	0.122	Standard deviation	0.062

6.4.5 Tensile strength tests on strut to membrane connection

In tensile strength tests of connection systems, two types of connections (one with steel cable typed keder core and one with nylon rope typed keder core) are

investigated. For each type of connection, forces are applied in both warp and weft directions of the main membrane.

Figure 6.21 shows the force-extension curves for connection systems discussed in Section 6.2.3. The force-extension curves show the similar pattern with those from uniaxial strength tests of membrane strip except that the lower stiffness at the very beginning region because of the initial adjustment at the strut and keder interface. As can be seen from Figure 6.21, steel cable typed connections have higher stiffness compared with nylon rope typed connections in both directions. This is due to steel cable typed connections experience smaller deformation at the aluminium strut and keder core interface than nylon rope typed connections. These two types of connections have the similar ultimate tensile strength in both warp and weft directions.

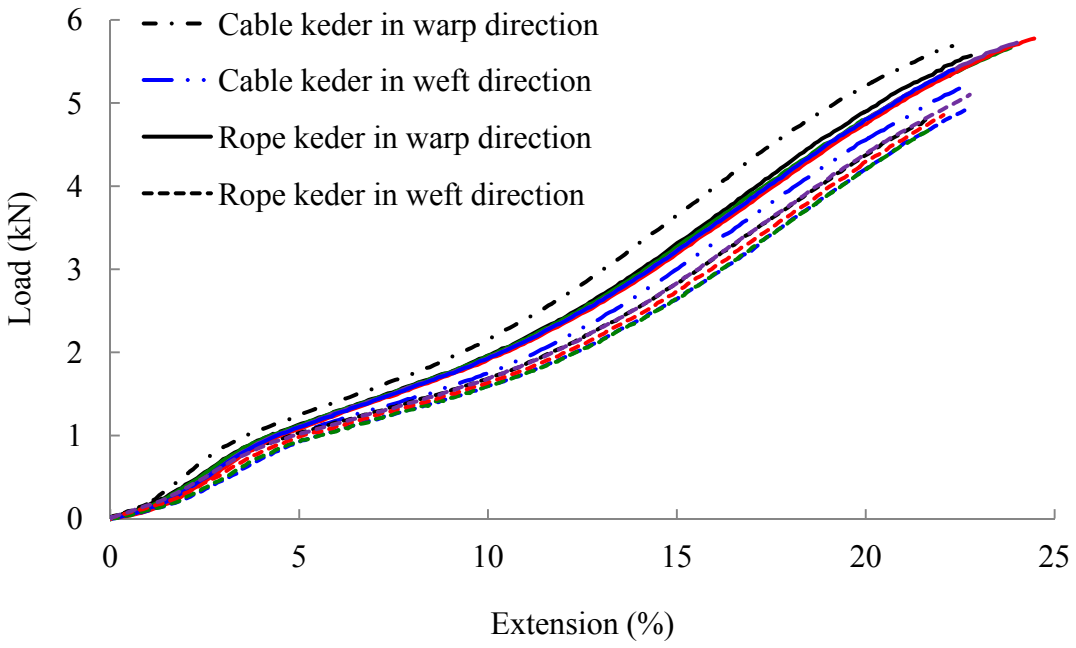

Figure 6.21: Force-extension diagram for connection systems in both warp and weft directions.

Table 6.6 summarizes the ultimate tensile strength of two types of connection systems

in warp and weft directions, respectively. Assuming that the uniaxial strength of membrane strips is proportional to the width, the mean ultimate strength for nylon rope typed connection systems is 97% of that for membrane strips in warp direction; while the mean ultimate strength for nylon rope typed connection systems is 95% of that for membrane strips in weft direction. This shows the connection systems using nylon rope is satisfactory.

Table 6.6: Tensile strength of connection systems.

Warp direction		Weft direction	
Specimen No.	Connection strength (kN/10 cm)	Specimen No.	Connection strength (kN/10 cm)
Rope keder 1	5.57	Rope keder 1	4.82
Rope keder 2	5.40	Rope keder 2	4.94
Rope keder 3	5.67	Rope keder 3	4.71
Rope keder 4	5.78	Rope keder 4	4.86
Rope keder 5	5.73	Rope keder 5	5.10
Cable keder	5.69	Cable keder	5.20
Mean value for rope keder	5.627	Mean value for rope keder	4.883
Standard deviation for rope keder	0.132	Standard deviation for rope keder	0.132

6.4.6 Monotonic load tests on Tension Strip Columns

Three Tension Strip Columns are fabricated and tested with the detailed dimension shown in Table 6.7. The cross section of the struts and membrane material used for the lateral restraints are given in Sections 6.2.2 and 6.2.3. The heights are the same for these columns while the gross depth is ranging from 184 to 342 mm. L/d ratios for these tested Tension Strip Columns vary from 8.4 to 25.

Results from the monotonic load test are shown and discussed in this section, including the failure modes, load-displacement curves, etc.

Table 6.7: Main dimension of tested Tension Strip Columns.

TSS	Height L (mm)	Pin space (mm)	Gross depth (mm)	Effective depth d (mm)	L/d
1	2000	104	184	80	25
2	2000	104	264	160	12.5
3	2000	104	342	238	8.4

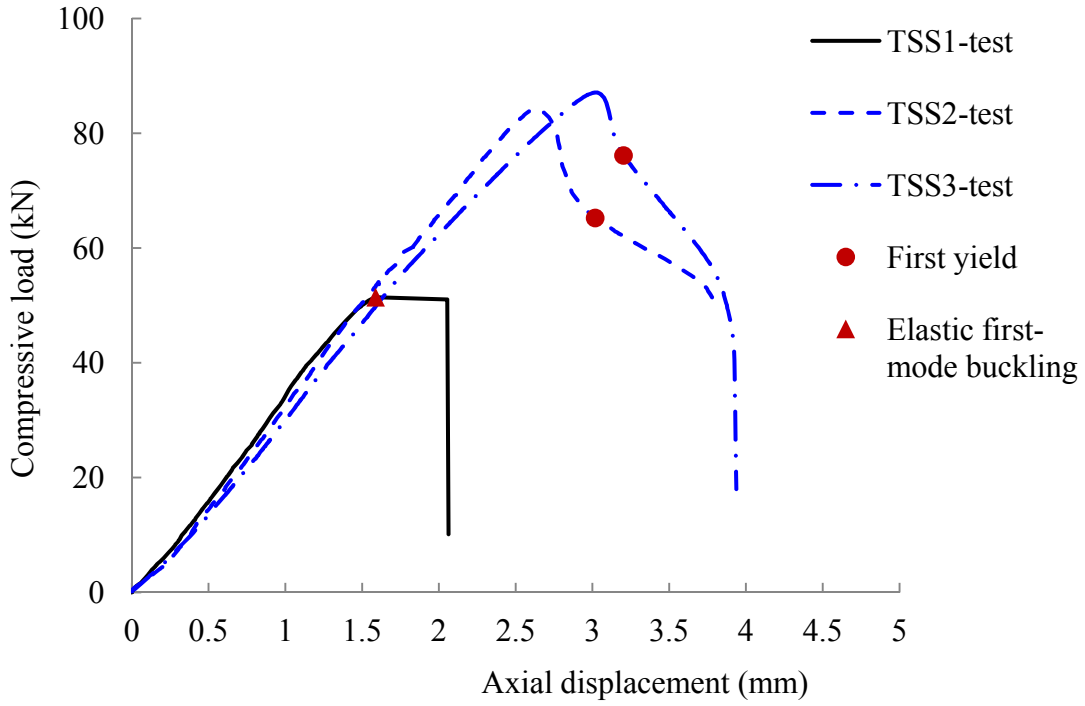

Figure 6.22: Load-displacement curves of test column specimens.

Figure 6.22 shows the applied load versus the axial shortening curves obtained from the experiments. The measured response can be partitioned into four phases as shown in Figure 6.23, where the load-displacement curve for TSS3 is taken as a typical example. In the initial phase, the column adapts itself to the applied axial compressive load and the membrane starts stretching. Lower slope compared to the second phases can be seen in this stage, which is due to the lower membrane resistance with small extension as discussed in Section 6.4.2. Comparisons among these three specimens show that TSS1 has the highest initial stiffness and TSS3 has the lowest. This trend is

consistent with the predictions by the simplified analytical and proposed numerical models as given in Section 5.2.2. The second phase, indicated as main compressive phase, may apply to the practical situation where Tension Strip Columns are used to resist axial compressive load. Almost consistent stiffness can be observed for each specimen. In the next two phases, Tension Strip Columns experience instability and large displacement. Ultimate load can be found in the buckling phase.

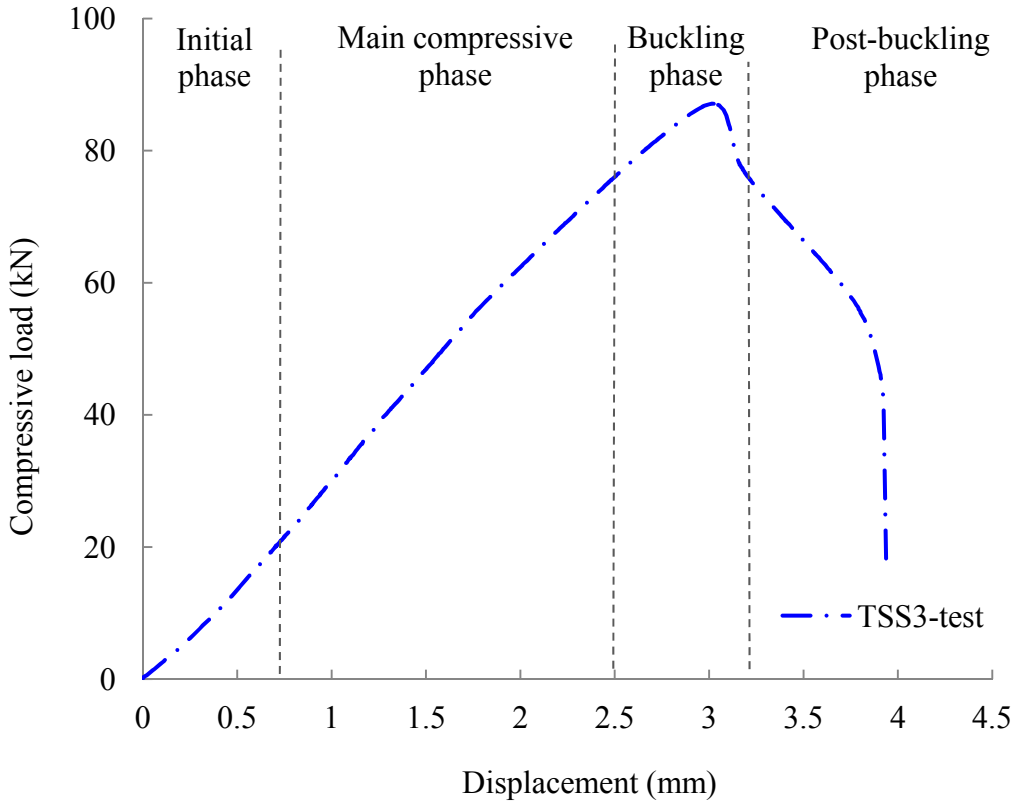

Figure 6.23: Different phases in typical load-displacement curve.

Figure 6.24 depicts the buckling load against the length to depth ratio for all three columns. Buckling load drops 3% as length to depth ratio changes from 8.4 to 12.5; this value drops 40% as the length to depth ratio changes from 8.4 to 25. The failure mode of all columns is dominated by the failure of a strut. Figure 6.25 shows TSS1 fails because a strut reverses the deflection direction and moves inward, resulting in

elastic buckling in the first mode. It is worthy to note that this first mode elastic buckling is induced by an initial anti-symmetric deformation as shown in Figure 6.25. Figure 6.26 and Figure 6.27 show the deformed configurations for TSS2 and TSS3, respectively. Both specimens fail because a strut experiences the anti-symmetric buckling and yields. As a result, the buckling load of TSS2 is very close to that of TSS3 while TSS1 shows significant reduction. It is hence suggested that high length to depth ratio (L/d > 20) should be avoided in the design of TSSs.

In addition, no failure in the membrane or connection area is observed after the tests, which indicates the connections between membrane and struts are reliable for these tested specimens.

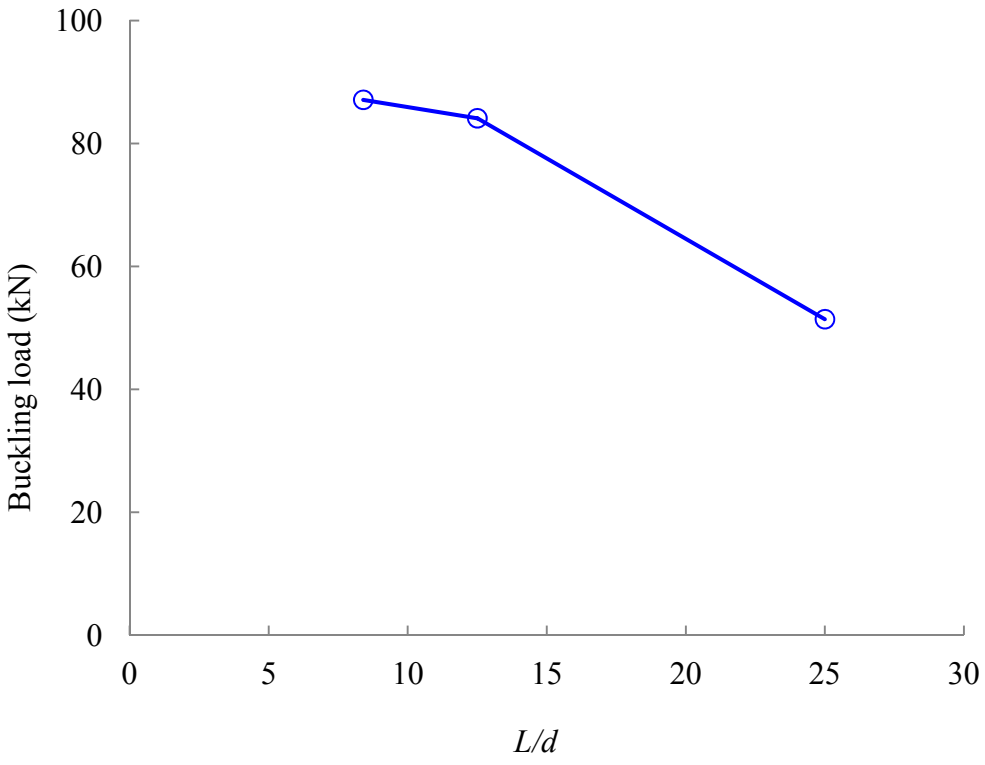

Figure 6.24: Effect of length to depth ratio on the experimental buckling load.

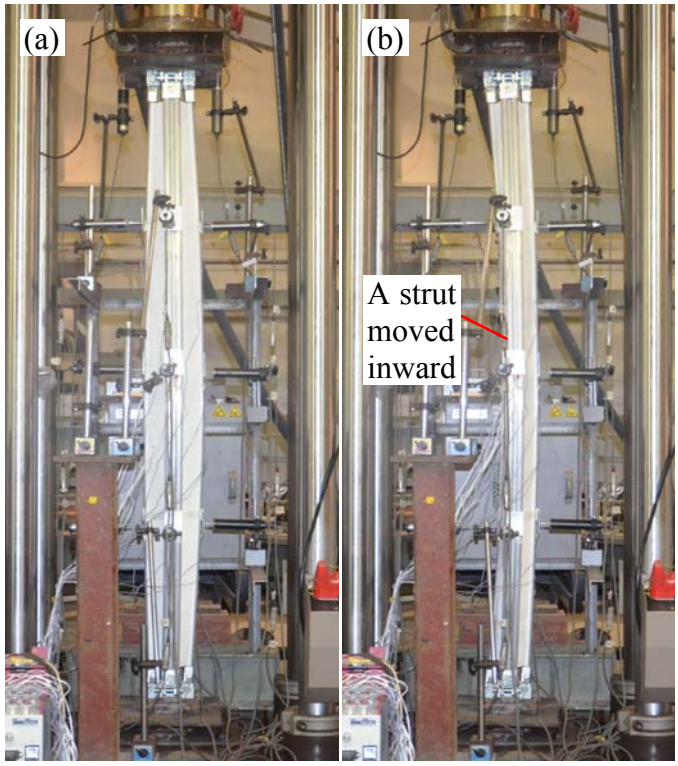

Figure 6.25: Experimental deformed configurations of TSS1: (a) anti-symmetric buckling mode; (b) a strut yielded.

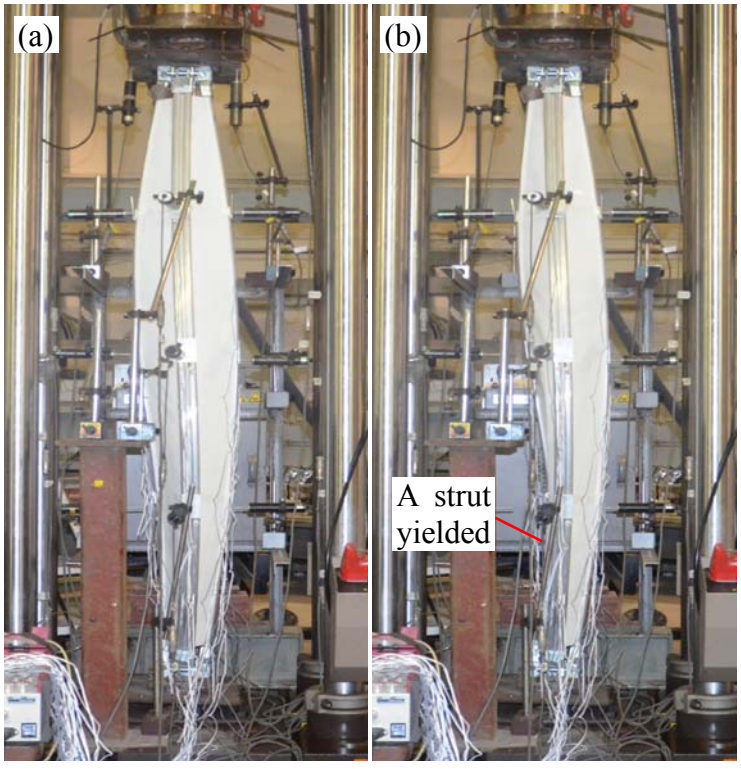

Figure 6.26: Experimental deformed configurations of TSS2: (a) anti-symmetric buckling mode; (b) a strut yielded.

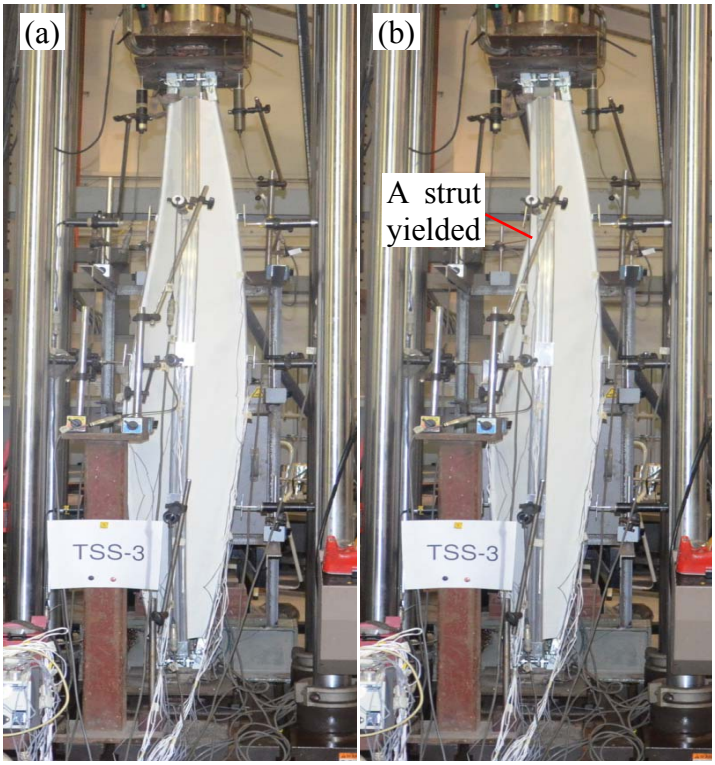

Figure 6.27: Experimental deformed configurations of TSS3: (a) anti-symmetric buckling mode; (b) a strut yielded.

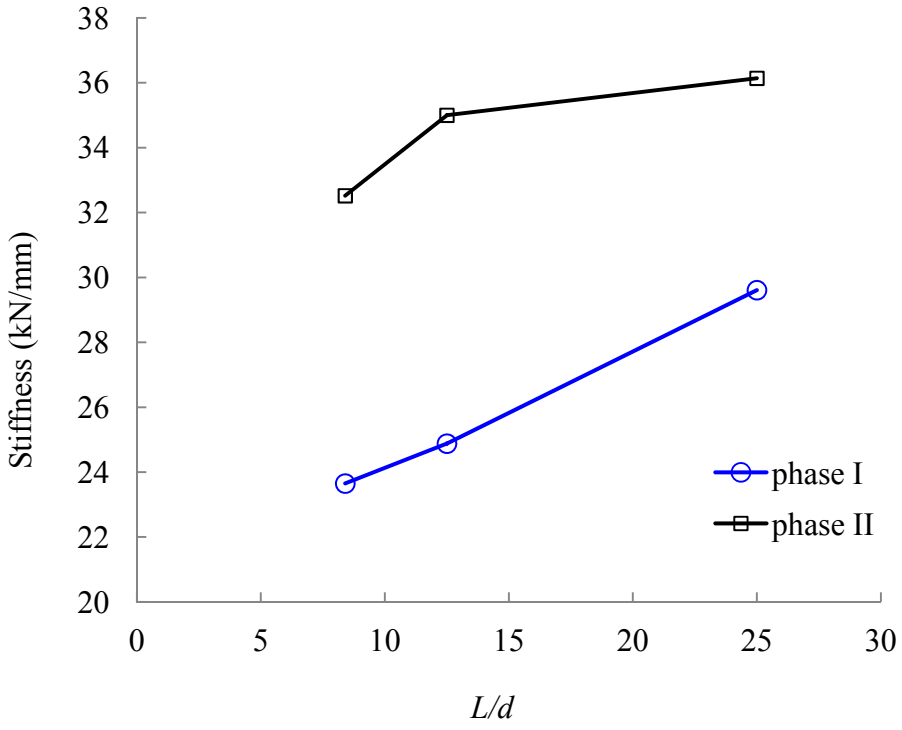

Figure 6.28: Effect of length to depth ratio on the experimental slope of the load-axial displacement curves.

Figure 6.28 compares the experimental slopes of the load-axial displacement curves for different Tension Strip Columns with different length to depth ratios. The comparison focuses on the slopes in initial phase and main compressive phase as indicated in Figure 6.23. In both phases TSS3 has the lowest stiffness while TSS1 has the highest stiffness among them. These observations from test results validate the conclusion drawn in Section 5.2.2 that structural stiffness of TSS increases with an increase in the height to depth ratio as the height remains same.

6.5 Comparison of load-displacement behaviour obtained from test and analysis

To verify the numerical model proposed in Chapter 4, the load-axial displacement curves for specimens TSS1 to TSS3 predicted by the model are compared with test results. TSS columns are simulated by a 2-dimensional model with two struts and a piece of membrane as given in Figure 5.2. These two struts have the same cross sectional properties with those from TSS3 as shown in Figure 6.2. The mean values of the material properties from the column test as summarized in Table 6.2 are used in the model. The membrane used in the model has an equivalent property with the two adjacent pieces of membrane in the TSS so that same elastic stiffness of restraints can be obtained. Test results of the whole connection system are adopted to simulate the restraint effects to include the effect of keder connections as given in Figure 6.21. Pin-roller boundary conditions are used in the numerical model.

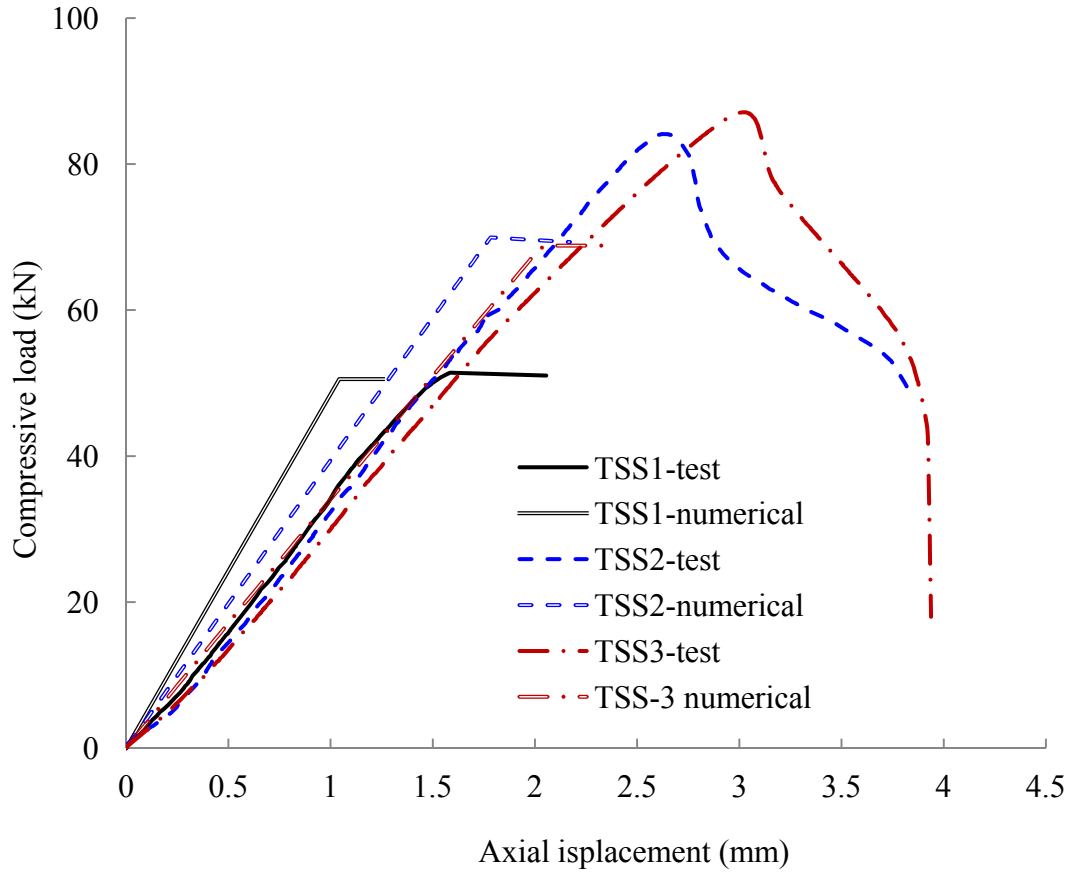

Figure 6.29: Comparison of the predicted load-displacement curve with test result of TSS3.

Figure 6.29 compares the predicted load-displacement at the tip curve against the test results for all three specimens. The predicted stiffness values by the proposed method for all specimens are higher than those obtained from the test in the main compressive phase as defined in Figure 6.23. Ineffective restraints due to the wrinkles caused by the fabrication imperfection in the tested specimen may attribute to this. In the numerical model, ideal restraints from all membranes are assumed leading to overestimated stiffness prediction. Figure 6.30 shows that some wrinkles distributed on the membrane surface after the TSS is tensioned.

The predicted buckling load for all specimens is lower than those observed in the tests. This is due to the fact that the roller-roller boundary conditions in the test as

shown in Figure 6.13 allow only in-plane rotation of the specimen. The out-of-plane rotation is restrained in such setup, leading to semi-rigid boundary conditions. In the numerical model, the pin-roller boundary condition is simply assumed. In such a case, it is reasonable for the numerical model to predict lower buckling load.

Figure 6.30: Wrinkles on the tensioned membrane surface.

Table 6.8 summarizes the stiffness for all specimens from both experimental measurements and numerical simulations. Table 6.8 also compares the predicted stiffness by the proposed numerical method with the stiffness of the specimens in the main compressive phase (i.e. Phase II) measured from the test results for all three specimens. It can be seen that satisfactory prediction can be obtained from the proposed method for TSSs with lower L/d ratios (TSS1 and TSS2). The difference between stiffness by prediction and test measurement for TSS3, however, reaches 25%. The possible explanation is as follows. Slender TSS (TSS3) with high L/d ratios suffers from premature buckling that affects the structural stiffness. In addition, elastic restraints in slender TSS (TSS3) are more sensitive to the fabrication imperfection because of the smaller membrane size used, although that imperfection remains on the same level for all specimens.

Table 6.8: Comparison of predicted stiffness with test results.

Specimen	L/d	Stiffness from tests (kN/mm)		Predicted Stiffness (kN/mm)	Difference from Phase II
		Phase I	Phase II		
TSS1	25	29.6	36.1	48.5	25%
TSS2	12.5	24.9	35.0	39.4	11%
TSS3	8.4	23.7	32.5	33.9	4%

Table 6.9: Comparison of predicted buckling load with test results.

Specimen	L/d	Buckling load (kN)	Predicted buckling load (kN)	Difference
TSS1	25	51.4	50.6	2%
TSS2	12.5	84.1	70.0	17%
TSS3	8.4	87.1	68.8	21%

All buckling loads obtained from the numerical method are lower than those measured in the tests, leading to conservative predictions. The predicted buckling loads for TSS2 and TSS3 are 17% and 21% lower than those observed from tests. The predicted buckling loads for TSS1 agree well with the test results. The

underestimation is attributed to the simplified boundary conditions used in the numerical model as explained above. The buckling mode captured from the numerical simulation is illustrated in Figure 6.31, which has the exact shape observed during the tests.

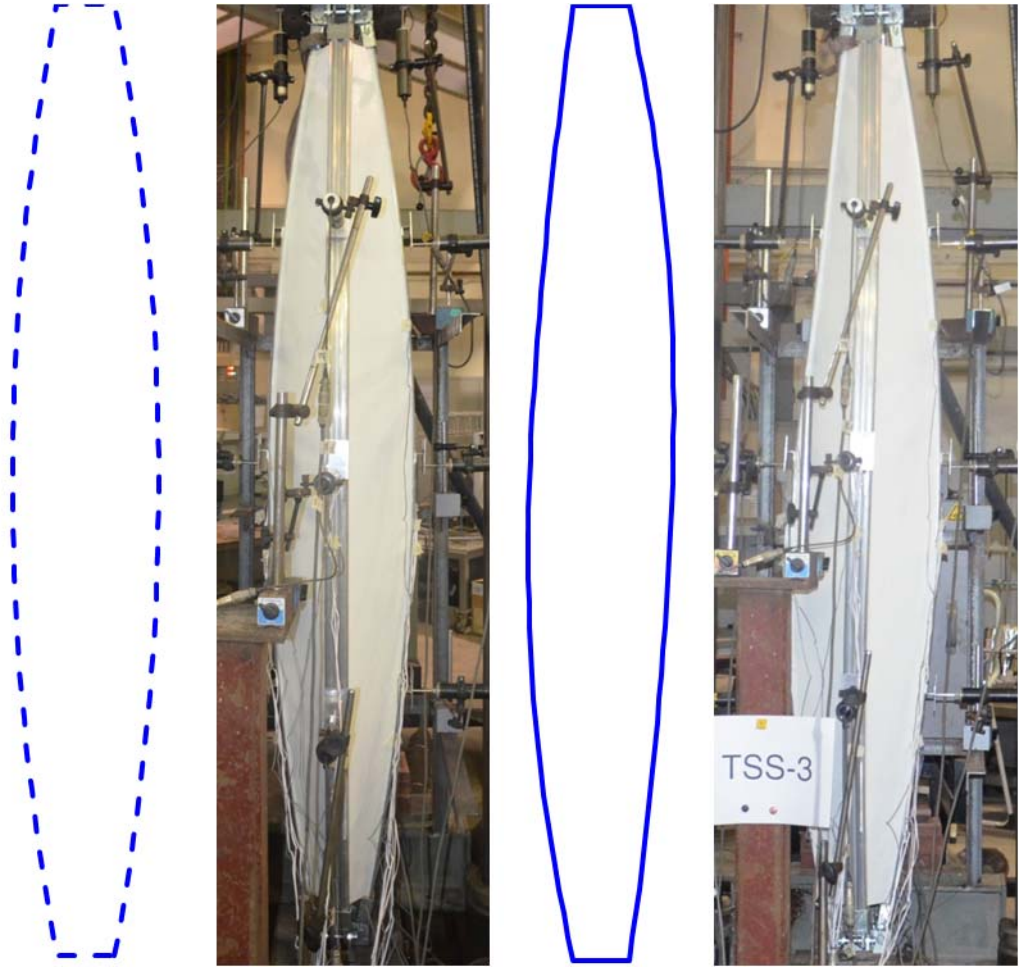

(a) (b) (c) (d)

Figure 6.31: Initial and buckling configurations: (a) Initial outline in proposed TSS numerical model; (b) Initial configuration of TSS specimen; (c) Deformed outline in proposed TSS numerical model; (d) Deformed configuration of TSS specimen.

6.6 Summaries

Three full scale specimens for TSSs are manufactured and tested. The challenges during the fabrication and installation are highlighted and practical recommendations

are given. The designed system including connections, joints, etc., has been proven to be able to realize rapid assembly and dismount. Structural behaviours of TSSs such as failure modes, critical loads and load-displacement curves are investigated in the tests. The experimental results show that the stiffness of TSS increases as the length to depth ratio increases from 8.3 to 25. The critical loads for the specimens remain similar when L/d changes from 8.3 to 12.5. However, the critical load drops by about 40% when L/d reaches 25 due to premature buckling of a strut in the first mode. The test demonstrates the adopted connection between membrane and strut is robust and reliable. The methods proposed in Chapter 4 can achieve reasonable predictions of the stiffness and buckling load for Tension Strip Structures.

Experiments on components including aluminium struts, membrane, and connection systems provide necessary mechanical properties for the numerical modelling. These experiments also offer technical insights on the desirable features in design details of tensile restrained structural systems.

Chapter 7

Conclusions

The main contributions of this thesis include: (a) developing new efficient structural forms using a self-balancing system involving compression struts restrained by tensile elements, (b) studying the response and behaviour of proposed structures with advanced analyses, and (c) design, implementation, and validation by prototypes and tests. The thesis proposes two novel lightweight structures under the similar concept of utilizing tensile restrained arch/truss for better structural performance. The main findings are summarized in the following sections.

7.1 Tension Strip Structures

Tension Strip Structure (TSS) has been proposed with the intention to combine the structural advantages of arch as lightweight compressive elements and membrane as lightweight tensile elements. In this new design, tensile restrained arches are used as a column-like member resisting axial load rather than as a conventional arch resisting gravity load. The buckling resistance of slender structural systems may be significantly improved by restraining the compression members laterally by tensile membrane.

Different TSS systems of various purposes such as planar or 3-dimensional shapes

have been proposed. Reliable connection details have been developed to join the tensile membrane to the struts so that they can act as an integral system to resist compression loads. Practical recommendations regarding the fabrication and assembly of TSSs have been provided based on full scale prototypes.

Key attributes of TSS are summarized as follows.

(a) Given the same height and cross sections of the compression components (struts), the initial stiffness of TSSs rises with an increase of the length to depth ratio. High length to depth ratio (>20) leads to premature first mode buckling toward the structural axis as observed from tests.

(b) The axial stiffness of TSSs increases with an increase in the elastic stiffness of restraints provided by membrane.

(c) The stiffness of the TSS with more struts is higher than those with fewer struts while the total weight remains same. However, maximum four struts are recommended because otherwise the joints become very complex.

(d) Higher elastic stiffness of restraints by membrane leads to higher normalized buckling load.

(e) Low buckling resistance of very slender column is associated with the first fundamental mode of buckling, which can be avoided in design by providing lateral restraints. A careful tuning of the combination of length to depth ratio, the cross sectional resistance of the strut and the elastic stiffness of restraints by membrane would result in an optimum least weight design.

7.2 Deployable Cable Chain Structures

Deployable Cable Chain Structures is proposed for shelters with a small to medium span following the similar concepts as Tension Strip Structures with an added function of deployablility. In this new structure, cable restrained compressive elements consisting of discretized struts forming barrel vault or dome shapes providing enclosure space as a shelter.

Deployable Cable Chain Structure (DCCS) is different from commonly used deployable pantographic structures and deployable tension-strut structures because eccentricity of the strut axes is avoided by using hinged connections rather than pivot connections. Various structural forms such as barrel vaults, geodesic domes, boom structures and their combinations have been generated by morphology studies. Investigation on the deployment pattern shows that the pyramid module based pattern has higher deployment ratio than the origami-like deployment pattern. Based on the pyramid module, the geometry relationship among struts, surrounding cables and connecting cables is derived. Honeycomb socket joint has been proposed for DCCSs to allow free rotation of the struts about their own axes

Nonlinear inelastic analysis on DCCSs has been carried out and comparison with other existing foldable shelters indicates that the proposed structure offers excellent structural efficiency in term of strength to weight ratio. In the robustness analysis, dynamic effects of accidental removal of cables are investigated, which shows the structure is sensitive to sudden loss of cable forces. However, the robustness of proposed structures against dynamic impact due to sudden damage of cables can be enhanced by providing safety ties at strategic locations.

7.3 Nonlinear analysis methods for Tension Strip Structures

Efficient and accurate locking-free beam element formulas for the analysis of beams with small strains and large displacements are developed. The element stiffness matrices are further expanded to include membrane restraints which are modelled as continuous springs. The attributes and advantages of the presented method are summarized as follows:

(a) Bending-tension coupling effect of the curved beam is circumvented to avoid membrane or shear locking problems.

(b) Axial strain caused by both end translations and end rotations is considered in the calculation of internal force steps.

(c) The proposed element is implemented into a generalized displacement control method with a capacity to trace equilibrium path involving both snap through and snap back problems.

(d) The applicability and accuracy of the developed method have been demonstrated by solving a series of classical problems from literature including large deflection of cantilever beams, planar frames, shallow/deep arches, as well as straight and curved beams on elastic foundations.

(e) The proposed numerical scheme suits the analysis of TSS, which is validated by comparing with test results of three TSS specimens.

7.4 Future research recommendations

Deep insights of the structural behaviour under different external loads require more comprehensive future researches on proposed structures in this thesis. Some research recommendations are given as follows.

(a) TSS has shown high potential for compressive elements used as members in temporary or semi-permanent structures. It is also known that TSS performs especially well as members with large length. Thus, it is interesting to develop deployable Tension Strip Columns for economic transportation and storage.

(b) The membrane strut interface connection plays important roles for the structural behaviour of the Tension Strip Columns. It is critical to investigate the connection performance under cyclic loads and the possible degeneration after long-time service (i.e., months).

(c) Only axial load condition is considered in this thesis, different load combinations including the end moment as well as torsion should be taken into account. Because it is practically hard to avoid low-level moments and/or torsional forces even for axial loading members such as a pole used in a tent.

(d) Laboratory tests on a module of DCCS or the full-scale specimen can provide solid result of the structural behaviour, which may verify the qualification of such structure for practical usage.

Besides, another research direction is to seek new lightweight structural forms following the concept used in this thesis with the emerging new structural material especially the tensile material.

Reference

ABAQUS (2010). Abaqus/standard: User's manual version 6.10.Pawtucket USA.

Akoz AY and Kadioglu F (1996). "The mixed finite element solution of circular beam on elastic foundation." Computers & Structures **60**(4): 643-651.

Alpermann H and Gengnagel C (2009). "Membranversteifte bogentragwerke." Stahlbau **78**(8): 531-536.

Alsafadie R, Hjiaj M, et al. (2010). "Corotational mixed finite element formulation for thin-walled beams with generic cross-section." Computer Methods in Applied Mechanics and Engineering **199**(49-52): 3197-3212.

Alsafadie R, Hjiaj M, et al. (2011). "A comparative study of displacement and mixed-based corotational finite element formulations for elasto-plastic three-dimensional beam analysis." Engineering Computations **28**(7-8): 939-982.

Argyris JH (1964). "Recent advances in matrix methods of structural analysis." Proceedings of Progress in Aeronautical Science, New York, Pergamon Press.

Argyris JH, Balmer H, et al. (1979). "Finite-element method - natural approach." Computer Methods in Applied Mechanics and Engineering **17-8**(JAN): 1-106.

ASTM D5587-08 (2008). Standard test method for tearing strength of fabrics by trapezoid procedure. ASTM International. West Conshohocken, PA.

ASTM E8/E8M-08 (2008). Standard test methods for tension testing of metallic materials. ASTM International. West Conshohocken, PA.

Balling RJ and Lyon JW (2011). "Second-order analysis of plane frames with one element per member." Journal of Structural Engineering-Asce **137**(11): 1350-1358.

Banan MR, Karami G, et al. (1989). "Finite-element analysis of curved beams on elastic foundations." Computers & Structures **32**(1): 45-53.

Bathe K-J and Bolourchi S (1979). "Large displacement analysis of three-dimensional beam structures." International Journal for Numerical Methods in Engineering **14**(7): 961-986.

Belytschko T and Glaum LW (1979). "Applications of higher-order corotational stretch theories to non-linear finite-element analysis." Computers & Structures **10**(1-2): 175-182.

Bletzinger K-U and Ramm E (2001). "Structural optimization and form finding of light weight structures." Computers & Structures **79**(22–25): 2053-2062.

Brayley KE, Davids WG, et al. (2012). "Bending response of externally reinforced,

inflated, braided fabric arches and beams." Construction and Building Materials **30**(0): 50-58.

Breuer JCM and Luchsinger RH (2010). "Inflatable kites using the concept of tensairity." Aerospace Science and Technology **14**(8): 557-563.

Burford NK and Gengnagel C (2004). "Mobile shelter systems - 2 case studies in innovation." Proceedings of IASS symposium. 334-335.

Burford NK and Smith FW (1999). "Developing a new military shelter system: A technical study in advanced materials and structures." Building Research and Information **27**(2): 64-83.

Burford NK, Smith FW, et al. (2009). The evolution of arches as lightweight structures - a history of empiricism and science. Proceedings of the 3rd International Congress on Construction History. Cottbus.

Calladine CR (1978). "Fuller,buckminster tensegrity structures and maxwell,clerk rules for construction of stiff frames." International Journal of Solids and Structures **14**(2): 161-172.

Chakraborty S and Majumdar S (1997). "An arbitrary-shaped arch element for large deflection analysis." Computers & Structures **65**(4): 593-600.

Chakraborty S and Sarkar SK (2000). "Analysis of a curved beam on uncertain elastic foundation." Finite Elements in Analysis and Design **36**(1): 73-82.

Chan SL and Gu JX (2000). "Exact tangent stiffness for imperfect beam-column members." Journal of Structural Engineering-Asce **126**(9): 1094-1102.

Chan SL, Shu GP, et al. (2002). "Stability analysis and parametric study of pre-stressed stayed columns." Engineering Structures **24**(1): 115-124.

Chan SL and Zhou ZH (1995). "2nd-order elastic analysis of frames using single imperfect element per member." Journal of Structural Engineering-Asce **121**(6): 939-945.

Chen HH, Lin WY, et al. (2006). "Co-rotational finite element formulation for thin-walled beams with generic open section." Computer Methods in Applied Mechanics and Engineering **195**(19-22): 2334-2370.

Chu KH and Berge SS (1963). "Analysis and design of struts with tension ties." Journal of the Structural Division - ASCE **89**(1): 127-163.

Conci A (1992). "Large displacement analysis of thin-walled-beams with generic open section." International Journal for Numerical Methods in Engineering **33**(10): 2109-2127.

Crisfield MA (1991). Nonlinear finite element analysis of solids and structures. Volume 1: Essentials

D'Anza G (2008). Forten 3000 user guide. TSI s.r.l. Naples.

Dasgupta S and Sengupta D (1988). "Horizontally curved isoparametric beam element with or without elastic-foundation including effect of shear deformation." Computers & Structures **29**(6): 967-973.

de Araujo RR, de Andrade SAL, et al. (2008). "Experimental and numerical assessment of stayed steel columns." Journal of Constructional Steel Research **64**(9): 1020-1029.

de Souza RM (2000). Froce-based finite element for large displacement inelastic analysis of frames. PhD thesis, Dept. of Civil and Environmental Engineering, UC Berkeley. Berkeley.

De Temmerman IaN, Mollaert M, et al. (2007). "Design and analysis of a foldable mobile shelter system." International Journal of Space Structures **22**(3): 161-168.

Dorfi HR and Busby HR (1994). "An effective curved composite beam finite-element based on the hybrid-mixed formulation." Computers & Structures **53**(1): 43-52.

Drew P (1976). Frei otto: Form and structure. Westview Press.

Escrig F (1996). "General survey of deployability in architecture." Mobile and Rapidly Assembled Structures II, Computational Mechanics Publications. 3-22.

European Committee for Standardization (2002). Eurocode: Basis of structural design.Brussels.

European Committee for Standardization (2006). Eurocode 1: Actions on structures - part 1-7: General actions - accidental actions. Brussels.

Felippa CA and Haugen B (2005). "A unified formulation of small-strain corotational finite elements: I. Theory." Computer Methods in Applied Mechanics and Engineering **194**(21-24): 2285-2335.

Friedman Z and Kosmatka JB (1998). "An accurate two-node finite element for shear deformable curved beams." International Journal for Numerical Methods in Engineering **41**(3): 473-498.

Gantes CJ (2001). Deployable structures analysis and design. Wit Press. Great Britain.

Guest SD and Pellegrino S (1994a). "The folding of triangulated cylinders .1. Geometric considerations." Journal of Applied Mechanics-Transactions of the Asme **61**(4): 773-777.

Guest SD and Pellegrino S (1994b). "The folding of triangulated cylinders .2. The folding process." Journal of Applied Mechanics-Transactions of the Asme **61**(4): 778-783.

Guest SD and Pellegrino S (1996). "The folding of triangulated cylinders .3. Experiments." Journal of Applied Mechanics-Transactions of the Asme **63**(1): 77-83.

Hachem C, Karni E, et al. (2005). "Evaluation of biological deployable systems." International Journal of Space Structures **20**(4): 189-200.

Hafez HH, Temple MC, et al. (1979). "Pre-tensioning of single-crossarm stayed columns." Journal of the Structural Division-Asce **105**(2): 359-375.

Hanaor A (1999). "Joint instability in lattice structures - lessons from a recent collapse." International Journal of Space Structures **14**(4): 257-267.

Hanaor A, Dallard PRB, et al. (2000). "Member buckling with joint instability - design application." International Journal of Space Structures **15**(3-4): 205-213.

Hanaor A and Levy R (2001). "Evaluation of deployable structures for space enclosures." International Journal of Space Structures **16**(4): 211-229.

Heinrich B (1979). Am anfang war der balken: Zur kulturgeschichte der steinbrücke. Deutsches Museum.

Hellan Ø, høgskole Nt, et al. (1995). Nonlinear pushover and cyclic analyses in ultimate limit state design and reassessment of tubular steel offshore structures. Norwegian Institute of Technology, Division of Marine Structures.

Herzog T (1976). Pneumatic structures: A handbook for the architect and engineer. Crosby Lockwood Staples.

Hetenyi M (1946). Beams on elastic foundation. The University of Michigan Press. Ann Arbor.

Huntington CG (2004). The tensioned fabric roof. American Society of Civil Engineers.

Kassabian PE, You Z, et al. (1999). "Retractable roof structures." Proceedings of the Institution of Civil Engineers-Structures and Buildings **134**(1): 45-56.

Khosravi P, Ganesan R, et al. (2007). "Corotational non-linear analysis of thin plates and shells using a new shell element." International Journal for Numerical Methods in Engineering **69**(4): 859-885.

Kim J-G and Park Y-K (2006). "Hybrid-mixed curved beam elements with increased degrees of freedom for static and vibration analyses." International Journal for Numerical Methods in Engineering **68**(6): 690-706.

Kim SE and Chen WF (1996). "Practical advanced analysis for unbraced steel frame design." Journal of Structural Engineering-Asce **122**(11): 1259-1265.

Krishnapillai A (1988). "Deployable structures." U.S. Patent 5167100.

Le van A and Wielgosz C (2007). "Finite element formulation for inflatable beams." Thin-Walled Structures **45**(2): 221-236.

Li ZX (2007a). "A co-rotational formulation for 3d beam element using vectorial rotational variables." Computational Mechanics **39**(3): 309-322.

Li ZX (2007b). "A mixed co-rotational formulation of 2d beam element using vectorial rotational variables." Communications in Numerical Methods in Engineering **23**(1): 45-69.

Liew JYR and Krishnapillai A (2009). "Deployable structures." U.S. Patent 20090199503.

Liew JYR, Lee BH, et al. (2003). "Innovative use of star prism (sp) and di-pyramid (dp) for spatial structures." Journal of Constructional Steel Research **59**(3): 335-357.

Liew JYR and Li JJ (2006). "Advanced analysis of pre-tensioned bowstring structures." International Journal of Steel Structures **6**(2): 153-162.

Liew JYR, Punniyakotty NM, et al. (2001). "Limit-state analysis and design of cable-tensioned structures." International Journal of Space Structures **16**(2): 95-110.

Liew JYR and Tang LK (2000). "Advanced plastic hinge analysis for the design of tubular space frames." Engineering Structures **22**(7): 769-783.

Liew JYR and Tran TC (2006). "Novel deployable strut-tensioned membrane structures." Journal of the International Association for Shell and Spatial Structures **47**(150): 17-29.

Liew JYR, Vu KK, et al. (2008). "Recent development of deployable tension-strut structures." Advances in Structural Engineering **11**(6): 599-614.

Luchsinger R and Crettol R (2006). "Experimental and numerical study of spindle shaped tensairity girders." International Journal of Space Structures **21**(3): 119-130.

Luchsinger RH, Pedretti M, et al. (2004). "Pressure induced stability: From pneumatic structures to tensairity®." Journal of Bionics Engineering **1**(3): 141-148.

Luchsinger RH, Sydow A, et al. (2011). "Structural behavior of asymmetric spindle-shaped tensairity girders under bending loads." Thin-Walled Structures **49**(9): 1045-1053.

Lukasiewicz S and Warner H (2010). "Air beam with stiffening members and air beam structur." U.S. patent 2010/0146868 A1.

Miura K and Tanizawa K (2000). Tension truss antenna - concept, reality and future

Mourelatos ZP and Parsons MG (1987). "A finite element analysis of beams on elastic foundation including shear and axial effects." Computers & Structures

27(3): 323-331.

Natori M (1985). "Jointed extendible truss beam." U.S. Patent 4655022.

Nojima T (2002). "Modelling of folding patterns in flat membranes and cylinders by origami." JSME International Journal, Series C: Mechanical Systems, Machine Elements and Manufacturing **45**(1): 364-370.

O'Connor C (1993). Roman bridges. Cambridge University Press.

Omidvar B and Ghorbanpoor A (1996). "Nonlinear fe solution for thin-walled open-section composite beams." Journal of Structural Engineering-Asce **122**(11): 1369-1378.

Onoda J (1986). "Collapsible truss unit, and frameworks constructued by combinations of such units." U.S. Patent 4667451.

Onoda J (1987a). "Collapsible truss unit for use in combinations with other like units for the construction of frameworks." U.S. Patent 4771585.

Onoda J (1987b). "Deployable truss." U.S. Patent 4819399.

Onoda J (1988). "Deployable truss structures." U.S. Patent 4745725.

Onoda J (1991). "Collapsible truss structures." U.S. Patent 5040349.

Oran C (1973). "Tangent stiffness in plane frames." Journal of the Structural Division - ASCE **99**(6): 973-985.

Oran C and Kassimali A (1976). "Large deformations of framed structures under static and dynamic loads." Computers & Structures **6**(6): 539-547.

Pedretti M and Luscher R (2007). "Tensairity-patent – eine pneumatische tenso-struktur." Stahlbau **76**(5): 314-319.

Pi Y-L and Trahair NS (1998). "Non-linear buckling and postbuckling of elastic arches." Engineering Structures **20**(7): 571-579.

Pi YL, Bradford MA, et al. (2007). "Geometric and material nonlinear analyses of elastically restrained arches." Engineering Structures **29**(3): 283-295.

Plagianakos TS, Teutsch U, et al. (2009). "Static response of a spindle-shaped tensairity column to axial compression." Engineering Structures **31**(8): 1822-1831.

Plaut RH and Johnson ER (1981). "The effects of initial thrust and elastic-foundation on the vibration frequencies of a shallow arch." Journal of Sound and Vibration **78**(4): 565-571.

Prathap G (1985). "The curved beam deep arch finite ring element revisited." International Journal for Numerical Methods in Engineering **21**(3): 389-407.

Prathap G and Babu CR (1986). "An isoparametric quadratic thick curved beam element." International Journal for Numerical Methods in Engineering **23**(9): 1583-1600.

Prathap G and Bhashyam GR (1982). "Reduced integration and the shear-flexible beam element." International Journal for Numerical Methods in Engineering **18**(2): 195-210.

Rasch J (1985). "Die kuppel in der römischen architektur. Entwicklung, formgebung, konstruktion." Architectura **15**(2): 117-139.

Ritzel DV, Parks SA, et al. (2009). Blast, ballistic, and earthquake response of a deployable air-beam shelter system. Proceedings of the 8th International Conference on Shock and Impact Loads on Structures**:** 545-552.

Saito D and Wadee MA (2009a). "Buckling behaviour of prestressed steel stayed columns with imperfections and stress limitation." Engineering Structures **31**(1): 1-15.

Saito D and Wadee MA (2009b). "Numerical studies of interactive buckling in prestressed steel stayed columns." Engineering Structures **31**(2): 432-443.

Saleeb AF and Chang TY (1987). "On the hybrid-mixed formulation of c0 curved beam elements." Computer Methods in Applied Mechanics and Engineering **60**(1): 95-121.

Seidel M (2009). Tensile surface structures. A practical guide to cable and membrane construction. Ernst & Sohn, Verlag für Architektur und technische Wissenschaften GmbH & Co. KG. Berlin.

Shaeffer RE (1996). Tensioned fabric structures: A practical introduction. American Society of Civil Engineers, Task Committee on Tensioned Fabric Structures.

Silveira RAM, Pereira WLA, et al. (2008). "Nonlinear analysis of structural elements under unilateral contact constraints by a ritz type approach." International Journal of Solids and Structures **45**(9): 2629-2650.

Singapore BaCSCo (2009). National annex to ss en 1991-1-4. Singapore.

Skelton RE (1995). "Deployable tendon-controlled structure." U.S. Patent 5642590.

Smith EA (1985). "Behavior of columns with pretensioned stays." Journal of Structural Engineering-Asce **111**(5): 961-972.

Smith RJ, McCaffrey GT, et al. (1975). "Buckling of a single-crossarm stayed column." Journal of the Structural Division-ASCE **101**(NST1): 249-268.

Standardization ECf (2005). Eurocode 1: Actions on structures-part 1-4: General actions - wind actions. Brussels.

Stolarski H and Belytschko T (1983). "Shear and membrane locking in curved c-0

elements." Computer Methods in Applied Mechanics and Engineering **41**(3): 279-296.

Temple MC, Prakash MV, et al. (1984). "Failure criteria for stayed columns." Journal of Structural Engineering-Asce **110**(11): 2677-2689.

Tibert G (2002). Deployable tension structures for space applications. PhD dissertation, Dept. of Mechanics, Royal Institute of Technology. Sweden.

Timoshenko SP and Woinowsky-Krieger S (1959). Theory of plates and shells. McGraw-Hill. New York.

Tran CT (2007). Novel deployable membrane structures: Design and implementation, Dept. of Civil Engineering, National University of Singapore. Singapore.

Trometer S and Krupna M (2006). "Development and design of glass folded plate structrues." Journal of the International Association for Shell and Spatial Structures **47**(152): 253-260.

Troyano LF (2003). Bridge engineering: A global perspective. Thomas Telford.

Urthaler Y and Reddy JN (2005). "A corotational finite element formulation for the analysis of planar beams." Communications in Numerical Methods in Engineering **21**(10): 553-570.

USFOS (2012). Usfos: User's manual.SINTEF GROUP.

Veldman SL (2005). Design and analysis methodologies for inflated beams. Ios Pr Incorporated.

Volterra E (1952). "Bending of a circular beam resting on an elastic foundation." Journal of Applied Mechanics-Transactions of the Asme **19**(1): 1-4.

Volterra E (1953). "Deflections of circular beams resting on elastic foundations obtained by methods of harmonic analysis." Journal of Applied Mechanics-Transactions of the Asme **20**(2): 227-232.

Vu KK (2007). Deployable tension-strut structures: Concept, structural behavior, and implementation. PhD, Dept. of Civil Engineering, National University of Singapore. Singapore.

Vu KK, Liew JYR, et al. (2006). "Deployable tension-strut structures: From concept to implementation." Journal of Constructional Steel Research **62**(3): 195-209.

Vu KK, Liew JYR, et al. (2007). "Deployable boom structures - concept and evaluation." Proceedings of the 9th International Conference on Steel, Space & Composite Structures. 469-478.

Wang BB (1998). "Cable-strut systems: Part ii - cable-strut." Journal of Constructional Steel Research **45**(3): 291-299.

Wang BB (2004). Free-standing tension structures: From tensegrity systems to cable-

strut systems. Spon Research. Oxfordshire.

Wang DD and Chen JS (2006). "A locking-free meshfree curved beam formulation with the stabilized conforming nodal integration." Computational Mechanics **39**(1): 83-90.

Wasserman Y (1977). "The influence of the behaviour of the load on the frequencies and critical loads of arches with flexibly supported ends." Journal of Sound and Vibration **54**(4): 515-526.

Wasserman Y (1978). "Spatial symmetrical vibrations and stability of circular arches with flexibly supported ends." Journal of Sound and Vibration **59**(2): 181-194.

Wei XZ, Yao YA, et al. (2006). "A new method of creating expandable structure for spatial objects." Proceedings of the Institution of Mechanical Engineers Part C-Journal of Mechanical Engineering Science **220**(12): 1813-1818.

Wempner G (1969). "Finite elements, finite rotations and small strains of flexible shells." International Journal of Solids and Structures **5**(2): 117-153.

Wever TE, Plagianakos TS, et al. (2010). "Effect of fabric webs on the static response of spindle-shaped tensairity columns." Journal of Structural Engineering-Asce **136**(4): 410-418.

Williams FW (1964). "An approach to the non-linear behavior of the members of a rigid jointed plane framework with finite deflections." The Quarterly Journal of Mechanics & Applied Mathmatics **17**(4): 451-469.

Wong KC and Temple MC (1982). "Stayed column with initial imperfection." Journal of the Structural Division-Asce **108**(7): 1623-1640.

Wong YW and Pellegrino S (2006). "Wrinkled membranes part iii: Numerical simulations." Journal of Mechanics of Materials and Structures **1**(1): 63-95.

Wu MG and Sasaki M (2007). "Structural behaviors of an arch stiffened by cables." Engineering Structures **29**(4): 529-541.

Yang YB and Kuo SR (1994). Theory and analysis of nonlinear framed structures. Prentice Hall. Singapore.

Yang YB, Lin SP, et al. (2007a). "Rigid body concept for geometric nonlinear analysis of 3d frames, plates and shells based on the updated lagrangian formulation." Computer Methods in Applied Mechanics and Engineering **196**(7): 1178-1192.

Yang YB, Lin SP, et al. (2007b). "Solution strategy and rigid element for nonlinear analysis of elastically structures based on updated lagrangian formulation." Engineering Structures **29**(6): 1189-1200.

Yang YB and Shieh MS (1990). "Solution method for nonlinear problems with multiple critical points." AIAA Journal **28**(12): 2110-2116.

Yau JD and Yang YB (2008). "Geometrically nonlinear analysis of planar circular arches based on rigid element concept - a structural approach." Engineering Structures **30**(4): 955-964.

Yoo EJ, Roh JH, et al. (2007). "Wrinkling control of inflatable booms using shape memory alloy wires." Smart Materials & Structures **16**(2): 340-348.

You Z and Pellegrino S (1996). "Cable-stiffened pantographic deployable structures .1. Triangular mast." AIAA Journal **34**(4): 813-820.

You Z and Pellegrino S (1997a). "Cable-stiffened pantographic deployable structures .2. Mesh reflector." AIAA Journal **35**(8): 1348-1355.

You Z and Pellegrino S (1997b). "Foldable bar structures." International Journal of Solids and Structures **34**(15): 1825-1847.

Zeigler T (1997). "Collapsible self-supporting structures." U.S. Patent 4026313.